Development of a biofilm penetrant delivery system for oligonucleotide-based antimicrobials to treat *Burkholderia pseudomallei* infections

By

Adam James Pattinson

Submitted for the Degree of Doctor of Philosophy

2022

ABSTRACT

Burkholderia species are a group of environmental Gram-negative bacteria that are clinically difficult to treat due to a combination of chromosomally encoded resistance mechanisms, low membrane permeability and a propensity to form biofilms. *Burkholderia pseudomallei* is the etiological agent of melioidosis, a tropical disease that infects around 165,000 people annually and results in approximately 89,000 deaths. The current treatment regime employs a biphasic approach consisting of intravenous meropenem or ceftazidime followed by a long term course of co-trimoxazole or co-amoxiclav. Despite this, mortality still occurs in up to 40% of cases. Due to its high aerosol infectivity, the ability to present as an aggressive disease with non-specific symptoms, and the lack of rapidly scalable treatment, *B. pseudomallei* is classified as a biothreat agent by the Centre of Disease Control and the National Institute for Allergy and Infectious Disease. Hence, there is a need for novel treatment approaches.

Transcription factor decoys (TFDs) are oligonucleotide-based antimicrobials that selectively inhibit bacterial transcription factors that are essential for viability and virulence. 12-bis-THA is a lipophilic cation that self-assembles to form particles that bind TFDs with high affinity and protect them from enzymatic degradation. These particles deliver TFDs to the cytoplasm of Gram-positive and Gram-negative bacteria through electrostatic and lipophilic interactions with prokaryote-specific membrane components including cardiolipin and lipopolysaccharide. This technology is an attractive platform for antimicrobial development as it acts on novel targets and circumvents traditional antimicrobial resistance mechanisms whilst sparing the host microbiota.

In this thesis, a multidisciplinary approach was used to examine whether this platform was suitable for the delivery of TFDs to *Burkholderia* biofilms. Firstly, antimicrobial susceptibility testing showed that 12-bis-THA particles alone inhibited the growth of *B. thailandensis*. A proteomic and metabolomic study outlined in this thesis showed that 12-bis-THA induced changes in central metabolism and caused the suppression of bacterial respiratory complexes. 12-bis-THA is a structural analogue of dequalinium, an antiseptic that is known to inhibit the same respiratory chains suggesting that these molecules share a similar mechanism of action. Additionally, Checkerboard assays and time-kill studies showed that 12-bis-THA particles synergised with trimethoprim and co-trimoxazole, and had an additive effect with rifampin and tobramycin against *B. thailandensis* suggesting it may have utility as an adjuvant.

The capsule produced by *B. pseudomallei* and its propensity to form biofilms are considerable challenges for TFD delivery. Confocal microscopy studies showed that 12-bis-THA particles delivered TFD to the cytoplasm of planktonic cells and the body of the biofilm however data was inconclusive regarding the location of TFD inside the biofilm. Additionally, a second TFD version, polymeric TFD particles, that used a rhodamine derived delivery molecule showed good transfection efficiency against planktonic *B. thailandensis* strain E555 in the absence of 12-bis-THA particles.

Using a proteomic and literature review approach, four candidates for TFD development were taken forward. For two candidates, Bcam1349 and GvmR, computational analysis using Prodoric was performed to identify possible transcription factor binding sequences. Antimicrobial testing was performed on TFDs in two formats. Firstly, Bcam1349 and TEX TFDs were formulated with 12-bis-THA particles, but no TFD specific activity was observed. In contrast, GvmR and Zur TFDs had been formulated as polymeric TFD particles and exhibited MICs of 2.5 μg/mL and 0.16 – 0.32 μg/mL.

This thesis shows that the multi-omic workflow used to study the mechanism of action of 12-bis-THA particles has considerable utility to investigate the stress response of an organism and to identify regulatory factors that govern the stress response. Additionally, this work serves as a proof of principle that TFD technology has great potential for the development of *Burkholderia* specific antimicrobial compounds.

LIST OF FIGURES

Figure 3.1: Deaths caused by antimicrobial resistance. Figure taken from the "Antimicrobial Resistance: Tackling a crisis for the health and wealth of nations", The Review on Antimicrobial Resistance Chaired by Jim O'Neill, December 2014.

Figure 3.2: The chemical structures of (A) 12-bis-THA and (B) Dequalinium.

Figure 3.3: Time-kill assay showing the antimicrobial activity of 12-bis-THA particles at MIC concentration against (A) unencapsulated *B. thailandensis* strain E264 and (B) capsulated *B. thailandensis* strain E555. Data are representative of 3 independent experiments, each consisting of 3 technical replicates.

Figure 3.4: Time-kill assay showing the antimicrobial activity of 12-bis-THA particles at MIC concentration against encapsulated *B. thailandensis* strain E555. Data are representative of 3 independent experiments each consisting of 3 technical replicates.

Figure 3.5: Morphological changes in *B. thailandensis* strain E264 following exposure to 4 µg/mL of 12-bis-THA particle for 6 h. **A** and **B** shows treated colonies grown on LB agar for 24 and 48 h, respectively. **C** shows the morphology of untreated E264 colonies grown for 48 h.

Figure 3.6: Growth kinetics of small, normal and untreated (WT) *B. thailandensis* strain E264 colonies in cation-adjusted Muller Hinton broth. Data are representative of 2 independent replicates consisting of 4 technical replicates

Figure 3.7: CLSM images of (A-F) *B. thailandensis* strain E264 and (G-L) strain E555 stained with FM4-64 FX (red) and challenged with 50 µg /mL 12-bis-THA particles (blue) for 120 minutes. (A-C and G-I) The untreated controls show that no autofluorescence was detected with the laser settings used. (**D-F** and **J-L**) Images show that 12-bis-THA particles transfected both unencapsulated (**D-F**) and encapsulated (**J-L**) *B. thailandensis* strains under the tested conditions. 12-bis-THA particle fluorescence was capture in the blue channel using the Hoechst filter (laser settings (λ_{ex} 405 nm/λ_{em} 455nm). The bacterial membrane was captured in the red channel using the FM4-64 FX filter (laser settings (λ_{ex} 515 nm/λ_{em} 630nm). Scales bars are representative of 5 µm except for **ABC** which shows 2 µm. Images were captured using Zen LSM 800 confocal microscope and uniformly edited to increase brightness using Zen software and Microsoft PowerPoint. The assay is represetantive of three independent replicates each consisting of at least five fields of view.

Figure 3.8: CLSM images of (A-F) *B. thailandensis* strain E264 and (G-L) strain E555 stained with FM4-64 FX (red) and challenged with 50 µg /mL CM2 particles (blue) for 30 minutes. (A-C and G-I) The untreated controls show that no autofluorescence was detected with the laser settings used. (**D-F** and **J-L**) Images show that 12-bis-THA particles transfected both unencapsulated (**D-F**) and encapsulated (**J-L**) *B. thailandensis* strains under the tested conditions. 12-bis-THA particle fluorescence was capture in the blue channel using the Hoechst filter (laser settings (λ_{ex} 405 nm/λ_{em} 455nm). The bacterial membrane was captured in the red channel using the FM4-64 FX filter (laser settings (λ_{ex} 515 nm/λ_{em} 630nm). Scales bars are representative of 5 µm. Images were captured using Zen LSM 800 confocal microscope and uniformly edited to increase brightness using Zen software and Microsoft PowerPoint. The assay is represetantive of three independent replicates each consisting of at least five fields of view.

Figure 3.9: Isoboles showing drug interactions between (AB) Trimethoprim and CM2 particles and (CD) Cotrimoxazole and 12-bis-THA particles against B. thailandensis E264 and *B. thailandensis* strain E555. Data show the FIC values along the turbid/non-turbid border of 1 of 3 independent replicates.

Figure 3.10: Isoboles showing drug interactions between (AB) rifampin and 12-bis-THA particles and (CD) tobramycin and 12-bis-THA particles against *B. thailandensis* strains E264 and E555. Data show the FIC values along the turbid/non-turbid border of 1 of 3 independent replicates.

Figure 3.11: Dynamic light scattering (DLS) profiles of 12-bis-THA particles (AB), tobramycin and 12-bis-THA particle (CD), trimethoprim and 12-bis-THA particles (EF) and rifampin and 12-bis-THA particles (GH) in H2O or 0.1X PBS.

Figure 3.12: Time-kill analysis of (A) rifampin (8 µg/mL) and 12-bis-THA particles (2.6 µg/mL), (B) tobramycin (8 µg/mL) and 12-bis-THA particles (2.6 µg/mL), (C) trimethoprim (4 µg/mL) and 12-bis-THA particle (1.3 µg/mL), and (D) co-trimoxazole (1 µg/mL) and (0.3 µg/mL)12-bis-THA particles activity against *B. thailandensis* strain E555. Timepoints were recorded at 0, 3, 6, and 24 . Data are representative of 3 independent experiments each consisting of 3 technical replicates.

Figure 4.1: The process of bacterial biofilm formation. (1) Bacteria reversibly attach to a surface. (2) Once attached, the biofilms form microcolonies that are encapsulated within a self-produced matrix. At this point the bacteria are irreversibly attached. (3) Bacteria within the biofilm proliferate and the biofilm matures and grows. (4) Bacteria on the surface are shed to colonise niches elsewhere. Figure taken from reference 396.

Figure 4.2: Establishing the biofilm growth conditions for the MBEC studies. (**A**) Photograph of *B. thailandensis* strain E555 biofilms grown on the Calgary biofilm device for 72 h. (**B**) Biofilm biomass of *B. thailandensis* strain E555 biofilms in CAMHB (red), LB (blue), or MVBM (green) that had been quantified using 2% crystal violet. (**C**) Bacterial density of biofilms represented as colony-forming units per. The data is representative of 2 independent replicates and the error bars show standard deviation.

Figure 4.3: Activity of antimicrobials and 12-bis-THA particles against *B. thailandensis* strain E555 biofilms. Biofilms were formed using the Calgary biofilm deviced and tested for 24 h before crystal violet staining and quantification. The values shown are relative to the untreated control. $MBEC_{50}$ values were calculated using Graphpad Prism to perform hill slope non-linear regression. The data are representative of 2 independent replicates and the error bars show standard deviation.

Figure 4.4: Activity of synergistic combinations against *B. thailandensis* E555 biofilms. Biofilms were formed using the Calgary biofilm and tested for 24 h before crystal violet staining and quanitifcation. The values shown are relative to the untreated control. $MBEC_{50}$ values were calculated using Graphpad Prism to performed hill slope non-linear regression. Data are representative of 2 independent replicates and error bars show standard deviation.

Figure 4.5: Growth kinetics of *B. thailandensis* strain E555 expressing RFP in MVBM supplemented with 50 µg/mL of chloramphenicol. Images were recorded at 24, 48, and 72 h using a Zeiss LSM 800 confocal microscope. Biofilm Z-stacks were captured using 1 µm slices and the thickness was quantified by Zeiss Blue software. Images were representative of a single independent experiment and 5 fields of view per slide. Scale bars show 10 µm.

Figure 4.6: Confocal micrographs of *B. thailandensis* E555 RFP 72 h old biofilms incubated with 50 ug/mL of 12-bis-THA particles. Biofilms were incubated with 12-bis-THA particles for 15 minutes, 30 minutes, or 60 minutes. Red and blue is representative of bacteria and 12-bis-THA particles respectively. Images were captured with a Zeiss LSM 800 microscope and represent 5 fields of view from 3 independent experiments. Scale bars show 10 µm.

Figure 4.7: Confocal micrographs of *B. thailandensis* strain E555 expressing RFP 72 h old biofilms incubated with 50 ug/mL of 12-bis-THA particles loaded with fluorescently labelled TFD. Biofilms were incubated with 12-bis-THA particles loaded with Alexa-488 labelled TFD 15 minutes, 30 minutes, or 60 minutes. Red, blue, and green are representative of bacteria, 12-bis-THA particles, and TFD respectively. Images were captured with a Zeiss LSM 800 microscope and represent 5 fields of view from 3 independent experiments. Scale bars show 10 μm.

Figure 4.8: Confocal micrographs of *B. thailandensis* strain E555 expressing RFP 72 h old biofilms incubated with 5 μg/mL of rhodamine green Fur TFD conjugate. Biofilms were incubated with TFD-Rhodamine conjugates for for 15 minutes, 30 minutes, or 60 minutes. Red, and green are representative of bacteria and TFD-conjugate, respectively. Images were captured with a Zeiss LSM 800 microscope and represent 5 fields of view from 1 independent experiments. Scale bars show 5 μm.

Figure 4.9: Physical properties of 12-bis-THA particles in water. Correlograms of (**A**) 12-bis-THA particles alone and (**B**) 12-bis-THA particles loaded with 5 μg/mL of TFD. (**C**) The size, polydispersity, derived count rate of 12-bis-THA particles alone or in combination with 5 μg/mL of TFD.

Figure 5.1: The impact of 12-bis-THA on mid-log cultures of *B. thailandensis* E555. Blue, pink and red lines represent untreated cultures or those incubated with 0.1X MIC (0.8μg/mL) or 1X MIC (8.0 μg/mL) of 12-bis-THA particles respectively. The time point marked with the arrow represents the addition of 12-bis-THA particles. Statistical significance was determined using a two-way ANOVA with a Bonferroni post-hoc test where *$P < 0.05$ and **$P < 0.01$

Figure 5.2: Imputation of missing values in the proteomics data set. Data present is plotted in blue whereas missing values that were computationally generated are plotted in orange. Imputation of missing values and generation of histograms was performed by Perseus

Figure 5.3: Principal component analysis (PCA) plots of the proteomics data set. Green dots represent the proteomes of untreated *B. thailandensis* whereas the pink and red dots represent the proteomes of bacteria incubated with 0.1X MIC 12-bis-THA particles or 1X MIC of 12-bis-THA particles respectively. PCA plots were generated using Perseus.

Figure 5.4: Multi-scatter plots of all proteomic data sets showing the correlation between technical and independent experiments. Numerical values are representative of Spearman's rank correlation values which were calculated using Perseus.

Figure 5.5: Volcano plots showing changes in protein abundance in *B. thailandensis* following incubation with 12-bis-THA particles. (**A**) shows the proteome of bacteria treated with 0.1X MIC of 12-bis-THA particles compared to the untreated control. (**B**) shows the proteome of bacteria treated with 1X MIC of 12-bis-THA particles compared to the untreated control. Data points in green represents a significant increase in protein abundance whereas data points in red show a significant reduction in protein abundance. Fold change significance was determined using FDR of 0.01 and an S0 value of 1.

Figure 5.6: Principal component analysis of the metabolomic data sets. Blue, red, and green dots are representative of the metabolomes of untreated bacterial and those treated with 0.1X MIC or 1X MIC of 12-bis-THA particles, respectively. PCA plots were generated using TopSpin version 3.2.

Figure 5.7: Cytoplasmic abundance of metabolic by-products and intermediates in *B. thailandensis* in untreated bacteria or those incubated with 0.1X MIC or 1X MIC of 12-bis-THA particles. Metabolite concentration was calculated using Chenomx NMR Suite 7.0 and comparing peak area to a known concentration of TSP. Statistical significance was determined using a one-way ANOVA followed by a Bonferroni correction. Significance was denoted using the following markers *P < 0.05; **P < 0.01; ***P < 0.001.

Figure 5.8: Cytoplasmic abundance of osmolytes in *B. thailandensis* in untreated bacteria or those incubated with 0.1X MIC or 1X MIC of 12-bis-THA particles. Metabolite concentration was calculated using Chenomx NMR Suite 7.0 and comparing peak area to a known concentration of TSP. Statistical significance was determined using a one-way ANOVA followed by a Bonferroni correction. Significance was denoted using the following markers *P < 0.05; **P < 0.01; ***P < 0.001.

Figure 5.9: Cytoplasmic abundance of nucleotides and nucleotide derivatives in *B. thailandensis* in untreated bacteria or those incubated with 0.1X MIC or 1X MIC of 12-bis-THA particles. Metabolite concentration was calculated using Chenomx NMR Suite 7.0 and comparing peak area to a known concentration of TSP. Statistical significance was determined using a one-way ANOVA followed by a Bonferroni correction. Significance was denoted using the following markers *P < 0.05; **P < 0.01; ***P < 0.001.

Figure 5.10: Cytoplasmic abundance of amino acids in *B. thailandensis* in untreated bacteria or those incubated with 0.1X MIC or 1X MIC of 12-bis-THA particles. Metabolite concentration was calculated using Chenomx NMR Suite 7.0 and comparing peak area to a

known concentration of TSP. Statistical significance was determined using a one-way ANOVA followed by a Bonferroni correction. Significance was denoted using the following markers *P < 0.05; **P < 0.01; ***P < 0.001.

Figure 5.11: Cytoplasmic abundance of amino acids in *B. thailandensis* in untreated bacteria or those incubated with 0.1X MIC or 1X MIC of 12-bis-THA particles. Metabolite concentration was calculated using Chenomx NMR Suite 7.0 and comparing peak area to a known concentration of TSP. Statistical significance was determined using a one-way ANOVA followed by a Bonferroni correction. Significance was denoted using the following markers *P < 0.05; **P < 0.01; ***P < 0.001.

Figure 5.12: The stress response of B. thailandensis to 12-bis-THA particles. (**A**) A cartoon schematic showing central metabolism under normal physiological conditions. (**B**) A cartoon schematic showing the down regulation of electron transport chain, glyoxylate shunt and glycolysis, and the upregulation of beta-oxidation in response to 12-bis-THA particles.

Figure 6.1: Volcano plots showing changes in transcription factor abundance in *B. thailandensis* strain E555 following incubation with 12-bis-THA particles. (**A**) shows the transcription factor proteome of bacteria treated with 0.1X MIC of 12-bis-THA particles compared to the untreated control. (**B**) shows the transcription factor proteome of bacteria treated with 1X MIC of 12-bis-THA particles when compared to the untreated control. Data points in green represents a significant increase in protein abundance whereas data points in red show a significant reduction in protein abundance. Fold change significance was determined using FDR of 0.01 and an S0 value of 1.

Figure 6.2: Amino acid sequence alignment of FNR in *E. coli* strain K12 with homologues in B. pseudomallei strain K96243 and B. thailandensis strain E264. Residues highlighted in red represent amino acids which are essential for the function of FNR in E. coli through the formation of an Fe-S cluster.

Figure 6.3: Identification of LysR type transcriptional regulator binding motif patterns in the 500 base pair region preceding GvmR in *B. pseudomallei*. The nucleotide sequence was taken from the *Burkholderia* genome browse and interrogated using Prodoric virtual footprint.

Figure 6.4: Prodoric analysis of the intergenic region preceding BTH_I1883 (TseM).

Figure 6.5: Confocal microscopy of TFD delivery to encapsulated *B. thailandensis* strain E555 using 12-bis-THA particles. Bacterial cells grown to mid-log phase were incubated with

50 μg/mL of 12-bis-THA loaded with 5 μg/mL of alexa-488 labelled FUR TFD for 1.5 h. Red, green and blue show the bacteria, TFD and 12-bis-THA particles respectively. Images were captured with a Zeiss LSM 800 microscope and represent 5 fields of view from 3 independent experiments. Scale bars show 5 μm

Figure 6.6: Activity of TFD loaded 12-bis-THA particles against *B. thailandensis* strain E555 biofilms. Biofilms were formed using the Calgary biofilm and tested for 24 h in the present of TFD before crystal violet staining and quantification. The values shown are relative to the untreated control. Data are representative of 2 independent replicates and error bars show standard deviation.

Figure 6.7: Investigation of the minimum biofilm inhibitory concentration (MBIC) for BFNR or TEX targeting TFD in *B. thailandensis*. Empty 12-bis-THA particles or those loaded with TFD were incubated with planktonic bacteria within the Calgary biofilm device and incubated at 37^{o}C for 24 h before using crystal violet staining to quantify the biofilm biomass. The values shown are relative to the untreated control. Data are representative of two independent experiments and error bars show the standard deviation.

Figure 6.8: TFD polymeric particle delivery to *B. thailandensis* strain E555. Bacterial cells grown to mid-log phase were incubated with 5 μg/mL of TAMRA labelled TFD polymeric particles for 1.5 h. Red and green show the bacteria and TFD respectively. Images were captured with a Zeiss LSM 800 microscope and represent 5 fields of view from 3 independent experiments. Scale bars show 5 μm.

Figure 10.1: Physical characterisation of rifampin suspending in water at 300 μg/mL using dynamic light scatter. (**A**) is a correlogram showing the correlation coefficient of rifampin suggesting it forms unstable, polydispersed particles. (**B**) shows the predicted size of the populations present.

Figure 10.2: Isoboles showing compounds that did not interact with 12-bis-THA particles in the checkerboard assay. A and **B** show interactions between 12-bis-THA particles and meropenem, **C** and **D** show interactions between 12-bis-THA particles and ciprofloxacin, and **E** and **F** show interactions between 12-bis-THA particles and ceftazidime. Data representative of 1/3 independent replicates.

LIST OF TABLES

LIST OF ABBREVIATIONS

ABC – ATP-binding Cassette

ADP - Adenosine diphosphate

AMP - Adenosine monophosphate

AMR – Antimicrobial resistance

ATP - Adenosine triphosphate

BCC – *Burkholderia cepacia* complex

BSA – *Burkholderia* Secretion Apparatus

CAMHB – Cation-Adjusted Muller Hinton Broth

cAMP - Cyclic adenosine monophosphate

CDC – Centre of Disease Control

CF – Cystic fibrosis

CFTR – Transmembrane Conductance Regulator

CFU/mL – Colony forming units per Millilitre

ChIP – Chromatin Immunoprecipitation

CLSM - Confocal Laser Scanning Microscopy

CoTMP – Co-trimoxazole

CV – Crystal Violent

Dam - DNA adenine methylase

Dcm - DNA cytosine methyltransferase

DLS – Dynamic light Scattering

eDNA – Extracellular DNA

EPS - Extracellular polymeric substance

ETC – Electron transport chain

$FADH_2$ – Flavin Adenine Dinucleotide

FDR – False Detection Rate

FIC – Fractional Inhibitory Concentration

FICi – Fractional Inhibitory Concentration Index

HPMC - Hydroxypropyl Methylcellulose

IDT – Integrated DNA Technologies

LB – Luria Bertani (Miller) Broth

LFQ – Label-Free Quantification

LNA – Locked Nucleic Acid

LPS – Lipopolysaccharide

MALDI-TOF – Matrix-Assisted Laser Desorption/Ionisation-Time Of Flight

MATE – Multidrug and Toxic Compound Extrusion

MBEC – Minimum Biofilm Eradication concentration

MBIC – Minimum Biofilm Inhibitory concentration

MFS – Major Facilitator Superfamily

MIC – Minimum Inhibitory Concentration

MVBM – Modified Vogel and Bonner's medium

NADH – Nicotinamide Adenine Dinucleotide

NMR – Nuclear Magnetic Resonance

OD_{600} – Optical Density at 600 nm

PACE – Proteobacterial Antimicrobial Compound Efflux

PAGE – Poly Acrylamide Gel Electrophoresis

PCA - Principal Component Analysis

PMF – Proton Motive Force

pMIC – Planktonic MIC

Prodoric – Prokaryotic Database Of Gene Regulation

Q - ubiquinone

QH_2 - ubiquinol

RFP – Red Fluorescent Protein

Rif - Rifampin

RND – Resistance Nodulation Cell Division

ROS – Reactive Oxygen Species

SCV – Small Colony Variant

SiRNA – Small Interfering RNA

SMR – Small Multidrug Resistance

T3SS-3 – Type 3 Secretion System cluster 3

T5SS – Type 5 Secretion System

T6SS – Type 6 Secretion System

T6SS-5 – Type 6 Secretion System cluster 5

TBE – Tris-Borate-EDTA

TCA cycle – Tricarboxylic Acid Cycle

TFBS – Transcription factor binding sequence

TMP - Trimethoprim

TMT – Tandem Mass Tagging

Tob - Tobramycin

Transcription factor decoy – TFD

Tss – Type Six Subunit

UT – Untreated

ACKNOWLEDGEMENTS

Firstly, I would like to thank the University of East Anglia and the Defence Science and Technology Laboratory for funding my PhD.

I would also like to thank my supervisory team Professor Michael McArthur, Dr Sarah Harding and Dr Chris Morris for their continued patience, guidance, and faith throughout the project. Additionally, I would like to thank Dr Gwenaelle Le Gall for the NMR analysis, and Professor Esh Mahenthiralingam and Dr Laura Rushton for the BCC work in this thesis.

Thanks to my former lab members Louis, Nichola, Jay, Elina and Sandeep for coffee breaks and for letting me steal your reagents. I'd also like to thank Marytn, Jayna, Dan, Conor and Abe for always giving me an excuse for a second lunch.

I'd also like to thank my former master's degree supervisor Professor Mihalis I. Panagiotidis for supporting and encouraging me to take the next step in my academic career.

Finally, I would like to thank my mum Susan Pattinson for supporting me throughout nine years of higher education and three degrees. I am eternally grateful for everything you have done, this is as much your accomplishment as it is mine.

CONTENTS

CHAPTER 1 - GENERAL INTRODUCTION

1.1 *BURKHOLDERIA CEPACIA COMPLEX*

The *Burkholderia* genus is comprised of over 80 species that occupy a diverse range of environmental niches (1,2) . The majority of these species are non-pathogenic, soil-dwelling saprophytes however several are successful human pathogens that induce severe disease.

The *Burkholderia cepacia* complex (BCC) is a group of 24 phenotypically similar but genetically distinct *Burkholderia* species that are opportunistic pathogens (3)(397) with another two awaiting classification (398, 399). BCC species rarely cause infections in immunocompetent individuals as bacterial cells are cleared by functional airway mucociliary activity (3). In contrast, these species cause opportunistic infections in those with cystic fibrosis (CF) or chronic granulomatosis (4–6). Infections have also been observed in individuals with compromised immune systems such as those with cancer or human immunodeficiency virus, or those undergoing chemotherapy (7–9). The most common risk factors associated with BCC infections are the use of venous and urinary catheters, endotracheal tubes for those on mechanical ventilation, hemodialysis, and long hospitalization periods in intensive care units (10).

CF is an autosomal recessive disorder caused by mutations in the gene encoding for the cystic fibrosis transmembrane conductance regulator (CFTR) (11). It affects approximately 1 in 2500 - 3500 newborns and is predominantly found in those of European descent (12). The CFTR is a chloride ion channel that is present on the apical surface of epithelial cells (13). The malfunction of the CFTR results in the secretion and accumulation of highly viscous fluids within multiple organ systems and is characterised by chronic lung malfunction, pancreatic insufficiency, and high levels of chloride in sweat. Pulmonary disease is a major cause of morbidity and mortality in individuals with CF (14). This is characterised by structural airway changes that give rise to increased dilation (bronchiectasis), mucoid impaction, a partial or complete collapse of the lung (atelectasis), fibrosis and vascular changes (15). This causes a decline in lung function that limits the effective clearance of thick, sticky mucus containing microbial pathogens that have entered the respiratory tract resulting in chronic bacterial infection and airway inflammation.

The microbiota of the CF airways is complex and differs throughout the lifespan of a patient. During the first decade of life, the pathogens *Staphylococcus aureus* and *Haemophilus influenzae* are routinely cultured from the sputum of individuals with CF (16).

After the age of 20, *Pseudomonas aeruginosa* is commonly identified as the main cause of respiratory infection in patients with CF. *P. aeruginosa* is a clinically important pathogen that is associated with ventilator associate pneumonia, catheter associated infection, central-line associated infections, burns, wound infections, and surgery related infections (400). Chronic *P. aeruginosa* lung infections common in CF individuals as this bacterium displays a propensity to form biofilms (401, 402) and gain resistance mechanisms to multiple antimicrobials making therapeutic eradication challenging.

Stenotrophpmonas maltophilia is a well-known respiratory pathogen that can be isolated from the respiratory tracts of 8.14% - 13.8% of individuals with CF (403, 404). Isolation of *S. maltophilia* is positively correlated with the use of intravenous antimicrobials and oral quinolone use (405 – 407). This is consistent with findings by Denton showed that the isolation of *S. maltophilia* was positively associated with the use of anti-pseudomonal therapeutics (408).

The incidence of infections caused by nontuberculous *Mycobacteria*, specifically the *Mycobacterium avium* complex and the *Mycobacterium abscessus* complex, in CF patients has risen from 3.3% to 22.6% over the last two decades and has resulted in an increase in both morbidity and mortality (409 – 411). Such poor prognosis is likely associated with accelerated lung function decline which is exacerbated by the requirement for long term therapeutic intervention that only results in a successful outcome in 30% of patients (412, 413).

Achromobacter species, including *Achromobacter xylosoxidans,* are emerging CF pathogens. These bacteria are environmental opportunistic pathogens that are associated with infections in the elderly (414, 415). The prevalence of these species in CF infections is unclear but these bacteria are isolate from up to 17% of individuals with CF (414, 416 – 418). Additionally, *Achromobacter* species are associate with temporary pulmonary exacerbation but not with long-term prognosis (419).

Though the BCC species infect relatively few patients, it represents a major clinical challenge and it is difficult to predict patient outcomes. Patients infected with these species can experience asymptomatic carriage to ‘cepacia syndrome’ which manifests as necrotizing pneumonia, worsening respiratory failure, and bacteremia (17). Despite consisting of approximately 24 different bacterial species, *Burkholderia cenocepacia* and *Burkholderia multivorans* are the most prevalent species identified in the CF community. Although it is not a member of the BCC, *Burkholderia gladioli* accounts for 15% of CF infections caused by

Burkholderia species (18). This is higher than other members of the BCC species including *Burkholderia vietnamiensis* (5%), *Burkholderia dolosa* (3%) and *Burkholderia cepacia* (3%) (19).

1.2 *BURKHOLDERIA MALLEI*

Burkholderia mallei is a highly pathogenic member of the *Burkholderia genus*. It is a Gram-negative, aerobic, non-motile bacillus and is a host-adapted pathogen that is unable to persist in the wider environment. It is believed to share a common progenitor with *Burkholderia pseudomallei* and is considered a divergent clone that has adapted to become an obligate pathogen by in-host evolution (20,21). It is the causative agent of glanders which is an infectious disease common in equine species such as horses, donkeys and mules. Glanders has been eradicated in Western Europe, the USA and Canada through the adoption of a stringent test and slaughter policy (22). However, it is still endemic to the Middle East, Asia, Africa, and South America (22). Infections in humans and are best described in the context of an accidental laboratory exposure (23–25). In these cases, glanders typically manifested as tachycardia, lymphedema, splenic and hepatic abscesses, pneumonia and bacteraemia. Though mortality was not observed in these cases, all patients required a long term course of antimicrobials to clear the disease (23,25).

1.3 *BURKHOLDERIA PSEUDOMALLEI*

1.3.1 Epidemiology

B. pseudomallei, the etiological agent of melioidosis, was first identified by Alfred Whitmore and C.S. Krishnaswami during autopsies performed on deceased opium addicts in Rangoon, Burma in 1911 (26). *B. pseudomallei* is a Gram-negative, facultative intracellular bacterium that can survive in low nutrient environments (27). It is saprophyte that is routinely cultured from rice paddies, stagnant waters and moist soil in the tropics and sub-tropics where it is endemic. The global distribution of *B. pseudomallei* is not well understood and subsequently, the rate of infection is poorly characterised. Poor diagnosis due to diverse clinical presentation and inadequate diagnostic tools have limited epidemiological analysis which has resulted in poor disease awareness even in areas where melioidosis is endemic (28). *B. pseudomallei* is especially prevalent in South-East Asia and Northern Australia although sporadic cases are recorded throughout Asia, Africa and South America. Studies by Limmathurotsakul *et al* present a new epidemiological model to predict the global distribution of melioidosis(29). **Figure 1.1** was modelled using an evidence-based consensus

and geo-locating reported cases, and has estimated there to be 165,000 human melioidosis cases each year, of which 89,000 cases result in mortality.

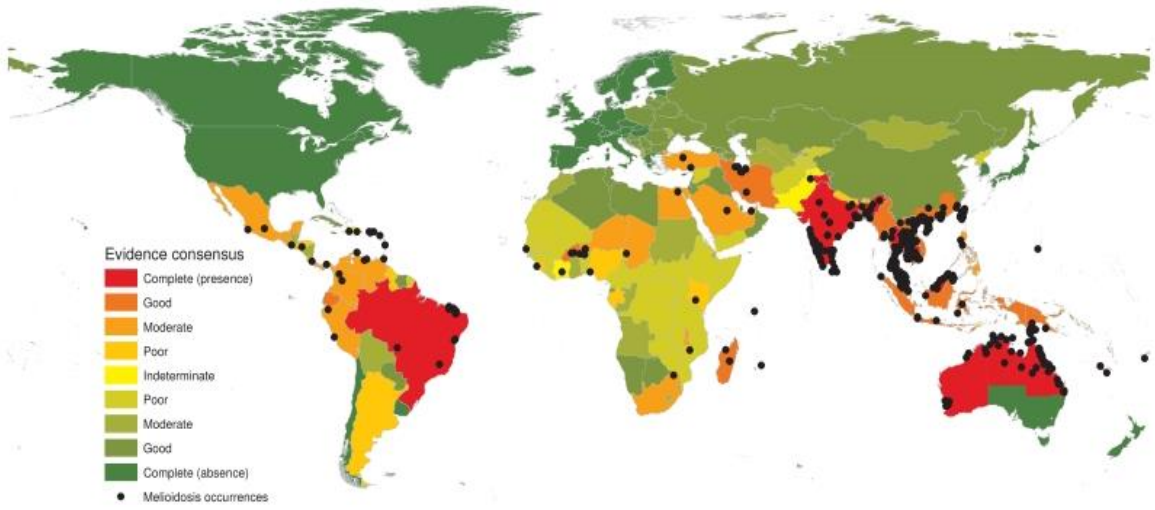

Figure 1.1: Estimated global distribution of *B. pseudomallei*. Green indicates a low evidence-based consensus whilst red represents high evidence-based consensus for the presence of *B. pseudomallei*. Black dots present geo-located records of melioidosis cases. Evidence was based on 22,338 human and animal recorded cases between 1910-2014. Figure taken from reference 29.

1.3.2 Routes of infection

Melioidosis develops following the inhalation, ingestion, or subcutaneous inoculation of *B. pseudomallei.* In South-East Asia and Northern Australia, the monsoon season has been closely associated with an increase in melioidosis cases by 75-85% possibly due to extreme weather causing aerosols containing the bacterium (30,31). Similarly, during the Vietnam war, inhalation of dust containing *B. pseudomallei* was believed to have infected American servicemen (32,33). As previously mentioned, *B. pseudomallei* is known to persist in low-nutrient environments including water (34). Multiple studies in Northern Australia and Southern Thailand have shown that *B. pseudomallei* has been cultured from unchlorinated, bore drinking water (35–37). Currie *et al* showed that a *B. pseudomallei* strain that was isolated from drinking water was matched to a clinical isolate from a patient, providing evidence for ingestion as a route of infection (37). In a 20 year prospective study of melioidosis cases in Northern Australia, Currie *et al* found that 75% of cases likely occurred as a result of environmental exposure to *B. pseudomallei* (38). Of these cases, 22% had specific exposure events such as sustaining wounds while gardening or playing sports, or

chasing feral pigs through tropical savannah swamps. In Northern Thailand, 81% of cases were observed in rice farmers who had likely come into contact with contaminated water or soil (39). Because of this, there have been education programs implemented to promote the use of rubber boots and gloves on rice farms with the aim of preventing infection (40).

1.3.3 Clinical manifestation

Clinical presentation can range from localized subcutaneous infections to sepsis and death. Bacteremia develops in 40-60% of cases which can develop into sepsis in 20% of these cases (38,41) . Bacteremia and sepsis allow bacterial cells to disseminate throughout the body and colonize varying niches including the respiratory, neurological, gastrointestinal and genitourinary systems (**Figure 1.2**) (38,42). Melioidosis pneumonia accounts for approximately 50% of melioidosis cases presenting in the clinic (41,43). It is a diverse illness that can present as acute, fulminant sepsis with multifocal infiltrates (44) or chronic respiratory colonization which emulates tuberculosis, both radiologically and by the clinical presentation (45).

Approximately 85% of melioidosis cases present as the acute form of the disease which arises from recent exposure incidents (38). Most of these patients present with an aggressive form of the disease such as sepsis, with or without pneumonia, or localized lesions. In contrast, approximately 11% of patients present with chronic melioidosis defined as a symptomatic infection that lasts longer than 2 months (38). These patients generally present with non-specific symptoms which slows the diagnosis and effective management of melioidosis.

Typically, the symptoms of melioidosis manifest 1 to 21 days (average of 9 days) following inoculation, however this is dependent on the route of transmission, host risk factors and the infecting strain (46). Melioidosis predominantly infects those with pre-existing co-morbidities. The most common risk factor is diabetes mellitus which was present in up to 75% of cases in Malaysia (41). Other pre-existing conditions such as a compromised immune system, chronic kidney disease, chronic lung disease, chronic alcohol use and cancer have also been associated with melioidosis (38,41). Additionally, individuals with CF have also been diagnosed with melioidosis which is consistent with the susceptibility of these patients to infections by BCC species (47,48).

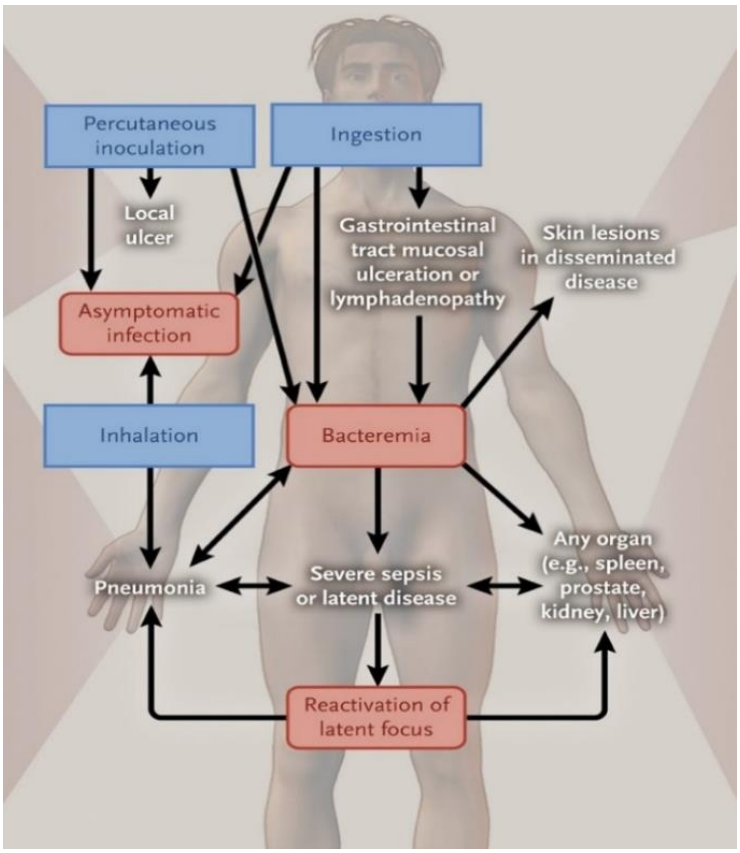

Figure 1.2: Clinical presentation of melioidosis highlighting route of infection and following dissemination. The blue boxes represent the initial infection event and the red boxes demonstrated clinical events. Figure taken from reference 42.

1.3.4 Molecular pathophysiology

To establish infection, *B. pseudomallei* first enter cells in the host epithelial layer or the mucosal surface where the bacterial cells replicate before spreading to neighbouring cells (**Figure 1.3**) (49). Attachment to the surface of host cells is driven by the type IV pili, which are hair-like filaments on the bacterial surface, and the capsular polysaccharide (50). Studies by Chuaygud *et al* and Allwood *et al* have shown that mobility helps bacterial cells navigate the mucosal lining but its role in surface attachment is still unclear (51,52). *B. pseudomallei* encodes multiple secretion systems which support the secretion of bacterial effector proteins into neighbouring cells or the intracellular milieu and several have been implicated with a role in cellular invasion. The type 5 secretion system (T5SS) exports the adhesins BoaA and BoaB which support bacterial attachment but are not essential (53). Similarly, the type 3 secretion system cluster 3 (T3SS-3) exports BopE, which causes actin rearrangement in the

host cell membranes facilitating ingress, and BsaQ which have been shown to support bacterial attachment (54). However, mutants of BoaA, BoaB, BopE, and BsaQ have shown that they are not essential for bacterial attachment suggesting multiple effectors are required to act in combination (54,55).

Most *Burkholderia* species including *B. pseudomallei* can invade phagocytotic and non-phagocytotic cells (56,57). Bacterial cells then can cause cell lysis or can invade neighbouring cells. Upon entering the host cell through phagocytosis, *B. pseudomallei* must rapidly escape before fusion with the lysosome which contains an array of enzymes that are capable of degrading biological molecules (**Figure 1.3**). The T3SS-3 plays a critical role in this with multiple studies showing that mutant strains of *B. pseudomallei* have a reduction in intracellular survival (58–60). For example, mutations in *bipD* and *bsaZ* have been shown to reduce or prevent the formation of actin tails which are used by *B. pseudomallei* for intracellular motility (58). Similarly, BimA (420) and BimC (421) are also required for actin-tail based intracellular motility.

The formation of multinucleated giant cells has been proposed as a mechanism to facilitate the cell-to-cell dissemination of *B. pseudomallei* (61). Additionally, cell fusion likely enables *B. pseudomallei* to access more nutrients from the newly fused cells (**Figure 1.3**). Both the T3SS-3 and the type 6 secretion system cluster 5 (T6SS-5 but also termed T6SS-1) are important virulence factors that play a role in the formation of multinucleated giant cells (61). Mutations in the T3SS-3 effector protein *bipB* have resulted in a reduction of cell-to-cell spreading and the formation of multinucleated giant cells (62). Similarly, other studies have shown that *B. pseudomallei* strains deficient in components of the T6SS-5 had reduced cell-to-cell fusion and the ability to form of multinucleated giant cells (63,64). *In vivo* studies have shown that mutations in the components of the T3SS-3 or the T6SS-5 resulted in an attenuation of virulence, suggesting that these pathways are important in the development of acute melioidosis in humans (61). *B. pseudomallei* can also induce cellular cytotoxicity resulting in host cell death. *B. pseudomallei* stimulates apoptosis in macrophages in response to the formation of multinucleated giant cells and membrane destabilisation as a result of actin scavenging (65). In addition, intracellular *B. pseudomallei* can induce caspase-1 dependent cell lysis in macrophages (66).

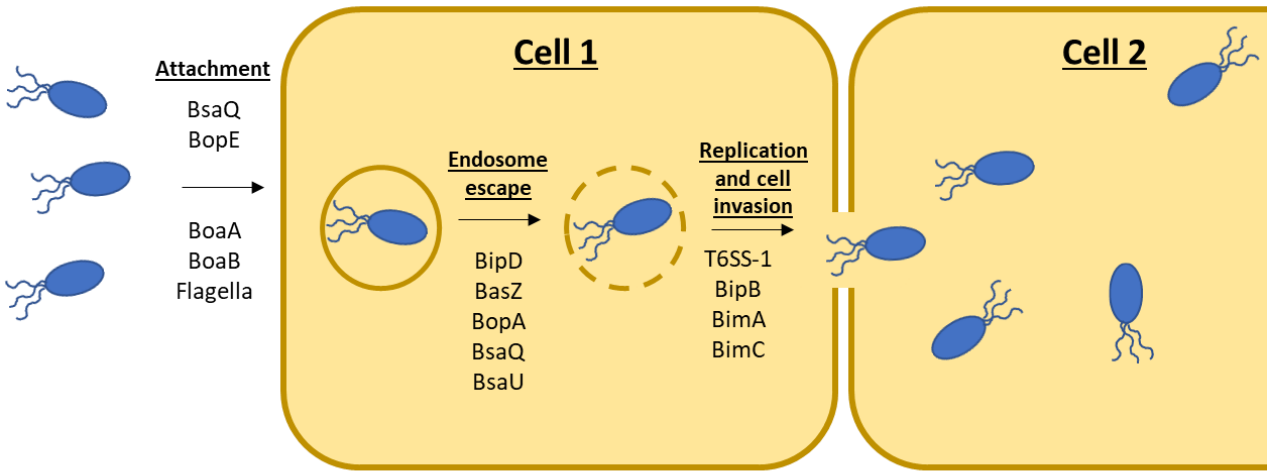

Figure 1.3: Cartoon schematic of intracellular invasion and replication of *Burkholderia pseudomallei* in the cytoplasm of host cells. *B. pseudomallei* can invade both phagocytotic and non-phagocytotic cells. Initial attachment occurs through the use of flagella and type IV pilli which is supported by the secretion of BoaA and BoaB. In non-phagocytotic cells, bacteria stimilate their own internatilsation using the T3SS which expels BsaQ and BopE causing membrane ingress. Next the bacteria escape the phagosome into the cytoplasm through the excretion of T3SS-3 effectos including BopA and BipD. Once into the cytoplasm the bacterial cells replicate bacteria use the T6SS-1 to expel effectors such as BimA and BimC which sequester host actin to facilitate actin-tail formation and the invasion of neighbouring host cells. Figure adapted from reference 422.

1.3.5 Diagnosis

Detection of *B. pseudomallei* from clinical specimens is the gold standard method for the diagnosis of melioidosis. Typically, blood, urine and respiratory samples including throat and rectal swabs may be cultured in suspected cases of systemic melioidosis (67). Wound swabs and pus/exudate should also be cultured to identify cutaneous melioidosis. Though bacterial culture is the gold standard, it has a low diagnostic sensitivity (60.2% sensitivity) to patients with melioidosis (68). A culture-based diagnosis requires experienced laboratory staff as *B. pseudomallei* can be misidentified as other species such as *Pseudomonas* spp, *B. cepacia*, or *Bacillus* spp (28). Diagnostic workshops have been implemented in areas where *B. pseudomallei* is endemic to educate and train laboratory staff to recognise *B. pseudomallei* using culture-based methods (28). *B. pseudomallei* grows on most routine laboratory agars but tends to grow much slower than commensal organisms which might outgrow it therefore selective agar is used to isolate *B. pseudomallei* from mixed cultures. Ashdown's media is used to isolated *B. pseudomallei* and traditionally contains trypticase soy agar, glycerol,

crystal violet, neutral red, and gentamicin (69) but can also be supplemented with colistin to reduce the growth of other Gram-negative species (70). When grown on this media, *B. pseudomallei* typically forms dry, flat, purple colonies that have a metallic sheen. *B. pseudomallei* is not a part of the human microbiota and identification within clinical specimens should be regarded as diagnostic of melioidosis.

Misidentification of *B. pseudomallei* is not uncommon and it is recommended that multiple methods are used to establish a diagnosis. Clinical proteomics using matrix-assisted laser desorption/ionization-time of flight (MALDI-TOF) has been shown to provide accurate identification of *B. pseudomallei* (71). 16s ribosomal sequencing (72) and PCR based methods (73,74) have also been developed however these are not used clinically but are instead used in research and reference laboratories.

Individuals can be screened for the presence of anti-*B. pseudomallei* antibodies using an indirect hemagglutination antibody test (75,76). However, this approach has limited application as approximately 70% of Thai children produced these antibodies in the absence of infection which likely occurs through environmental exposure (77). Instead, a method has been developed that uses a monoclonal antibody to recognise an antigen on the capsular polysaccharide of *B. pseudomallei* and *B. mallei* (78). It has displayed excellent sensitivity (99.1% sensitivity) and is particularly useful for screening suspect colonies (78).

1.3.6 Treatment strategies

Early diagnosis and implementation of the appropriate antimicrobial treatment is essential in melioidosis and has been linked with patient outcomes. Mortality occurs in approximately 10% of cases where healthcare professionals have access to state-of-the-art facilities (38). However, these facilities are not available in many locations where *B. pseudomallei* is endemic resulting in patient mortality increasing up to 40% (79).

The current treatment regime is composed of a biphasic approach consisting of an acute phase and an eradication phase (80). During the acute phase, antimicrobials are delivered intravenously for $\geq$ 10 days to prevent death from overwhelming sepsis. Ceftazidime is typically used in uncomplicated cases whereas meropenem is used in individuals within intensive care, who have neurological involvement or display persistent bacteremia (80). The treatment length can also be extended up to four weeks for patients entering intensive care with pneumonia or those with deep-seated abscesses. It can be further extended to six weeks for those with osteomyelitis, and up to eight weeks for individuals with arterial infection or central nervous system involvement (81). A recent

review of the treatment guidelines suggested that the acute phase should be extended to a minimum of three weeks for patients with concurrent bacteremia and pneumonia involving only a single lobe and those with bilateral and unilateral multi-lobar pneumonia who do not have bacteremia (81). Treatment in those with concurrent bacteraemia and bilateral or unilateral multi-lobar pneumonia should be treated for a minimum of four weeks.

The eradication phase is comprised of oral co-trimoxazole or co-amoxiclav to kill residual bacteria and reduce the risk of relapse (80). This typically lasts for three months but maybe extended up to six months in individuals with osteomyelitis, arterial infection, or neurological involvement (81). In a large, multicentre study, co-trimoxazole was non-inferior and produced fewer side effects when compared to patients treated with co-trimoxazole and doxycycline (82). Emerging resistance to co-trimoxazole presents a clinical challenge as up to 18% of clinical isolates show reduced susceptibility (83,84).

1.3.7 Resistance mechanisms

The frequency of resistance of *B. pseudomallei* to clinically relevant β-lactams is unclear. A screen of 4,000 clinical isolates performed by Wuthiekanun *et al* showed that only 0.6% of strains were resistant to ceftazidime (n=8), amoxicillin + clavulanic acid (n=8) or both antimicrobials (n=13) (85). In contrast, Rao *et al* performed a screen of 164 clinical isolates and 21 (11.6%) were resistant to ceftazidime (86). It was proposed that this was due to the misuse of antimicrobials however this is difficult to determine considering the difference in samples sizes (4000 compared to 164).

PenA is a class A β-lactamase that is commonly associated with β-lactam resistance in most *B. pseudomallei* clinical isolates (87). This can develop due to two reasons. Structural mutations in or near the β-lactamase site have been shown to result in resistance to ceftazidime, co-amoxiclav, or both. Alternatively, some clinically isolates that are resistant to ceftazidime have shown the presence of a point mutation in the promoter region of *penA* which may increase its transcription (88). Large genomic rearrangements or deletions have been associated with resistance to ceftazidime in clinical *B. pseudomallei* isolates (89). This was caused by a 71 kb deletion from chromosome two which contained three penicillin-binding proteins which are known targets of β-lactam antimicrobials.

Efflux pumps are important resistance determinants in *B. pseudomallei* and other *Burkholderia* species. Bacterial efflux pumps are separated into six groups: 1) The major facilitator (MFS) superfamily; 2) The resistance nodulation cell division (RND) family; 3) The small multidrug resistance (SMR) family; 4) The multidrug and toxic compound extrusion

(MATE) family; 5) The ATP-binding cassette (ABC) family; and 6) The proteobacterial antimicrobial compound efflux (PACE) family (90). RND efflux pumps are clinically important due to their ability to span both the cellular envelope. By doing so, they act synergistically with the Gram-negative outer membrane by simultaneously reducing antimicrobial penetration into the bacterial cell and efficiently expelling compounds that successfully enter the cytoplasm (91).

B. pseudomallei encodes for ten efflux pumps, seven are located on chromosome one and three are located on chromosome two (92). Of the ten pumps, three are well characterised. AmrAB-OprA was the first pump to be identified and is responsible for expelling aminoglycoside and macrolide antimicrobials from the cytoplasm. Rare, naturally occurring deletions or regulatory mutations have been identified and are susceptible to aminoglycosides (93,94). AmrAB are possible homologues of MexXY which is expressed in some aminoglycoside resistant strains of *Pseudomonas aeruginosa* (95).

The BpeAB-OprB efflux pump was initially described in *B. pseudomallei* strain KWH and confers resistance to low-levels of chloramphenicol, fluoroquinolone, tetracycline, aminoglycoside and macrolides (96,97). Further characterisation of *B. pseudomallei* strain 1026b showed that the BpeAB-OprB efflux pump confers resistance to aminoglycosides in this strain (98). BpeAB-OprB is related to MexAB-OprM in *P. aeruginosa* however their functions are different (99). The MexAB-OprM efflux pump is widely expressed and contributes to antimicrobial resistance against a range of compounds (99). In contrast, it is not widely expressed in *B. pseudomallei* and may only play a minor role in the resistance profile of this bacterium.

BpeEF-OprC was first identified as a chloramphenicol and trimethoprim efflux pump through its expression in an efflux compromised strain of *P. aeruginosa* (100). It is not widely expressed in wild type strains but is expressed in naturally occurring mutants where the transcriptional activator *bpeT* is constitutively expressed (101). When expressed, BpeEF-OprC expels chloramphenicol, fluoroquinolones, tetracyclines, and trimethoprim, and is responsible for trimethoprim resistance in clinical settings (102).

The Gram-negative membrane acts as a permeability barrier that prevents the internalisation of compounds that would be toxic to the bacteria. It is an asymmetrical bilayer made up of an outer membrane that is comprised of lipopolysaccharide (LPS) and the inner membrane which comprised of glycerophospholipids (103). LPS is made up of three components, lipid A, the core oligosaccharide, and the o-antigen, and it is the structure of

LPS that reduces the permeability of the lipid bilayer (103). The acyl chains that anchor the lipid A into the membrane help stabilise LPS and prevents the passage of hydrophilic molecules across the membrane. Conversely, the core oligosaccharide and o-antigen are hydrophilic which helps prevent hydrophobic molecules from crossing the lipid bilayer (104). *B. cepacia* has extremely low membrane permeability and demonstrates only 11% of the permeability of *E. coli* (105). This likely occurs as *B. cepacia* produces comparatively fewer membrane porins than *E. coli* (105). The structure of LPS can also be modified to confer resistance to cationic peptides and polymyxins such as colistin. Extreme resistance to polymyxin class molecules is a common characteristic of *Burkholderia* species and occurs due to the inclusion of an Ara4N group to the lipid A of the LPS. This neutralises the negative charge of a phosphate by adding a sugar with a positively charged amine group (106).

1.3.8 *Burkholderia* genomics

B. pseudomallei has a large genome (7.2 Mb) that is GC rich (67.9%) and is comprised of two chromosomes. The first chromosome is 4.07 Mb and contains genes that are associated with core functions such as metabolism and growth (423). In contrast, the second chromosome, which is smaller (3.17 Mb), contains accessory genes that support bacterial adaption and including iron acquisition, osmotic protection, and secondary metabolism genes (423). Though the second chromosome contains genes associated with plasmid replication, it has been classified as a chromosome as it contains genes that are associated with central metabolism and essential function (423). BCC species also contain two cromosomes but also have a third replicon which is a megaplasmid named pC3 (formerly chromosome III). This has been shown to contribute to stress resistance and virulence in addition to antifungal and proteolytic activity in a number of strains (424, 425). However, this megaplasmid is not essential for bacterial viability with approximately 4% of BCC isolates having lost this replicon (424).

The comparison of clinical and environmental isolates against *B. pseudomallei* strain K96243 allowed for the allocation of genes into core and accessory genomes (426). 86% of the K96243 genome was common across all environmental and core isolate representing the core genome. Alternatively, 14% of the K96423 genome was found at varying frequencies across the isolates which represent the accessory genome. Gene order between strains of *B. pseudomallei* is remarkably well preserved despite the diversity of genes that can be found in the accessory genome. New genes are acquired through horizontal gene transfer but are integrated within specific regions of the genome such as genomic islands (427). These sites account for around 4% of the *B. pseudomallei* genome (427).

Burkholderia thailandensis is closely related to both *B. pseudomallei* and *B. mallei*. Like *B. pseudomallei, B. thailandensis* can be isolated from contaminated soil and stagnant water in the tropics and subtropics (109). *B. thailandensis* also has a large genome (6.7 Mb) comprised of two chromosome (chromosome 1 - 3.8 Mb and chromosome - 2.9 Mb) (428). *B. thailandensis* is genetically distinct as it can assimilate arabinose due to the presence of the BTH_II1626 – 1633 operon found on chromosome two of *B. thailandensis* but is absent from *B. pseudomallei* (111). Comparative genomics has shown that *B. thailandensis* has retained 71% of virulence genes from *B. pseudomallei* (428). Despite the conservation of virulence genes, *B. thailandensis* is avirulent and rarely causes infections in humans.

The genomes of both *B. pseudomallei* and *B. thailandensis* contain regions of unusually high GC content which act as markers for genomic islands. These are an important source of genomic diversity which allow for the acquisition and integration of new genes into the genome. In *B. pseudomallei*, the number of genomic islands varies depending on strain and sites can vary between strains (429). Similarly, the genome of *B. thailandensis* also contains genomic islands which are in similar locations to those in *B. pseudomallei* (428). The clinical importance of genomic islands is not full clear but they have the potential to be a source of virulence and AMR resistance genes. This has been observed in *B. thailandeneis* strain E555. Most *B. thailandensis* strains do not produce a capsular polysaccharide as they usually lacks the gene cluster BPSL2790 – 2810 which is responsible for the synthesis and trafficking of CPS. *B. thailandensis* strain E555 has acquired a genomic island that allows this strain to produce a capsular polysaccharide that is highly similar to that present in *B. pseudomallei* (112,113). This is important as the capsule in *B. pseudomallei* is a conserved virulence factor that provides protection from host immunity by lowering the efficiency of the membrane attack complex (430).

1.3.9 Biothreat pathogen

B. pseudomallei is classified as a biothreat agent due to its high aerosol infectivity, the ease with which it can be isolated from the environment, and its ability to cause severe disease with non-specific symptoms. It is classified as a category B biothreat agent by the National Institute of Allergy and Infectious Diseases (107). This rank also includes *B. mallei* and is reserved for species that are moderately easy to disseminate, result in moderate morbidity rates and low mortality rates, and require specific enhancements for diagnostic capacity and enhanced disease surveillance (107). Similarly, it is ranked as a tier 1 select agent by the Centre for Disease Control, and the United States Department of Agriculture as it is capable of causing severe disease in humans (108). Because of this, there is considerable

interest in developing novel therapeutic approaches that are more scalable than the traditional biphasic therapeutic regime. However, as *B. pseudomallei* is a Containment Level 3 pathogen it requires extended containment facilities which can slow the screening of novel compounds. One approach is to use a surrogate organism to identify lead compounds which can then be tested in the target organism at a later date.

1.3.10 B. thailandensis as a surrogate organism

As previously mentioned, *B. thailandensis* closely related to *B. pseudomallei* (431) . Despite sharing a high degree of genomic similarity, *B. thailandensis* is considerably less virulent in *in vivo* models as *B. pseudomallei* has a lethal dose 50 (LD_{50}) of <10 organisms whereas *B. thailandensis* has an LD_{50} of 10^6 bacteria (432, 433). Infections caused by *B. thailandensis* have been recorded however are exceedingly rare compared to cases of melioidosis (434 – 437). Despite being less virulent, *B. thailandensis* shares important virulence factors including the T3SS and the T6SS which are both important for cellular invasion. Due to the conservation of these systems, *B. thailandensis* is a well-established surrogate model for *B. pseudomallei* to study the molecular basis of cellular invasion and survival (438 – 440).

Though *B. thailandensis* has comparably lower virulence, it still primers the host immune system and can provide cross-protection from *B. pseudomallei* infections either using live *B. thailandensis* cells (441) or using *B. thailandensis*-derived products such as outer membrane vesicles (442) or heat killed cells (443). This suggests that *B. thailandensis* is a surrogate organism for studying the host-immune response to *B. pseudomallei* and that *B. thailandensis* may have the potential for the development of a melioidosis vaccine.

B. thailandensis produces many of the same antimicrobial resistance mechanisms such as efflux pumps and LPS modification that are observed in both *B. pseudomallei* and BCC species (444). For this reason, *B. thailandensis* displays similar minimum inhibitory concentrations to those observed in *B. pseudomallei* (114). This indicates that *B. thailandensis* is a useful surrogate organism to investigate the activity of novel antimicrobial molecules (115). Therefore, in this thesis, we use *B. thailandensis* strains E264 and E555 to investigate the activity of novel antimicrobial compounds.

1.4 TRANSCRIPTION FACTOR DECOYS (TFDS)

Transcription factors are regulatory proteins that control gene expression by binding to a specific nucleotide sequence called a transcription factor binding site (TFBS) which is in

the promoter of a target gene. This can occur independently or in combination with other transcription factors and/or nucleoid associated proteins to promote (by transcriptional activators) or block (by transcriptional repressors) recruitment of RNA polymerase. Numerous approaches have been performed to identify TFBS such as DNA footprinting (116), protein-nucleic acid pull-downs, Chromatin Immunoprecipitation (ChIP assays) (117), the use of reporter strains (118), and mutational studies (119). Alternatively, computational tools such as the prokaryotic database of gene regulation (Prodoric) have been used to predict TFBS in promoter regions by identifying nucleotide sequences that are similar to characterised binding motifs (120). Transcription factor binding sequences are generally direct or inverted repeats of five to seven nucleotide motifs that are separated by a short spacer sequence. This is indicative of transcription factors binding as a dimer in the same or opposing orientation (121).

Under normal conditions, a transcriptional activator will bind to a transcription factor binding motif upstream of a target gene. The DNA-bound transcription factor then recruits RNA polymerase initiating transcription (**Figure 1.4A**). Transcription factor decoys (TFDs) are nucleic acid-based therapeutics that contain the binding sequence of a transcription factor, resulting in the competitive inhibition of the TFD target. By doing so, this prevents the transcription factor from binding its cognate genomic target resulting in the suppression of downstream gene expression (**Figure 1.4B**) (121).

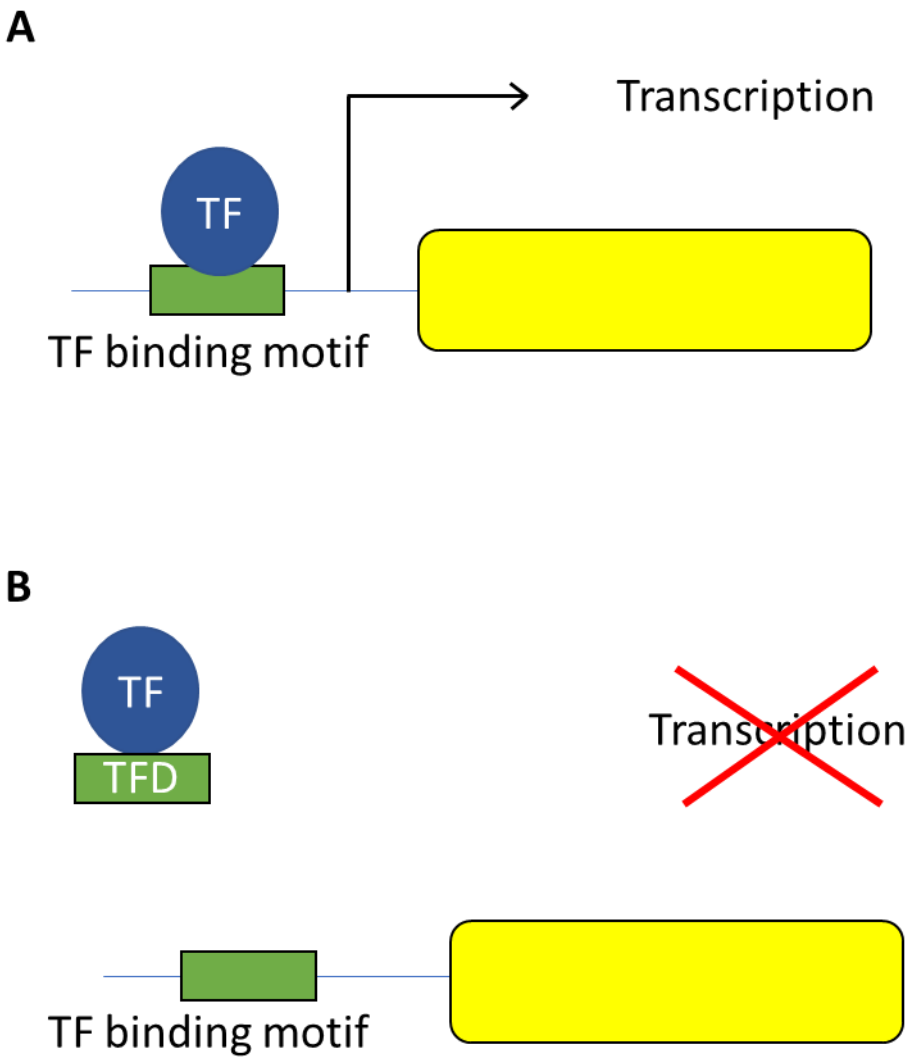

Figure 1.4: Cartoon schematic showing the mechanism of action of transcription factor decoys (TFDs). (**A**) Transcriptional activators bind to a transcription factor binding motif resulting in the recruitment of RNA polymerase and the induction of transcription. (**B**) TFDs sequester the target transcription factor preventing the initiation of transcription and suppressing downstream gene expression.

TFDs have distinct advantages over other nucleic-acid based therapeutics such as short interfering RNAs (siRNA) and locked nucleic acids (LNAs) which work by preventing the translation of mRNA transcripts. TFDs control gene expression by competitively inhibiting a transcription factor which prevents it from binding to its genomic target and flooding the bacterial cell with numerous mRNA copies (122). Alternatively, antisense-based therapeutics inhibits gene expression on a post-transcriptional level by targeting mRNA and either stimulating its enzymatic degradation or by binding mRNA (123) and sterically preventing its translation (124). mRNA transcripts are numerous within the cytoplasm and require micromolar concentrations of antisense therapeutics to inhibit bacterial growth (125,126). In contrast, transcription factors are present in relatively lower copy numbers meaning that fewer TFDs are required to elicit antimicrobial activity (127). Another challenge for antisense-based strategies is the identification of a nucleotide sequence that allows for efficient oligo-mRNA binding as mRNA transcripts often have complex secondary structures (128). Instead, TFDs can be quickly synthesized and tested once a transcription factor binding sequence has been identified.

Resistance to TFDs is considered unlikely but may occur following certain independent events. Previous candidates for TFD development were based on the essentiality of the TFD target meaning that deletion of this gene would result in bacterial death. Mutations to a transcription factor that reduces its ability to recognize its binding sequence would reduce its affinity for the TFD. However, this would also result in a reduced affinity to its genomic target which would reduce gene expression. Similarly, mutations within the TFBS would prevent the binding of its own transcription factor consequently resulting in the suppressed expression of downstream genes. To effectively become resistant to a TFD, a bacterium would have to develop complementary mutations in both the transcription factor and its binding site.

Multiple challenges must be considered when developing antimicrobial TFDs. Firstly, there is inherent redundancy in bacterial regulatory networks which could affect TFD activity if the inhibition of the target transcription factor could be compensated by the activation of a second transcription factor. Another challenge is the identification of new transcription factors for TFD development that have a known phenotype and transcription factor binding motifs. Previously, the McArthur group has utilized a combined approach to identify candidates for TFD development. Proteomic studies have been performed to identify transcription factors that were induced in response to stress (data not shown). By inhibiting these transcription factors, it has led to the sensitization of the bacteria under certain

conditions. This approach is best used in organisms such as *E. coli* (129) or *P. aeruginosa* (130) as considerable work has been performed to understand the molecular function of regulatory factors and their respective bind domains in these species. Alternatively, candidates have been identified by reviewing the literature. Candidates identified this way typically have a known phenotype and transcription factor binding motif which allows for the quick development and testing of TFDs against these targets.

1.5 TFD DELIVERY AGENTS

The considerable challenge to oligonucleotide therapeutics is the delivery of high molecular weight, polyanionic TFD through the negatively charged bacterial envelope. The ideal transfection agent for TFDs should have three main properties: (1) the ability to efficiently bind TFDs; (2) the ability to selectively target bacteria without causing bacterial and cellular lysis; and (3) the ability to protect TFDs from degradation in biological fluids. Cationic cell-penetrating peptides can be used for nucleic acid delivery but this approach requires chemically modified nucleotides that are neutrally charged to prevent precipitation (131). This highlights the need for a delivery system that does not require the need for nucleotide modification.

An alternative to this approach is to use bola-amphiphilic lipids such as 12,12'-(dodecane-1,12-diyl)bis(9-amino-1,2,3,4tetrahydroacridinium) hereafter termed 12-bis-THA (132). It is a structural analogue of the antiseptic dequalinium and is comprised of two hydrophilic tetrahydroacridinium molecules containing a delocalized cationic charge that are connected by a lipophilic alkane linker (**Figure 1.5A**). 12-bis-THA spontaneously self-assembles in dilute aqueous solution to form unstable nanosized aggregates called 12-bis-THA particles. These particles rapidly bind TFDs (**Figure 1.5B**) through a combination of intercalation and electrostatic interactions to form loaded 12-bis-THA particles that are colloidally stable in dilute aqueous solution (**Figure 1.5C**). When loaded onto 12-bis-THA particles, TFDs are condensed and lose their β canonical structure which provides protection from enzymatic degradation in biological fluids (132).

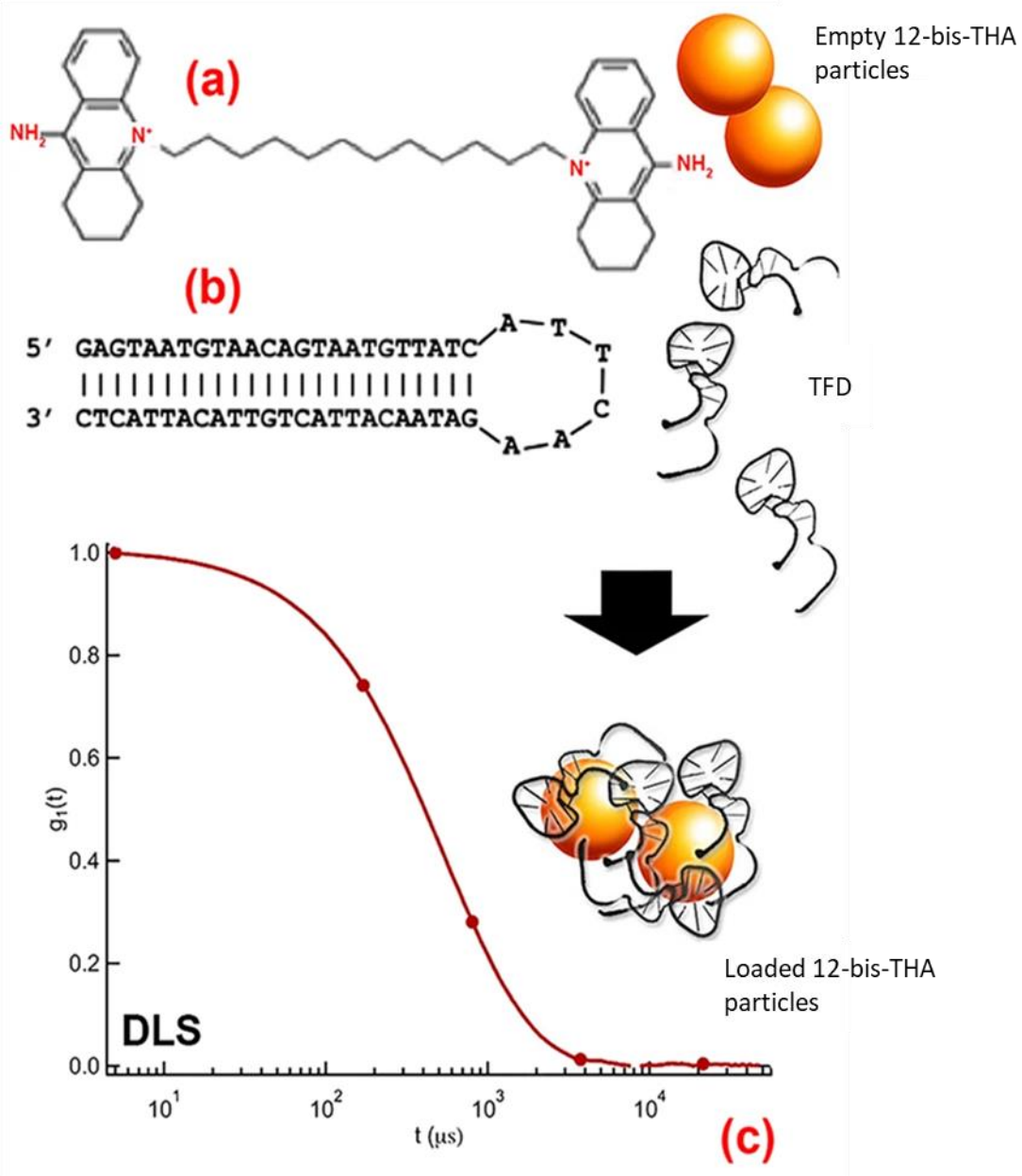

Figure 1.5: The formation of loaded 12-bis-THA particles. (**A**) shows the chemical structure of 12-bis-THA particles, a bola-amphiphilic molecule that forms unstable, nanosized aggregates in dilute aqueous solution. (**B**) TFDs used with 12-bis-THA particles are designed as hairpin. (**C**) When mixed, the 12-bis-THA particles bind and encapsulate the TFD, collapsing the DNA helix structure and forming stable, homogenous particles. Figure adapted from reference 132.

12-bis-THA particles can overcome the permeability barrier of the bacterial membrane and deliver TFD to a wide range of Gram-positive and Gram-negative bacterial species including those producing a polysaccharide capsule (132,133). The bacterial envelope is comprised of three main lipids: phosphatidylethanolamine, phosphatidylglycerol,

and cardiolipin (134). Phosphatidylethanolamine is zwitterionic and accounts for approximately 80% of the lipids in the *E. coli* membrane whereas cardiolipin and phosphatidylglycerol are anionic and account for approximately 15% and 8% respectively (135). Though these lipids are present in the membrane of *B. cenocepacia* their concentration is unknown (136). Biophysical studies showed that interactions between 12-bis-THA particles and cardiolipin drives TFD transfection in artificial membranes in the absence of ATP or protein machinery (132). Similar studies have shown that interactions with LPS drives TFD transfection under the same conditions (137). Further studies by Montis *et al* showed that 12-bis-THA particles interacted with LPS in two ways; through electrostatic interactions between the positively charged 12-bis-THA headgroup and the negatively charged phosphates on the GlcN-A of the lipid A, and through the integration of the alkane linker within the artificial membrane (137). The lipophilic interaction of the 12-bis-THA linker likely accounts for the formation of transient pores in artificial membranes which was observed by Di Blasio *et al* (138). This suggests that 12-bis-THA particles utilise both lipophilic and electrostatic interactions to release TFD into the bacterial cytoplasm.

As 12-bis-THA is derived from the antiseptic dequalinium, it has its own antimicrobial activity that is independent of the TFD component. It is well tolerated when delivered topically however demonstrates an unfavourable toxicity profile when delivered systemically (139). To counter this, alternative TFD delivery systems have been developed. Rhodamine is a fluorescent label that exploits proton motive force (PMF) to accumulate within the mitochondria of eukaryotic cells (140,141). In the context of drug delivery, Santos *et al* showed that rhodamine efficiently delivers active pDNA to the mitochondria of eukaryotic cells (142). The TFD-rhodamine conjugate was developed by attaching a rhodamine molecule to the 3' end of a synthetic, hairpin TFD. Studies by the McArthur group have shown that TFD-conjugates can transfect both Gram-positive and Gram-negative species including clinical isolates of *P. aeruginosa*.

Recently, this technology has been further developed using an approach described by Yuan *et al* (143). Cyclised DNA containing the transcription factor binding motif of a target transcription factor was amplified using rolling circle amplification. Doing so produces a large net of DNA strands containing the TFD sequences. Rhodamine derived, 5-Carboxytetramethylrhodamine (TAMRA) modified nucleotides were incorporated into the TFD nets which are then condensed through the addition of cationic magnesium pyrophosphate to form polymeric TFD particles. The resultant polyplexes have a hydrodynamic radius of approximately 100 nm and it is estimated that this will represent

many thousands of copies per particle. The MIC value is calculated based on the concentration of the DNA and the molecular weight of the cassette containing the double stranded TFBS used in the amplification procedure. Preliminary studies performed by Professor McArthur have shown that polymeric TFD particles can be engineered to induce bactericidal antimicrobial activity at nanomolar concentrations (data not shown). However, further studies are required to determine whether this platform is suitable for delivery against encapsulated Gram-negative species including *B. pseudomallei*.

1.6 PROJECT AIMS

Burkholderia species are clinically difficult to treat due to a combination of chromosomally encoded resistance mechanisms, low membrane permeability that limits antimicrobial penetration, and the propensity to form biofilms. This project aims to investigate if TFD technology is a suitable platform to counter *Burkholderia* infections by:

1. Investigating if 12-bis-THA particles can transfect capsulated and unencapsulated *Burkholderia* species
2. Investigating if 12-bis-THA particles can penetrate *B. thailandensis* biofilms
3. Identifying transcription factors for TFD development using a proteomic and literature review approach
4. Designing TFDs that inhibit the growth of *B. thailandensis*

CHAPTER 2 - MATERIALS AND METHODS

2.1 CULTURING BACTERIA

2.1.1 Culture media

All microbiology culture media was prepared using ultrapure water and autoclaved at 121°C for 20 minutes unless stated otherwise. All materials were purchased from Sigma-Aldrich unless stated otherwise.

- **Luria-Bertani (LB) (Miller)** – Tryptone (10 g/L), NaCl (10 g/L), Yeast Extract (5 g/L)
- **2X Cation-adjusted Mueller Hinton broth (2X CAMHB)** (Fisher Scientific) – Caesin acid hydrolysate (35 g/L), beef extract (6 g/L), starch (3 g/L), magnesium (25 mg/L), calcium (50 g/L)
- **Modified Vogel and Bonner's medium (MVBM)** (144) – MgSO4 (0.2 g/L), citric acid (2 g/L), $NaNH_4HPO_4$ (3.5 g/L), and K2HPO4 (10 g/L) were dissolved in order into 919 mL of ultrapure water and autoclaved at 121°C for 20 minutes. 1 mL of $CaCl_2$ (from a 36 g/100mL stock) and 80 mL of D-gluconate (25% w/v) that had been filter sterilised were added. The final pH was adjusted to 7.2.

2.1.2 Bacterial strains and growth conditions

The bacterial strains used in this thesis are listed in **Table 2.1.** *B. thailandensis* strain E264 and strain E555 were provided by the Defense Science and Technology Laboratory (DSTL), Porton Down. A *B. thailandensis* strain E555 that expressed red fluorescent protein (RFP) was provided by Professor Rick Titball from the University of Exeter.

Table 2.1: List of organisms and growth conditions used in this thesis.

Strain name	Growth Conditions	Medium
B. thailandensis strain E264	37 °C, aerobic, 200 rpm	LB (Miller) or CAMHB
B. thailandensis strain E555	37 °C, aerobic, 200 rpm	LB (Miller), MVBM or CAMHB
B. thailandensis strain E555 expressing RFP	37 °C, aerobic, 200 rpm	MVBM supplemented with 50 µg / mL chloramphenicol

Stocks of the *B. thailandensis* strains were prepared by growing cultures to mid-log phase (0.3 – 0.4 optical density 600 nm) and stored in 50% glycerol and at -80 °C. Cell densities were measured using a UV-Vis spectrophotometer (FLUOstar Omega Microplate Reader) at a wavelength of 600 nm.

2.2 PREPARATION OF ANTIMICROBIAL COMPOUNDS

2.2.1 Stocks of small-molecule antimicrobials.

Table 2.2 provides a list of the antimicrobial compounds used in this thesis including the solvent used, the final concentration of stock solutions and the supplier. All compounds except for 12-bis-THA were stored at -20 °C and were discarded after two freeze-thaw cycles.

Table 2.25: A list of antimicrobials used in this thesis.

Compound	Solvent	Stock concentration	Supplier
Meropenem	Ultrapure water	1 mg/mL	Alfa Aesar
Ceftazidime	1 X phosphate-buffered saline	1 mg/mL	Alfa Aesar
Co-trimoxazole (trimethoprim and sulfamethoxazole)	100% DMSO	10:50 mg/mL	Alfa Aesar
Doxycycline	Ultrapure water	1 mg/mL	Alfa Aesar
Ciprofloxacin	Ultrapure water	1 mg/mL	Alfa Aesar
Tobramycin	Ultrapure water	5 mg/mL	Sigma-Aldrich
Polymyxin B	Ultrapure water	5 mg/mL	Alfa Aesar

2.2.2 Preparation of hairpin and ssRNA TFDs

Hairpin and single-strand RNA TFDs were provided as lyophilised powders by Integrated DNA Technologies (IDT). TFDs were suspended in ultrapure water to a final concentration of 1 mg/mL before being separated into 10 µL aliquots and stored at -20 °C. TFDs in the hairpin format were heated to 95 °C for 30 seconds and were then left to anneal at room temperature for 1 h to allow for the TFD to fold.

The concentration of TFD oligonucleotides was confirmed using a Nanodrop 2000 (Thermo Scientific). The Nanodrop sampler was cleaned by transferring 2 µL of ultrapure water to the pedestal and closing the lid for 30 seconds. The pedestal was then wiped with a clean tissue and 2 µL of TFD was analysed using the nucleic acid option which measures absorbance at 260 nm. TFD quality was established by a 260/280 ratio of >1.7.

2.2.3 Polyacrylamide gel electrophoresis

Polyacrylamide gel electrophoresis (PAGE) was performed to investigate if TFDs had folded into the correct format. Firstly, 5X Tris-Borate-EDTA (TBE) was prepared by mixing tris base (5.4 g), boric acid (27.5 g), 0.5M Ethylenediaminetetraacetic acid – pH 8.0 (20 mL) in 1 L of ultrapure water. A 1X TBE working stock was prepared by transferring 20 mL of the 5X stock to 1 L of ultrapure water.

Next, 20% PAGE gels were prepared by using the recipe shown in **Table 2.3**. The gel solution was then added to the casting system and the comb was added. Gels were left at room temperature for 1 h to polymerise. Excess set gels were wrapped in a paper towel soaked in ultrapure water, then clingfilm, and stored at 4 °C.

Table 2.3: Recipe for 20% polyacrylamide gels

Gel%	40% Acrylamide (mL)	Ultrapure water (mL)	5x TBE (mL)	Ammonium persulfate (10% w/v) (µL)	TEMED (µL)
20	6	3.6	2.4	200	10

Gels were run using a Mini-ProTEAN Tetra Vertical Electrophoresis Cell (Biorad). An aliquot of 1 µg of TFD was mixed with SDS free 6X loading buffer (New England Biolabs) to a final volume of 10 µL which was loaded onto the gel. An aliquot of 4 µL of O'Range 5 base pair ladder (ThermoFisher) and low molecular weight ladder (New England Biolabs) were also added to wells of the 20% PAGE gel. Gels were run in 1X TBE buffer at 110V for 90 minutes. They were then stained in 1X TBE buffer containing 10 µg/mL of Sybr safe (Biorad). Gels were imaged using a ChemicDoc-It^2 UVP gel imaging station.

2.3 ANTIMICROBIAL SUSCEPTIBILITY TESTING

2.3.1 Preparation of TFD loaded 12-bis-THA particles

Nanoparticles were formed using the bola-amphiphilic lipid 12-bis-THA which had been synthesized by Concept Life Sciences limited. To form the nanoparticles, 12-bis-THA was dissolved in ultrapure water to a final concentration of 1 mg/mL. The solution was then vortex for 30 seconds and then sonicated in a water bath at 40°C until clear. 12-bis-THA particles were stored at 4°C for up to one week. To form loaded 12-bis-THA particles, 12-bis-THA particles were mixed in a 10:1 ratio with hairpin or ssRNA. This was performed by mixing 100 µg/mL of 12-bis-THA particles with 10 µL of TFD stock (1 mg/mL). The solution was then vortexed for 30 seconds resulting in the spontaneous formation of loaded 12-bis-THA particles. New batches of loaded 12-bis-THA particles before every experiment.

2.3.2 Dynamic light scattering

Empty and loaded 12-bis-THA particles were prepared as described in section 2.3.1. Additionally, combinations of antimicrobials and 12-bis-THA particles were analysed by diluting these compounds into ultrapure water to a final concentration of 300 µg/mL and 100 µg/mL, respectively. All compounds were vortexed for 30 seconds before analysis. Dynamic Light Scattering analysis (DLS) was carried out using a Malvern Zetasizer Nano. Samples were equilibrated for 120 seconds at 25°C before analysis. Particle measurements were generated by performing 3 independent runs consisting of 11 reads, and data was captured in backscatter mode. The size and polydispersity of samples were determined using distribution analysis. For size and polydispersity analysis, samples were contained in a semi-micro cuvette. Zeta-potential measurements were recorded with a Malvern Zetasizer Nano using laser doppler viscometry and phase analysis light scattering. For zeta-potential analysis, samples were contained in folded capillary cells.

2.3.3 Minimum inhibitory concentration testing

Compounds were tested to determine their Minimum Inhibitory Concentration (MIC) against *B. thailandensis* strains E264 and E555 using the broth microdilution method. Bacterial colonies were isolated from a streak plate and suspended in 1X PBS to a turbidity equivalent to a 0.5 McFarland standard. The bacterial suspension was then diluted 1:500 into 2X CAMHB and vortexed to break up bacterial aggregates. 100 µL of bacterial culture was transferred to the wells of a 96-well plate containing treatments. Treatments were prepared by serially diluting compounds 2-fold in sterile water in a 96-well plate to produce a final volume of 100 mL (total 200 µL for treatments and bacterial culture). Plates were incubated

at 37°C with agitation for 18 h and the MIC was defined as the concentration of a compound that inhibited the presence of visible growth.

2.3.4 Time Kill studies

An overnight culture was prepared by suspending a single bacterial colony from a streak plate into 1X CAMHB which was then incubated overnight at 37°C and 180 rpm. The bacterial culture was diluted to an optical density ($O.D_{600}$) of 1.0 in 1X PBS and then diluted 1:1000 (1 x 10^5 colony-forming units per millilitre (CFU/mL)) into prewarmed 1X CAMHB containing treatments. Bacterial cultures were then incubated for 24 h at 37°C and 200 rpm. To measure the antimicrobial activity of compounds against *B. thailandensis* strains E264 and E555, 20 µL aliquots were taken at 0, 3, 6 and 24 h and serially diluted 10-fold in 180 µL of 1X PBS. The bacterial inoculum was spot plated into LB agar and incubated at 37°C for 24 h before counting. Bactericidal activity was defined as a >3 log10 reduction in CFUs when compared to the starting inoculum. Antimicrobial synergy was determined using this method and was defined as a >2 log10 reduction in CFUs 24 h in an antimicrobial combination when compared to the most effective of the two monotherapies (145).

2.3.5 Growth kinetics

The growth kinetics of small and normal *B. thailandensis* colonies was analysed by isolating colonies with the tip of a p200 pipette and mixing them in 1X PBS to an optical density equivalent to a 0.5 McFarland standard. The bacterial suspension was diluted 1:500 into 1X CAMHB and vortexed for 30 seconds. An aliquot of 100 µL of the bacterial inoculum were then transferred to a 96-well plate. The edge of the plate was wrapped in parafilm to prevent the evaporation of wells. The plate was then placed into a spectrophotometer (FLUOstar Omega Microplate Reader) set at 37°C and the OD_{600} was recorded every 30 minutes for 16 h.

2.3.6 Checkerboard testing

Synergy testing using the checkerboard method was used to investigate interactions between 12-bis-THA particles and antimicrobials trimethoprim, co-trimoxazole, ceftazidime, meropenem, doxycycline, colistin, tobramycin and rifampicin.

The checkerboard assay was performed by diluting 12-bis-THA particles through the columns and antimicrobials through the rows of separate 96 well plates. The first column was filled with 200 µl of 12-bis-THA particles which was serially diluted 2-fold in distilled water and antimicrobials were diluted through the rows of a separate plate in the same fashion. An aliquot of 50 µl of each compound were transferred to the relevant well of a third plate. Row

H and column 12 contained a single compound to determine the MIC of the respective compound as shown in **Figure 2.1**. *B. thailandensis* colonies were suspended in PBS to a turbidity equivalent to 0.5 McFarland and then diluted 1:300 into (2X) LB broth. An aliquot of 100 µl of the bacterial inoculum were transferred to the wells of the checkerboard plate. The plates were then incubated for 16-18 h at 37 °C and 160 rpm.

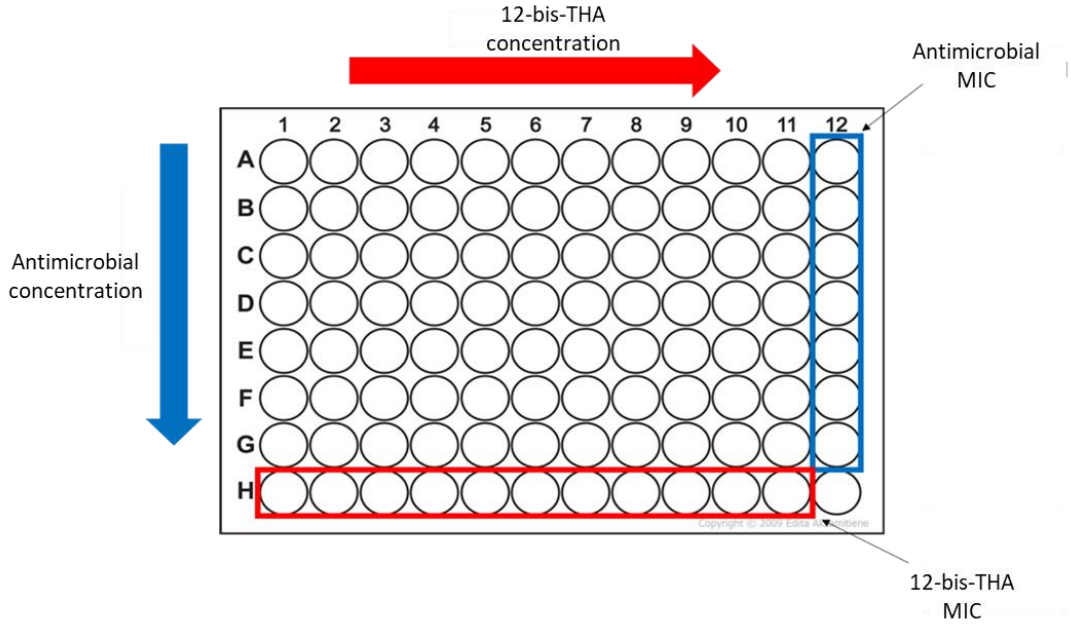

Figure 2.1: Cartoon schematic of a checkerboard plate to investigate interactions between antimicrobial compounds.

Drug interactions were evaluated by calculating fractional inhibitory concentration index (FICi) values of wells absent of growth along the turbid/non-turbid. FICi values are calculated by dividing the MIC of compounds in combination with the MIC of the compound alone (equation shown below). The FICi scores of both compounds are then added together to produce the ΣFICi value. ΣFICi scores of ≤ 0.5 are representative of drug synergy, while values between 0.5 – 1 indicate an additive or weakly synergistic effect. Scores between 1 – 4 demonstrate indifference while scores > 4 show drug antagonism.

$$\Sigma FICI = \frac{MIC_A \text{ in combination}}{MIC_A \text{ Alone}} + \frac{MIC_B \text{ in combination}}{MIC_B \text{ Alone}}$$

2.3.7 Confocal microscopy – planktonic studies

An overnight culture of either *B. thailandensis* strains E264 and E555 was diluted 2% v/v into 1X CAMHB and incubated at 37°C and 200 rpm. Bacterial cultures were grown to mid-log phase (0.3 – 0.5 OD_{600}) and then diluted by transferring 500 µL of bacteria into an Eppendorf tube containing either 500 µL of 12-bis-THA particles (100 µg/mL) or 500 µL of PBS. *B. thailandensis* which were then incubated with 12-bis-THA particles for either 30 or 90 minutes at 37 °C with agitation. Alternatively, mid-log cultures of *B. thailandensis* strain E555 were incubated with 50 µg/mL of 12-bis-THA particles loaded with 5 µg/mL Alexa-488 labelled TFD or 5 µg/mL of TAMRA-labelled polymeric TFD particles to investigate TFD transfection. Bacteria were stained for a further 30 minutes using the lipophilic dye FM4-64 FX (Thermo Fisher Scientific, UK) (1 mg/mL stock solution) by transferring 10 µL of dye.

Bacterial cultures were pelleted at 4000 x g for 5 minutes and resuspended in 100 µL of PBS. Poly-d-lysine slides (Fisher Scientific) were prepared by marking the boundaries using a PAP pen (ThermoFisher) to confine bacteria to a small area. 100 µL of bacteria were smeared onto the slide within the boundaries and left to incubate at room temperature in the dark for 30 minutes. Slides were gently rinsed with 1X PBS to remove the loosely attached bacteria and left to dry for 5 minutes at 37°C in the dark. Coverslips were mounted using Fluoromount aqueous mounting media before imaging. Slides were imaged using a Zeiss LSM800 confocal microscope (Zeiss). 12-bis-THA particles fluorescence was captured using the Hoechst H3258 emission filter at λ_{ex} 405 nm and λ_{em} 455nm and FM4-64 FX was captured at λ_{ex} 515 nm and λ_{em} 630 nm.

2.4 MULTI-OMIC ANALYSIS

2.4.1 Microbiological growth analysis

An overnight culture of *B. thailandensis* strain E555 was diluted to an OD_{600} of 0.05 into 100 mL of LB broth and grown at 37°C and 200 rpm for 16 h. When at an OD_{600} of 0.5, the culture was split into three 10 mL aliquots and challenged with ultrapure water (untreated), 0.1X MIC (0.8 µg/mL) or 1X MIC (8 µg/mL) of 12-bis-THA particles. These were incubated for 2.5 h following the challenge. Cultures were then centrifuged at 6000 XG and 4°C, and pellets were washed twice with 1X PBS. Following the final wash, the supernatant was discarded, and the pellet was stored at -80°C.

2.4.2 Protein extraction and quantification

Bacterial pellets were suspended in 500µL of lysis buffer (8M urea and 25 mM $NaHCO_3$) and sonicated at 4°C on the high setting of a Bioruptor plus sonicator for 10 cycles each lasting 30 seconds. The samples were then centrifuged at 16,100 x *g* for 40 min at room temperature. Following centrifugation, the supernatant was retained, and the pellet was discarded. Protein concentration was measured using the Pierce™ BCA Protein Assay Kit (Thermofisher). Liquid protein extracts were sent to the Bristol proteomics facility on ice for analysis using tandem mass tagging (TMT).

2.4.3 TMT Labelling and High pH reversed-phase chromatography*

Aliquots of 25µg of each sample were digested with trypsin (2.5µg trypsin per 100µg protein; 37°C, overnight), labelled with Tandem Mass Tag (TMT) ten plex reagents according to the manufacturer's protocol (Thermo Fisher Scientific) and the labelled samples pooled.

The pooled sample was evaporated to dryness, resuspended in 5% (v/v) formic acid, and then desalted using a SepPak cartridge according to the manufacturer's instructions (Waters, Milford, Massachusetts, USA). The eluate from the SepPak cartridge was again evaporated to dryness and resuspended in buffer A (20 mM ammonium hydroxide, pH 10) before fractionation by high pH reversed-phase chromatography using an Ultimate 3000 liquid chromatography system (Thermo Scientific). In brief, the sample was loaded onto an XBridge BEH C18 Column (130Å, 3.5 µm, 2.1 mm X 150 mm, Waters, UK) in buffer A and peptides eluted with an increasing gradient of buffer B (20 mM ammonium hydroxide in acetonitrile, pH 10) from 0-95% over 60 min. The resulting fractions were evaporated to dryness and resuspended in 1% (v/v) formic acid prior to analysis by nano-LC MSMS using an Orbitrap Fusion Lumos mass spectrometer (Thermo Scientific).

2.4.4 Nano-LC Mass Spectrometry *

High pH reversed phase fractions were further fractionated using an Ultimate 3000 nano-LC system in line with an Orbitrap Fusion Lumos mass spectrometer (Thermo Scientific). In brief, peptides in 1% (v/v) formic acid were injected onto an Acclaim PepMap C18 nano-trap column (Thermo Scientific). After washing with 0.5% (v/v) acetonitrile 0.1% (v/v) formic acid peptides were resolved on a 250 mm × 75 µm Acclaim PepMap C18 reverse phase analytical column (Thermo Scientific) over a 150 min organic gradient, using 7 gradient segments (1-6% solvent B over 1min., 6-15% B over 58min., 15-32%B over 58min., 32-40%B over 5min., 40-90%B over 1min., held at 90%B for 6min and then reduced to 1%B over 1min.) with a flow rate of 300 nl min−1. Solvent A was 0.1% formic acid and Solvent B was aqueous

80% acetonitrile in 0.1% formic acid. Peptides were ionized by nano-electrospray ionization at 2.0kV using a stainless steel emitter with an internal diameter of 30 µm (Thermo Scientific) and a capillary temperature of 275°C.

All spectra were acquired using an Orbitrap Fusion Lumos mass spectrometer controlled by Xcalibur 4.1 software (Thermo Scientific) and operated in data-dependent acquisition mode using an SPS-MS3 workflow. FTMS1 spectra were collected at a resolution of 120 000, with an automatic gain control (AGC) target of 200 000 and a max injection time of 50ms. Precursors were filtered with an intensity threshold of 5000, according to charge state (to include charge states 2-7) and with monoisotopic peak determination set to Peptide. Previously interrogated precursors were excluded using a dynamic window (60s +/-10ppm). The MS2 precursors were isolated with a quadrupole isolation window of 0.7m/z. ITMS2 spectra were collected with an AGC target of 10 000, maximum injection time of 70ms and CID collision energy of 35%.

For FTMS3 analysis, the Orbitrap was operated at 50 000 resolution with an AGC target of 50 000 and a maximum injection time of 105ms. Precursors were fragmented by high-energy collision dissociation (HCD) at a normalised collision energy of 60% to ensure maximal TMT reporter ion yield. Synchronous Precursor Selection (SPS) was enabled to include up to 5 MS2 fragment ions in the FTMS3 scan.

2.4.5 Data Analysis

The raw data files were processed and quantified using Proteome Discoverer software v2.1 (Thermo Scientific) and searched against the UniProt *B. thailandensis* strain E264 database (downloaded August 2019: 5565 entries) using the SEQUEST algorithm. Peptide precursor mass tolerance was set at 10ppm, and MS/MS tolerance was set at 0.6Da. Search criteria included oxidation of methionine (+15.9949) as a variable modification and carbamidomethylation of cysteine (+57.0214) and the addition of the TMT mass tag (+229.163) to peptide N-termini and lysine as fixed modifications. Searches were performed with full tryptic digestion and a maximum of 2 missed cleavages were allowed. The reverse database search option was enabled, and all data was filtered to satisfy a false discovery rate (FDR) of 5%.

Data handling and analysis were performed using Perseus (146). Reverse hits and contaminants were removed, and missing values were imputed before performing statistical analysis. The intensity data were transformed to Log_2 and filtered to contain at least three values. Statistical significance was determined by performing Students' *t*-tests with a

Bonferroni post hoc test to correct for multiple hypothesis testing. Volcano plots were produced using the statistical parameters false detection rate (FDR) of 0.01 and an S0 value of 1.

2.4.6 Metabolite extractions

The metabolome of *B. thailandensis* pellets retained from the growth curve assay (**2.4.1**) was extracted as described by Moreira *et al* (147). Briefly, glass beads were added to the bacterial pellet that was resuspended in 600 µL of 80 °C ethanol (75% v/v). Samples were vortexed for 30 s and then incubated at 80 °C for 3 min. The samples were vortexed again for 30 s. The supernatant was collected by centrifugation at 10000 x *g* at -10 °C for 10 min. This process was repeated once. The supernatant was dried under a vacuum using a Savant SC210A SpeedVac Concentrator and the extracts were stored at -20 °C until analysis.

2.4.7 Metabolome analysis

The extracts were prepared by dissolving pellets in 0.6 ml NMR buffer (100 mL D_2O containing 0.26 g NaH_2PO_4, 1.41 g K_2HPO_4, and 1 mM deuterated trimethyl silylpropionate (TSP) as a reference compound). The spectra were recorded using Bruker Avance NEO 600 MHz NMR spectrometer equipped with a TCI CryoProbe. The data were collected at 25 °C using TSP as a reference compound and processed using the TopSpin version 3.2 software package. The metabolites were quantified using the software Chenomx NMR Suite 7.0.

2.4.8 Statistical analysis

GraphPad Prism 5.0 was used for the statistical analysis of bacterial growth curves and metabolite concentration. For the statistical comparison of three groups, a two-way ANOVA followed by a Bonferroni test was used. Probability (p) values were considered significant when below 0.05 (*), 0.01 (**) or 0.001 (***). Sample sizes (n) are representative of the number of independent experiments performed.

* Methods marked with a star (*) were provided by Dr Kate Heesom at Bristol Proteomic Facility.

2.4.9 Identification of transcription factor homologues

Regulatory factors were identified in the proteomic database provided Dr Kate Heesom by performing a keyword search to identify proteins with the following annotations: transcription, factor, transcription factor, two-component, DNA-binding, regulatory, regulator, and sensory kinase. Proteins fulfilling the criteria were then transferred to a new Excel document which was processed using Perseus as described in section 2.4.5. The amino

acid sequences of proteins of interest were taken from the *Burkholderia* genome browser (148). Homology searches were performed using BlastP to investigate homologues of *B. thailandensis* regulatory factors in *P. aeruginosa, Acinetobacter baumannii, E. coli* and *Salmonella typhi.*

2.4.10 PRODORIC

Prodoric virtual footprint version 1.0 was used to interrogate the promoter region of genes in *B. thailandensis* to identify possible transcription factor binding sequences based on binding motifs characterised in other bacteria species (120,149). To do so, the 500 base pair nucleotide sequence upstream of the genes of interest were taken from the *Burkholderia* genome browser. These sequences were then compared to a repository of characterised transcription factor binding sequences (TFBS) from a variety of transcription factor families and bacteria. Potential TFBS that had been identified in the *Burkholderia* sequences were allocated a position weight matrix score based on its similarity to the characterised binding sequence. Higher scores indicated greater similarity.

2.5 BIOFILM TESTING

2.5.1 Establishing biofilm growth conditions

An overnight culture of *B. thailandensis* strain E555 was prepared by suspending a single bacterial colony into CAMHB and incubating at 37°C with shaking at 180 rpm for 18 h. This was then diluted to an optical density of 0.11 OD_{600} in MVBM, LB, or CAMHB. 150 µL of all cultures were transferred to separate wells within a Calgary biofilm device, in which pegs extend from the lid into each well. This was incubated at 37°C with shaking at 120 rpm for 72 h. At 24, 48 and 72 h, pegs were broken off the lid with angled needle-nosed pliers and placed into wells containing 200 µL of PBS. The plate was gently agitated by hand for 30 seconds to remove loosely attached cells before bacterial colony counting or biomass quantification with crystal violet was performed.

For colony counting, the pegs were placed into a 1.5 mL Eppendorf tube containing 200 µL of PBS which was vortexed for 30 seconds to detach the biofilm. 20 µL of PBS was serially diluted 10-fold in PBS and the bacterial density was enumerated by spot plating 20 µL of each dilution onto LB agar. LB plates were incubated at 37°C for 24 h before counting.

Biofilm biomass was measured with crystal violet (Arcos Organics) using a method adapted from O'Toole (150). Rinsed pegs were removed from PBS and fixed for 15 minutes in a well containing 200 µL methanol. The pegs were then transferred to an empty well

and dried for 30 minutes at 37 °C to evaporate any excess methanol. The pegs were then transferred to a 96-well plate with each well containing 200 µL of 2% (w/v) crystal violet solution and incubated for 5 minutes at room temperature without agitation. Pegs were rinsed three times in clean PBS to remove the excess stain before drying at 37 °C for 30 minutes. Crystal violet was solubilised by transferring the biofilms to a 96-well plate containing 200 µL of 100% methanol for 10 minutes at room temperature under gentle agitation. Absorbance was recorded at 595 nm using a FLUOstar Omega Microplate Reader.

2.5.2 Minimum Biofilm Eradication Concentration (MBEC) and Planktonic Minimum Inhibitory Concentration testing (pMIC)

An overnight culture of *B. thailandensis* strain E555 was prepared by inoculating CAMHB with a single bacterial colony and incubating at 37°C with shaking at 180 rpm for 18 h. This was diluted to an optical density of 0.11 OD_{600} in MVBM. Biofilms were grown by transferring 150 µL of bacterial culture to the wells of a Calgary biofilm device which was incubated at 37°C with shaking at 120 rpm for 24 h.

Following this, lids of the Calgary biofilm device were transferred to a 96 well plate containing 200 µL of PBS to remove loosely attached cells from the pegs. Once rinsed, the lids were transferred to a treatment plate containing the test compounds. These were made in a similar manner to a broth microdilution MIC plate. Antimicrobials, 12-bis-THA particles, and synergy combinations were diluted 2-fold in MVBM through the columns of a 96-well plate to a final volume of 200 µL. Lids were then incubated at 37°C with shaking at 120 rpm for 24 h. Following this, biofilm biomass was measured as described in above.

The planktonic MIC (pMIC) is the minimum inhibitory concentration of antimicrobials, 12-bis-THA particles, and synergy combinations that prevented biofilm shedding. The pMIC was determined by recording planktonic growth following the incubation of the biofilms with the treatments and was defined as media that displayed an optical density of <0.1 OD_{600}. Absorbance was recorded at 600 nm using a FLUOstar Omega Microplate Reader.

2.5.3 Minimum biofilm inhibitory concentration (MBIC)

An overnight night culture of *B. thailandensis* strain E555 was prepared by suspending a bacterial colony in CAMHB which was then incubated at 37°C with shaking at 180 rpm for 18 h. The culture was then diluted into PBS to a turbidity equivalent to a

0.5 McFarland standard. This was then diluted 1:1000 into MVBM media and vortexed. 100 µL of the bacterial culture was transferred to the wells of the treatment plate.

The treatment plate was prepared in a similar manner to the MIC plates described in section 2.3.3 however compounds were serially diluted 2-fold in MVBM instead of ultrapure water. After the bacterial culture had been added to the treatment plate, the Calgary biofilm device lid was then placed onto the plate. This was then incubated at 37°C with shaking at 120 rpm for 16 h. The biofilm biomass was then quantified using crystal violet staining described in section 2.5.1.

2.5.4 Confocal microscopy - biofilm studies

An overnight culture of *B. thailandensis* E555 strain expressing red fluorescent protein (RFP) was prepared by inoculating CAMHB broth containing 50 µg/mL of chloramphenicol with a single bacterial colony and incubating at 37°C with shaking at 180 rpm for 18 h. 1 mL of this culture was transferred to 9 mL of MVBM containing 50 µg/mL of chloramphenicol and grown for a further 24 h at 37°C with shaking at 180 rpm. 1 mL of culture was then transferred to a 50 mL Falcon tube containing 13 mL of MVBM supplemented with 50 µg/mL of chloramphenicol and a microscope slide coated with poly-D-lysine (ThermoFisher). The culture was gently mixed by pipetting up and down and then incubated statically at 37°C for 72 h.

Following incubation, the bacterial growth on the neutrally charged side of the microscopy slide was removed with a Kleenex tissue soaked in 100% Chemgene. The slides were then gently rinsed with PBS and transferred to a 50 mL Falcon tube containing 14 mL of MVBM supplemented with 50 µg/mL chloramphenicol. Subsequently, the following agents were added to the broth to achieve the following concentrations: 50 µg/mL of 12-bis-THA particles, 50 µg/mL of 12-bis-THA particles loaded with 5 µg/mL of Alexa-488 Fur hairpin TFD, 5 µg/mL of rhodamine green-Fur hairpin TFD conjugate, or a no treatment control. These were incubated with the biofilms for 15, 30, or 60 minutes. Before imaging, the slides were rinsed with PBS to remove loosely attached matter and stored at 37°C for 5 minutes. Coverslips were attached using Fluoromount (Sigma-Aldrich) and the slides were imaged using a Zeiss LSM 800 confocal microscope. **Table 2.4** shows the settings used to visualise and record images of the slide. For biofilms incubated with either empty 12-bis-THA particles or those loaded with TFD, the assay was repeated three times and five fields of view were record. The assay was repeated once for biofilms incubated with the TFD conjugate and five fields of view were recorded.

Table 2.4.: Setting used to record images of *B. thailandensis* strain E555 biofilms incubated with 12-bis-THA particles, 12-bis-THA particles loaded with Alexa-488 labelled Fur TFD, or Rhodamine labelled TFD. Images were recorded using a Zeiss LSM800 confocal microscope

Component	Laser (nm)	Laser intensity (%)	Gain	Pinhole (nm)
B. thailandensis E555 RFP	561	1.5	700	65
Alexa-488 labelled TFD	488	1.5	650	50
Rhodamine labelled TFD	488	1	650	65
12-bis-THA particles	405	3	75	750

CHAPTER 3 - THE ANTIMICROBIAL PROPERTIES OF 12-BIS-THA PARTICLES AGAINST *B. THAILANDENSIS*

3.1 INTRODUCTION

Penicillin was discovered in 1928 by Alexander Fleming. By 1940, before its clinical implementation (151), a bacterial penicillinase had been identified (152). During his Nobel Prize speech, Fleming acknowledged the ease with which antimicrobial resistance (AMR) could develop stating that "It is not difficult to make microbes resistant to penicillin in the laboratory by exposing them to concentrations not sufficient to kill them, and the same thing has occasionally happened in the body" (153). Today AMR is a global threat as there are emerging resistance mechanisms to even last-line antimicrobials (154–156). The loss of effective antimicrobials and the scarcity of novel antimicrobials in the pipeline may render common infections potentially life-threatening and compromise our ability to deliver modern medicine. Current predictions by the Centre for Disease Control (CDC) estimate that AMR contributes to two million infections and 23,000 mortalities annually within the United States (157). Furthermore, the O'Neill report states that failure to address the lack of effective treatment strategies for resistant infections could result in ten million deaths a year by 2050 (**Figure 3.1**) (158).

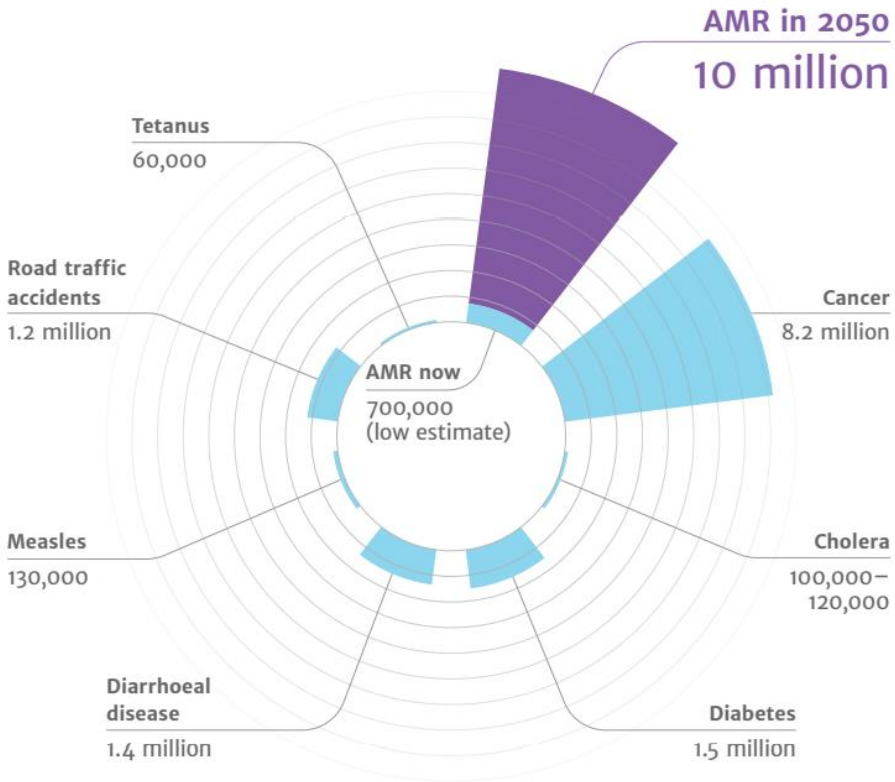

Figure 3.1: Deaths caused by antimicrobial resistance. Figure taken from the "Antimicrobial Resistance: Tackling a crisis for the health and wealth of nations", The Review on Antimicrobial Resistance Chaired by Jim O'Neill, December 2014 (158).

The paucity of antimicrobials in the pipeline escalates the impact of AMR. In 2004, only 1.6% of drugs in development by large pharmaceutical companies were antimicrobials primarily due to lower economic return (159). Potent antimicrobials such as carbapenems are used sparingly, which sends the message that new treatments will be administered infrequently leading to lower financial return. Secondly, antimicrobial regimes are often cheap, brief and curative and as such are less attractive financially than therapies to treat chronic disorders. The development of resistance to novel antimicrobials may also influence the financial return if the therapeutic is rendered rapidly ineffective. Financial incentives offered by governments have been put forward to generate momentum and accelerate the development of novel antimicrobials (160,161). As of 2019, there were only 40 molecules in phases I to III of the development pipelines with 18 demonstrating activity against ESKAPE pathogens (*Enterococcus faecium, Staphylococcus aureus, Klebsiella pneumoniae, A. baumannii, P. aeruginosa,* and *Enterobacter* species) (162).

There is a clear need to identify new therapeutic approaches to compliment traditional small molecule and natural product-based discovery. One approach is to use antimicrobial combinations that act synergistically. Antimicrobial synergy occurs when the combined activity of two or more compounds is greater than the individual activity, and this can happen in several ways. Synergism may occur when antimicrobials target the same pathway target but at different steps such as trimethoprim and sulfamethoxazole (163). Alternatively, synergy occurs when one compound enhances the uptake of a second compound. For example, tobramycin is a positively charged aminoglycoside that binds to negatively charged components of the bacterial membrane. By doing so, it permeabilises the bacterial membrane of *P. aeruginosa* resulting in the improved activity of carbapenem antimicrobials (164). Thirdly, antimicrobial synergy occurs when one compound inhibits the resistance mechanism for a second compound (165). For example, therapeutic regimes such as piperacillin/tazobactam or co-amoxiclav are comprised of a β-lactamase inhibitor (tazobactam and clavulanic acid) that restore the activity of β-lactam antimicrobials (piperacillin and amoxicillin) in drug-resistant strains (166).

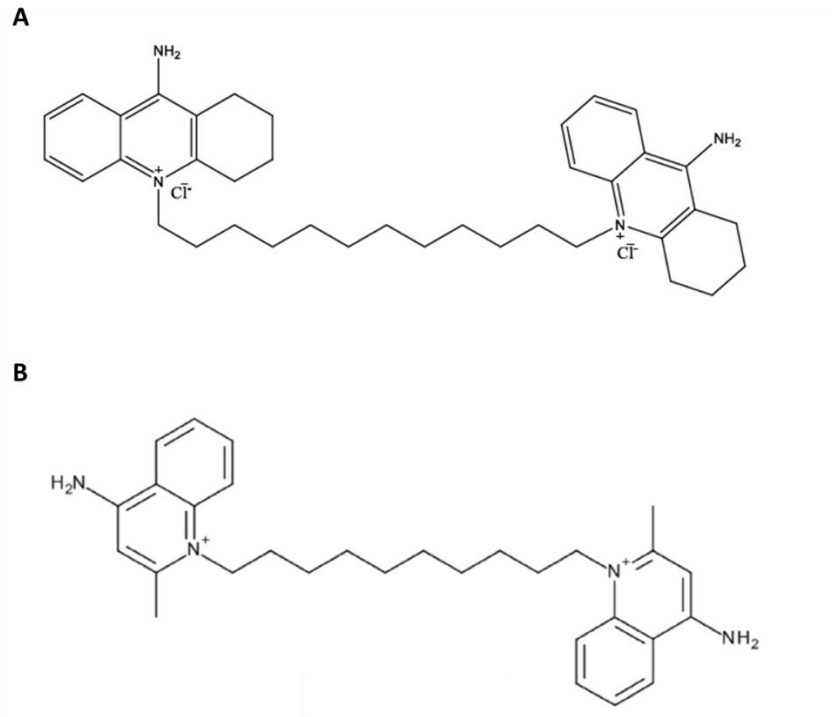

Figure 3.2: The chemical structures of (A) 12-bis-THA and (B) Dequalinium.

Dequalinium chloride is the parental molecule of 12-bis-THA, the compound studied in this thesis. Previous studies by the McArthur group have shown that 12-bis-THA particles are endowed with antimicrobial activity against Gram-positive and Gram-negative species (data not shown) and show potential for synergistic interactions. Studies by Di Blasio *et al* demonstrated that 12-bis-THA particles synergised colistin and tobramycin against multidrug-resistant *P. aeruginosa* (138). It is unclear whether this was due to membrane activity of the 12-bis-THA particles enhancing uptake or whether different steps of targeted pathways were being inhibited. Given the challenges of *B. pseudomallei* treatment due to chromosomally encoded resistance mechanisms (167) we investigated whether 12-bis-THA particles could synergize in combination with clinically-relevant antimicrobials such as meropenem, ceftazidime and co-trimoxazole. In this chapter we aim to:

- Investigate the antimicrobial activity of 12-bis-THA particles against capsulated and unencapsulated strains of *B. thailandensis*
- Investigate interactions between 12-bis-THA particles and extant antimicrobials against *B. thailandensis* to identify synergist combinations

3.2 RESULTS

3.2.1 Biological activity of 12-bis-THA particles against encapsulated and unencapsulated *B. thailandensis* strains

To investigate the antimicrobial activity of 12-bis-THA particles, the MIC was determined along with a panel of antimicrobials against *B. thailandensis* E264 (unencapsulated) and *B. thailandensis* E555 (encapsulated). No differences were observed for meropenem, ceftazidime, co-trimoxazole, doxycycline, ciprofloxacin, and 12-bis-THA particles when comparing the MIC values for strains E264 and E555 (**Table 3.1**). A 4-fold increase in the MIC of tobramycin was observed in E555 compared to E264 suggesting the capsule may affect its antimicrobial activity. No MIC was determined for polymyxin B in either strain which is consistent with the literature (168).

Table 3.1: The MIC of 12-bis-THA particles and a panel of antimicrobials against *B. thailandensis* strains E264 and E555. MIC assays were performed in CAMHB and data are representative of a minimum of 3 independent experiments.

Compound	***B. thailandensis* E264 (µg/mL)**	***B. thailandensis* E555 (µg/mL)**
12-bis-THA particles	2-8	2-8
Meropenem	0.25-1	0.5-1
Ceftazidime	1-2	1-2
Co-trimoxazole	2	2-4
Doxycycline	1	1
Ciprofloxacin	1	2
Tobramycin	32-64	128-256
Polymyxin B	>1024	>1024

3.2.2 Killing kinetics of 12-bis-THA particles against *B. thailandensis*

Time-kill assays were performed to investigate if the antimicrobial activity of 12-bis-THA particles were bacteriostatic or bactericidal against both *B. thailandensis* strains. Bactericidal antimicrobials are generally preferable for clinical use, as bacteriostatic antimicrobials are reliant on the immune system of the host to clear the infection. The time-kill data shows that 12-bis-THA particles were bactericidal against E264 at 4 and 8 µg/mL but bacteriostatic against strain E555 at all concentrations. This suggests that the presence of the polysaccharide capsule may provide protection against the antimicrobial activity of 12-bis-THA particles at MIC concentrations (**Figure 3.3**).

12-bis-THA particles reduced the bacterial load of E264 in a concentration-dependent manner at 3 and 6 h (**Figure 3.3**). Those cultures challenged with 2 µg/mL were reduced by 1.86 and 1.32 $\log_{10}$ CFU/mL at 3 and 6 h whereas those challenged with 4 µg/mL were reduced by 2.87 $\log_{10}$ CFU/mL at 3 h and consistently reduced below the limit of detection (10^2 CFU/mL) by 6 h. Cultures challenged with 8 µg/mL of 12-bis-THA particles were reduced below the limit of detection of the assay at both 3 and 6 h. At 24 h, all cultures had regrown with those challenged with 2 µg/mL and 4 µg/mL of 12-bis-THA particles surpassing the starting inoculum by 2.21 and 1.68 $\log_{10}$ CFU/mL, respectively. Cultures challenged with 8 µg/mL exhibited regrowth but remained 0.58 $\log_{10}$ below the starting inoculum.

Unlike the activity demonstrated against strain E264, the antimicrobial activity of 12-bis-THA particles occurs in a time-dependent manner (**Figure 3.3**). Strain E555 was less sensitive to 12-bis-THA particles following 3 h of exposure irrespective of the concentration as bacterial densities were reduced by only 0.24, 0.26, and 0.39 $\log_{10}$ CFU/mL at 2, 4, and 8 µg/mL respectively. Bacterial killing increased at 6 h as bacterial cultures were reduced 1.32, 2.33, and 2.00 $\log_{10}$ CFU/mL at 2, 4, and 8 µg/mL, respectively. 24 h after treatment, E555 challenged with 2 and 4 µg/mL regrew and surpassed the starting inoculum by 3.17 and 1.67 $\log_{10}$ CFU/mL, respectively. Cultures challenged with 8 µg/mL remained below the starting inoculum by 0.98 $\log_{10}$ CFU/mL.

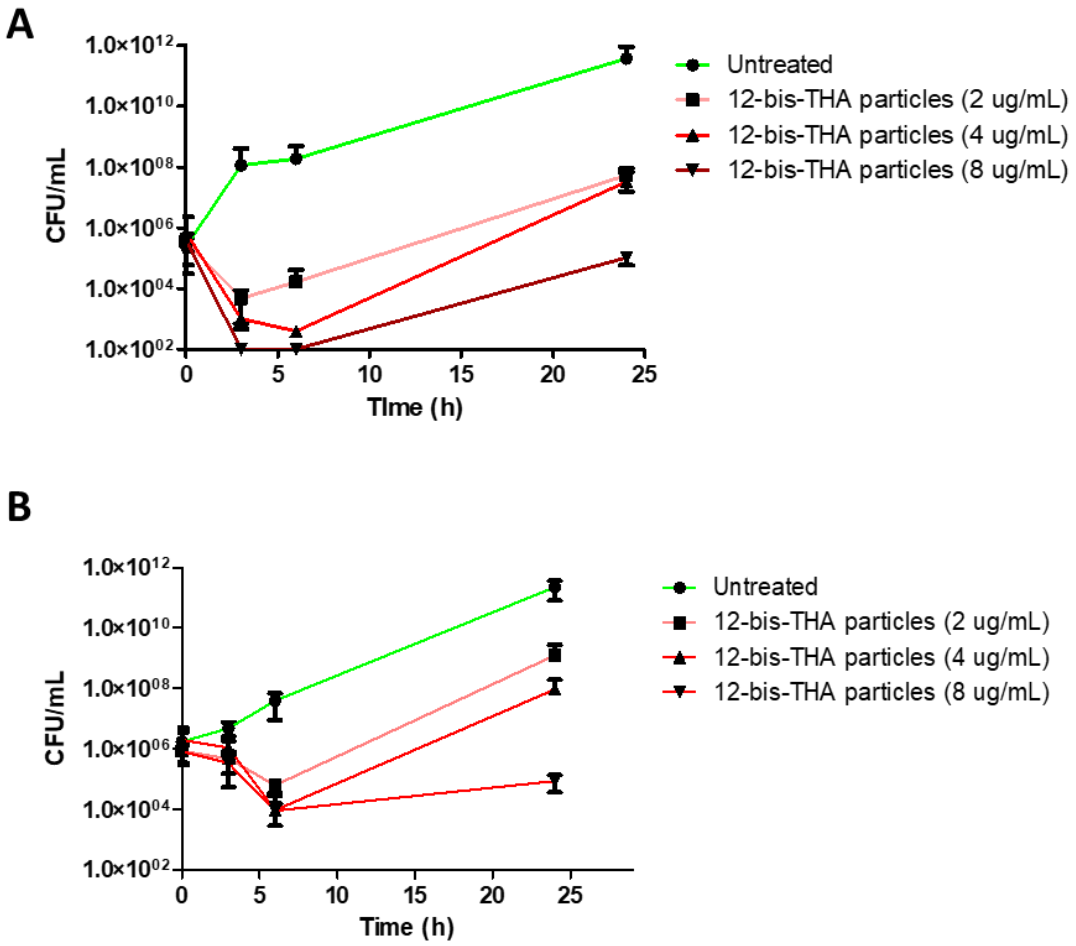

Figure 3.3: Time-kill assay showing the antimicrobial activity of 12-bis-THA particles at MIC concentration against (A) unencapsulated *B. thailandensis* strain E264 and (B) capsulated *B. thailandensis* strain E555. Data are representative of 3 independent experiments each consisting of 3 technical replicates.

3.2.3 Evidence for adaptive resistance to 12-bis-THA particles

The growth of both small and normal sized colonies was observed in both strains of *B. thailandensis* following exposure to 12-bis-THA particles (**Figure 3.4**). This phenomenon was more common for strain E264 and was not influenced by the length of exposure or 12-bis-THA particle concentration. The emergence of small colonies in addition to bacterial regrowth at 24 h following treatment might suggest that 12-bis-THA particles may induce the development of heteroresistant subpopulations in *B. thailandensis*.

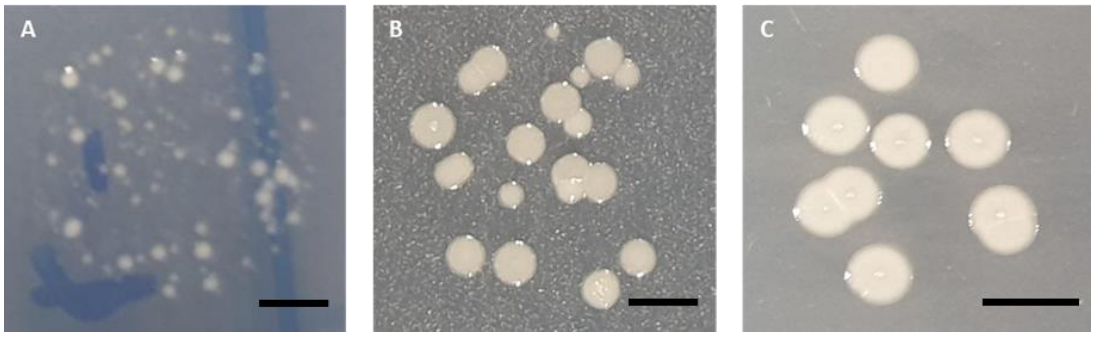

Figure 3.4: Morphological changes in *B. thailandensis* strain E264 following exposure to 4 µg/mL of 12-bis-THA particle for 6 h. **A** and **B** shows treated colonies grown on LB agar for 24 and 48 h, respectively. **C** shows the morphology of untreated E264 colonies grown for 48 h. Images representative of observations from 3 independent replicates. Scale bar shows 5 mm

The growth kinetics of small and normal sized E264 colonies, and untreated bacteria were studied to investigate if there was a change in growth rate following exposure to 12-bis-THA particles. However, the data shows no difference in the growth kinetics of all colonies (**Figure 3.5**).

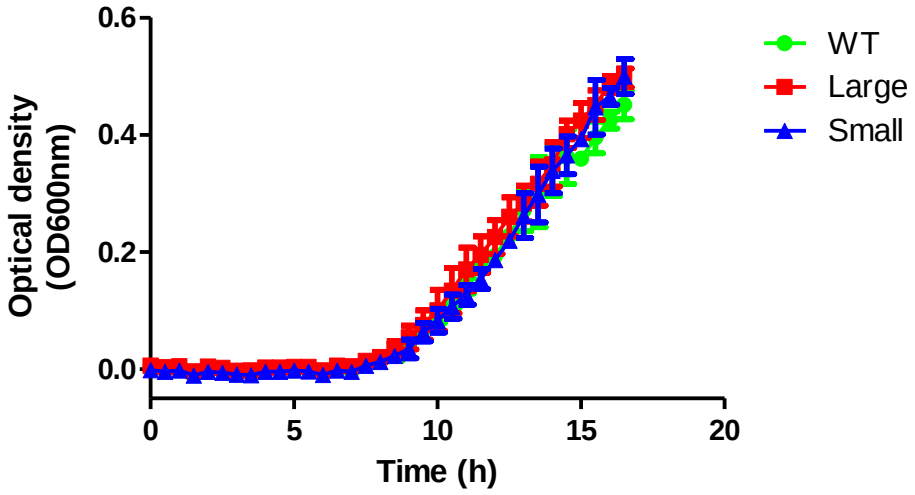

Figure 3.5: Growth kinetics of small, normal and untreated (WT) *B. thailandensis* strain E264 colonies in cation-adjusted Muller Hinton broth. Data are representative of 2 independent replicates consisting of 4 technical replicates

In some bacteria, small colony variants (SCVs) are typified by their reduced susceptibility to antimicrobials. A comparison of a *B. pseudomallei* SCV with its clonal parent strain showed the SCV was less susceptible to clinically relevant antimicrobials ceftazidime, meropenem and co-trimoxazole (169). MICs were determined for these different colony forms to investigate they had a change in susceptibility to 12-bis-THA particles following previous exposure. No difference in the MIC of 12-bis-THA particles was observed between normal, small and untreated colonies suggesting that these are not a resistant sub-population of *B. thailandensis* cells (**Table 3.2**).

Table 3.2: The MIC of 12-bis-THA particles against small, normal, and untreated *B. thailandensis* strain E264 colonies. Data are representative of 3 independent replicates consisting of 2 technical replicates.

E264 colony morphology	12-bis-THA particles (μg/mL)
Untreated	2
Treated (Small colony)	2
Treated (Normal colony)	2

3.2.4 Evidence for transfection

Confocal Laser Scanning Microscopy (CLSM) was performed to investigate if 12-bis-THA particles interacted with the bacterial membrane and to investigate if transfection was influenced by the polysaccharide capsule in *B. thailandensis* strain E555. In the first set of experiments, both strains were grown to an OD_{600} of approximately 0.3 and incubated with 50 μg/mL of 12-bis-THA particles for 120 minutes. The bacterial membrane of both strains was labelled with FM4-64 FX (**Figure 3.6A-C** and **G-I**), a cationic, lipophilic molecule that becomes embedded within the plasma membrane (170). Strain E555 was observed to self-associate into large clumps whereas strain E264 did not (**Figure 3.6A** and **G**). This likely occurs due to the presence of a polysaccharide capsule which can cause cellular adhesion in bacterial species (171). CLSM images shows that 12-bis-THA particles bind to the bacteria and associate with, or within the cell wall, and likely accumulates within the cytoplasm of both strains. This suggests that the presence of the polysaccharide capsule did not affect the ability of 12-bis-THA particles to penetrate bacteria (**Figure 3.6EF** and **KL**).

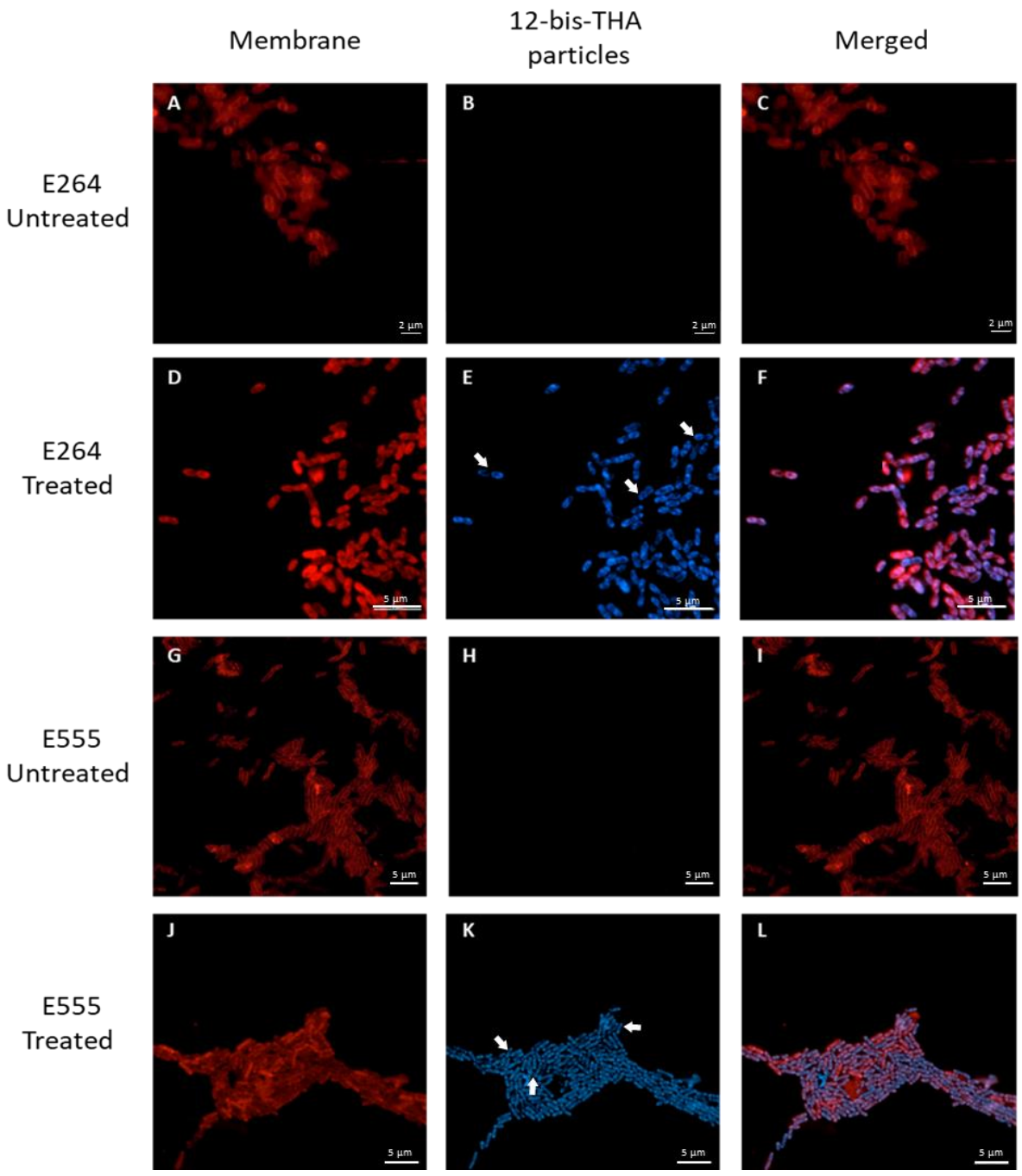

Figure 3.6: CLSM images of (A-F) *B. thailandensis* strain E264 and (G-L) strain E555 stained with FM4-64 FX (red) and challenged with 50 µg /mL 12-bis-THA particles (blue) for 120 minutes. (A-C and G-I) The untreated controls show that no autofluorescence was detected with the laser settings used. (**D-F** and **J-L**) Images show that 12-bis-THA particles transfected both unencapsulated (**D-F**) and encapsulated (**J-L**) *B. thailandensis* strains under the tested conditions. 12-bis-THA particle fluorescence was capture in the blue channel using the Hoechst filter (laser settings (λ_{ex} 405 nm/λ_{em} 455nm). The bacterial membrane was captured in the red channel using the FM4-64 FX filter (laser settings (λ_{ex} 515 nm/λ_{em} 630nm). Scales bars are representative of 5 µm except for **ABC** which shows 2 µm. Images were captured using Zen LSM 800 confocal microscope and uniformly edited to increase brightness using Zen software and Microsoft PowerPoint.The assay is represetantive of three independent replicates each consisting of at least five fields of view.

In order to assess the effect of the capsule on the timing of the penetration of 12-bis-THA particle a set of images were captured by CLSM at an earlier timepoint of 30 minutes. The CLSM images show the 12-bis-THA particles rapidly become associated with the bacterial membrane of both strains and preferentially accumulate at the poles and septum of the bacteria (**Figure 3.7EF** and **KL**). Similar observations were made by Di Blasio and Mason with data showing that 12-bis-THA particles accumulated at the poles of *P. aeruginosa* during the early phase of transfection (138). These regions are enriched with cardiolipin which is known to interact with 12-bis-THA particles and to drive the transfection and delivery of TFD cargo (172). Additionally, the binding of membrane components by 12-bis-THA particles may also explain why the resolution of FM4-64 FX diminishes upon exposure to 12-bis-THA particles as both are cationic, lipophilic molecules that interact with the bacterial plasma membrane (170).

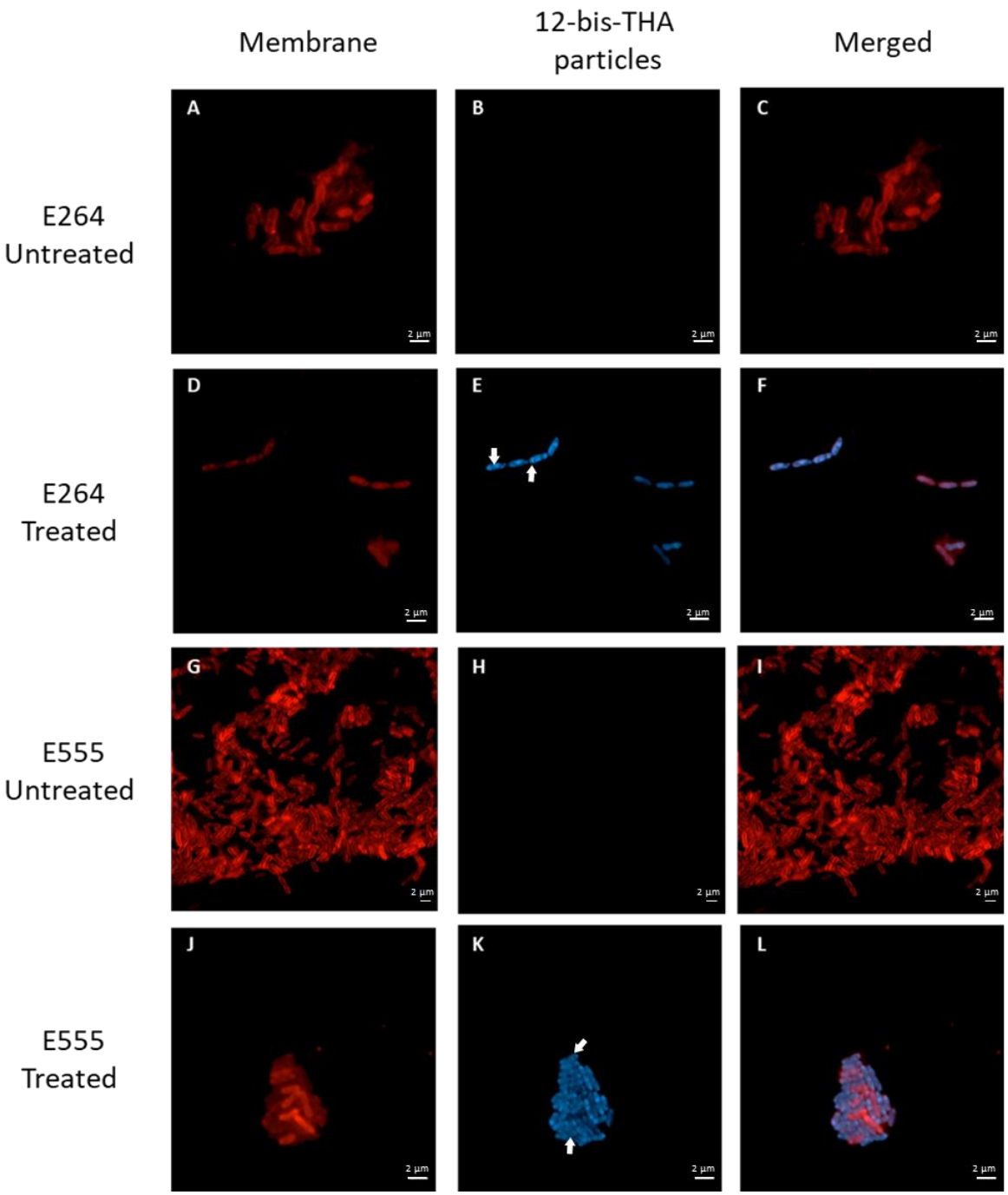

Figure 3.7: CLSM images of (A-F) *B. thailandensis* strain E264 and (G-L) strain E555 stained with FM4-64 FX (red) and challenged with 50 µg /mL CM2 particles (blue) for 30 minutes. (A-C and G-I) The untreated controls show that no autofluorescence was detected with the laser settings used. (**D-F** and **J-L**) Images show that 12-bis-THA particles transfected both unencapsulated (**D-F**) and encapsulated (**J-L**) *B. thailandensis* strains under the tested conditions. 12-bis-THA particle fluorescence was capture in the blue channel using the Hoechst filter (laser settings (λ_{ex} 405 nm/λ_{em} 455nm). The bacterial membrane was captured in the red channel using the FM4-64 FX filter (laser settings (λ_{ex} 515 nm/λ_{em} 630nm). Scales bars are representative of 5 µm. Images were captured using Zen LSM 800 confocal microscope and uniformly edited to increase brightness using Zen software and Microsoft PowerPoint. The assay is represetantive of three independent replicates each consisting of at least five fields of view.

3.2.5 Investigation of synergy between 12-bis-THA particles and antimicrobials against *B. thailandensis*

12-bis-THA particles are bactericidal against strain E264 at the MIC concentration but are bacteriostatic against the capsulated strain E555. Bactericidal antimicrobials are preferable to treat infections caused by *Burkholderia* species as infections are more common in immunocompromised individuals. CLSM shows that 12-bis-THA particles bind to the membranes of both strains and where they may interact with cardiolipin and LPS. These interactions may induce stress to the bacteria either through the accumulation of 12-bis-THA monomers within the cytoplasm or through the destabilisation of the bacterial membrane resulting in increased permeability and interference with the electron transfer chain. These properties may result in synergistic interactions with other antimicrobials that are either limited by uptake or act on similar pathways.

This was investigated using checkerboard assays were performed using both *B. thailandensis* strains to determine fractional inhibitory concentration index (FICi) of various combinations of 12-bis-THA and antimicrobials against both strains. The antimicrobials tested were co-trimoxazole, trimethoprim, sulfamethoxazole, ciprofloxacin, doxycycline, polymyxin B, tobramycin, rifampin, and metronidazole. In this study, synergy was defined as a fractional inhibitory concentration index (FICi) of $\leq$ 0.5, additivity as a FICi of 0.5 – 1, and antagonism as an FICi $\geq$ 4.

It was found that 12-bis-THA particles act synergistically with trimethoprim against both strain E264 (FICi - 0.44 $\pm$ 0.08) and strain E555 (FICi - 0.31 $\pm$ 0.05). Similarly, co-trimoxazole synergised with 12-bis-THA particles against strains E264 (FICi – 0.35 $\pm$ 0.04) and E555 (FICi - 0.33 $\pm$ 0.06). Checkerboard assays were performed to investigate interactions between 12-bis-THA particles and sulfamethoxazole; however, no synergy was observed as the MIC of sulfamethoxazole was greater than the maximum concentration tested of 512 µg/mL. This suggests that the synergy observed with co-trimoxazole is due to trimethoprim rather than sulfamethoxazole. Additivity was observed with tobramycin against strains E264 (FICi - 0.53 $\pm$ 0.02) and E555 (0.54 $\pm$ 0.03) and rifampin against strains E264 (FICi - 0.60 $\pm$ 0.11) and E555 (FICi - 0.55 $\pm$ 0.12) as shown in **Table 3.3**.

Table 3.3: **Fractional inhibitory concentration index (FICi) of interactions between 12-bis-THA particles and antimicrobials against *B. thailandensis* strains E264 and E555.** Data are representative of at least 3 independent experiments the standard deviation is shown.

Combination	**FICi value (*B. thailandensis* E264)**	**FICi value (*B. thailandensis* E555)**
Trimethoprim + 12-bis-THA particles	0.44 ± 0.08	0.31 ± 0.05
Co-trimoxazole + 12-bis-THA particles	0.35 ± 0.04	0.33 ± 0.06
Rifampin + 12-bis-THA particles	0.60 ± 0.11	0.55 ± 0.12
Tobramycin + 12-bis-THA particles	0.53 ± 0.02	0.54 ± 0.03

Isoboles can be used as a graphical representation of synergy and show changes in the MIC of synergistic antimicrobials by plotting the fractional inhibitory concentrations (FICs) along the turbid/non-turbid border. 12-bis-THA particles combined with trimethoprim reduce both MICs by up to 16-fold and 4-fold respectively in strain E264 (**Figure 3.8A**), and by up to 8-fold and 8-fold respectively in strain E555(**Figure 3.8B**). The MICs of co-trimoxazole and 12-bis-THA particles were reduced 8-fold and 8 to 16-fold in strain E264 (**Figure 3.8C**), and by 8-fold and 8 to 16-fold in strain E555, respectively (**Figure 3.8D**).

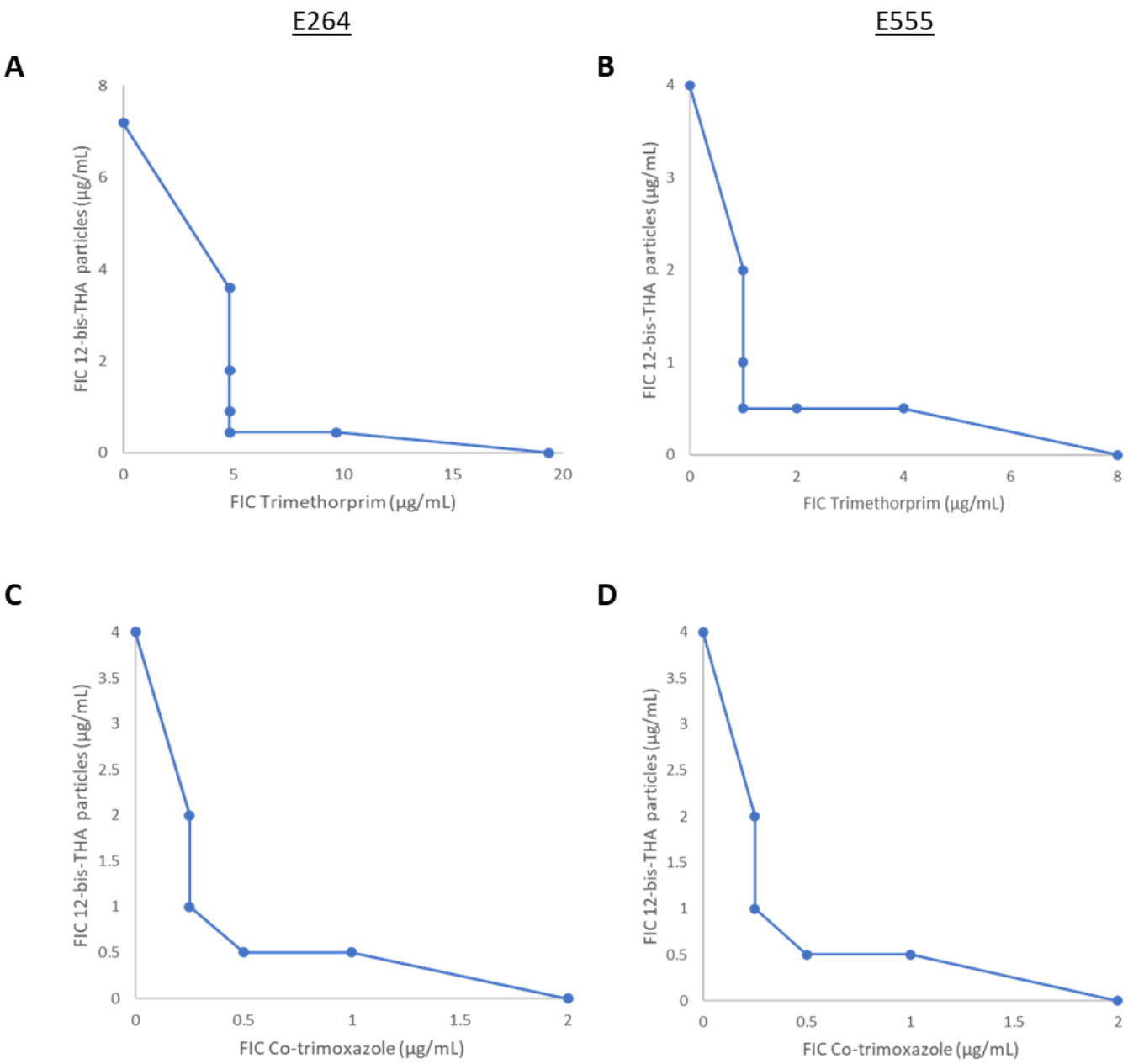

Figure 3.8: Isoboles showing drug interactions between (AB) Trimethoprim and CM2 particles and (CD) Cotrimoxazole and 12-bis-THA particles against B. thailandensis E264 and *B. thailandensis* strain E555. Data show the FIC values along the turbid/non-turbid border of 1 of 3 independent replicate.

Isoboles show that the MIC of 12-bis-THA particles and rifampin was reduced 2-fold and up to 32-fold respectively in *B. thailandensis* E264 (**Figure 3.9A**). In E555, additivity was observed twice and synergism once. In the context of the observed synergy, MIC values of 12-bis-THA particles and rifampin were reduced by 4-fold and 8-fold respectively (**Figure 3.9B**), however, for the plates with additivity, the MIC of 12-bis-THA particles was reduced 2-fold in both cases. Similar results were observed between 12-bis-THA particles and tobramycin. Generally, the MIC of 12-bis-THA particles were consistently reduced 2-fold whereas the MIC in tobramycin was reduced 16-fold and 32-fold in E264 (**Figure 3.9C**) and E555 (**Figure 3.9D**) respectively.

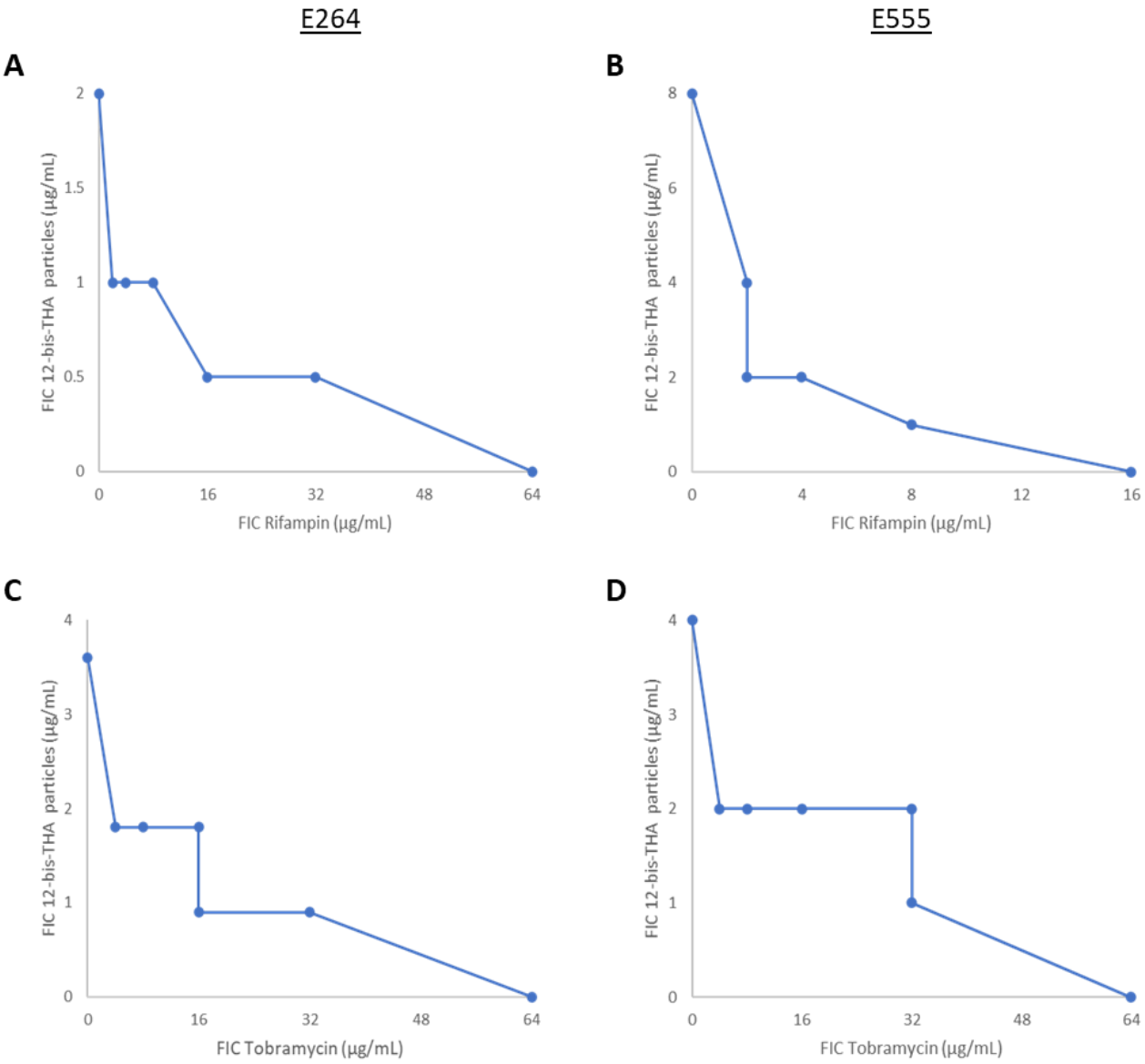

Figure 3.9: Isoboles showing drug interactions between (AB) rifampin and 12-bis-THA particles and (CD) tobramycin and 12-bis-THA particles against *B. thailandensis* strains E264 and E555. Data show the FIC values along the turbid/non-turbid border of 1 of 3 independent replicate.

3.2.6 Effect of varying weight ratios of 12-bis-THA and antimicrobial combinations

Multiple synergistic drugs that are used clinically are formulated as weight ratios (w/w) and have been optimized to achieve the best synergistic effect. For example, co-amoxiclav is a combination of amoxicillin and clavulanic acid that is commonly delivered as a 4:1 ratio using doses of either 250:62.5 mg or 500:125 mg (173). In order to investigate whether altering the w/w ratio of combinations with 12-bis-THA affected synergism we tested a number of combinations against *B. thailandensis* strain E555 for use in *in vitro* studies including time-kill assays and to investigate activity against a panel of *B. cepacia* complex clinical isolates. Combinations of antimicrobials and 12-bis-THA particles were prepared with the following w/w ratios of antimicrobials to 12-bis-THA particles: 8:1, 5:1, 3:1, 1:1, 1:3, 1:5, and 1:8. Selected MIC results are shown in **Table 3.4** with the w/w ratios of 1:3 to 1:8 excluded as no difference in MIC was observed when compared to the MIC of 12-bis-THA alone. Similarly, enhanced antimicrobial activity was not observed in the 1:1 combination.

The MICs of the 3:1, 5:1 and 8:1 ratios of trimethoprim to 12-bis-THA particles were 2 : 0.67, 2 - 4 : 0.4 - 0.8 and 4 : 0.5 µg:µg/mL respectively. These values were in line with the findings of the checkerboard assays where the concentration of trimethoprim and 12-bis-THA particles were reduced to 1 and 0.5 µg/mL respectively against E555 (**Figure 3.8B**). For the tobramycin and 12-bis-THA particle mixtures, the MICs were 4 - 8 : 1.3 - 2.7, 4 - 8 : 0.8 – 1.6 and 16 : 2 µg/mL for the 3:1, 5:1 and 8:1 mixtures respectively (**Table 3.4**). Again, these values are consistent with the checkerboard assays where the MIC of tobramycin reduced from 64 µg/mL to 2-4 µg/mL whereas the MIC of 12-bis-THA particles was consistently reduced 2-fold from 4 to 2 µg/mL (**Figure 3.9D**). The MICs of the 3:1 and 5:1 ratios of rifampin to 12-bis-THA particles were 2-4 : 0.67 – 1.33 and 4 : 0.8 µg:µg/mL respectively. No MIC was determined for the 8:1 ratio as E555 grew in the highest concentration tested (16:8 µg:µg/mL). The MICs for the rifampin and 12-bis-THA particle combinations are in line with the values from the checkerboard assay where MICs were reduced approximately 8-fold to 2 µg/mL whereas the MICs of 12-bis-THA particles were reduced 2 to 4-fold to 2 µg/mL. The 3:1 ratio of antimicrobial to 12-bis-THA particles was selected for future studies as it produced the lowest MICs of the ratios tested and was broadly consistent with the findings of the checkerboard assays.

Table 3.4: The MICs of trimethoprim, tobramycin or rifampin in combination with 12-bis-THA particles at different weight/weight ratios. The ratios 1:1, 3:1, 5:1, and 8:1 were tested in the range of 0.5 – 16 μg/mL. Values denoted as ND were above the tested range in *B. thailandensis* strain E555. Data are representative of 3 independent replicates and 2 technical replicates.

Ratio (Antimicrobial: 12-bis-THA particles)	Trimethoprim:12-bis-THA particles (μg:μg/mL)	Tobramycin:12-bis-THA particles (μg:μg/mL)	Rifampin:12-bis-THA particles (μg:μg/mL)
1:1	2 : 2	4-8 : 4 - 8	4 : 4
3:1	2 : 0.67	4-8 : 1.3 – 2.7	2-4 : 0.67 – 1.33
5:1	2-4 : 0.4-0.8	8 : 1.6	4 : 0.8
8:1	4 : 0.5	16 : 2	ND
Trimethoprim only	8	-	-
Tobramycin only	-	ND	-
Rifampin only	-	-	ND

3.2.7 Biophysical characterisation of 12-bis-THA particle: antimicrobial combinations

Synergism with 12-bis-THA particles may occur due to enhanced uptake either through permeabilization of the cell wall or the second antimicrobial associating with the particle. Traditionally, entrapment efficiency can be assessed using techniques such as liquid chromatography (LC) that separates and quantifies the free antimicrobial from the particle, typically a liposome. However, given 12-bis-THA particles were not amenable to LC as they bound tightly to the matrix of the columns.

Alternatively, dynamic light scattering (DLS) has been used to study interactions between oligonucleotide TFDs which bind to the surface of 12-bis-THA particles causing a change in the biophysical characteristics. A DLS study was performed to investigate whether there were changes in the physical characteristics of 12-bis-THA particles when combined with synergistic antimicrobials. Combinations were formed at a 3:1 ratio in either water or 0.1x PBS at RT and their hydrodynamic ratios of the resultant particles were measured. 0.1x

PBS was tested to assess the effect of a mild ionic strength solvent and the samples were measured immediately after formation.

No difference was observed when comparing the histograms of 12-bis-THA particles and trimethoprim or tobramycin with 12-bis-THA particles alone suggesting no interaction between the molecules. A change in the histogram was seen in 12-bis-THA particles when combined with rifampin but this may be due to rifampin forming nanoparticles in aqueous conditions. The rifampin particles were unstable in 0.1X PBS at the concentration tested (100 µg/mL) irrespective of the presence of 12-bis-THA particles (**Figure 3.10H**).

As previously mentioned, physical interactions between oligonucleotide TFDs and 12-bis-THA particle have resulted in changes to the 12-bis-THA strucutre which has been observed using DLS. This was observed when empty particles which are typically polydispersed (i.e multiple populations of varying sizes) and had an average diameter of approximately 300 nm. However, when mixed with TFD, the particles became monodispersed (i.e a single population which are the same size) which had an average diameter of 120 nm.

The aim of this assay, shown in **figure 3.10**, was to investigate whether physical interactions occurred between the synergistic antimicrobials and 12-bis-THA particle which might be observed as changes in the biophysical properties of the particles. However, no discernable difference was detect using this approach suggesting that either no interaction between the antimicrobials occur or that DLS is not sensitive or suitable to determine possible interactions. The lack of change in the physical properties of the combinations may occur because: (1) the interaction may not yield a change that is detectable by DLS; (2) there is no interaction between the 12-bis-THA particles and the antimicrobials; (3) the current data are representative of a single time point (0 h) and interactions may occur at later time points.

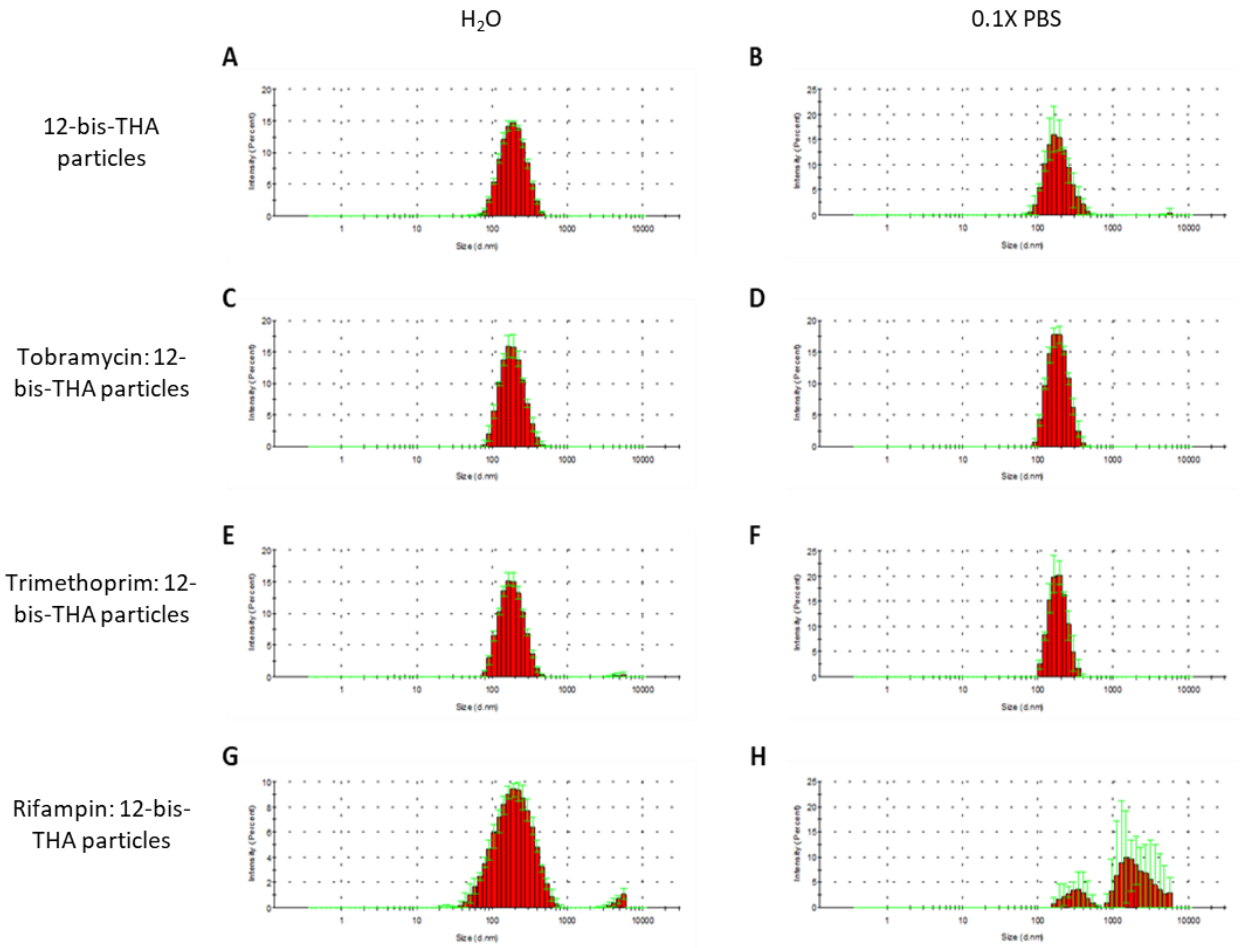

Figure 3.10: Dynamic light scattering (DLS) profiles of 12-bis-THA particles (AB), tobramycin and 12-bis-THA particle (CD), trimethoprim and 12-bis-THA particles (EF) and rifampin and 12-bis-THA particles (GH) in H2O or 0.1X PBS.

3.3 ASSESSMENT OF SYNERGISTIC INTERACTIONS USING TIME-KILL ASSAYS

Time-kill assays were performed to determine if synergy was retained in the selected 3:1 ratios and to investigate if the combination were bacteriostatic or bactericidal. For this study, antimicrobial synergy was defined as a >2 $\log_{10}$ reduction in CFUs when compared to the most effective monotherapy at 24 h (145). Rifampin and 12-bis-THA particles act synergistically against *B. thailandensis* strain E555 as a 4.8 $\log_{10}$ reduction in CFUs was observed when comparing the activity of 12-bis-THA particles to the rifampin: 12-bis-THA particle combination (**Figure 3.11A**). The antimicrobial activity of the rifampin and 12-bis-THA particle combination was bacteriostatic as a 1.8 $\log_{10}$ decrease in CFUs/mL relative to starting inoculum was observed at 24 h. Tobramycin and 12-bis-THA particles act synergistically as a 2.3 $\log_{10}$ reduction in CFUs was observed when comparing cultures at 24 h that had been challenged with 12-bis-THA particles to those challenged with tobramycin and 12-bis-THA particles (**Figure 3.11B**). Interestingly, the combination was rapidly bactericidal as the bacterial density was reduced by 2.7 and 3.9 $\log_{10}$ CFUs at 3 and 6h, respectively. However, by 24h had regrown and surpassed the bacterial density of the starting inoculum by 0.34 $\log_{10}$. Trimethoprim and 12-bis-THA particles act synergistically as a $\log_{10}$ 3.7 difference in CFUs were observed when comparing *B. thailandensis* cultures at 24h which had been challenged with either 12-bis-THA particles alone or trimethoprim and 12-bis-THA particles (**Figure 3.11C**). Additionally, the combination of trimethoprim and 12-bis-THA particles was bacteriostatic against *B. thailandensis* strain E555 as the bacterial density was reduced 1.6 $\log_{10}$ following 24 h of treatment. 12-bis-THA particles act synergistically with co-trimoxazole as a 3.2 $\log_{10}$ reduction in CFUs were observed at 24 h when comparing co-trimoxazole as a single agent to co-trimoxazole and 12-bis-THA particles (**Figure 3.11D**). The antimicrobial activity of the 12-bis-THA particle and co-trimoxazole combination was bacteriostatic as the starting inoculum was reduced 2.7 $\log_{10}$ CFUs.

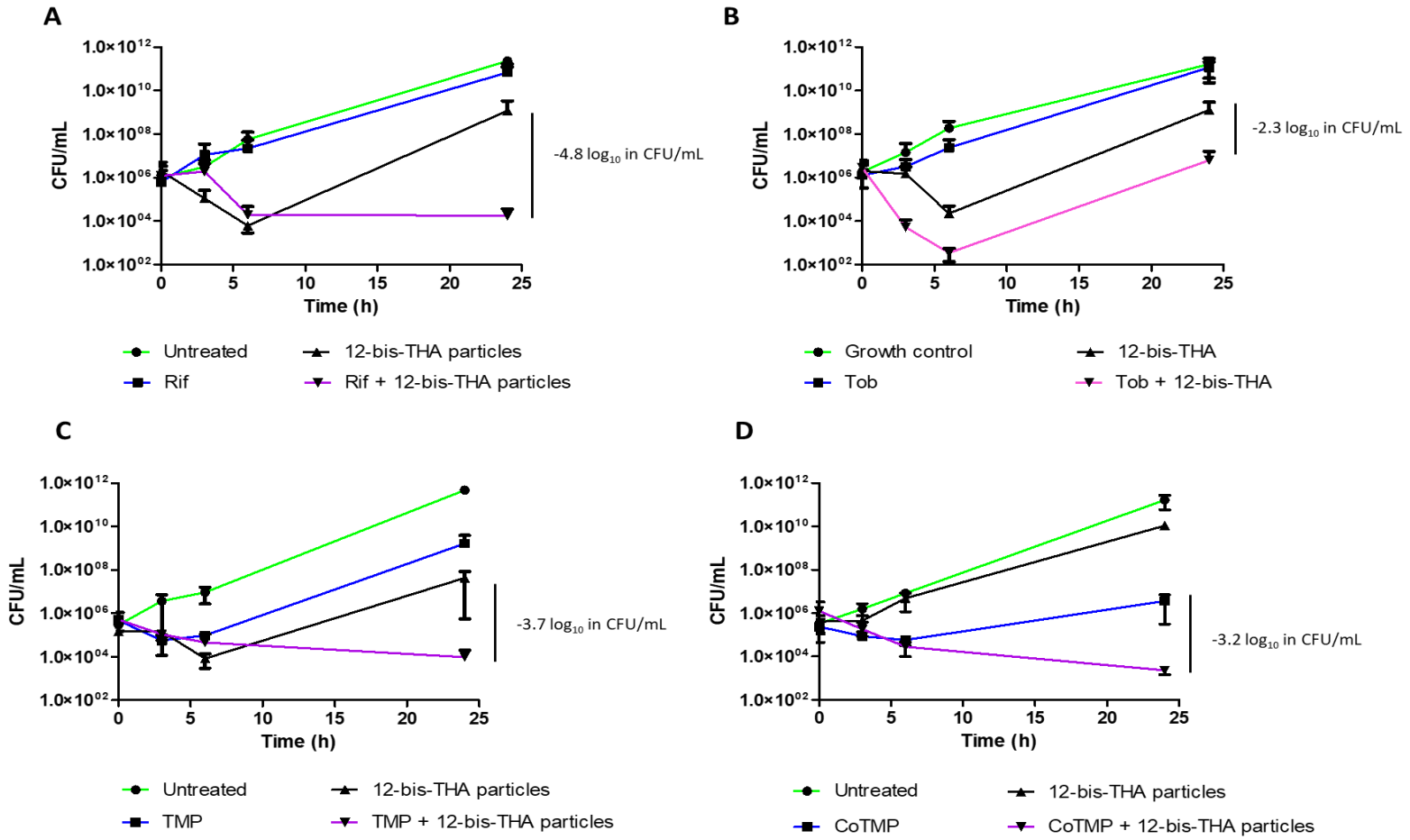

Figure 3.11: Time-kill analysis of (A) rifampin (8 µg/mL) and 12-bis-THA particles (2.6 µg/mL), (B) tobramycin (8 µg/mL) and 12-bis-THA particles (2.6 µg/mL), (C) trimethoprim (4 µg/mL) and 12-bis-THA particle (1.3 µg/mL), and (D) co-trimoxazole (1 µg/mL) and (0.3 µg/mL)12-bis-THA particles activity against *B. thailandensis* strain E555. Timepoints were recorded at 0, 3, 6, and 24 . Data are representative of 3 independent experiments each consisting of 3 technical replicates.

3.3.1 Activity of 12-bis-THA particles and the antimicrobial combinations against a panel of *B. cepacia* complex clinical isolates

The activities of trimethoprim, rifampin, tobramycin, and 12-bis-THA were determined as monotherapies or combinations against a panel of BCC clinical isolates including *B. gladioli* in collaboration with Professor Mahenthiralingam and Dr Rushton at Cardiff University. These formulations were supplemented with the excipient agent hydroxypropyl methylcellulose (HPMC) which has been shown to slightly improve the activity of 12-bis-THA particles and also improve their stability (139).

All BCC strains tested were highly resistant to rifampin and tobramycin except for *B. gladioli* that was sensitive to tobramycin. Most strains were sensitive to trimethoprim excluding *B. cenocepacia* J2315 which has a point mutation in dihydrofolate reductase (DfrA) conferring resistance to trimethoprim (174). 12-bis-THA particles exhibited antimicrobial activity against all strains in the panel with MICs of 2 – 8 μg/mL for *B. multivorans* and *B. cepacia,* 1 μg/mL in *B. gladioli* and 8 - 32 μg/mL in *B. cenocepacia*. The literature was reviewed to investigate the LPS chemotype of each BCC isolate used in **Table 3.5** to evalute whether LPS chemotype influenced the MIC of 12-bis-THA particles (**Appendix - Table 10.1**). By doing so, we identified 8/12 LPS chemotypes for the strains used. However, no clear difference in the MIC of 12-bis-THA particles was observed (**Appendix - Table 10.2**).

The combinations showed varying levels of activity against the BCC panel. The rifampin: 12-bis-THA formulation showed improved efficacy against 1 strain and antagonism against 1 strain. The trimethoprim: 12-bis-THA combination showed improved efficacy against 2 strains and antagonism against 1 strain. The tobramycin: 12-bis-THA formulation was the most active and showed improved efficacy, relative to tobramycin and 12-bis-THA alone, against 9 of the 12 strains.

Table 3.5: The MIC of 12-bis-THA particles, rifampin, tobramycin and trimethoprim determined as monotherapies, and antimicrobial combinations against a panel of BCC clinical isolates. All formulations containing 12-bis-THA were supplemented with HPMC (0.1% V/V). MICs were defined as an 80% reduction in turbidity relative to an untreated control. Data are representative of 3 independent experiments. Boxes highlighted in **GREEN** show a reduction in antimicrobial and 12-bis-THA MIC when administered together compared to the appropriate monotherapy. Boxes highlighted in **RED** show a decrease in antimicrobial and 12-bis-THA activity when administered as a combination compared to the monotherapies

		Monotherapies				Combination therapies					
Organism	**Strain ID**	**12-bis-THA**	**Rifampin**	**Tobramycin**	**Trimethoprim**	**Rifampin: 12-bis-THA particles**		**Tobramycin: 12-bis-THA particles**		**Trimethoprim: 12-bis-THA particles**	
B. multivorans	17616	8	8	8-16	8	16-32	5.33-10.67	4-8	1.33-2.67	2	0.67
B. multivorans	BCC764	4-8	128	32-128	4	16	5.33	8	2.67	2-4	0.67-1.33
B. multivorans	BCC710	4	64-128	64-128	16	16	5.33	8	2.67	16	5.33
B. multivorans	BCC008	8	128	256	4	32	10.67	8-16	2.67-5.33	4-8	1.33-2.67
B. multivorans	BCC032	2	16-64	64-256	2-4	16	5.33	8	2.67	2	0.67
B. cenocepacia	J2315	16	128	128-256	256<	64	21.33	64	21.33	128	42.67
B. cenocepacia	K56-2	32	64-256<	64-128	8	32-64	10.67-21.33	8	2.67	32	10.67
B. cenocepacia	AU1054	16	16-32	64-128	2	32	10.67	8	2.67	2-8	0.67-2.67
B. cenocepacia	BCC0018	8-16	16-32	128-256	2	16	5.33	8-16	2.67-5.33	2	0.67
B. cenocepacia	BCC0020	8	16-32	256<	<2	16	5.33	16	5.33	2	0.67
B. gladioli	MA4	1	16	0.5	1-2	8	2.67	2	0.67	4-8	1.33-2.67
B. cepacia	BCC0001	4-8	8-16	32-64	4	8-16	2.67-5.33	8	2.67	4	1.33

3.4 DISCUSSION

3.4.1 Are 12-bis-THA particles affected by modified LPS or the presence of a polysaccharide capsule?

Burkholderia species are profoundly resistant to cationic antimicrobials as the core oligosaccharide and lipid A components of their LPS are modified with Ara4N groups (175). This neutralizes the negative charge of the phosphate by providing a sugar with a positively charged primary amine group which lowers the affinity of cationic molecules to the LPS (176). Unlike other Gram-negative species where this modification is dispensable and is only induced under selective pressure, it is essential for viability in *Burkholderia* species (177). The data presented in this chapter are consistent with the literature and demonstrate that both *B. thailandensis* strains were able to grow in 1024 μg/mL of polymyxin B, whereas 12-bis-THA particles inhibit the growth of both strains at 2 – 8 μg/mL. 12-bis-THA particles and polymyxin B have a similar binding affinity to *E. coli* LPS (5.1 μM and 0.5 μM respectively). This interaction is driven by the electrostatic interactions between the cationic 12-bis-THA headgroup and the negative glucosamine within the lipid A and the insertion of the 12-bis-THA linker into the membrane (137). Our findings suggest that, unlike polymyxin B, 12-bis-THA activity is not driven solely though LPS interactions as the particles were not influenced by the Ara4N modification to LPS in which gives rise to profound resistance to cationic molecules in *Burkholderia* species.

No difference in the MIC was observed for 12-bis-THA particles when strains E264 and E555 were compared suggesting that the activity of the particles is unaffected by the polysaccharide capsule. However, this cannot be accurately determined when measuring MIC as an endpoint because it provides data at a single time point and is based on turbidity which does not distinguish between live and dead cells. Therefore, confocal microscopy was performed to investigate if the presence of the capsule affected the transfection efficiency of 12-bis-THA particles into *B. thailandensis*. After 2 h of exposure, the images suggest that bacterial cells exhibit a high degree of transfection where 12-bis-THA particles had accumulated in the bacterial cytoplasm or had become embedded within the membrane, however, no difference in uptake efficiency in E264 and E555 was observed under these conditions. This may be an artifact of the experimental design as this assay required a high concentration of 12-bis-THA particles (50 μg/mL) to exploit its fluorescence.

Previously, the McArthur group has used radiolabeled 12-bis-THA particles in pharmacokinetic studies (data not published). An alternative approach to microscopy could be to treat capsulated and unencapsulated with MIC concentration of radiolabelled 12-bis -THA. Cytoplasm could then be extracted from treated cells to determine the presence of 12-bis-THA particles in the cytoplasm and

to establish their concentration. From this, we may also be able to determine uptake kinetics of the particles to investigate the influence of the polysaccharide capsule.

The images show that the poles of both strains were consistently enriched with 12-bis-THA particles. Cardiolipin is an essential, anionic phospholipid found in the inner membrane of bacteria and mitochondria. It preferentially accumulates in areas of great curvature such as the pole or septum of bacteria (178,179) and forms cardiolipin micro-domains (179,180). It is involved in the stabilization of respiratory complexes (181,182), generation of membrane potential ($\Delta\psi$), and controlling bacterial cell division (183). The localization of 12-bis-THA particles at the bacterial poles and the membrane may be representative of 12-bis-THA particles binding to cardiolipin which has been shown to drive transfection in artificial membranes (172).

The presence of the capsule did result in a difference in the antimicrobial activity of 12-bis-THA particles in time-kill studies. Strain E264 was more susceptible than E555 to 12-bis-THA particles resulting in a reduction in bacterial CFU counts in a time and concentration-dependent manner. 12-bis-THA particles demonstrated bactericidal activity against *B. thailandensis* E264 at a concentration of 8 µg/mL as CFUs were reduced >3 $\log_{10}$. In contrast, 12-bis-THA particles were bacteriostatic against *B. thailandensis* E555 and CFUs were reduced in a time-dependent manner irrespective of concentration suggesting the capsule may absorb the particles to limit transfection at MIC concentrations. It is not clear how the presence of the polysaccharide capsule provides a small degree of protection from 12-bis-THA particles. In *B. pseudomallei*, the polysaccharide capsule provides protection from host serum by limiting complement factor deposition and reducing the efficiency of the membrane attack complex (184,185). In the context of this work, one possibility is that the capsule slows transfection at MIC concentrations by providing a physical barrier which shields the membrane from the lipophilicity of 12-bis-THA particles. Multiple biophysical studies have shown that 12-bis-THA particles interact strongly with artificial prokaryotic membranes through a combination of charge and hydrophobic based interactions, causing the formation of transient pores or even the collapse of the membrane through invagination in these models (137,138).

3.4.2 Why does *B. thailandensis* regrow at 24 h?

By the 24 h time point of the time-kill study, almost all cultures which had been challenged with 12-bis-THA particles displayed some degree of regrowth. Cultures incubated with 2 and 4 µg/mL regrew whereas those incubated with 8 µg/mL showed less regrowth. Additionally, small and normal colonies were observed in both strains when incubated with 12-bis-THA particles. The combination of small *B. thailandensis* colonies and bacteria regrowth at MIC concentrations of 12-bis-THA particles

may suggest the development of adaptive resistance that may give rise to heteroresistant subpopulations of *B. thailandensis*.

Heteroresistant subpopulations are groups of bacteria within an isogenic culture that exhibit varying antimicrobial susceptibility profiles (186). These are distinct from persister cells as they rapidly grow in the presence of an antimicrobial (187) unlike persister cells which are generally considered to be dormant (188). Heteroresistant subpopulations develop due to genetic mutations and are classified as either stable or unstable which is contingent on the fitness cost of its causal mutation. Stable heteroresistant subpopulations are retained in the absence of an antimicrobial and are caused by mutations that have no or low fitness costs such as TF repressors of RND pumps, overexpression of genes encoding RND efflux pump components, or small molecule transporters (189). Unstable heteroresistant subpopulations develop when mutations occur in genes involved in essential processes such as the electron transport chain (ETC) which confers a high fitness cost. Alternatively, unstable heteroresistance can occur due to spontaneous amplification of resistance genes which are quickly lost following the removal of selective pressure (190).

Gene expression can be regulated in prokaryotes through the methylation of cytosine and adenine nucleotides, by DNA cytosine methyltransferase (Dcm) and DNA adenine methylase (Dam) (191)which can influence the binding of regulatory factors such as transcription factors and nucleoid associated proteins (192). For example, the expression of transposon *Tn*10 was 1000 fold higher in a strain with a partially methylated promoter region compared to one with a completely methylated promoter region (193). The relationship between antimicrobial resistance and DNA methylation is not well understood. However, data generated by Stephenson and Brown show that *E. coli* strains deficient in *dam* were more susceptible to antimicrobials compared to the parental strain (194). Dam is essential in *Enterobacteriaceae* for efficient DNA mismatch repair by the SOS system (195). Adaptive resistance may occur through the upregulation of Dam if 12-bis-THA particles cause DNA damage and induce the SOS system

A series of microbiological assays were performed to investigate if small and normal colonies of strain E264 exhibited phenotypic changes when compared to an untreated control. However, no difference in the growth kinetics or susceptibility to 12-bis-THA particles was observed in any of the colonies. Additionally, the small and normal colonies reverted to the morphology of the untreated control when subcultured onto LB agar and grown for 72 h (appendix). It is more likely that the observed small colonies are not a heteroresistant sub-population. Small colony variants have been observed when bacteria accumulate mutations in genes encoding components of the electron transport chain (196) which is possible given the structure of 12- bis-THA, given its similarity to

dequalinium that is known to damage respiratory chains (197). Therefore, it is more likely that the small colonies observed in this chapter are associated with temporary respiratory damage rather than the formation of drug resistant sub-populations.

3.4.3 Mechanism of synergy with tobramycin

Tobramycin is an aminoglycoside that is hydrophilic and cationic at physiological pH. Because of these physiochemical properties it is unable to passively cross the bacterial membrane but must exploit proton motive force (PMF) to be internalized. As tobramycin is cationic and stimulates its own uptake by destabilizing the bacterial membrane, this also contributes to bacterial killing at high concentrations (198). Upon entering the bacterial cytoplasm, tobramycin inhibits growth by binding to the 30S and 50S ribosomal subunits inhibiting translation (199). The mechanism of action of tobramycin is multifarious; destabilization of the outer membrane stimulates the uptake of tobramycin causing bacterial killing at high concentrations while also preventing mRNA translation to protein at low concentrations.

Checkerboard assays show additivity between 12-BIS-THA particles and tobramycin against E264 (FICi - 0.53 $\pm$ 0.02) and E555 (FICi – 0.54 $\pm$ 0.03). Time-kill studies showed that this combination is bactericidal against E555 at 6 h and induce small colony formation suggesting that 12-bis-THA particles and tobramycin share a potential mechanism of action. For drugs to act synergistically they can: (1) improve uptake of one another; (2) prevent efflux; (3) counter a resistance mechanism of a second drug; or (4) stimulate pathways that are targeted by the second drug. For example, *P. aeruginosa* cultures supplemented with fumarate were more susceptible to tobramycin as the PMF was stimulated leading to increased tobramycin uptake (200). Synergy has been observed between tobramycin and baicalin in *B. cenocepacia.* Baicalin enhanced the reactive oxygen species (ROS) mediated bactericidal activity of tobramycin in addition to improving tobramycin uptake through stimulating the tricarboxylic acid cycle (TCA) and PMF (201). Tobramycin has also been shown to act synergistically with bismuth-thiols against *B. multivorans* and *B. cenocepacia* (202). Bismuth-thiols are cations that bind the bacterial outer membrane and lead to a reduction in cytoplasmic levels of ATP which may occur either through inhibition of ATP synthase due to a loss of membrane integrity or by neutralizing the negative charge of the membrane and countering reuptake of H^+ ions (203).

Cardiolipin has been shown to enhance the activity of respiratory complex I (204) which is responsible for proton translocation across the inner membrane contributing to PMF (205). 12-bis-THA particles may synergise with tobramycin through the binding of cardiolipin which is known to stabilise respiratory chains (204). Alternatively, dequalinium has been shown to inhibit both respiratory complex III (Coenzyme Q – cytochrome C reductase) and V (ATP synthase), the latter of

which catalyzes the phosphorylation of ADP to ATP at the expense of PMF (206,207). By inhibiting respiratory complexes III and V the bacteria may upregulate complex I in an attempt to stimulate the electron transport chain. Conversely, inhibition of respiratory complexes may lead to a depletion of ATP which may reduce the activity of ATP dependent transporters including RND efflux pumps resulting in decreased tobramycin efflux.

Hence, there may be several ways that 12-bis-THA and tobramycin synergise, and these include improving its penetration into the cytoplasm either through the destabilization of the bacterial membrane or through inducing changes in central metabolism and PMF. Alternatively, synergy may occur if 12-bis-THA particles suppress respiratory chains by binding cardiolipin which may reduce the cytoplasmic concentration of ATP and indirectly suppress efflux.

3.4.4 12-bis-THA particles act synergistically with trimethoprim and co-trimoxazole but not sulfamethoxazole

Strong synergy was observed between the 12-bis-THA particles and trimethoprim in strains E264 (FICi – 0.44 $\pm$ 0.08) and E555 (FICi – 0.31 $\pm$ 0.05). Additionally, strong synergy was also observed between 12-bis-THA particles and co-trimoxazole against E555 (FICi – 0.33 $\pm$ 0.06). Time-kill assay data showed that 12-bis-THA particles in combination with trimethoprim or co-trimoxazole exhibited bacteriostatic activity against strain E555 by 24 h post incubation. The presence of small colonies or regrowth was not observed for strain E555 following incubation with these combinations suggesting that they are may not be affected by the potential 12-bis-THA particle adaptive resistance mechanism.

Trimethoprim is a pyrimidine analogue that inhibits bacterial growth by blocking the reduction of dihydrofolate to tetrahydrofolate, an essential step in folate production that leads to the inhibition of nucleic acid synthesis (208). In the context of melioidosis, trimethoprim is used in combination with sulfamethoxazole as co-trimoxazole, both compounds inhibit enzymes in the biosynthetic pathway for tetrahydrofolate synthesis. Sulfamethoxazole is a structural analogue of para-aminobenzoic acid which is a metabolite that is required for the formation of dihydrofolate by dihydropteroate synthase (209). Sulfamethoxazole acts synergistically with trimethoprim as it competes with para-aminobenzoic acid to bind dihydropteroate synthase which leads to a decrease in the production of dihydropteroic acid and tetrahydrofolic acid. It is unlikely that 12-bis-THA particles target the biosynthetic pathway for tetrahydrofolate as no synergy was observed between 12-bis-THA particles and sulfamethoxazole.

Synergy between trimethoprim and nitrofurantoin, and mecillinam has been observed against *E. coli.* Fatsis-Kavalopoulos *et al* proposed that sensitisation to trimethoprim may occur due to two key events: (1) the ablation of ATP synthesis; (2) the removal of secreted extracellular polysaccharides. In *E. coli,* an *atpF* mutant was substantially more sensitive to trimethoprim suggesting that ATP is

required for survival against trimethoprim (210). Additionally, *E. coli* strains that were deficient in producing secreted polysaccharides and LPS were also susceptible to trimethoprim, as were wild type strains that had been pre-treated with EDTA (210). Confocal microscopy shows that 12-bis-THA particles interact with the membrane of *B. thailandensis* where they may destabilise the outer membrane. Additionally, 12-bis-THA particles may inhibit respiratory complexes as they are stabilised by cardiolipin. This may lead to the ablation of ATP synthase and account for the synergy between 12-bis-THA particles and trimethoprim.

3.4.5 12-bis-THA particles improve the antimicrobial activity of rifampin

An additive effect was observed between 12-bis-THA particles and rifampin against strains E264 (FICi - 0.60 $\pm$ 0.11) and E555 (FICi - 0.55 $\pm$ 0.12). This was confirmed using a time-kill study which showed that 12-bis-THA particles and rifampin exhibit bacteriostatic activity against E555. Additionally, no small colonies or regrowth was observed following incubation with this combination of compounds suggesting that, like 12-bis-THA particles and trimethoprim/co-trimoxazole, 12-bis-THA particles and rifampin may prevent the adaptive resistance mechanism that gives rise to regrowth at 24 h. Rifampin is bactericidal and prevents DNA transcription by irreversibly binding to RNA polymerase (66). Rifampin is commonly used in combination with isoniazid, ethambutol and pyrazinamide as a first-line treatment for those with pulmonary tuberculosis (67). Rifampin exhibits poor in vitro activity against *Burkholderia* species as a monotherapy (68,69). There is data showing moderate in vivo activity against *B. pseudomallei* in a murine model however this is at concentrations higher than what is clinically achievable in humans with traditional dosing regimens (71). Combining 12-bis-THA particles with rifampin may provide a method of reducing the required concentration of rifampin to a more clinically achievable level.

12-bis-THA particles are membrane active and strongly bind to LPS and cardiolipin (132,137). Biophysical modelling showed that 12-bis-THA particles caused invagination and lysis of these giant unilamerallar vescicles and patch clamp studies showed that 12-bis-THA particles caused the formation of transient pores within liposomes (138). In addition, an NMR metabolomics study indicated that 12-bis-THA particles induced changes in membrane lipids in *E. coli* and *P. aeruginosa.* Our confocal microscopy data shows that 12-bis-THA particles interact with the membrane of both strains E264 and E555. This may suggest that 12-bis-THA particles permeabilise the membrane of *B. thailandensis* which allows improved internalisation of rifampin and concomitant antimicrobial activity.

Alternatively, a proteomic study showed that the transcription factor fumarate and nitrate reductase (FNR) was strongly induced by 12-bis-THA particles in *E. coli* (data not published). FNR

regulates the transition between aerobic and anaerobic respiration in *Enterobacteriaceae* by measuring the cytoplasm concentration of oxygen (211). This implies that 12-bis-THA particles may disturb redox homeostasis by inducing anaerobic respiration in the presence of oxygen. Redox homeostasis is regulated by numerous transcription factors such as OxyR, SoxR, FNR, NarPL, and FUR, and must be tightly controlled to prevent death overwhelming concentrations of reactive intermediates from respiratory pathways (212). Rifampin may act synergistically by inhibiting transcriptional regulators which control the stress response to 12-BIS-THA particles.

3.4.6 12-bis-THA particles are active against a panel of BCC clinical isolates and retain the ability to potentiate the activity of tobramycin

The data presented in this chapter shows that most BCC strains are highly resistant to tobramycin and rifampin. *Burkholderia* species including *B. thailandensis* and *B. pseudomallei* are intrinsically resistant to many antimicrobials which is predominantly mediated by low membrane permeability and efficient extrusion of antimicrobials by RND efflux pumps (91). To date, 6 RND efflux pumps have been identified in BCC species which confer resistance to aminoglycosides, fluoroquinolones, quinolones and chlorohexidine (213–215). Resistance to aminoglycosides is also influenced by low activity against the outer membrane of *Burkholderia* species as the outer membrane of *B. cepacia* is less permeable than *E. coli* (216). Like *B. pseudomallei,* the LPS of BCC contains Ara4N modifications to the Lipid A which limits the activity of cationic molecules such as tobramycin, colistin, and EDTA (217). All BCC strains were susceptible to trimethoprim except *B. cenocepacia* strain J2315 (MIC > 256 μg/mL) which contains a non-synonymous mutation in *dfrA*, the target of trimethoprim (174).

12-bis-THA particles as a monotherapy showed varying antimicrobial activity against the panel. *B. multivorans* and *B. cepacia* were moderately susceptible to 12-bis-THA and had MIC's that were similar to those for *B. thailandensis* (2 – 8 μg/mL). *B. gladioli* was the most susceptible species to 12-bis-THA and had an MIC of 1 μg/mL. *B. cenocepacia* strains were the least susceptible to 12-bis-THA and had MIC's ranging from 8 – 32 μg/mL.

The rifamipin and trimethoprim combinations showed limited activity against the clinical panel whereas the tobramycin combination retained activity against 9/12 strains. The lack of trimethoprim and rifampin potentiation by 12-bis-THA particles may indicate that: (1) 12-bis-THA particles do not act synergistically with these antimicrobials against BCC strains; (2) 12-bis-THA particles do not act synergistically at the tested ratio. This could be investigated by performing checkerboard assays to investigate if 12-bis-THA particles synergise with these antimicrobials against BCC strains.

Burkholderia species, particularly those in the BCC, have a propensity to remodel their LPS through reduced or ablated production of the LPS O-antigen or components of the inner core oligosaccharide (218) which may give rise to variable susceptibility to membrane active molecules. The inner core oligosaccharide of LPS is essential for *in vitro* resistance to polymyxin B in both *B. pseudomallei* (219) and *B. cenocepacia* (220). In contrast, the loss of the O-antigen does not affect susceptibility of *B. cenocepacia* to polymyxin B (220) but increases the susceptibility of *B. pseudomallei* strains to polymyxin B (221). Studies by Montis *et al* showed that 12-bis-THA particles and polymyxin B had a similar binding affinity to LPS (5.1 µM and 0.5 µM respectively) (manuscript in preparation). An NMR study showed that the positively charged nitrogen group of the 12-bis-THA headgroup interacted with the GlcN-A LPS subunit which exhibits a negative charge as it is located next to a phosphate group. It is difficult to understand from the current BCC data if the LPS chemotype correlated with 12-bis-THA particle susceptibility as these strains are from different species which exhibit different genotypes. To investigate the effect of LPS chemotype, MICs and CLSM could be performed using a series of deep rough mutants which are derived from the same parental strain (222).

CHAPTER 4 - INTERACTIONS BETWEEN 12-BIS-THA PARTICLES AND *B. THAILANDENSIS* BIOFILMS

4.1 INTRODUCTION

Biofilms are clinically important, surface-attached bacterial communities that are encapsulated within a self-produced extracellular polymeric substance (EPS). Published data suggest that biofilms are implicated in 80% of microbial infections (223). These bacterial communities are highly resistant to antimicrobial therapy (224) and disinfectants (225) and are associated with disease persistence and relapse (226). However, the role of biofilm formation is not clear in relapse and pathogenicity in BCC species as no biofilm biomass was observed in 21 explanted lungs from individuals with CF that were colonised by a member of the BCC (445). In contrast, there is compelling evident which suggests biofilms may play a role in the relapse of melioidosis as clinical isolates with a propensity to form biofilms *in vitro* was correlated with relapse following the completion of treatment (227).

Biofilm formation is comprised of four steps. Firstly, planktonic bacteria reversibly attach to a surface using flagella and pili-based motility. Such genes were highly expressed in a high-biofilm forming strain of *B. pseudomallei* strain UM6 (228). Genome-wide mutagenesis of *B. pseudomallei* strain Bp82 identified 59 genes involved in biofilm formation including 9 encoding flagella involved in motility and chemotaxis, and several fimbriae genes with likely roles in attachment (229). This is generally considered the most 'druggable' stage of biofilm formation as the bacterial attachment is reversible. Next, as the bacteria repress their motility functions they multiply and produce an EPS to form a microcolony that is irreversibly attached to the surface. The EPS is comprised of exopolysaccharides, lipids, proteins, and extracellular DNA (eDNA), which facilitates the attachment to a surface and structural stability of the biofilm (230,231). Thirdly, the microcolony undergoes maturation which is mediated by quorum sensing. Bacteria coordinate an increase in the production and export of EPS components. In *B. thailandensis,* mutations in quorum sensing genes prevented biofilms from forming three-dimensional, dome-like structures which is a characteristic of mature biofilms (232). As the biofilm matures and grows, it develops gradients of nutrients and oxygen which can affect the growth of bacteria at the base or within the core of the biofilm as these nutrients are scarce. To alleviate this, water channels are formed to facilitate solute transport throughout the biofilm (233). Finally, once matured, biofilms undergo shedding whereby bacteria are dispersed from the surface of the biofilm to restart the cycle as planktonic bacteria that may disseminate to other niches to perpetuate the infection.

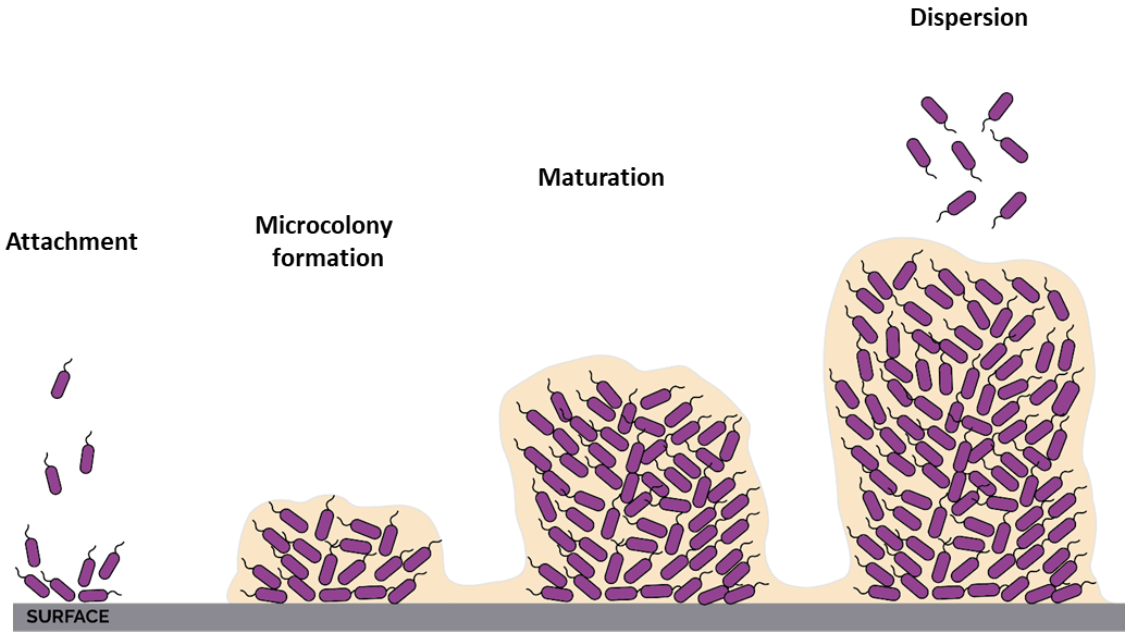

Figure 4.1: The process of bacterial biofilm formation. (1) Bacteria reversibly attach to a surface. (2) Once attached, the biofilms form microcolonies that are encapsulated within a self produced matrix. At this point the bacteria are irreversibly attached. (3) Bacteria within the biofilm proliferate and the biofilm matures and grows. (4) Bacteria on the surface are shed to colonise niches elsewhere. Image adapted from reference (396).

B. pseudomallei and *B. thailandensis* biofilms are highly resistant to antimicrobials because of a combination of several factors (234). The relative conditions of starvation throughout the structure of the biofilm gives rise to multiple populations of bacteria that exhibit different levels of metabolic activity. An example is persister cells. As they are dormant, they tolerate antimicrobials that target active processes but can reactivate, potentially once therapy has eradicated other cells in the biofilm, maintaining the infection. Persister cells have been studied in *B. pseudomallei* and are induced by nutrient starvation, exposure to sub-inhibitory concentrations of antimicrobials including trimethoprim, or anaerobiosis (235–237). *B. pseudomallei* persisters are tolerant to a range of antimicrobials including the clinically important antimicrobial ceftazidime (238). This implies that there may be a role for persister cells in the relapse of melioidosis following treatment. Additionally, the physical and chemical properties of the EPS can form a substantial barrier to antimicrobial compounds and increase the effective doses needed for biofilm eradication. In *B. pseudomallei* biofilms the EPS has been shown to influence the penetration of clinically relevant

antimicrobials ceftazidime and imipenem (239). Similarly, the EPS of BCC biofilms can reduce the efficacy of tobramycin (240) and also protect bacterial cells from phagocytosis and reactive oxygen species produced by the host immune system (241).

There are other potential antimicrobial resistance mechanisms displayed by bacteria within biofilms however published data in *B. pseudomallei* is inconclusive or suggest that it may not be essential in this species. For example, the increased expression of efflux pumps during biofilms formation in other species, such as *E. coli* and *P. aeruginosa*, has been associated with EPS export influencing cell aggregation and biofilm maturation, export of quorum sensing molecules, and the extrusion of antimicrobials and harmful metabolic products (242). Proteomic analysis of samples of biofilm formed by *B. thailandensis* showed that efflux components predominantly decreased in abundance in mature *B. thailandensis* biofilms (243). This implies that efflux pumps may not play a central role in the reduction of antimicrobial susceptibility in *B. thailandensis* biofilms. Changes to the hydrophobicity and structure of the LPS layer in Gram-negative bacteria also influences biofilm formation (244). Modifications to the LPS have also been associated with decreased susceptibility to antimicrobials in planktonic cells suggesting a potential link between biofilm formation, LPS chemotype, and antimicrobial resistance (245). However, Sawasdidoln *et al* have shown that the LPS chemotype did not correlate with the antimicrobial resistance of *B. pseudomallei* in biofilms (234). In summary, the literature suggests that *B. thailandensis* and *B. pseudomallei* biofilms are more resistant to their planktonic counterparts due to the sequestration of antimicrobials by the EPS matrix and through the formation of tolerant persister cells.

High doses of antimicrobials are needed to eradicate recalcitrant biofilms. However, at high doses they can exact non-specific activity resulting in damage to the host microbiota, potentially leaving patients susceptible to secondary infections, in addition to system toxicity (246). Considerable research is ongoing in the field of nanomedicine to identify nanomaterials that are either have antimicrobial activity or are capable of encapsulating antimicrobials to improve delivery and offset toxicity. Research has shown that the physical properties of nanomaterials influence their ability to interact with biofilms. An important characteristic is the surface charge of a particle as positively charged particles (247,248) more readily interact, penetrate and diffuse through a biofilm compared to negative or neutrally charged particles and liposomes (248,249).

Considering this, bola-amphiphiles are a promising class of molecule that could be useful in forming nanomedicines to counter bacterial biofilms. Both 12-bis-THA particles and other bola-amphiphiles studied by Hegarty *et al* demonstrated effective encapsulation efficiency of oligonucleotide antimicrobials that were protected from enzymatic degradation. Once loaded with

TFD antimicrobials, 12-bis-THA particles retain a slight cationic charge which may facilitate biofilm interactions and lead to the delivery of oligonucleotide cargo to bacteria within the biofilm. 12-bis-THA particles loaded with the oligonucleotide antimicrobial TFD were well tolerated when delivered topically and have shown *in vivo* efficacy against *Clostridium difficile* and *Enterobacteriaceae* in the gut while sparing the rest of the microbiota (132,139).

In the previous chapter, it has been shown that 12-bis-THA particles cross the capsule and membrane of *B. thailandensis* E555 to accumulate in the bacterial cytoplasm and have an MIC of 2 - 8 µg/mL. Due to the cationic nature and its ability to deliver TFD oligonucleotide cargo to Gram-negative bacteria, and its synergy with other antimicrobials, this chapter will investigate:

- The antimicrobial activity of 12-bis-THA particles and different antimicrobial combinations against mature *B. thailandensis* E555 biofilms
- The ability of 12-bis-THA particles to deliver TFD cargo to bacterial cells within a biofilm

4.2 RESULTS

4.2.1 Establishing the growth conditions for the MBEC assays

To test the antimicrobial activity of 12-bis-THA particles as a sole therapy and in combination with different antimicrobials against *B. thailandensis* strain E555 biofilms, it was necessary to establish the appropriate biofilm growth conditions for the Calgary biofilm device. To date, there is no standardised growth media for producing biofilms therefore we compared the biofilm biomass and bacterial density of E555 biofilms grown in two nutrient-rich media, CAMHB and LB, and one minimal medium (MVBM) following incubation at 37^{o}C for 24, 48 or 72 h. For each growth condition and time point, the cell density was measured for two pegs, similarly, biomass determination was performed on two pegs using crystal violet staining.

At 24 h, the biofilms grown in LB and CAMHB had similar levels of bacterial density. At the same time point, there was less growth of biofilms produced in MVBM. Similar observations were made at 48 h where the biofilms grown in LB and CAMH displayed comparable bacterial densities however the biofilm grown in LB had a lower biomass compared to the biofilm grown in CAMH. In contrast, biofilms grown in MVBM for 48 h were similar to those produced after 24 h. At 72 h, biofilms grown in CAMHB had the greatest biomass compared to LB and MVBM (**Figure 4.2A**). Despite the broad range of biomasses observed, no significant difference between bacterial densities was observed when comparing the growth media across the time points. This implies that biofilms are established at 24 h and are stable up to 72 h.

Biofilms that had grown for 24 h in LB or CAMHB displayed a higher biofilm biomass and bacterial density than those grown in MBVM. This could make it challenging to investigate the antimicrobial activity of compounds against biofilms as it would be difficult to distinguish if a high MBEC value relative to the traditional MIC is representative of biofilm mediated resistance or simply due to a higher starting inoculum (MIC assay starting inoculum - 5 x 10^5 CFU/mL). Therefore, MVBM was selected as the growth media for the MBEC studies as biofilms grown for 24 h in this medium had a bacterial density of approximately 10^6 CFUs/peg. By doing so, this allows for the comparison between the MICs determined in **Chapter 3** with the MBEC values measured below.

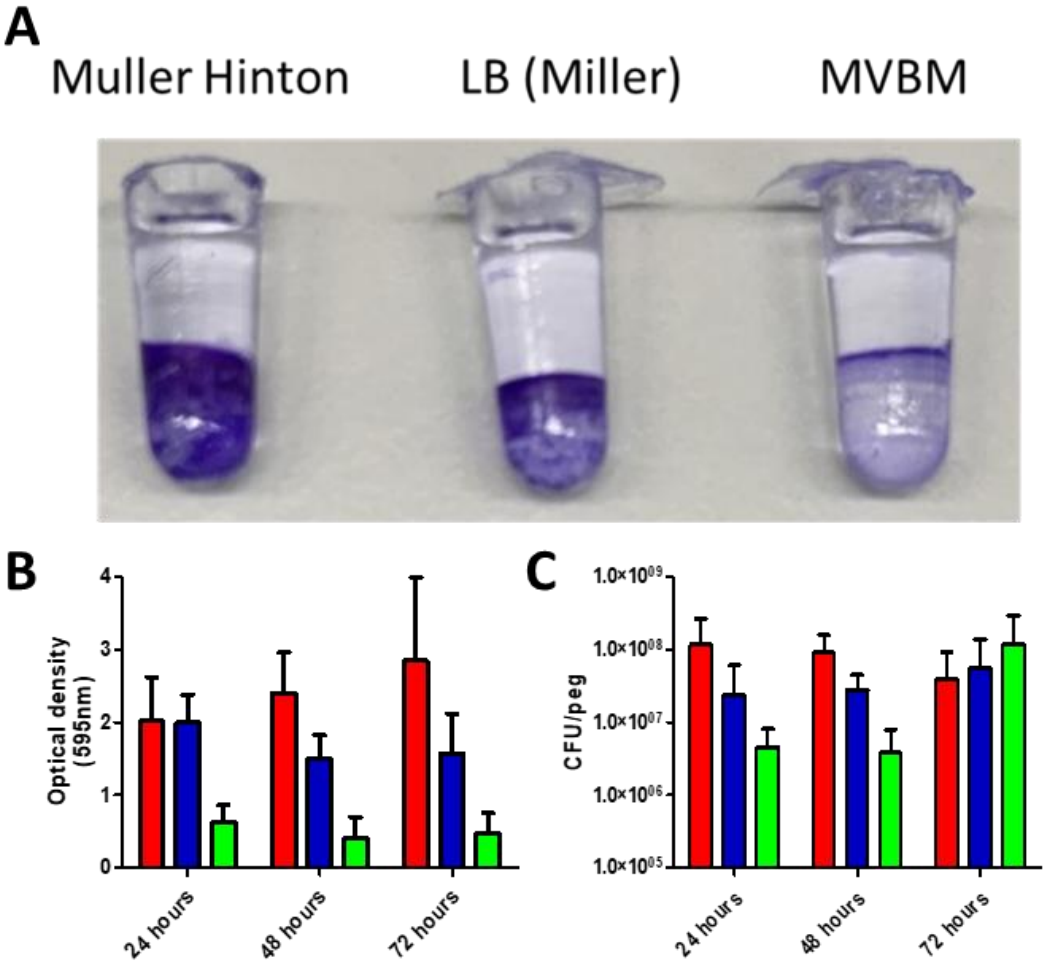

Figure 4.2: Establishing the biofilm growth conditions for the MBEC studies. (**A**) Photograph of *B. thailandensis* strain E555 biofilms grown on the Calgary biofilm device for 72 h. (**B**) Biofilm biomass of *B. thailandensis* strain E555 biofilms in CAMHB (red), LB (blue), or MVBM (green) that had been quantified using 2% crystal violet. (**C**) Bacterial density of biofilms represented as colony-forming units per. The data is representative of 2 independent experiments and the error bars show standard deviation.

4.2.2 Investigating antimicrobial activity against *B. thailandensis* strain E555 biofilms

The antimicrobial activity of 12-bis-THA particles and antimicrobials against *B. thailandensis* E555 biofilms were tested using the Calgary biofilm device which is a standardised assay for examining biofilms. $MBEC_{50}$ values were calculated using non-linear regression analysis to establish the concentration of a compound that reduced the biofilm biomass by 50% relative to the untreated control. The MBEC data showed that Co-trimoxazole (CoTMP), an important antimicrobial used in the treatment of melioidosis, reduced the biomass of *B. thailandensis* biofilms to below 50% at all concentrations tested and it was therefore not possible to calculate an $MBEC_{50}$ value (**Figure 4.3**). Trimethoprim (TMP), which is a component of CoTMP, showed moderate activity against *B. thailandensis* biofilms with an $MBEC_{50}$ value of 0.81 µg/mL (**Figure 4.3**). 12-bis-THA particles also exhibited moderate activity against *B. thailandensis* biofilms with an $MBEC_{50}$ value of 2.17 µg/mL. Higher concentrations of rifampin (Rif) and tobramycin (Tob) were required to reduce the biomass of *B. thailandensis* biofilms at relatively higher concentrations with $MBEC_{50}$ values of 53.32 µg/mL and 100.90 µg/mL respectively (**Figure 4.3**). Interestingly, biofilms increased in biomass when incubated with low concentrations of 12-bis-THA particles (1 µg/mL) or Rif (0.25 – 2 µg/mL) suggesting that they may have a stimulatory effect.

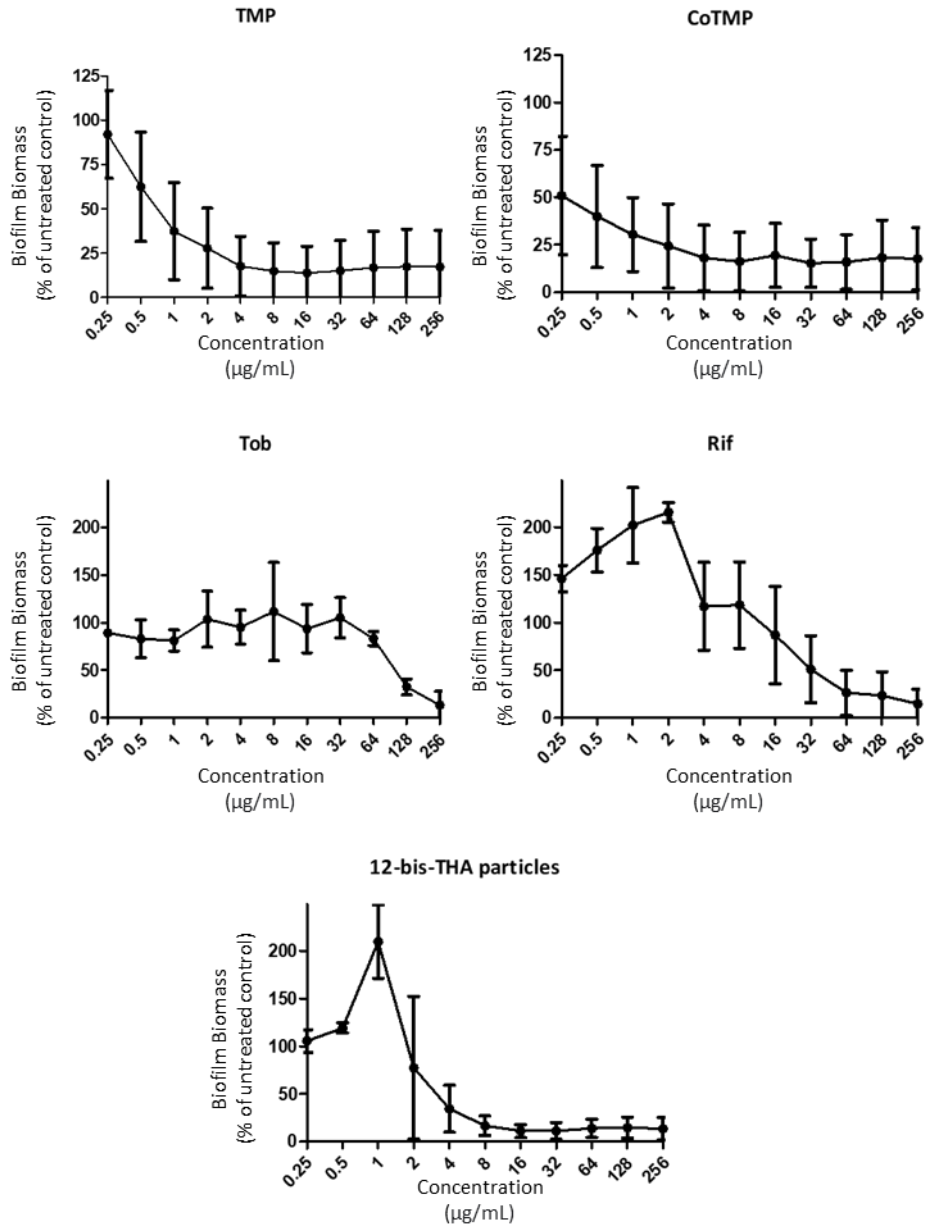

Figure 4.3: Activity of antimicrobials and 12-bis-THA particles against *B. thailandensis* strain E555 biofilms. Biofilms were formed using the Calgary biofilm deviced and tested for 24 h before crystal violet staining and quantification. The values shown are relative to the untreated control. $MBEC_{50}$ values were calculated using Graphpad Prism to perform hill slope non-linear regression. The data are representative of 2 independent experiments and the error bars show standard deviation.

The data in **Figure 4.3** showed that Rif and Tob displayed poor antimicrobial activity against *B. thailandensis* E555 biofilms. We have previously demonstrated that these antimicrobials act synergistically with 12-bis-THA particles against planktonic *B. thailandensis* (**Chapter 3**). Therefore, we investigated whether the combination of these agents with 12-bis-THA particles could improve their antibiofilm activity. To do so, we mixed Rif or Tob with 12-bis-THA particles in a 3:1 ratio as outlined in **Chapter 3**. For example, 128 µg/mL of CoTMP:12-bis-THA particles contained 128 µg/mL of CoTMP and 42.7 µg/mL of 12-bis-THA particles.

The CoTMP: 12-bis-THA particles combination showed the best antimicrobial activity against the *B. thailandensis* biofilms, reducing them to below 50% of the untreated control. As with CoTMP evaluated alone, it was not possible to calculate an $MBEC_{50}$ value as all recorded values were less than 50% and no regression could be calculated (**Figure 4.4**). The TMP: 12-bis-THA particles combination showed moderate antimicrobial activity against *B. thailandensis* biofilms and had an $MBEC_{50}$ value of 3.59 µg/mL (**Figure 4.4**). However, the $MBEC_{50}$ value of TMP alone was lower than the $MBEC_{50}$ value of TMP: 12-bis-THA particles which might occur if 12-bis-THA particles stimulate biofilm formation at low concentrations. The Tob: 12-bis-THA particles and Rif: 12-bis-THA particles combinations demonstrated similar antimicrobial activity against *B. thailandensis* biofilms with values of 7.34 µg/mL and 4.74 µg/mL respectively (**Figure 4.4**). Both Tob and Rif combinations showed better antimicrobial activity when compared to Tob and Rif alone (**Figure 4.3**).

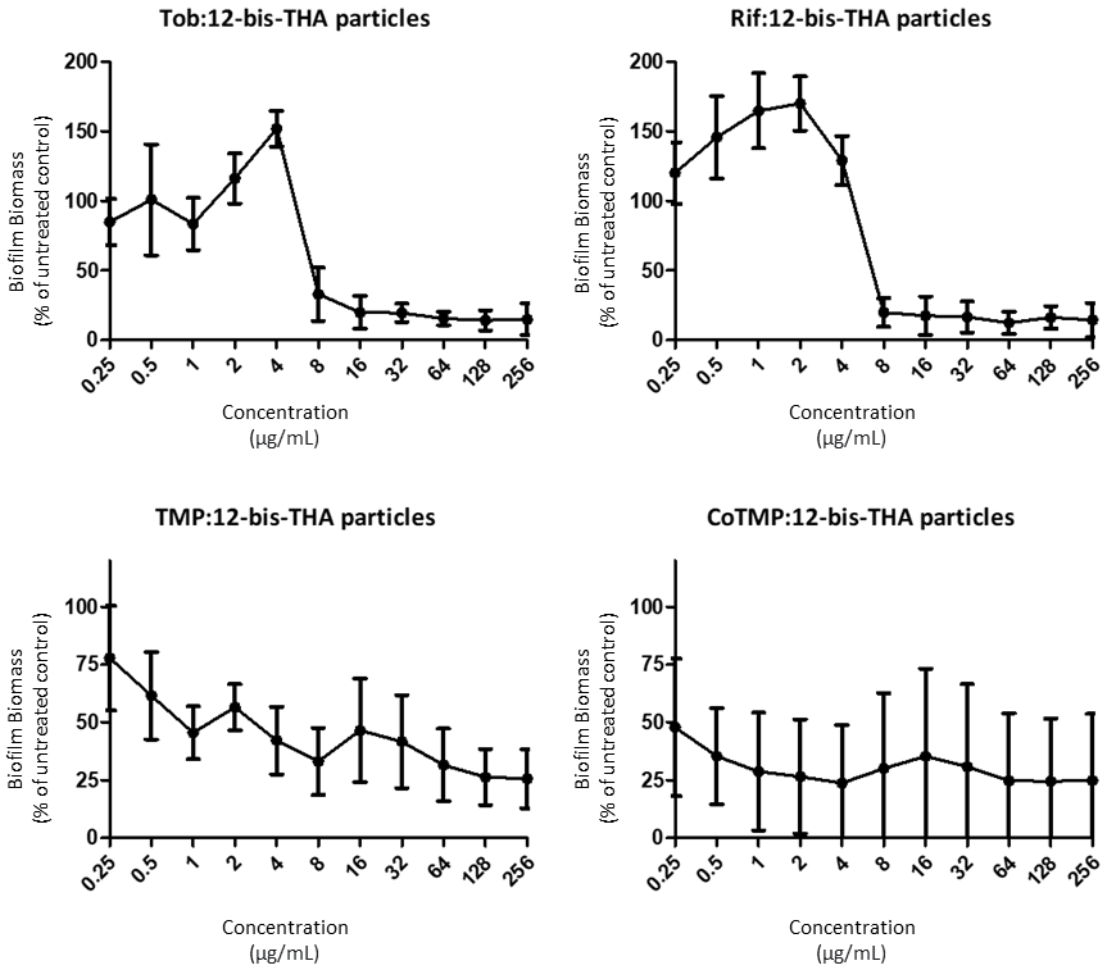

Figure 4.4: Activity of synergistic combinations against *B. thailandensis* E555 biofilms. Biofilms were formed using the Calgary biofilm and tested for 24 h before crystal violet staining and quanitifcation. The values shown are relative to the untreated control. $MBEC_{50}$ values were calculated using Graphpad Prism to performed hill slope non-linear regression. Data are representative of 2 independent experiments and error bars show standard deviation.

The Calgary biofilm device can also be used to investigate the pMIC which is the minimum concentration of a compound that prevents biofilm shedding. This is observed in the wells of the treatment plate following the antimicrobial challenge and the pMIC is the lowest concentration that inhibited visible planktonic growth within the well. **Table 4.1** shows the pMIC of the compounds tested against the *B. thailandensis* biofilms compared to previously determined MIC values. The MIC and pMIC of CoTMP, TMP, 12-bis-THA particles, Tob, and all combinations tested were within one dilution of each other. In contrast, Rif showed a 2 to 16-fold increase in inhibitory concentration when comparing the MIC and pMIC however this may occur as the MICs were performed in a different culture media to the pMIC's (CAMHB and MVBM respectively).

$MBEC_{50}$ values were also compared to the pMIC and MIC of antimicrobial compounds. The $MBEC_{50}$ of TMP was lower than both its MIC and pMIC. The $MBEC_{50}$ for 12-bis-THA particles (2.17 µg/mL) was comparable to its MIC and pMIC values which were 2-8 µg/mL and 2-4 µg/mL, respectively. The $MBEC_{50}$ of Tob was 110.90 µg/mL was also comparable to its MIC (128-256 µg/mL) and pMIC (128 µg/mL). Rif had an $MBEC_{50}$ of 53.32 µg/mL which was higher than its MIC (16-32 µg/mL) but lower than its pMIC (64-256 µg/mL).

Table 4.1: Comparison of MIC and pMIC of antimicrobials, 12-bis-THA particles, and antimicrobials against *B. thailandensis* strain E555. MIC data are representative of at least 3 independent experiments, and the MBEC and pMIC data are representative of 2 independent experiments.

Compound	**MIC (μg/mL)**	**pMIC (μg/mL)**	**$MBEC_{50}$ (μg/mL)**
Co-trimoxazole	2-4	2-4	-
Trimethoprim	8-16	4-8	0.81
12-bis-THA particles	2-8	2-4	2.17
Tobramycin	128-256	128	110.90
Rifampin	16-32	64 - 256	53.32
Tobramycin: 12-bis-THA particles	4-8	8	7.34
Rifampin: 12-bis-THA particles	2-4	8	4.74
Trimethoprim: 12-bis-THA particles	2	4	3.59
Co-trimoxazole: 12-bis-THA particles	1	2	-

4.2.3 Microscopic analysis of *B. thailandensis* strain E555 biofilms expressing RFP

Confocal laser scanning microscopy was used to investigate how 12-bis-THA particles, either alone or loaded with fluorescently labelled TFD, or rhodamine-TFD conjugates would interact with *B. thailandensis* E555 RFP biofilms. Firstly, a time-course study was performed to investigate the thickness of *B. thailandensis* E555 biofilms grown on microscope slides in MVBM supplemented with 50 µg/mL of chloramphenicol for 24, 48, and 72 h. The thickness of the resultant biofilms was measured following imaging using a Zeiss LSM 800 and data analysis was performed on subsequent Z-stack experiments using Zeiss Blue software.

The images of the biofilms at the three-time points are shown in **Figure 4.5** with the top-down view and the Z-stack to assess the three-dimensional structure. At 24 h the biofilms displayed a honeycomb-like structure with a thickness of 3 - 4 µm (**Figure 4.5**) which has previously been observed before in *B. thailandensis* and *B. pseudomallei* (250). By 48 h, this structure was lost as the biofilms became thicker (measured at 6 - 8 µm) and more uniform at the air-surface interface. At 72 h biofilms displayed three-dimensional structures which are characteristic of mature biofilms. Analysis of biofilms at 72 h showed that the depth of these structures ranged between 13 and 22 µm. For studies investigating interactions between 12-bis-THA particles and biofilms, it is important that the biofilms are mature enough to visualise both interactions at the surface of the biofilm but also within the body of the biofilm. Therefore, for the biofilm penetration studies, we used biofilms grown for 72 h in MVBM to investigate if 12-bis-THA particles could penetrate biofilms to deliver oligonucleotide TFDs to cells within.

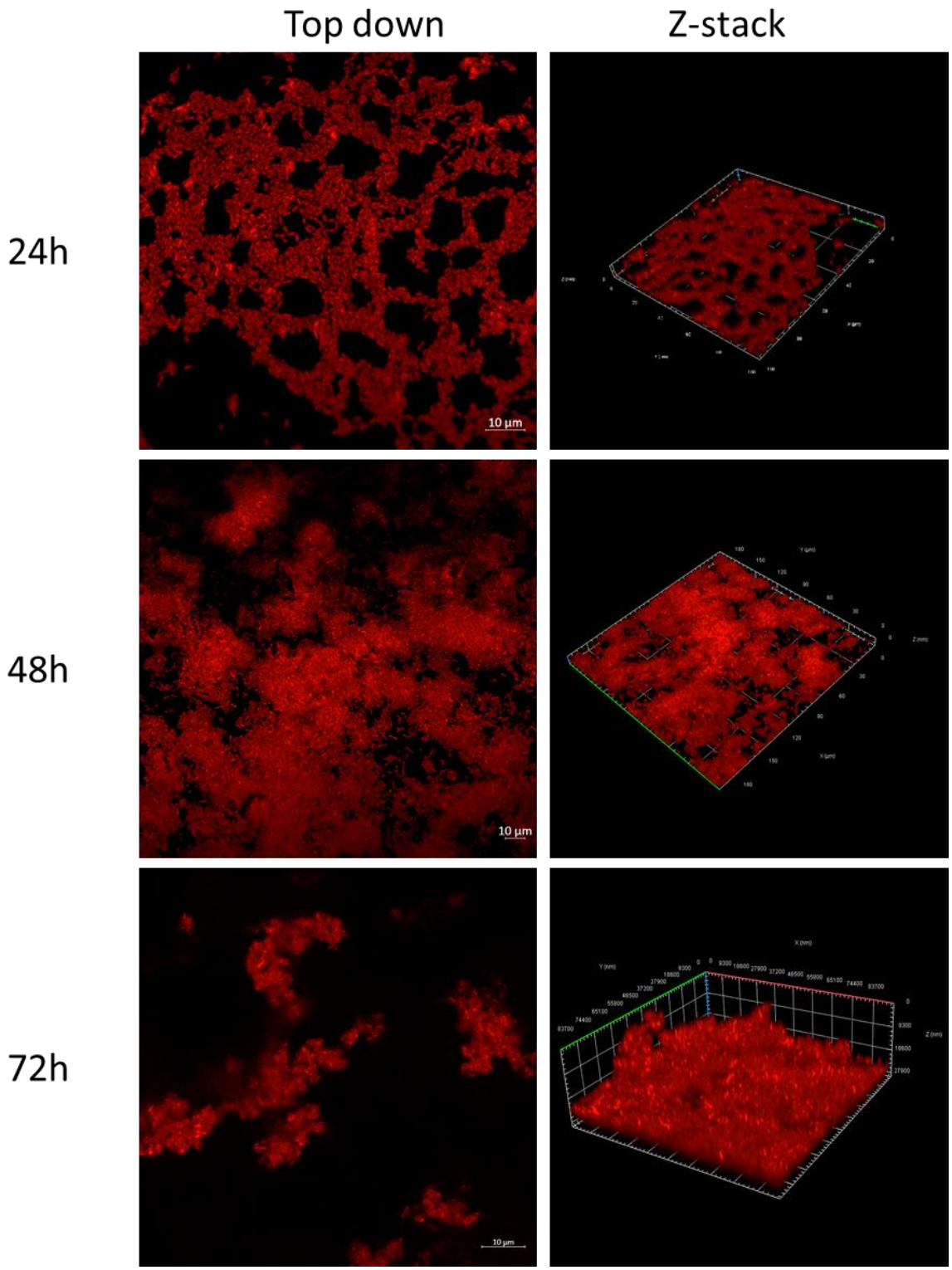

Figure 4.5: Growth kinetics of *B. thailandensis* strain E555 expressing RFP in MVBM supplemented with 50 µg/mL of chloramphenicol. Images were recorded at 24, 48, and 72 h using a Zeiss LSM 800 confocal microscope. Biofilm Z-stacks were captured using 1 µm slices and the thickness was quantified by Zeiss Blue software. Images were representative of a single independent experiment and 5 fields of view per slide. Scale bars show 10 µm.

4.2.4 Assessing interactions between empty 12-bis-THA particles and *B. thailandensis* strain E555 biofilms.

B. thailandensis was grown for 72 h in MVBM to generate biofilms which were then challenged with 50 µg/mL of 12-bis-THA particles for 15, 30, or 60 minutes. This concentration was used as the particles were detectable and although above the $MBEC_{50}$ the short duration of the experiment reduced the likelihood that damage to the biofilm structure would occur. CLSM imaging was used to determine how particles interacted with the mature biofilm and whether they were able to penetrate the biofilms. To detect the 12-bis-THA particles the 405 nm laser was used, and the particles were observed in the blue channel. By merging with the signal from the constitutively expressed RFP in the bacterial cells in combination with Z-stack analysis it was possible to determine whether the 12-bis-THA particles were located on the surface of the biofilm or had to any extent penetrated it.

The micrographs resulting from the time course are shown in **Figure 4.6**. The top-down view of the red (RFP), blue (12-bis-THA particles) and merged image are shown, alongside the merged images of the Z-stack. The cross-sectional images show that the blue fluorescence extends throughout the biofilm following 15 minutes of incubation (**Figure 4.6**) Similar observations were made in the biofilms challenged for 30 and 60 minutes as the blue fluorescence of the 12-bis-THA particles diffused throughout the biofilm at all time points tested (**Figure 4.6**). No consistent changes in biofilm depth were observed suggesting that 12-bis-THA particles did not uncouple the biofilms from the slide. 12-bis-THA particles may have transfected bacteria on the surface of the biofilm but it is difficult to tell without the use of a membrane stain. Overall, this data shows that 12-bis-THA particles quickly interacts with and penetrates *B. thailandensis* biofilms.

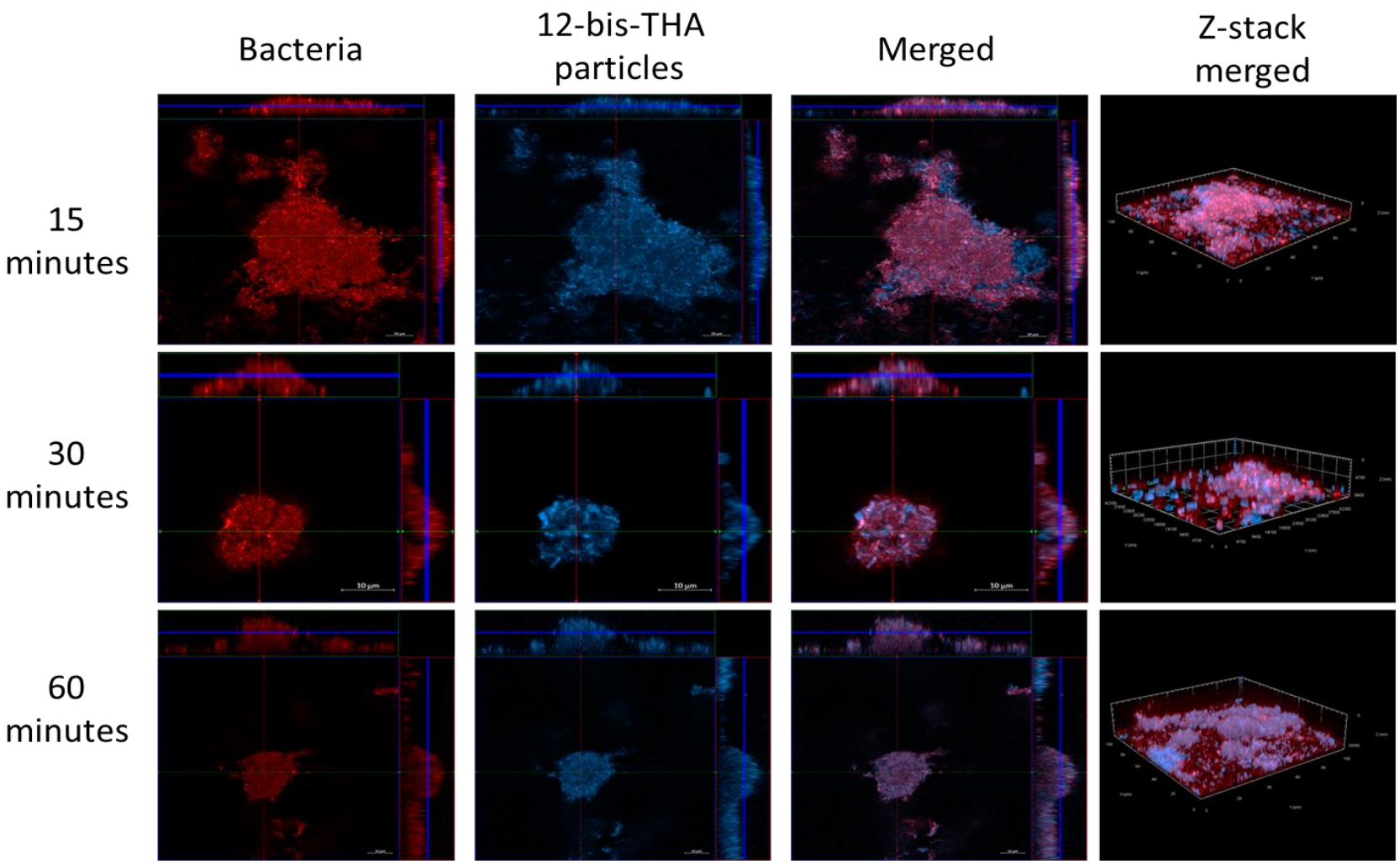

Figure 4.6: Confocal micrographs of *B. thailandensis* E555 RFP 72 h old biofilms incubated with 50 ug/mL of 12-bis-THA particles. Biofilms were incubated with 12-bis-THA particles for 15 minutes, 30 minutes, or 60 minutes. Red and blue is representative of bacteria and 12-bis-THA particles respectively. Images were captured with a Zeiss LSM 800 microscope and represent 5 fields of view from 3 independent experiment. Scale bars show 10 µm.

4.2.5 Assessing interactions between 12-bis-THA particles loaded with TFD and *B. thailandensis* strain E555 biofilms

To investigate if 12-bis-THA particles were a suitable delivery system for oligonucleotide TFDs against *B. thailandensis* biofilms a time course experiment was performed. Biofilms grown for 72 h were challenged with 50 µg/mL of 12-bis-THA particles loaded with 5 µg/mL of fluorescently labelled TFD for 15, 30, and 60 minutes. The RFP-expressing bacteria were observed in the red channel, the Alexa-488 labelled oligonucleotide TFD were observed in the green channel, and the fluorescent 12-bis-THA particles were observed in the blue channel (**Figure 4.7**).

After 15 minutes, the micrographs show that low levels of 12-bis-THA particles loaded with TFD were detected on the surface of the biofilm where they retained their spherical structure (**Figure 4.7**). 12-bis-THA particles (blue) and TFD (green) fluorescence were co-localised suggesting that they remain associated upon interacting with the biofilm (**Figure 4.7**). After 30 minutes the images suggest that the number of loaded 12-bis-THA particles on the surface of the biofilm increased and started to penetrate the biofilm (**Figure 4.7**). Most of the green and blue fluorescence remained co-localised however some diffuse green and blue fluorescence signal was observed which may suggest that the complex is breaking apart. Following 60 minutes of incubation, cross-sectional micrographs showed that loaded 12-bis-THA particles penetrated further into the biofilm (**Figure 4.7**). As with the previous time point, the green and blue fluorescence signals were predominantly co-localised with some diffusion of the signal. This data suggests that 12-bis-THA particles loaded with TFD quickly interact with *B. thailandensis* biofilms where they slowly break apart causing the release of TFD. The current data is inconclusive regarding the location of the free TFD; whether is within the bacterial cell or has otherwise been sequestered by the biofilm matrix.

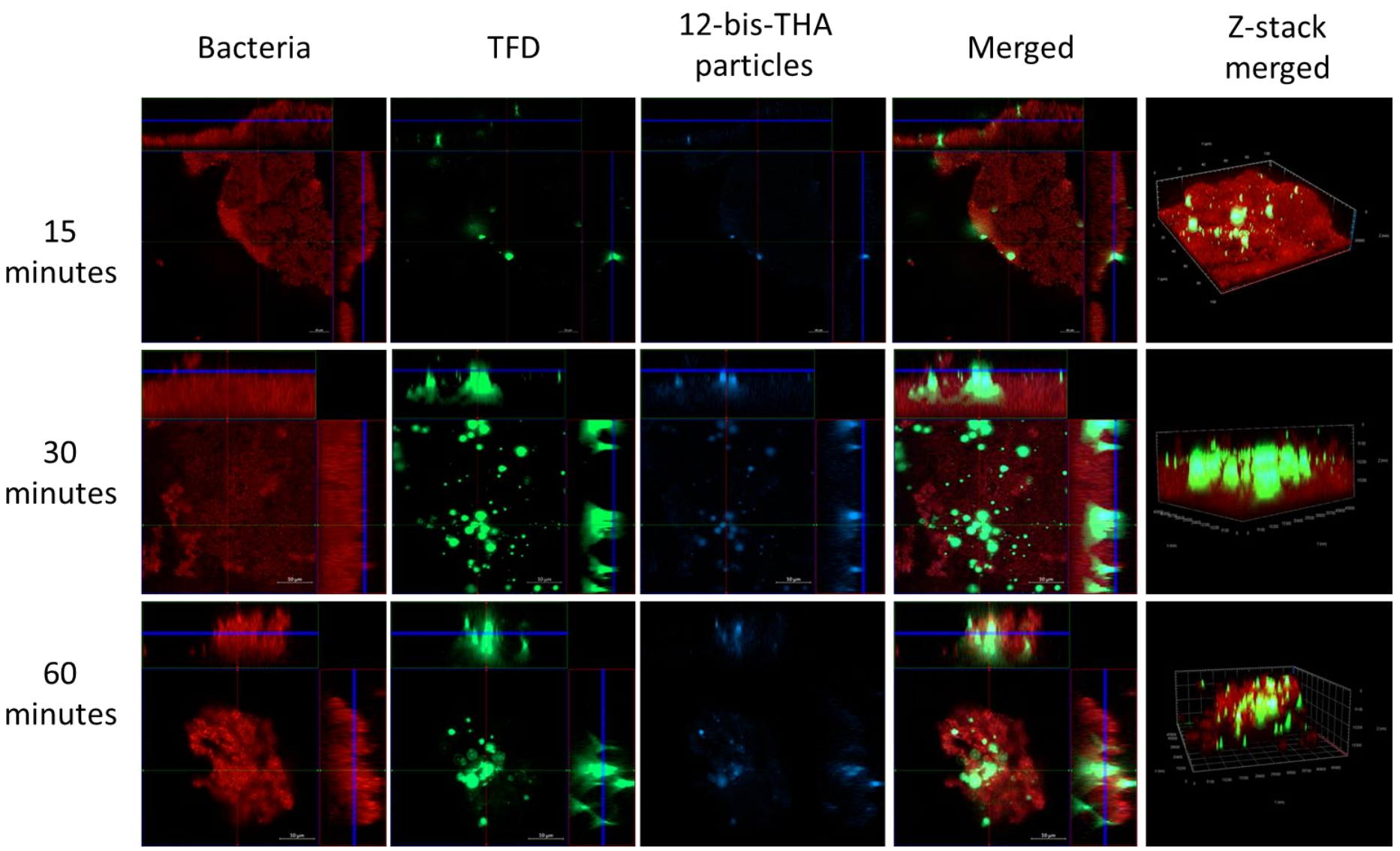

Figure 4.7: Confocal micrographs of *B. thailandensis* strain E555 expressing RFP 72 h old biofilms incubated with 50 ug/mL of 12-bis-THA particles loaded with fluorescently labelled TFD. Biofilms were incubated with 12-bis-THA particles loaded with Alexa-488 labelled TFD 15 minutes, 30 minutes, or 60 minutes. Red, blue, and green are representative of bacteria, 12-bis-THA particles, and TFD respectively. Images were captured with a Zeiss LSM 800 microscope and represent 5 fields of view from 3 independent experiment. Scale bars show 10 µm.

4.2.6 Assessing penetration of TFD-rhodamine conjugates to *B. thailandensis* strain E555 biofilms

Due to the cationic and lipophilic nature of rhodamine, a single rhodamine headgroup conjugated to a TFD may offer an alternative delivery molecule to 12-bis-THA particles (142). Additionally, the fluorescent nature of rhodamine allows us to use our model to determine any interactions between the TFD-rhodamine conjugate and *B. thailandensis* biofilms. Therefore, we investigated if TFD-rhodamine conjugates were capable of delivering TFD to bacterial biofilms. Confocal micrographs show no evidence of interactions between biofilms and TFD-rhodamine conjugates following 15 and 30 minutes of incubation (**Figure 4.8**). However, at 60 minutes, low levels of the conjugates were observed on the surface of the biofilm (marked by white arrows in **Figure 4.8**). No green fluorescence was observed in the body of the biofilm which suggests that the TFD-rhodamine conjugate does not penetrate *B. thailandensis* biofilms following 60 minutes of incubation.

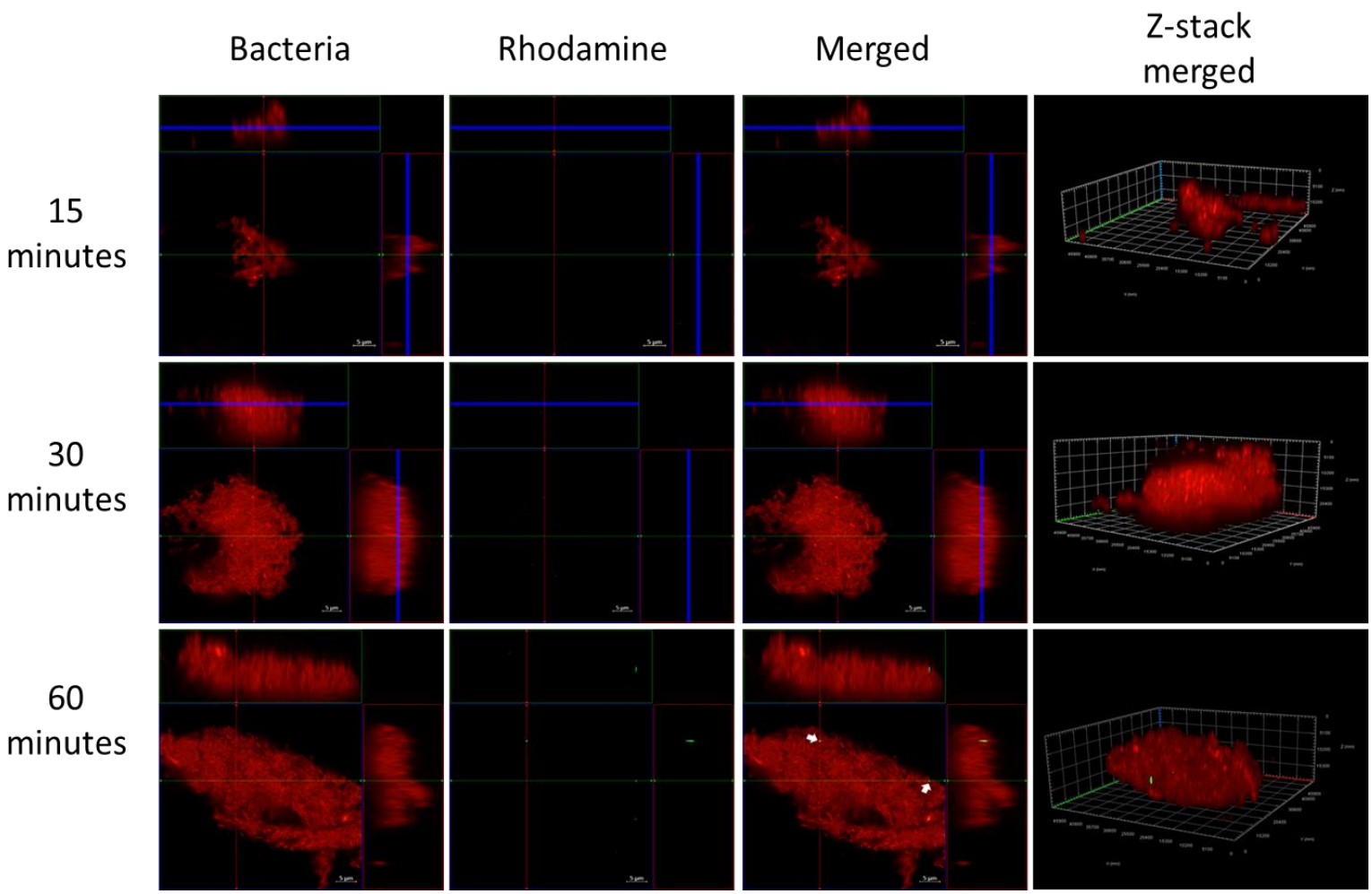

Figure 4.8: Confocal micrographs of *B. thailandensis* strain E555 expressing RFP 72 h old biofilms incubated with 5 µg/mL of rhodamine green Fur TFD conjugate. Biofilms were incubated with TFD-Rhodamine conjugates for for 15 minutes, 30 minutes, or 60 minutes. Red, and green are representative of bacteria and TFD-conjugate, respectively. Images were captured with a Zeiss LSM 800 microscope and represent 5 fields of view from 1 independent experiment. Scale bars show 5 µm.

4.2.7 The physical properties of 12-bis-THA particles alone or loaded with fluorescently labelled TFD

DLS was performed to investigate the physical characteristics of both empty and loaded 12-bis-THA particles. The correlograms of particles formed from (**Figure 4.9A**) 12-bis-THA particles or (**Fig 4.9B**) 12-bis-THA particles loaded with TFD showed smooth curves with a steep intercept suggesting that these particles are homogenous and free from large aggregates. The correlograms were used to calculate the hydrodynamic diameter of the particles using the Stokes-Einstein equation which is expressed as the z-average. Empty 12-bis-THA particles have a z-average of 169.8 $\pm$ 4.3 nm whereas those loaded with TFD had a z-average of 208 $\pm$ 63.3 nm (**Figure 4.9C**) By measuring the polydispersity index of both samples, the data showed that empty 12-bis-THA particles (0.11) were more monodispersed than 12-bis-THA particles with TFD (0.21) suggesting that the latter forms two or more populations of particles that exhibit different diffusion characteristics. As expected, empty 12-bis-THA particles were cationic under these ionic conditions with a zeta-potential value of 35.4 $\pm$ 0.4 mV. In contrast, when loaded with TFD the zeta-potential was 18.8 $\pm$ 0.7 mV which is consistent with the oligonucleotide shielding some of the positive charge of the 12-bis-THA headgroup.

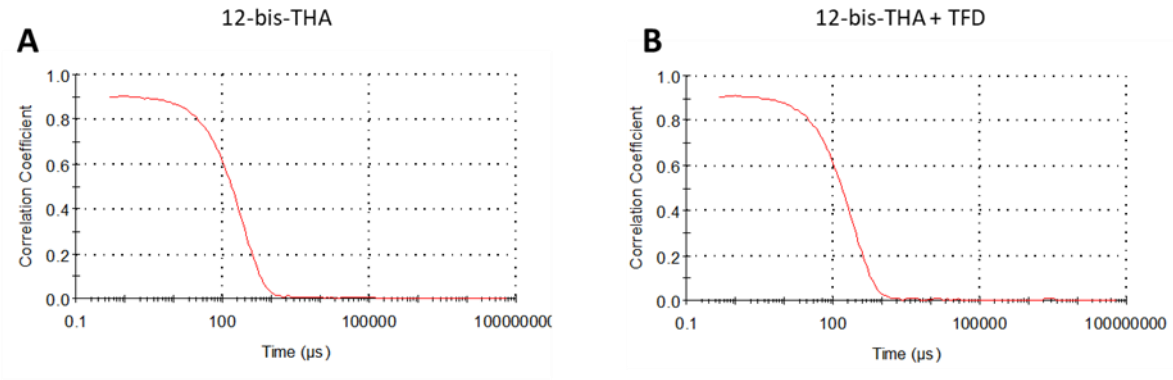

C

Particle	Z-average (nm)	Polydispersity index (pdi)	Zeta-potential (mV)
12-bis-THA particle	169.8 ± 4.3	0.11 ± 0.02	35.4 ± 0.6
12-bis-THA particle + TFD	208.1 ± 63.3	0.21 ± 0.09	18.8 ± 0.7

Figure 4.9: Physical properties of 12-bis-THA particles in water. Correlograms of (**A**) 12-bis-THA particles alone and (**B**) 12-bis-THA particles loaded with 5 µg/mL of TFD. (**C**) The size, polydispersity, derived count rate of 12-bis-THA particles alone or in combination with 5 µg/mL of TFD.

4.2.8 Investigating the antimicrobial properties of compounds against *B. thailandensis* strain E555 biofilms

Before studying the antimicrobial activity of compounds against *B. thailandensis* biofilms, we first investigated the growth conditions required to produce biofilm formation. To do so, we investigated the longitudinal biofilm formation of *B. thailandensis* E555 in two nutrient-rich media (CAMHB and LB) and one minimal media (MVBM). The aim of this was to identify conditions that would stimulate biofilm formation with the resultant biofilm film displaying a bacterial density similar to that found in an MIC assay (5 x 10^5 CFU/mL) to allow for a meaningful comparison of values. The data showed that *B. thailandensis* formed biofilms in all media tested. Those grown in nutrient-rich media showed a greater biomass and bacterial density compared to those grown in minimal media. Biofilms grown in MVBM minimal media had a bacterial density of ~10^6 CFU/peg at 24 and 48 h which increased to ~10^8 CFU/peg at 72 h, and also displayed low (~0.67 $\pm$ 0.2 OD_{595}) but stable biomass across all of the time points. *B. thailandensis* E555 biofilms grown in MVBM for 24 h were taken forward for antimicrobial testing as the bacterial density of these biofilms most closely resembled that starting inoculum of a broth microdilution MIC plate.

Next, we investigated the antimicrobial activity of 12-bis-THA particles alone, 12-bis-THA particles in combination with antimicrobials, and antimicrobials on biofilms grown for 24 h in MVBM using the Calgary biofilm method. The data showed that CoTMP demonstrated the best antimicrobial activity against *B. thailandensis* biofilms. It was not possible to calculate $MBEC_{50}$ values for this compound as the biofilm biomass was reduced below 50% (relative to the untreated control) at the lowest concentration tested. It is unlikely to be an artifact and a result of an undergrown control as all controls grew to an anticipated optical density of approximately 0.6 OD_{600}. Similar observations were made when calculating the $MBEC_{50}$ value of TMP (0.81 μg/mL) which was lower than its MIC (2 – 4 μg/mL). Unlike other findings in this study, the $MBEC_{50}$ values of CoTMP and TMP were lower than the MIC. The reason for this is not fully understood however Pibalpakee *et al* have shown that CoTMP can diffuse through *B. pseudomallei* biofilms unimpeded by the EPS (239). It may be that CoTMP and TMP can exact good antimicrobial activity against *B. thailandensis* biofilms as their penetration is not slowed by the matrix of the biofilm. Alternatively, the mechanism of TMP and CoTMP may be important in their activity against biofilms. Both compounds inhibit folate synthesis which is an essential precursor in DNA synthesis (251). As eDNA is an important component of *Burkholderia* biofilms, these compounds may prevent the production of DNA which could be exported into the EPS resulting in a structurally smaller biofilm or a biofilm

with a different EPS composition (230,231) . This could be further studied using mass spectrometry to determine the composition of biofilms before and after TMP or CoTMP treatment.

Our findings of CoTMP activity against *B. thailandensis* biofilms are considerably different from previously published findings investigating *B. pseudomallei* biofilms. Sawasdidoln *et al* showed that CoTMP had an MBEC of >128 µg/mL (234). Differences in MBEC values may occur due to biological differences between the species. Alternatively, Sawasdidoln *et al* used a different method to record MBEC values where treated biofilms are rinsed in PBS and transferred to a plate containing MHB and grown for 24 h at 37 ^{o}C. Sawasdidoln *et al* defined the MBEC as the absence of bacterial growth when removing the pegs from treatment to nutrient-rich media for 24 h. It is unlikely that the disparity between findings is due to species variation as Anutrakunchai *et al* show similar MIC, pMIC, and MBEC values using this method when comparing *B. thailandensis* and *B. pseudomallei* (252). The method used by Sawasdidoln *et al* defines the MBEC as total chemical sterilisation of the pegs. It is high throughput but low resolution as it does not detect changes in the bacterial density or in the biomass of biofilms following treatment. The differences between our findings and those of Sawasdidoln *et al* is most likely due to methodological differences as both studies measure different endpoints and have different definitions of MBEC. The method used in our study quantifies changes in the biomass of *B. thailandensis* biofilms following treatment using crystal violet staining. This has provided further information on whether compounds can reduce the biomass of biofilms and if they stimulate biofilm formation at sub-inhibitory concentrations. The caveat of this approach is that a reduction in biomass is not representative of changes in bacterial viability and therefore future studies are required to investigate the antimicrobial activity of the $MBEC_{50}$ values when measuring CFUs as an endpoint.

The data in **Figure 4.3** and **4.4** suggests that low concentrations of 12-bis-THA or Rif may stimulate the formation of biofilms in *B. thailandensis*. This phenomenon has been observed in both Gram-negative and Gram-positive species (253). For example, the growth or expansion of *P. aeruginosa* biofilms has been observed in response to aminoglycosides (254) whereas Rif can stimulate biofilm formation in *S. aureus* (255). An increase in biofilm biomass can occur as a non-specific defense mechanism against sub-inhibitory concentrations of antimicrobials possibly due to the increased production of matrix components. eDNA is an important component of bacteria biofilms as it contributes to biofilm structure and adhesion. Ranieri *et al* propose that eDNA may drive biofilm formation at sub-inhibitory concentrations when some of the bacterial cells die resulting in the release of their cytoplasmic contents (256). Some bacterial species such as *P. aeruginosa* undergo explosive lysis in response to antimicrobials which can result in the release of eDNA into the extracellular milieu (257). Oxidative stress has also been shown to stimulate biofilm

formation in multiple bacterial species (258–260) and may be driven through the initiation of the stringent stress response by the secondary messenger molecule c-di-GMP (261). In *Burkholderia* species, eDNA is an important component of the biofilm formation which facilitates the initial attachment of biofilms to a surface and later act as a scaffold supporting the three-dimensional structure of the biofilm (230,231). 12-bis-THA particles may reduce biofilm biomass by binding to the eDNA and displacing it causing the biofilm to disconnect from the surface. Exporting more eDNA by *B. thailandensis* may prevent biofilm uncoupling from occurring at low concentrations of 12-bis-THA particles. In addition, the proteomic data set (**Chapter 5**) showed an increase in the abundance of oxidative stress proteins. Whilst no change in the proteins involved with the stringent response was observed, *B. thailandensis* may increase biofilm production in response to drug stress independently of c-di-GMP signalling.

The different combination therapies showed modest antimicrobial activity against *B. thailandensis* biofilms. The CoTMP combination showed the greatest antimicrobial activity of the combinations tested. Like CoTMP alone, the $MBEC_{50}$ of CoTMP: 12-bis-THA particles was incalculable as biofilm biomass was below 50% at the lowest concentration tested which was 0.25 μg/mL. The TMP combination also demonstrated good activity with an $MBEC_{50}$ of 3.59 μg/mL which was higher than TMP alone (0.81 μg/mL) and more similar to 12-bis-THA particles alone (2.17 μg/mL). The Tob: 12-bis-THA particles and Rif: 12-bis-THA particles combinations showed modest activity with $MBEC_{50}$ values of 7.34 μg/mL and 4.74 μg/mL, respectively. It is unclear if the synergy between the 12-bis-THA particles and the antimicrobials is retained against *B. thailandensis* biofilms.

The antimicrobial activity of CoTMP:12-bis-THA particles and CoTMP was similar suggesting that there was no synergistic effect by combining the treatments however this was at the lower end of the tested concentrations. Further studies are required to investigate changes in bacterial density in response to the combinations to establish whether the compounds retain the synergistic effect observed in **Chapter 3**. Despite inconclusive data regarding potential interactions between the two compounds the data showed that low concentrations of CoTMP:12-bis-THA particles did not cause an increase in biofilm biomass at the concentrations tested unlike 12-bis-THA particles alone. Conversely, the TMP:12-bis-THA particle combination showed an increase in $MBEC_{50}$ when compared to TMP alone. The 12-bis-THA particles component was at 1.20 μg/mL at the $MBEC_{50}$ concentration of TMP: 12-bis-THA particle (3.59 μg/mL). The increase in $MBEC_{50}$ for TMP:12-bis-THA particles when compared to TMP alone (0.81 μg/mL) may occur if low concentrations of 12-bis-THA particles stimulated biofilm growth. It is therefore unclear if TMP and CoTMP affect the biomass of biofilms by preventing DNA synthesis and concomitant export of eDNA to the EPS.

Further investigations are required to determine the EPS composition following treatment with these compounds.

Rif: 12-bis-THA particles and Tob: 12-bis-THA particles combinations had $MBEC_{50}$ values of 4.74 μg/mL and 7.34 μg/mL, respectively, and showed greater activity when compared to their monotherapies. However, it is unclear whether this is synergy or demonstrates antimicrobial activity of 12-bis-THA which would be present 1.58 μg/mL or 2.45 μg/mL in the $MBEC_{50}$ concentrations of Rif:12-bis-THA particles and Tob:12-bis-THA particles. Interactions between 12-bis-THA particles and antimicrobials could be studied by treating mature biofilms with $MBEC_{50}$ concentrations of the synergy combinations alongside the calculated concentrations of the monotherapies. For example, to investigate synergy between Rif and 12-bis-THA particles biofilms would be incubated with 4.74 μg/mL of Rif: 12-bis-THA particles, 4.74 μg/mL of Rif alone, or 1.58 μg/mL of 12-bis-THA particles alone. After 24 h, the CFUs/peg could be determined to allow for the comparison of treatments. As with the time-kill studies in **Chapter 3**, synergy could be defined as a >2 log_{10} reduction in CFUs relative to the most active monotherapy.

Using the Calgary biofilm method, we also identified the concentrations of each compound that inhibited the shedding of *B. thailandensis* biofilms which is termed planktonic MIC and is referred to as pMIC. There was considerable overlap between the pMICs of most compounds tested and their MICs which had been previously determined using the broth microdilution method. This is consistent with findings by Anutrakunchai *et al* who only identified a difference in the MIC and pMIC of doxycycline in *B. thailandensis* and *B. pseudomallei* from a panel of clinically relevant antimicrobials (252). In comparison, Khan *et al* demonstrated that the pMIC of TMP was 1000-fold higher than the MIC in *B. thailandensis.* Our data showed no difference in the pMIC and MIC of TMP against *B. thailandensis* (4-8 μg/mL and 8-16 μg/mL, respectively) (243). This could be due to methodological difference as Khan *et al* grew biofilms for 24 h in nutrient-rich media and likely had a greater bacterial density compared to our biofilms grown in minimal media. Our data showed that the pMIC of rifampin was up to 8-fold higher than its MIC. Isogenic bacterial biofilms are known to be highly heterogenic and contain persister cells that are metabolically and transcriptionally dormant. A release of a subpopulation of persister cells into the media containing rifampin may account for an increase in pMIC. Alternatively, dispersal of the biofilm containing viable bacteria and biofilm matrix may cause an increase in optical density resulting in an artificial increase in pMIC.

4.2.9 12-bis-THA particles as a delivery molecule for TFD against biofilms.

Bacteria within a biofilm are resistant to antimicrobials due to multiple factors. One is that the EPS matrix provides a physical barrier that limits drug penetration by either slowing its diffusion or preventing the drug from reaching the bacteria. Therefore, we used confocal microscopy to investigate if empty 12-bis-THA particles or loaded with TFD were able to penetrate *B. thailandensis* biofilms and accumulate in bacterial cells. To do so, we firstly investigated the conditions required to grow mature *B. thailandensis* biofilms for imaging. Multiple studies have shown that *Burkholderia* species including *B. cenocepacia* (262,263)*, B. pseudomallei* (264)*,* and *B. thailandensis* (252) grow biofilms on glass slides and coverslips. In our study, biofilms were grown on poly-d-lysine coated microscopy slides in MBVM media supplemented with 50 µg/mL of chloramphenicol for 24, 48, and 72 h. A genetically modified strain of *B. thailandensis* E555 expressing red fluorescent protein was used to visualise bacterial structures using CLSM. The data showed that *B. thailandensis* biofilms increased in-depth in a time-dependent manner. At 72 h the biofilms were between 13 and 22 µm deep and exhibited three-dimensional structures that were consistent with those observed in the literature (446, 447). This suggests that *B. thailandensis* biofilms grown for 72 h are a suitable model to test interactions between 12-bis-THA particles (alone or loaded with TFD cargo) against *Burkholderia* biofilms.

Mature *B. thailandensis* biofilms were challenged with 50 µg/mL of 12-bis-THA particles alone, 50 µg/mL of 12-bis-THA particles loaded with 5 µg/mL of fluorescent TFD, or 5 µg/mL of a TFD-rhodamine conjugates Biofilms were incubated with these treatments for 15, 30, or 60 minutes before imaging to determine time-dependent changes. In all cases, regardless of treatment, the biofilm depth did not consistently change suggesting that the compounds did not cause uncoupling from the slide through the displacement of anionic EPS components (i.e eDNA). Microscopy images showed that empty 12-bis-THA particles rapidly penetrated the *B. thailandensis* biofilm as blue fluorescence was observed to span the depth of biofilms at all time points. In contrast, 12-bis-THA particles loaded with TFD interacted with the biofilm in a time-dependent manner. Following 15 minutes, loaded 12-bis-THA particles interacted with the surface of the biofilm whereas, at 30 and 60 minutes, the loaded 12-bis-THA particles proceeded to penetrate the biofilm. Interestingly, 12-bis-THA particles loaded with TFD retained their three-dimensional, particulate structure both on the surface and within the biofilm, unlike 12-bis-THA particles alone which were observed as a diffuse signal. This may imply that 12-bis-THA particles loaded with TFD penetrate the biofilm as a particle that proceeds to slowly dissociate unlike 12-bis-THA alone which may break apart upon entering the biofilm.

Rhodamine is an amphiphilic, potentiometric dye that has previously been shown to deliver pDNA to mitochondria (142). TFD-rhodamine conjugates have also been shown to have good transfection capability in *E. coli* and *P. aeruginosa.* Therefore, we investigated whether TFD-rhodamine conjugates were capable of penetrating *B. thailandensis* biofilms. Confocal micrographs showed that TFD-rhodamine conjugates did not interact with the biofilms at 15 and 30 minutes and only weakly interacted with the surface of the biofilm at 60 minutes. No penetration of TFD into the biofilm was observed at any time point. This may occur as the DNA oligonucleotide component holds multiple negative charges which are masked when combined with 12-bis-THA particles. Rhodamine may be insufficient at masking the charge with the resulting molecule exhibiting a net anionic charge which has been shown to slow or even prevent biofilm penetration (266).

The limited resolution makes it challenging to determine whether the 12-bis-THA particles or the TFD is within the cytoplasm of bacteria or the EPS. Some evidence suggests that 12-bis-THA particles, when given alone, are internalized by bacteria on the surface of the biofilm after 30 minutes. No evidence of TFD transfection, either delivered by 12-bis-THA particles or the rhodamine group, was observed at any of the time points. The images did show that the loaded 12-bis-THA particles penetrated and diffused within the main body of the biofilm slower than empty 12-bis-THA particles. It would be interesting to determine the location of both 12-bis-THA particles and TFDs to understand which EPS component could be limiting TFD transfection. For example, eDNA may limit the transfection of 12-bis-THA particles due to its polyanionic charge. Interactions between these could be observed by staining biofilm eDNA with the fluorescent stain TOTO-3 and measuring co-localisation (230). Alternatively, cationic polysaccharides in the EPS may sequester and prevent TFD transfection. This is challenging when using fluorescence microscopy as lectin stains, which have been used to stain polysaccharides in biofilms, are non-specific and generally give poor resolution (230,262). A potential alternative to this approach is to directly measure the binding of TFD to purified biofilm EPS such as cepacian or eDNA using isothermal titration calorimetry. Additionally, the development of a reporter strain could help determine if the TFD is in the cytoplasm or the extracellular matrix. This could be produced by transforming *B. thailandensis*, which is naturally competent (448), with a plasmid that constitutively expressed a reporter gene such as LacZ (in the presence of Isopropyl ß-D-1-thiogalactopyranoside), or with a reporter plasmids that had been optimised for constitutive expression in BCC species (449).

A clear difference in biofilm penetration was observed when comparing 12-bis-THA particles alone and 12-bis-THA particles loaded with TFD. Therefore, we performed DLS analysis on both combinations to investigated differences in their physical properties. Biofilms generally exhibit a net anionic charge due to EPS components and the negatively charged bacterial membrane.

Therefore, particle charge is an important factor that controls the interactions between nanoparticles and biofilms and cationic molecules are more likely to interact compared to negative and neutrally charged particles (247–249). Li *et al* have shown that neutral and anionic quantum dots (nanoparticles with a diameter between 7.5 and 24 µm) did not interact with *E. coli* biofilms following 1 h of incubation whereas cationic quantum dots both penetrated and diffused within the biofilm (248). The DLS data showed that particles formed of 12-bis-THA particles alone and those loaded with TFD were similar in size (169.8 nm vs 208.1 nm) however 12-bis-THA particles were more positively charged than those loaded with TFD (35.4 mV and 18.8 mV, respectively). Both exhibited a cationic charge which is likely the driving force behind the penetration of *B. thailandensis.* Interestingly, confocal microscopy showed that empty 12-bis-THA particles were diffuse within the biofilm which is comparable to findings by Li *et al*. 12-bis-THA particles loaded with TFD also penetrated the biofilm and diffused although at a lesser extent which may be due to its lower zeta-potential. Size is also a contributing factor when considering the penetration of nanomedicines against biofilms. Forier *et al* have shown that size is the main contributory factor governing the penetration of negatively charged polystyrene particles and liposomes into *P. aeruginosa* and *B. multivorans* biofilms (267). In the case of 12-bis-THA particles it is more likely that charge plays the most significant role in driving biofilm interaction and penetration.

To conclude, 12-bis-THA particles showed promising anti-biofilm activity against *B. thailandensis* E555 biofilms and potentially sensitized the biofilms to tobramycin and rifampin. Penetration studies using confocal microscopy showed that 12-bis-THA particles, alone or loaded with TFD, rapidly interacted and penetrated *B. thailandensis* biofilms however 12-bis-THA particles loaded with TFD showed a lower degree of diffusion. This may occur as loaded particles are less cationic than their empty counterpart. Future studies will explore the biofilm penetration characteristics of 12-bis-THA particles analogues with varying physical properties, such as size, charge, and hydrophobicity, to identify a compound that more readily diffuses through bacteria biofilms.

CHAPTER 5 - MULTI-OMIC ANALYSIS OF THE 12-BIS-THA STRESS RESPONSE IN *B. THAILANDENSIS*

5.1 INTRODUCTION

Empty 12-bis-THA particles demonstrated antimicrobial activity against *B. thailandensis* and BCC species. Their mechanism of action is not fully understood but is believed to be multifarious. Studies by Marín-Menéndez *et al* and Montis *et al* have shown that the internalisation of 12-bis-THA particles and their TFD cargo is driven, at least in part, through electrostatic interactions with the conserved, prokaryote-specific membrane components cardiolipin and lipopolysaccharide (LPS) (132,137). Cardiolipin is an important component of the bacterial inner membrane and mitochondria membrane where it is associated with respiration. It supports the activity of respiratory complexes that are responsible for synthesising adenosine triphosphate (ATP) through oxidative phosphorylation.

Dequalinium is a structurally similar molecule to 12-bis-THA that inhibits respiratory complexes in mitochondria (268) and bacteria (269,270). It has been proposed that dequalinium inhibits bacterial growth by destabilisation of the outer membrane resulting in a loss of enzyme function and the precipitation of nucleic acids (271). The mechanism of action of 12-bis-THA has not been fully characterised but is anticipated to be similar to that of dequalinium. Di Blasio *et al* have shown that 12-bis-THA particles form transient pores within artificial membranes and induce changes in proton motive force (PMF) of the bacterial membrane (138). Additionally, the tricyclic headgroup of the 12-bis-THA monomer intercalates with DNA which is consistent with the proposed mechanism of dequalinium.

In **Chapter 3**, time-kill studies showed that, following incubation of 12-bis-THA particles, *B. thailandensis* regrew at 24 h suggesting that bacteria may adapt and recover. As the mechanism of action is unclear, it is difficult to predict pathways that facilitate this possible adaption. Interestingly, a time-kill study showed that, despite an initial reduction in bacterial density, cultures incubated with tobramycin and 12-bis-THA also regrew by 24 h despite clear synergy at early time points (3 and 6 h). This may suggest that tobramycin and 12-bis-THA share similar adaption mechanisms which may include the overexpression of efflux pumps (272), LPS modifications (273), or shifts in central metabolism (200). The purpose of 12-bis-THA particles is to act as a delivery platform for TFD antimicrobials to the bacterial cytoplasm where they selectively inhibit the target transcription factor. There is particular interest in adaption mechanisms that involve the regulation of bacteria membrane components as the loss or modification of these may result in a reduction in the ability of 12-bis-THA particles to deliver TFD.

Untargeted 'omic approaches such as transcriptomics, proteomics, and metabolomics are useful techniques to assess global biological changes in response to stimuli. For example, RNA-seq is

used to measure changes at an mRNA level in response to stimuli (274,275). RNA-seq is a powerful technique that gives broad coverage and is sensitive to subtle changes in mRNA transcript levels. However, a potential issue of this technique is that it is not completely representative of a phenotype as not all mRNA is translated into protein (276). Alternatively, NMR based metabolomics methods can be used to measure global changes in the concentration of cytoplasmic (fingerprint) (147) and extracellular (footprint) metabolites (277). This can be associated with a phenotype, however, this approach may not be useful on its own as it provides little insight into the pathways associated with the identified metabolic products. Proteomic methods such as label-free quantification (LFQ) and isobaric tagging provide insight into changes at a protein level which can be more closely associated with a phenotype compared to RNA-seq and identify which pathways are induced. Untargeted proteomics methods have their own drawbacks as they have lower coverage than RNA-seq. Additionally, LFQ methods do not identify changes in protein activity but rather their abundance.

In this chapter, LC-MS/MS based proteomics and NMR based metabolomics were utilised to provide insight into the mechanism of action of 12-bis-THA against *B. thailandensis* E555 to address the following questions:

- Do 12-bis-THA particles inhibit bacterial respiratory chains like its parental molecule dequalinium?
- Are antimicrobial resistance pathways induced by 12-bis-THA particles?
- Do 12-bis-THA particles induce pathways associated with membrane changes?

5.2 RESULTS

5.2.1 12-bis-THA particles delay the growth of mid-log *B. thailandensis* cultures

Mid-log phase cultures of *B. thailandensis* were incubated with 0.1X MIC (0.8 µg/mL) and 1X MIC (8.0 µg/mL) of 12-bis-THA particles and grown for a further 2.5 h (**Figure 5.1**). No significant difference in growth was observed between untreated bacteria and those challenged with 0.1X MIC of 12-bis-THA particles. Bacteria challenged with 1X MIC of 12-bis-THA particle demonstrated a significant delay in growth at 1 ($p = <0.05$) and 2 ($p = <0.01$) h post-exposure however, there was no significant difference at 2.5 h.

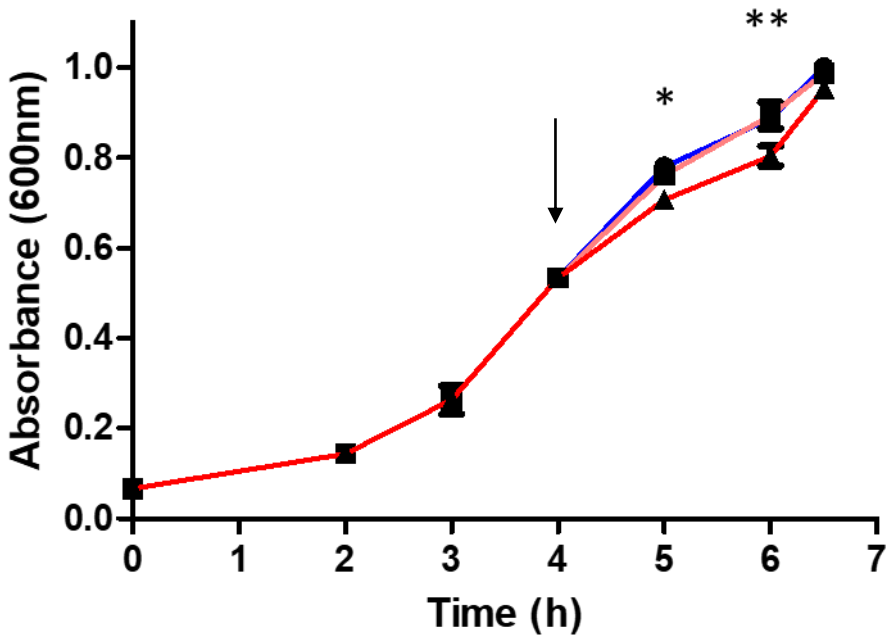

Figure 5.1: The impact of 12-bis-THA on mid-log cultures of *B. thailandensis* E555. Blue, pink and red lines represent untreated cultures or those incubated with 0.1X MIC (0.8µg/mL) or 1X MIC (8.0 µg/mL) of 12-bis-THA particles respectively. The time point marked with the arrow represents the addition of 12-bis-THA particles. Error bars show standard deviation and statistical significance was determined using a two-way ANOVA with a Bonferroni post-hoc test where *P < 0.05 and **P < 0.01. Data shows 3 independent replicates.

5.2.2 Processing, visualisation, and statistical analysis of the proteomic data set

To investigate the mechanism of action of 12-bis-THA particles on *B. thailandensis*, the proteomes of bacteria that had been incubated with water (hereafter termed untreated), 0.1X MIC, or 1X MIC of 12-bis-THA particles were analysed by the Bristol proteomics facility using TMT labelled MS3 proteomic analysis. Mass spectra were assigned to the appropriate protein using Proteome Discoverer. For this step, the mass spectra were mapped to the *B. thailandensis* strain E264 Uniprot database as the *B. thailandensis* E555 database was incomplete at the time of analysis. A total of 3150 *B. thailandensis* proteins were identified from a total of 5565 proteins giving a 56.6% proteome coverage.

Data visualisation and statistical analysis were performed on the Proteome Discoverer outputs using Perseus. Imputation was performed on the *B. thailandensis* proteomic data sets and is a technique that is used when proteins are identified in some technical replicates but not others. Histograms show data that are present in the proteomics data set in blue and missing values in orange (**Figure 5.2**). The low levels of orange within **Figure 5.2** indicates a low amount of missing data when comparing biological and technical replicates of the proteomic data set.

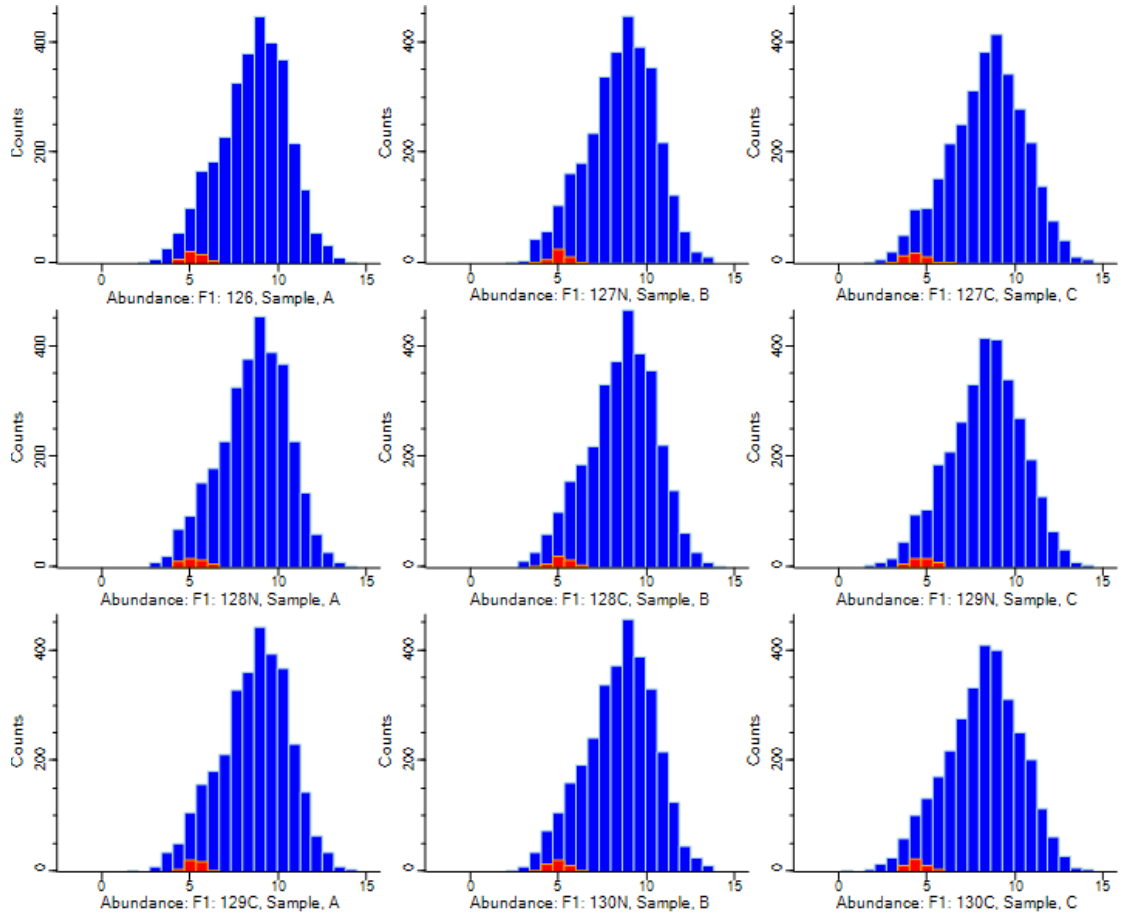

Figure 5.2: Imputation of missing values in the proteomics data set. Data present are plotted in blue whereas missing values that were computationally generated are plotted in orange. Imputation of missing values and generation of histograms was performed by Perseus.

Principal component analysis (PCA) plots were generated to assess the similarity of the proteomics data sets (**Figure 5.3**). The PCA plots show that the proteomics data sets separate into three distinct groups based on their growth conditions. The proteomes of bacteria incubated with 1X MIC of 12-bis-THA particles clustered far from untreated bacteria and those treated with 0.1X MIC of 12-bis-THA particles. The proteomes of bacteria challenged with 0.1X MIC of 12-bis-THA particles or those that were incubated with water clustered closely together. This suggests that 1X MIC of 12-bis-THA particles induces a stronger change in protein abundance compared to 0.1X MIC of 12-bis-THA particles when compared with the water control.

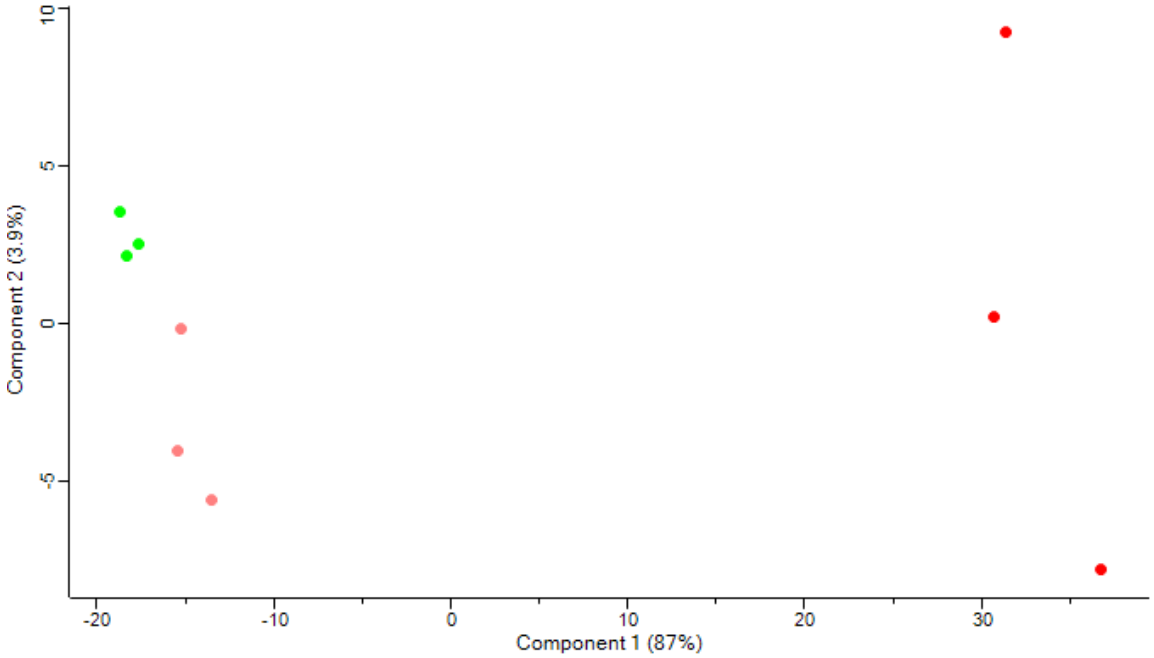

Figure 5.3: Principal component analysis (PCA) plots of the proteomics data set. Green dots represent the proteomes of untreated *B. thailandensis* whereas the pink and red dots represent the proteomes of bacteria incubated with 0.1X MIC 12-bis-THA particles or 1X MIC of 12-bis-THA particles respectively. PCA plots were generated using Perseus.

Multi-scatter plots were produced to investigate the reproducibility of data generated from individual replicates (**Figure 5.4**). The plots shows that proteins found in different independent experiments of the same treatment group were highly reproducible as they exhibited high Spearman's rank correlation values ($\geq$ 0.995). A high degree of similarity was observed between the proteomes of untreated bacteria and those challenged with 0.1X MIC of 12-bis-THA particles ($\geq$ 0.991) however this was slightly reduced when comparing the proteomes of untreated bacteria with those treated with 1X MIC of 12-bis-THA particles ($\leq$ 0.910). Additionally, similar Spearman rank correlation values were observed when comparing the proteomes of bacteria treated with 1X MIC of 12-bis-THA particles to those treated with 0.1X MIC of 12-bis-THA particles ($\leq$ 0.922). The multi-scatter plots show similar findings to the PCA plot which suggest that the proteomes of untreated bacteria and those treated with 0.1X MIC of 12-bis-THA particles are highly similar. A slightly lower correlation was observed in those treated with 1X MIC of 12-bis-THA particles suggesting substantial changes in protein abundance.

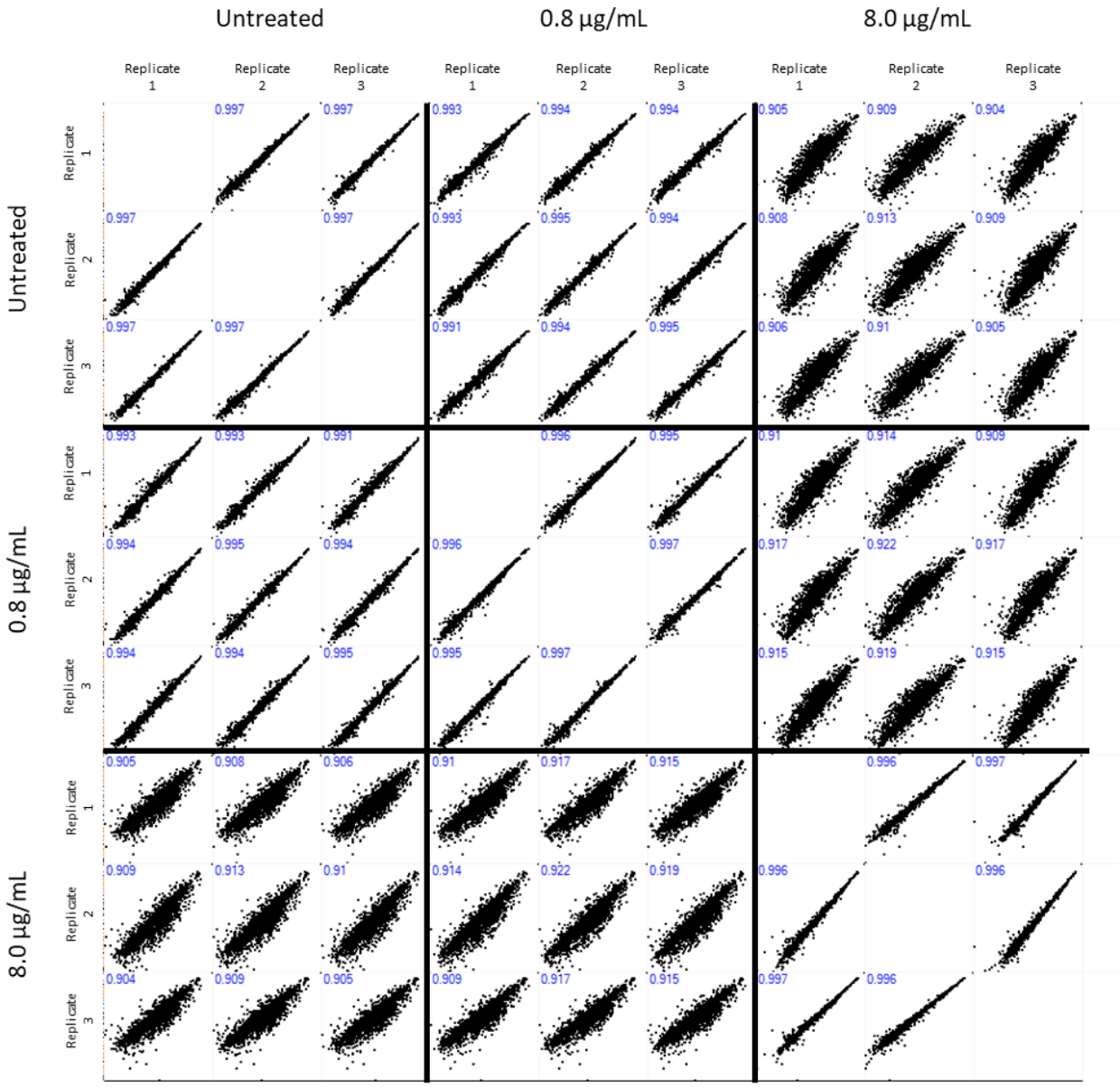

Figure 5.4: Multi-scatter plots of all proteomic data sets showing the correlation between technical and independent experiments. Numerical values are representative of Spearman's rank correlation values which were calculated using Perseus.

Perseus was used to determine significant changes in protein abundance which were visualised using volcano plots (**Figure 5.5**). Significance was determined using a two-sample t-test followed by the Bonferroni post-hoc test to limit the number of false-positive data points and a false detection rate (FDR) of 0.01 and an S0 value of 1 was used. These robust statistical parameters were selected to ensure strong confidence in the findings of the proteomics assay.

No significant changes in protein abundance were identified when comparing the proteome of *B. thailandensis* strain E555 treated with 0.1X MIC of 12-bis-THA particles with the untreated control (**Figure 5.5A**). This is consistent with the growth curve (**Figure 5.1**) which showed no difference between the bacteria incubated with 0.1X MIC of 12-bis-THA particles compared to the untreated group at any time point. Additionally, the PCA plot (**Figure 5.3**) and the multi-scatter plot (**Figure 5.4**) showed that the proteomes of these two groups are highly similar.

In contrast, 139 proteins increased in abundance and 671 proteins decreased in abundance when comparing the proteomes of *B. thailandensis* strain E555 incubated with 1X MIC of 12-bis-THA particles with the untreated control (**Figure 5.5B**). This is consistent with the growth curve which showed that 1X MIC of 12-bis-THA particles significantly delayed the growth of mid-log cultures of *B. thailandensis* for 2 h (**Figure 5.1**) in addition to the variation observed in the PCA (**Figure 5.3**) and multi-scatter plots (**Figure 5.4**).

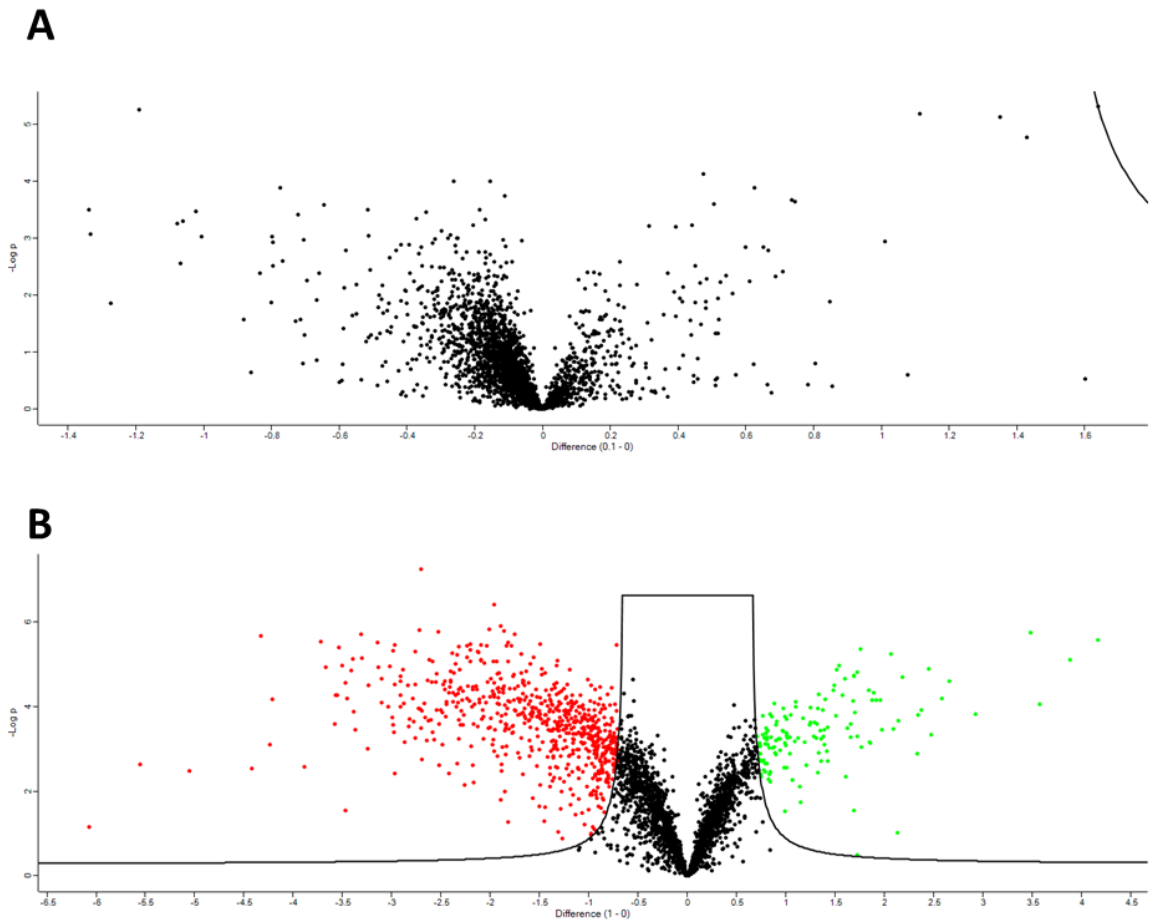

Figure 5.5: Volcano plots showing changes in protein abundance in *B. thailandensis* following incubation with 12-bis-THA particles. (**A**) shows the proteome of bacteria treated with 0.1X MIC of 12-bis-THA particles compared to the untreated control. (**B**) shows the proteome of bacteria treated with 1X MIC of 12-bis-THA particles compared to the untreated control. Data points in green represents a significant increase in protein abundance whereas data points in red show a significant reduction in protein abundance. Fold change significance was determined using FDR of 0.01 and an S0 value of 1.

5.2.3 12-bis-THA particles induce a shift in central metabolism from sugar to fatty acid metabolism

The proteomic data set was manually interrogated to identify pathways that were differentially abundant in response to 12-bis-THA particles compared to the untreated control. All data showing changes in the protein abundance is recorded on a Log_2 scale. **Table 5.1** shows that 12-bis-THA particles caused changes in the abundance of proteins of central metabolism. Four proteins involved in glycolysis were identified and two significantly decreased in abundance (BTH_II0415: -1.25-fold, BTH_I1085: -0.96-fold). In addition, four proteins involved in β-oxidation were identified and all increased in abundance (BTH_I0564: 1.69-fold, BTH_I0565: 1.89-fold, BTH_I0566: 1.57-fold, BTH_I0567: 1.00-fold). Several proteins involved with the tricarboxylic acid (TCA) cycle had increased in abundance in response to 1X MIC of 12-bis-THA particles. α-ketoglutarate dehydrogenase (SucAB) were both significantly increased by 0.89-fold. Components succinyl coenzyme A synthetase (SucCD) were increased 0.46-fold and 0.47-fold however these were not significant as this was below the cut-off for minimum fold change. AceA and AceB, which are enzymatic components of the glyoxylate cycle, were identified with AceA which deceased in abundance 1.33-fold. AceB also deceased in abundance 0.62-fold however this was also below the minimum fold change cut-off for significance.

Table 5.1: Changes in the abundance of proteins associated with central metabolism identified in the *B. thailandensis* proteomics data set. Fold changes in bold represent statistical significance using the volcano statistics FDR - 0.01 and S0 - 1.

				Fold change (Log_2)	
	Accession number	**Protein name**	**Gene**	**0.1X MIC**	**1X MIC**
Glycolysis	Q2SYG4	Phosphoglucomutase	BTH_I1489	-0.16	-0.39
	Q2T884	6-phosphofructokinase	BTH_II0415	0.04	**-1.25**
	Q2SZ59	Phosphoglycerate mutase	BTH_I1243	0.17	0.36
	Q2SZL1	Phosphoglycerate mutase	BTH_I1085	-0.21	**-0.96**
β-oxidation	Q2T128	acyl-CoA dehydrogenase domain-containing protein	BTH_I0564	0.002	**1.69**
	Q2T125	Enoyl-CoA hydratase	BTH_I0567	0.14	**1.00**
	Q2T127	3-hydroxyacyl-CoA dehydrogenase	BTH_I0565	0.06	**1.89**
	Q2T126	Acetyl-CoA acetyltransferase	BTH_I0566	0.08	**1.57**
TCA cycle	Q2T7J2	Mdh1	BTH_II0658	0.07	-0.03
	Q2T4T8	Mdh2	BTH_II1671	-0.13	**-0.79**
	Q2T7I5	GltA	BTH_II0665	0.06	0.47
	Q2T7J6	AcnA	BTH_II0654	-0.04	0.04
	Q2T0I4	Icd	BTH_I0759	-0.07	0.14
	Q2SVH6	SucA	BTH_I2556	-0.03	**0.89**
	Q2SVH7	SucB	BTH_I2555	-0.08	**0.89**
	Q2T0U7	SucC	BTH_I0646	0.02	0.46
	Q2T0U6	SucD	BTH_I0647	-0.08	0.47
Glyoxylate bypass	Q2SX27	AceA	BTH_I1998	-0.24	**-1.33**
	Q2SX31	AceB	BTH_I1994	-0.13	-0.62

5.2.4 12-bis-THA particles may suppress bacterial respiratory complexes

Changes in glycolysis, beta-oxidation and TCA cycle would likely cause changes in downstream metabolism therefore we interrogated the proteomic data set to identify changes in the abundance of protein subunits from respiratory complexes. Fourteen protein subunits of respiratory complex I, termed NADH dehydrogenase, were identified in the proteomic data however no change in protein abundance was observed in response to either concentration of 12-bis-THA particles. (**Table 5.2**)

Table 5.2: Protein subunits of respiratory complex I (NADH dehydrogenase) identified in the *B. thailandensis* proteomics data set. Fold changes in bold represent statistical significance using the volcano statistics FDR - 0.01 and S0 - 1.

				Fold change (Log_2)	
	Accession number	**Protein name**	**Gene**	**0.1X MIC**	**1X MIC**
Respiratory complex I (Type I NADH dehydrogenase)	Q2SZN5	NuoA	BTH_I1061	-0.14	0.30
	Q2SZN4	NuoB	BTH_I1062	-0.05	0.58
	Q2SZN3	NuoC	BTH_I1063	-0.04	0.35
	Q2SZN2	NuoD	BTH_I1064	-0.02	0.58
	Q2SZN1	NuoE	BTH_I1064	-0.06	0.49
	Q2SZN0	NuoF	BTH_I1066	-0.06	0.57
	Q2SZM9	NADH-quinone oxioreductase	BTH_I1067	-0.05	0.62
	Q2SZM8	NuoH	BTH_I1068	-0.09	-0.26
	Q2SZM7	NuoI	BTH_I1069	-0.13	0.42
	Q2SZM6	NuoJ	BTH_I1070	-0.16	0.58
	Q2SZM5	NuoK	BTH_I1071	-0.30	0.38
	Q2SZM4	NuoL	BTH_I1072	-0.14	0.39
	Q2SZM3	NuoM	BTH_I1073	-0.08	0.18
	Q2SZM2	NuoN	BTH_I1074	-0.16	0.46

Five protein subunits of respiratory complex II (succinate dehydrogenase) were identified in the proteomic data set which showed that respiratory complex II was not affected by 12-bis-THA particles. BTH_II0362 is annotated as succinate dehydrogenase subunit B which contains Fe-S clusters that are reduced by FADH2. BTH_II0362 was the only protein that was differentially abundant and deceased in abundance 1.66-fold following incubation with 1X MIC of 12-bis-THA particles (**Table 5.3**).

Table 5.3: Protein subunits of Respiratory complex II (succinate dehydrogenase) identified in the *B. thailandensis* proteomics data set. Fold changes in bold represent statistical significance using the volcano statistics FDR - 0.01 and S0 - 1.

				Fold change (Log_2)	
	Accession number	**Protein name**	**Gene**	**0.1X MIC**	**1X MIC**
Respiratory complex II (Succinate reductase)	Q2T7J0	succinate dehydrogenase, cytochrome b556 subunit (Likely SdhC)	BTH_II0660	-0.05	-0.09
	Q2T7I9	succinate dehydrogenase, hydrophobic membrane anchor protein	BTH_II0661	-0.16	-0.21
	Q2T7I8	SdhA	BTH_II0662	-0.01	0.11
	Q2T7I7	SdhB	BTH_II0663	-0.02	0.01
	Q2T8D7	succinate dehydrogenase subunit B	BTH_II0362	-0.33	**-1.66**

Three proteins from respiratory complex III (cytochrome c reductase) were identified in the proteomics dataset and all deceased in abundance following incubation with 1X MIC of 12-bis-THA particles (**Table 5.4**). PetA is the protein subunit that contains the Rieske center (278) and deceased in abundance 2.03-fold. Cytochrome c1, the sequential next step in trafficking electrons to cytochrome c, deceased in abundance 1.21-fold following incubation with 1X MIC of 12-bis-THA particles. Cytochrome B, which is responsible for scavenging a second electron from Q to form QH_2, also was significantly deceased in abundance 1.36-fold following incubation with 1X MIC of 12-bis-THA particles.

Table 5.46: Protein subunits of Respiratory complex III (cytochrome c reductase) identified in the *B. thailandensis* proteomics data set. Fold changes in bold represent statistical significance using the volcano statistics FDR - 0.01 and S0 - 1.

				Fold change (Log_2)	
	Accession number	**Protein name**	**Gene**	**0.1X MIC**	**1X MIC**
Respiratory complex III (Cytochrome c reductase)	Q2SUB8	PetA	BTH_I2977	0.04	**-2.03**
	Q2SUB9	Cytochrome B	BTH_I2976	-0.1	**-1.36**
	Q2SUC0	Cytochrome c1	BTH_I2975	-0.13	**-1.21**

Five cytochrome c oxidase proteins were identified in the proteomic dataset and two significantly deceased in abundance following incubation with 1X MIC of 12-bis-THA particles (**Table 5.5**). BTH_I2874 (cytochrome c oxidase subunit I) and BTH_I1786 (cytochrome c oxidase subunit III) are responsible for pumping protons from the cytoplasm to the periplasm and both significantly deceased in abundance 1.26-fold and 2.62-fold, respectively.

Table 5.5: Protein subunits of Respiratory complex IV (cytochrome c oxidase) identified in the *B. thailandensis* proteomics data set. Fold changes in bold represent statistical significance using the volcano statistics FDR - 0.01 and S0 - 1.

				Fold change (Log_2)	
	Accession number	**Protein name**	**Gene**	**0.1X MIC**	**1X MIC**
Respiratory complex IV (Cytochrome C oxidase)	Q2T1G4	Cytochrome c oxidase subunit 1	BTH_I0427	-0.08	-0.07
	Q2SUL3	Cytochrome c oxidase subunit 1	BTH_I2874	-0.20	**-1.26**
	Q2T1G5	Cytochrome c oxidase subunit 2	BTH_I0426	-0.11	0.15
	Q2T1G1	Cytochrome c oxidase subunit III	BTH_I0430	-0.01	-0.26
	Q2SXN1	Cytochrome c oxidase subunit III	BTH_I1786	-0.22	**-2.62**

Twelve protein subunits of ATP synthase were identified in the proteomics data set (**Table 5.6**). ATP synthase subunits c and a are components of the F_0 domain and were not differentially abundant. Unlike the other components of the F_0 domain, ATP synthase subunit b, which is the peripheral stack that holds the F_0 and F_1 domain together, deceased in abundance 3.39-fold following incubation with 1X MIC of 12-bis-THA particles. The F_1 domain is a section of the ATP synthase and is responsible for producing ATP from ADP and inorganic phosphate. All components of the F_1 domain that were identified in the proteomic data set deceased in abundance except for the δ subunit. The α and β subunits deceased in abundance 1.69 and 2.01-fold respectively following incubation with 1X MIC of 12-bis-THA particles. Under the same conditions, the γ and ε subunits deceased in abundance 2.97 and 1.29-fold respectively. The proteomic dataset shows that 12-bis-THA particles cause a decrease in the abundance of ATP synthase subunits that extend into the cytoplasm from the membrane.

Table 5.6: Protein subunits of Respiratory complex V (ATP Synthase) identified in the *B. thailandensis* proteomics data set. Fold changes in bold represent statistical significance using the volcano statistics FDR - 0.01 and S0 - 1.

				Fold change (Log_2)	
	Accession number	**Protein name**	**Gene**	**0.1X MIC**	**1X MIC**
Respiratory complex V (ATP synthase) F_0 domain	Q2T875	ATP synthase subunit c	BTH_II0424	0.02	0.21
	Q2STE4	ATP synthase subunit c	BTH_I3313	-0.17	-0.12
	Q2STE3	ATP synthase subunit a	BTH_I3314	-0.01	-0.43
	Q2T874	ATP synthase subunit b	BTH_II0425	0.04	**-3.39**
	Q2STE5	ATP synthase subunit b	BTH_I3312	-0.14	-0.08
Respiratory complex V (ATP synthase) F_1 domain	Q2STF0	ATP synthase epsilon chain	BTH_I3307	-0.10	0.03
	Q2T879	ATP synthase epsilon chain	BTH_II0420	0.06	**-1.29**
	Q2T872	ATP synthase F1 gamma subunit	BTH_II0427	0.08	**-2.97**
	Q2STE7	ATP synthase subunit alpha	BTH_I3310	-0.01	0.12
	Q2T873	ATP synthase subunit alpha	BTH_II0426	0.11	**-1.69**

	Q2STE9	ATP synthase subunit beta	BTH_I3308	-0.07	0.14
	Q2T880	ATP synthase subunit beta	BTH_II0419	0.05	**-2.01**

5.2.5 12-bis-THA particles induce manganese scavenging pathways

The data in the previous section suggests that 12-bis-THA particles have an effect on respiration which may lead to the formation of reactive oxygen species (ROS). ROS are natural products of respiration therefore bacteria have multiple mechanisms to manage the intracellular levels. The proteomics data set was analysed to investigate if 12-bis-THA particles caused the induction of oxidative stress pathways.

Two Sod family proteins, BTH_I0859 and BTH_I0744 were identified in the proteomics data set (**Table 5.7**) however neither were differentially abundant following incubation with 1X MIC of 12-bis-THA particles. KatG and catalase related peroxidase BTH_I0072 were identified in the proteomic data set (**Table 5.7**). Neither were differentially abundant following incubation with 0.1X MIC of 12-bis-THA particles, however, KatG significantly deceased in abundance 1.39-fold following incubation with 1X MICof 12-bis-THA particles while BTH_I0072 was not differentially abundant. Two AhpC proteins, BTH_II1926 and BTH_I2092, were identified in the proteomics dataset however neither were differentially abundant following exposure to 12-bis-THA particles. DpsA is a non-specific DNA binding protein that is expressed by *Synechococcus* species under oxidative stress conditions (279) and significantly deceased in abundance 1.75 fold following incubation with 1X MIC of 12-bis-THA particles (**Table 5.7**).

Table 5.7: Proteins identified in the *B. thailandensis* proteomics data set that are associated with protection from oxidative stress. Fold changes in bold represent statistical significance using the volcano statistics FDR - 0.01 and S0 - 1.

				Fold change (Log_2)	
	Accession number	**Protein name**	**Gene**	**0.1X MIC**	**1X MIC**
	Q2SWT3	AhpC	BTH_I2092	-0.16	-0.48
	Q2T3X9	AhpC	BTH_II1926	-0.05	-0.30
	Q2T2L6	Catalase-related peroxidase	BTH_I0072	-0.14	-0.37
	Q2SZ20	KatG	BTH_I1282	-0.05	**-1.39**
	Q2T084	Superoxide dismutase Cu-Zn	BTH_I0859	-0.01	0.20
	Q2T0J9	Superoxide dismutase	BTH_I0744	-0.13	-0.1
	Q2SZ21	OxyR	BTH_I1282	-0.11	-0.39
	Q2SZ18	DspA	BTH_I1284	-0.11	**-1.75**

Fifteen proteins that are associated with the type 6 secretion system cluster 2 (T6SS-2) were identified in the proteomics data set and all increased in abundance following incubation with 1X MIC of 12-bis-THA particles (**Table 5.8**). Both TseM and TseZ are responsible for scavenging manganese and zinc and they both increased in abundance 1.76 and 1.83-fold respectively. Type six subunits (Tss) are proteins that make up the needle-like structure. TssM, TssL, TssK, and TssJ increased in abundance 1.39, 1.41, 2.00, and 2.13-fold respectively following incubation with 1X MIC of 12-bis-THA particles. TssA, TssB, and TssC also increased in abundance 1.28, 1.72, and 1.66-fold respectively under the same conditions. VgrG-4a and VgrG-4b increased in abundance 1.96 and 0.84-fold respectively. Hcp, a protein that associates with VgrG to form the tip of the needle-like structure, also increased in abundance 1.33-fold following incubation with 1X MIC of 12-bis -THA particles. ClpV is an ATPase that recycles components of the T6SS-2 and increased in abundance 2.37-fold following incubation with 1X MIC of 12-bis-THA particles. Both TagB and TagAB also increased in abundance 1.42 and 2.92-fold respectively under the same conditions however their function is unknown.

Table 5.87: Identification of manganese scavenging T6SS-2 proteins in the *B. thailandensis* proteomics data set. Fold changes in bold represent statistical significance using the volcano statistics FDR - 0.01 and S0 - 1.

				Fold change (Log_2)	
	Accession number	**Protein name**	**Gene**	**0.1X MIC**	**1X MIC**
Oxidative stress (T6SS-4)	Q2T422	Hypothetical protein (TseM)	BTH_II1883	0.01	**1.76**
	Q2T421	TseZ	BTH_II1884	0.01	**1.85**
	Q2T420	TssM	BTH_II1885	-0.01	**1.39**
	Q2T419	TssL	BTH_II1886	-0.05	**1.41**
	Q2T418	TssK	BTH_II1887	0.22	**2.00**
	Q2T417	TssJ	BTH_II1888	0.16	**2.13**
	Q2T414	TagB	BTH_II1891	0.04	**1.42**
	Q2T413	TagAB	BTH_II1892	0.14	**2.92**
	Q2T412	VgrG-4b	BTH_II1893	0.14	**0.84**
	Q2T411	VgrG-4a	BTH_II1894	-0.03	**1.96**
	Q2T410	ClpV	BTH_II1895	0.01	**2.37**
	Q2T406	Hcp	BTH_II1899	-0.11	**1.33**
	Q2T405	TssC	BTH_II1900	0.12	**1.66**
	Q2T404	TssB	BTH_II1901	0.23	**1.72**
	Q2T403	TssA	BTH_II1902	-0.01	**1.28**

5.2.6 12-bis-THA particles induce the expression of efflux pumps but not beta-lactamases

Time kill studies detailed in **Chapter 3** showed that 12-bis-THA particles alone or in combination with tobramycin caused an initial reduction in bacterial CFUs prior to regrowth at later time points. This may indicate that 12-bis-THA particles are susceptible to resistance pathways expressed by *B. thailandensis.* To investigate this the proteomics data set was manually interrogated to investigate the production of efflux pump components and beta-lactamases.

The AmrAB-OprA RND efflux pump is conserved in *B. pseudomallei* where it gives rise to aminoglycoside and macrolide resistance (280). AmrA and AmrB increased in abundance 1.69 and 1.59-fold following incubation with 1X MIC of 12-bis-THA particles. BTH_I2443 is a homologue of OprA in *B. pseudomallei* and also significantly increased in abundance 0.92-fold under the same conditions. BpeA and BpeB, components of the BpeAB-OprB RND efflux pump, were identified in the proteomics dataset and increased in abundance 1.51 and 1.60-fold respectively following incubation with 1X MIC of 12-bis-THA particles (**Table 5.9**). BpeAB-oprB is conserved in *B. pseudomallei* and extrudes aminoglycoside and macrolide antimicrobials from the cytoplasm (281). The MacAB-TolC pump is a key determinant of macrolide resistance in *E. coli* (282) but is conserved in many Gram-negative species where it plays a role in the trafficking of membrane components and virulence factors (283–285). Only MacA increased in abundance 0.99-fold following incubation with 1X MIC of 12-bis-THA particles. BTH_I2289 is annotated as an RND family efflux transporter MFP subunit and increased in abundance 0.89-fold following exposure to 12-bis-THA particles. BTH_I2289 is conserved in *B. pseudomallei* (BPSL1568 and BPSL0308) where BPSL0308 is located immediately upstream of SilA, a component of the sil cation-efflux system which is responsible for protection against silver.

Table 5.98: Identification of efflux pump components in the *B. thailandensis* proteomics data set. Fold changes in bold represent statistical significance using the volcano statistics FDR - 0.01 and S0 - 1.

				Fold change (Log_2)	
	Accession number	**Protein name**	**Gene**	**0.1X MIC**	**1X MIC**
Efflux pump components	Q2SVT5	RND efflux system outer membrane protein	BTH_I2443	0.73	**0.92**
	Q2SVT4	AmrB	BTH_I2444	1.11	**1.59**
	Q2SVT3	AmrA	BTH_I2445	1.35	**1.69**
	Q2T0R3	BpeA	BTH_I0680	0.62	**1.51**
	Q2T0R2	BpeB	BTH_I0681	0.75	**1.60**
	Q2T4B4	MacA	BTH_II1791	0.16	**0.99**
	Q2T4B3	MacB	BTH_II1792	0.18	-0.02
	Q2T4B2	Outer membrane efflux protein	BTH_II1793	-0.17	0.53
	Q2SW89	RND family efflux transporter MFP subunit	BTH_I2289	-0.14	**0.89**

Seven beta-lactamase proteins were identified in the proteomics data set, two significantly deceased in abundance following incubation with 1X MIC of 12-bis-THA particles. BTH_I2282 and BTH_II0462 deceased in abundance 1.28 and 0.75-fold respectively (**Table 5.10**). Both are conserved in *B. pseudomallei* however their functions are unknown.

Table 5.10: Identification of beta-lactamase proteins in the *B. thailandensis* proteomics data set. Fold changes in bold represent statistical significance using the volcano statistics FDR - 0.01 and S0 - 1.

				Fold change (Log_2)	
	Accession number	**Protein name**	**Gene**	**0.1X MIC**	**1X MIC**
Beta-lactamases	Q2T1P4	metallo-beta-lactamase family protein	BTH_I0347	-0.10	0.18
	Q2SYQ9	metallo-beta-lactamase family protein	BTH_I1394	0.51	-0.60
	Q2SYM4	metallo-beta-lactamase family protein	BTH_I1429	-0.05	0.61
	Q2SXB1	metallo-beta-lactamase family protein	BTH_I1908	-0.09	-0.15
	Q2SW96	metallo-beta-lactamase family protein	BTH_I2282	-0.08	**-1.28**

	Q2STV4	metallo-beta-lactamase family protein	BTH_I3151	-0.08	-0.03
	Q2T837	metallo-beta-lactamase family protein	BTH_II0462	0.01	**-0.75**

5.2.7 12-bis-THA particles cause a reduction in the abundance of proteins controlling O-antigen production

12-bis-THA particle transfection is driven, at least in part, through electrostatic interactions with prokaryotic membrane components such as LPS and cardiolipin. Therefore, resistance to 12-bis-THA particles may arise through the remodeling or ablation of LPS to hinder transfection. The proteomics dataset was interrogated to investigate changes in LPS production and trafficking.

LpxABCD, LpxH, and LpxK were identified in the proteomics dataset but were not differentially abundant following incubation with either concentration of 12-bis-THA particles (**Table 5.10**). These proteins are responsible for the assembly of the lipid A component of LPS with deletions or mutations within these encoding genes resulting in resistance to polymyxin B (286,287).

LptABCDEFG are responsible for the trafficking of complete LPS molecules from the cytoplasm and across the cytoplasmic membrane and periplasm to the outer membrane. LptA, LptD and LptE were identified in the proteomics data set and were not differentially regulated following exposure to either concentration of 12-bis-THA particles (**Table 5.11**). LPS molecules can also be trafficked from the cytoplasm by MsbA which is a flippase protein. MsbA was also detected in the proteomics data set but was not differentially abundant (**Table 5.11**).

RfbH, RfbG, and RfbF significantly deceased in abundance 2.03, 2.41, and 2.97-fold respectively (**Table 5.11**). BTH_II1985 and BTH_II1986 are co-localised on chromosome 2 of *B. thailandensis* with *rfbHGF* and are predicted to be in the same operon. Both proteins significantly deceased in abundance 1.64 and 2.20- fold respectively. These proteins are members of the Rfb operon that plays a role in the production of rhamnose for cell wall polysaccharides (288). These enzymes are separated into 3 groups: (1) Enzymes that catalyse the formation of sugars that can be integrated into the O-antigen; (2) enzymatic transferases that assemble the sugars into the O-

subunit; (3) enzymes that assemble and traffic the O-antigen from the O-subunit (289,290). RfbFGH are conserved in *B. pseudomallei* however their function is not defined.

Table 5.11: Identification of proteins involved with LPS production and trafficking in the *B. thailandensis* proteomics data set. Fold changes in bold represent statistical significance using the volcano statistics FDR - 0.01 and S0 - 1.

				Fold change (Log_2)	
	Accession number	**Protein name**	**Gene**	**0.1X MIC**	**1X MIC**
O-antigen related	Q2T3S3	RfbH	BTH_II1982	-0.12	**-2.03**
	Q2T3S2	RfbG	BTH_II1983	-0.15	**-2.41**
	Q2T3S1	RfbF	BTH_II1984	-0.07	**-2.97**
	Q2T3S0	Chain length determining protein	BTH_II1985	-0.17	**-1.64**
	Q2T3R9	Polysaccharide biosynthesis protein	BTH_II1986	-0.12	**-2.20**
O-antigen related	Q2T3S7	RfaC-2	BTH_II1978	-0.04	**-2.30**
	Q2T3S8	Lipopolysaccharide core biosynthesis heptosyltransferase	BTH_II1977	-0.19	**-3.32**
	Q2T3S9	Galactoside O-acetyltransferase	BTH_II1976	-0.18	**-2.17**
	Q2T3T0	Glyco_trans_2-like domain-containing protein	BTH_II1975	-0.11	**-1.45**

Lipid A synthesis	Q2SWY6	LpxA	BTH_I2039	-0.07	0.14
	Q2SWY5	LpxB	BTH_I2040	-0.08	0.07
	Q2SYW0	LpxC	BTH_I1342	0.06	0.35
	Q2SZH6	LpxC	BTH_I1125	-0.29	-0.06
	Q2SWY8	LpxD	BTH_I2037	-0.04	0.16
	Q2SX82	LpxH	BTH_I1937	-0.03	-0.05
	Q2T0K1	LpxK	BTH_I0742	-0.02	-0.25
Lipid A trafficking	Q2T1A4	LptA	BTH_I0488	-0.03	0.39
	Q2T117	LptD	BTH_I0575	-0.17	-0.06
	Q2SZ90	LptE	BTH_I1212	-0.14	0.66
	Q2SZW0	MsbA	BTH_I0985	-0.13	-0.23

5.2.8 12-bis-THA particles suppress the production of T3SS-3 effector proteins

Burkholderia secretion apparatus (Bsa) proteins are structural proteins that make up the needle-like structure of the T3SS (291) except for BsaN which is the transcriptional regulator for this system (292). Nine Bsa proteins were identified in the proteomics data set but only one was differentially abundant (**Table 5.12**). BsaS significantly deceased in abundance 0.87-fold following exposure to 1X MICof 12-bis-THA particles. BsaS is the ATPase of the T3SS and is responsible for fuelling its activity through the hydrolysis of ATP (293,294). T3SS ATPases have been proposed to form hexameric rings in the inner membrane of bacteria where they unfold and traffic secreted effector proteins (295).

Six effector proteins were also identified in the proteomics data set and four significantly deceased in abundance following incubation with 1X MIC of 12-bis-THA particles (**Table 5.12**). BicP deceased in abundance 1.77-fold and is a predicted chaperone for BopA (296) which also deceased in abundance 1.90-fold. BopA contributes to intracellular survival and is a virulence determinant *in vivo*. Both BipC and BipB, which likely make up the translocation pore for secreted effectors (291), deceased in abundance 2.27-fold and 1.37-fold respectively.

Table 5.12: Identification of T3SS-3 virulence proteins in the *B. thailandensis* proteomics data set. Fold changes in bold represent statistical significance using the volcano statistics FDR - 0.01 and S0 – 1. changes in bold represent statistical significance

				Fold change (Log_2)	
	Accession number	**Protein name**	**Gene**	**0.1X MIC**	**1X MIC**
Secretory proteins	Q2T726	BsaM	BTH_II0826	-0.25	-0.60
	Q2T724	BsaO	BTH_II0828	-0.34	-0.43
	Q2T723	BsaP	BTH_II0829	-0.16	-0.58
	Q2T722	BsaQ	BTH_II0830	-0.19	-0.52
	Q2T721	BsaR	BTH_II0831	-0.17	-0.32
	Q2T720	BsaS	BTH_II0832	-0.14	**-0.87**

	Q2T718	BsaU	BTH_II0834	-0.03	-0.54
	Q2T717	BsaV	BTH_II0835	-0.22	-0.59
	Q2T725	BsaN	BTH_II0837	-0.18	0.02
Effector proteins	Q2T702	BicP	BTH_II0850	-0.20	**-1.77**
	Q2T703	BopA	BTH_II0849	-0.12	**-1.90**
	Q2T704	BopE	BTH_II0848	-0.18	-0.63
	Q2T708	BipD	BTH_II0844	-0.07	-0.58
	Q2T710	BipC	BTH_II0842	-0.16	**-2.27**
	Q2T711	BipB	BTH_II0841	-0.09	**-1.37**

5.2.9 12-bis-THA particles cause a decrease in the abundance of motility proteins

It was observed in the proteomics data set that proteins involved in flagellar-based motility were among the most strongly to reduce in abundance following incubation with 12-bis-THA particles. Thirty-two motility proteins were identified in the proteomics data set and seventeen significantly deceased in abundance (**Table 5.13**).

The C-ring which is comprised of FliM, FliN and FliG is responsible for torque generation and controlling the direction of rotation (297). FliM, FliN and FliG were detected in the proteomic data set and deceased in abundance 1.91, 2.00 and 0.93-fold respectively following incubation with 1X MIC of 12-bis-THA particles (**Table 5.13**). FliF is a component of the M-ring that acts as an anchor within the inner membrane (298) and deceased in abundance 2.00-fold under the same conditions. FlgH is a lipoprotein that makes up the L-ring which is located in the outer membrane (299). FlgH deceased in abundance 0.88-fold following incubation with 1X MIC of 12-bis-THA particles. BTH_I0029 (a homologue of FliO in *B. pseudomallei*), FliI and FliH-1 are components of the T3SS which is responsible for trafficking distal components of the flagella. These proteins deceased in abundance 1.23, 1.30 and 0.77-fold following exposure to 1X MIC of 12-bis-THA particles. FliC (flagellin) is a hollow, globular protein that forms the extracellular, membrane-bound filament of the flagellum. BTH_I3196 was identified in the proteomics data set and is a homologue of FliC. Following incubation with 1X MIC of 12-bis-THA particles, it deceased in abundance 1.32-fold. FliS-1 is an export chaperone that binds flagellin and facilitates its export (300) and deceased in abundance 2.70-fold following incubation with 1X MIC of 12-bis-THA particles. Once exported, flagellin is attached to the hook component by FlgL and FlgK which form the hook-filament junction. Both proteins were detected in the proteomics data set however only FlgL deceased in abundance 1.14-fold. FlgK and FlgL are trafficked to their site of action by FlgN which deceased in abundance 1.58-fold under the same conditions. The hook component of the flagella is around 55 nm long and is comprised of up to 120 FlgE subunits (301). The proteomic data set showed that FlgE deceased in abundance 1.11-fold under the same conditions. MotA and MotB are integral membrane proteins that generate torque through proton translocation resulting in the rotation of the flagella (302). Both proteins were identified in the proteomics data set and deceased in abundance 1.40 and 1.00-fold following exposure to 1X MIC of 12-bis-THA particles. YcgR is a flagellar brake protein that is negatively regulated by cyclic-di-GMP (303) and deceased in abundance 1.40-fold under the same conditions.

Table 5.13: Identification of proteins involved with the production, trafficking, and activation of flagella in the *B. thailandensis* proteomics data set. Fold changes in bold represent statistical significance using the volcano statistics FDR - 0.01 and S0 - 1.

				Fold change (Log_2)	
	0.1X MIC	**1X MIC**	**Gene**	**0.1X MIC**	**1X MIC**
Fli proteins	Q2T2F9	FliF	BTH_I0026	-0.27	**-2.00**
	Q2T2F8	FliM	BTH_I0027	-0.16	**-1.91**
	Q2T2F7	FliN	BTH_I0028	-0.22	**-2.00**
	Q2T2F6	Flagella biosynthesis protein	BTH_I0029	-0.08	**-1.23**
	Q2T246	Flagella hook-length control protein	BTH_I0195	-0.03	0.09
	Q2T245	FliJ	BTH_I0196	0.60	**-1.10**
	Q2T244	FliI	BTH_I0197	0.15	**-1.30**
	Q2T243	FliH-1	BTH_I0198	-0.02	**-0.77**
	Q2T242	FliG	BTH_I0199	-0.02	**-0.93**
	Q2T241	FliF-1	BTH_I0200	-0.02	-0.68
	Q2T239	FliS-1	BTH_I0202	-0.02	**-2.70**
	Q2T8X4	FliH-2	BTH_II0173	-0.25	0.04
	Q2T204	FlgN	BTH_I0237	0.13	**-1.58**
	Q2T200	FlgC-1	BTH_I0241	0.45	-0.18
	Q2T1Z8	FlgE	BTH_I0243	0.05	**-1.11**

Flg proteins	Q2T1Z7	FlgF	BTH_I0244	0.08	0.32
	Q2T1Z6	FlgH	BTH_I0245	0.08	**-0.88**
	Q2T1Z5	FlgH-1	BTH_I0246	-0.02	-0.30
	Q2T1Z4	FlgI-1	BTH_I0247	0.03	-0.36
	Q2T1Z2	YcgR	BTH_I0249	-0.11	**-1.40**
	Q2T1Z1	FlgK	BTH_I0250	0.21	-0.87
	Q2T1Z0	FlgL	BTH_I0251	0.30	**-1.14**
	Q2T8W4	FlgA	BTH_II0183	-0.13	0.22
	Q2T8W0	FlgE	BTH_II0187	-0.15	0.26
Flh proteins	Q2STT6	FlhA	BTH_I3169	-0.38	0.03
	Q2STT7	FlhH	BTH_I3168	0.06	-0.41
Motor proteins	Q2STS0	MotA	BTH_I3185	-0.32	**-1.40**
	Q2STS1	MotB	BTH_I3184	-0.15	**-1.00**
Misc.	Q2STQ9	Flagellin	BTH_I3196	-0.32	**-1.32**
	Q2T8Z6	Flagellin D	BTH_II0151	-0.48	0.21
	Q2T8X1	Flagella hook-associated protein	BTH_II0176	0.02	-0.21
	Q2T510	Flagella hook-associated protein 2	BTH_II1544	0.40	-0.36

5.2.10 Metabolomic analysis of the 12-bis-THA stress response in *B. thailandensis* strain E555

The proteomic data set suggested that 12-bis-THA particles induced changes in central metabolism in *B. thailandensis*. To investigate this further, we performed NMR-based metabolomic analysis on bacterial pellets retained from the growth assays (**Figure 5.1**). PCA analysis was performed to assess the similarity between the three different treatment groups. The PCA plot showing the proteomic data set showed that the three treatment groups separated into three distinct clades (**Figure 5.3**). In contrast, PCA analysis of the metabolomics data set showed some overlap between the three groups (**Figure 5.6**). The biggest overlap was observed between the metabolomes of bacteria incubated with 0.1X MIC of 12-bis-THA particles and the untreated control. The metabolomes of bacteria incubated with 1X MIC of 12-bis-THA particles formed a clade that overlapped slightly with the untreated control and but not with the metabolomes of bacteria treated with 0.1X MIC of 12-bis-THA particles. This suggests that the metabolomes of bacteria treated with 0.1X MIC or 1X MIC of 12-bis-THA particles are distinct from one another but share considerable overlap with the untreated control. This is in contrast with the PCA plots from the proteomics data set (**Figure 5.3**) which showed that the proteomes of all conditions were distinct. This may occur if the changes in the metabolomic data set are more subtle than those in the proteomic data set.

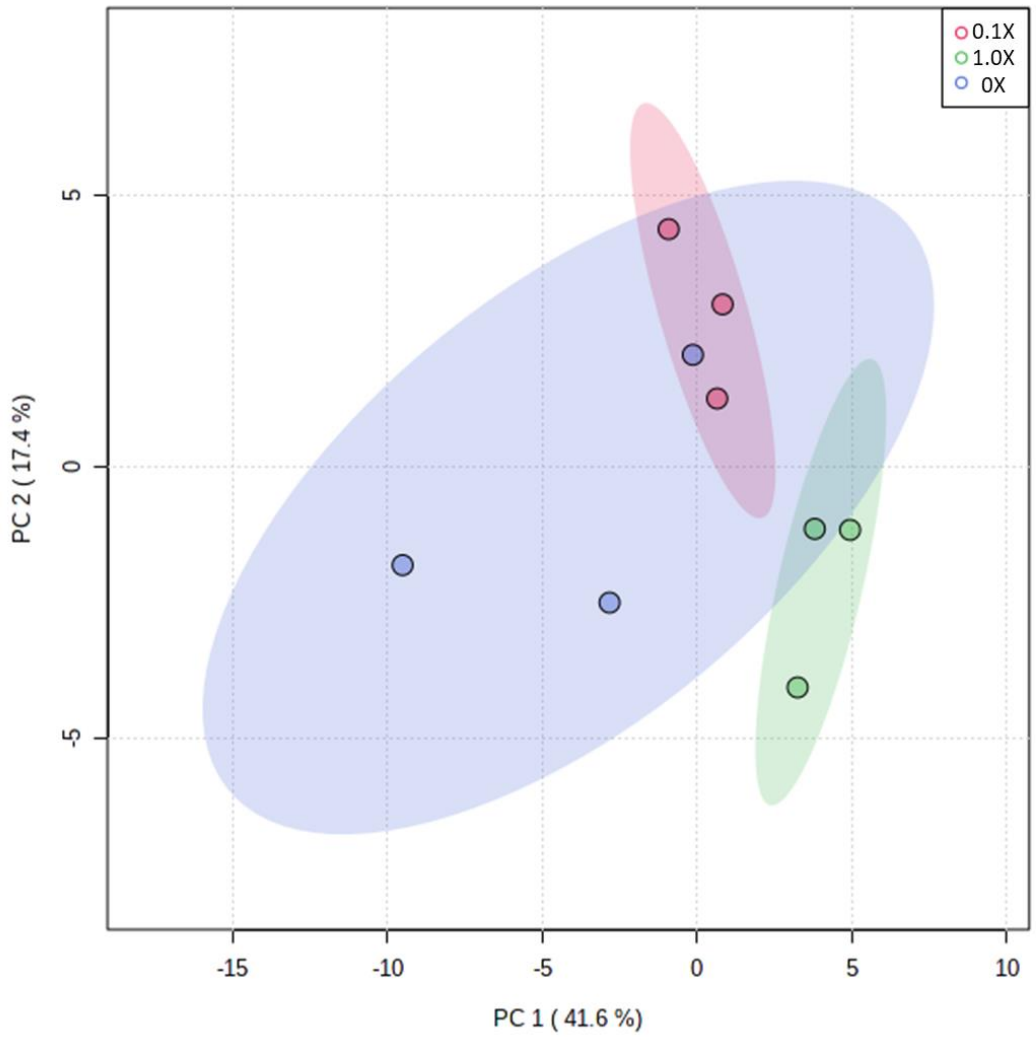

Figure 5.6: Principal component analysis of the metabolomic data sets. Blue, red, and green dots are representative of the metabolomes of untreated bacterial and those treated with 0.1X MIC or 1X MIC of 12-bis-THA particles, respectively. PCA plots were generated using TopSpin version 3.2.

NMR spectra were then interrogated to identify the constituents of the *B. thailandensis* metabolome and allowed for the identification of biomolecules including amino acids (glutamate, valine, serine, tyrosine, etc), osmolytes (glucose, trehalose, glycine betaine, etc), organic acids (fumarate, succinate, pyruvate, etc), cofactors (NAD+), nucleosides (guanosine, adenosine, uracil, etc) and metabolic intermediates and end-products (ATP, ADP, AMP, 3-hydroxybutyrate, etc).

Univariate analysis showed significant decrease in the abundance of succinate in response to 1X MIC of 12-bis-THA particles (**Figure 5.7**). Similarly, the cytoplasmic concentrate of fumarate was also reduced however this was not significant ($p = 0.0604$). 3-hydroxybutyrate, a ketone body that can be converted to acetyl-CoA, deceased in abundance in response to 1X MIC of 12-bis-THA particles. Again, this was not significant but had a p-value of 0.0501. Compounds of glycolysis were also detected in the metabolomic data set. Cytoplasmic glucose was reduced in response to 1X MIC of 12-bis-THA particles. The concentrations of cytoplasmic pyruvate also decreased in response to 1X MIC of 12-bis-THA particles however this was not significant ($p = 0.11$). AMP, ADP, and ATP were identified in the NMR spectra however none were differentially abundant following exposure to 12-bis-THA particles.

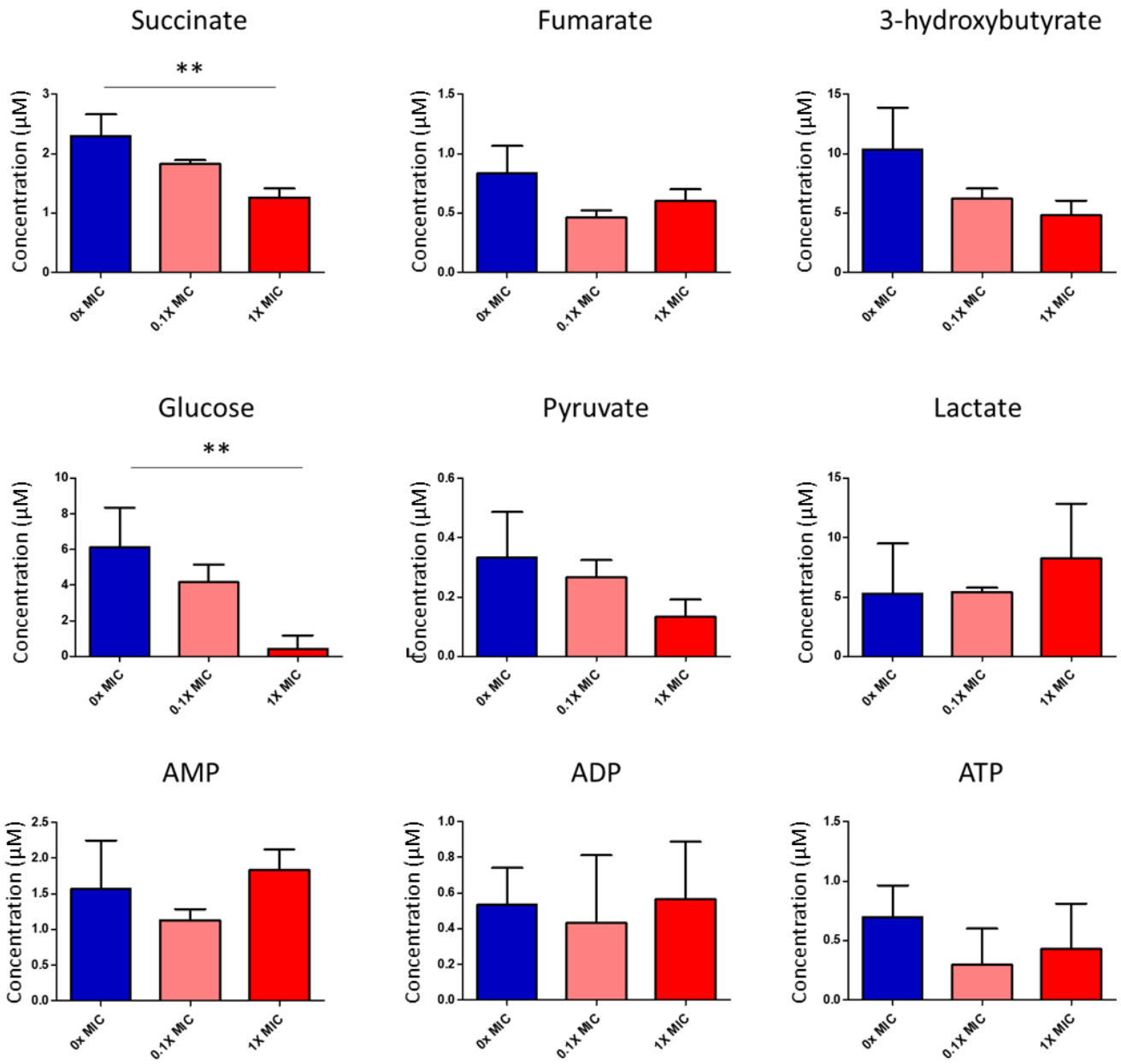

Figure 5.7: Cytoplasmic abundance of metabolic by-products and intermediates in *B. thailandensis* in untreated bacteria or those incubated with 0.1X MIC or 1X MIC of 12-bis-THA particles. Metabolite concentration was calculated using Chenomx NMR Suite 7.0 and comparing peak area to a known concentration of TSP. Statistical significance was determined using a one-way ANOVA followed by a Bonferroni correction. Significance was denoted using the following markers *P < 0.05; **P < 0.01; ***P < 0.001.

The NMR spectra showed that 12-bis-THA particles induced changes in the cytoplasmic concentration of osmotically active molecules. Statistical analysis showed that betaine, also known as trimethylglycine or glycine betaine, was the only metabolite that deceased in abundance in response to both 0.1X MIC and 1X MIC concentrations of 12-bis-THA particles (**Figure 5.8**). The osmolytes glutamate and trehalose both deceased in abundance however this was only observed in response to 1X MIC of 12-bis-THA particles (**Figure 5.8**).

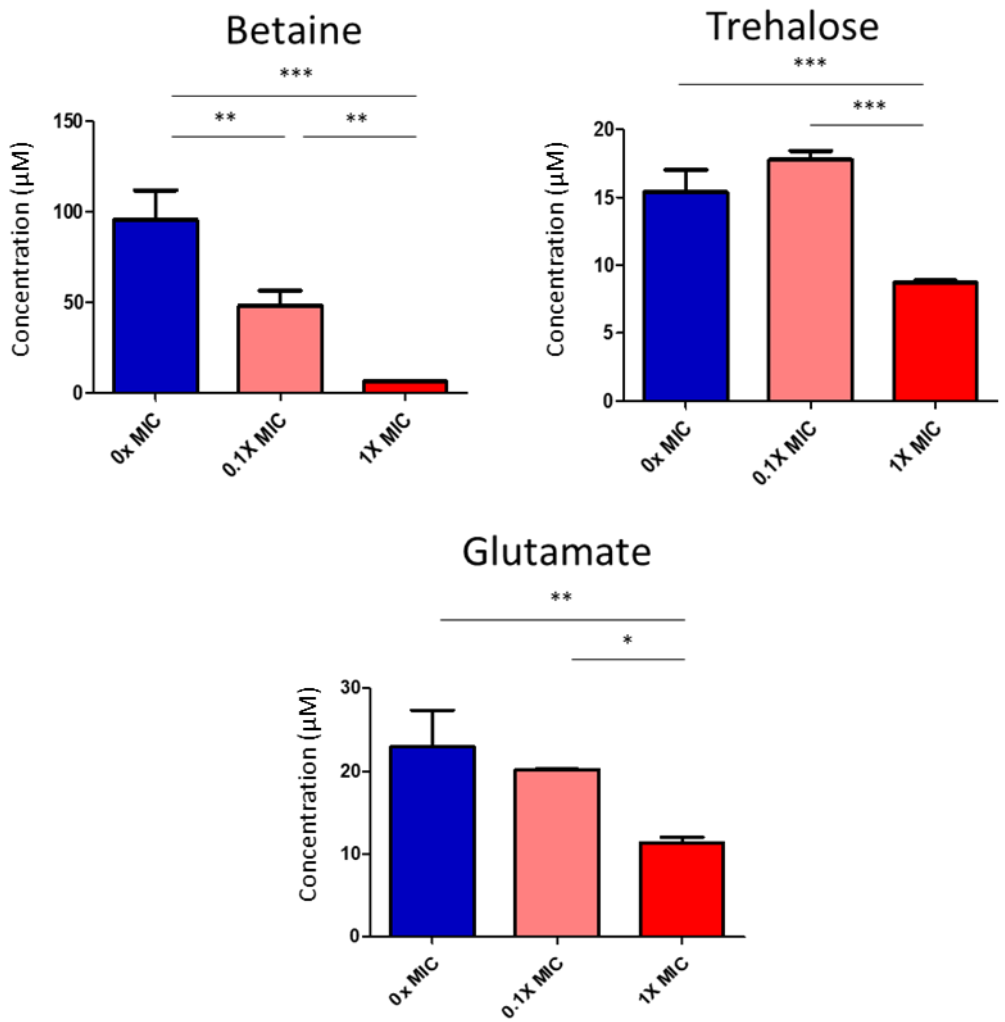

Figure 5.8: Cytoplasmic abundance of osmolytes in *B. thailandensis* in untreated bacteria or those incubated with 0.1X MIC or 1X MIC of 12-bis-THA particles. Metabolite concentration was calculated using Chenomx NMR Suite 7.0 and comparing peak area to a known concentration of TSP. Statistical significance was determined using a one-way ANOVA followed by a Bonferroni correction. Significance was denoted using the following markers *P < 0.05; **P < 0.01; ***P <

Three nucleoside sugars and one intermediate compound for nucleotide synthesis were identified in the NMR spectra. The cytoplasmic concentration of uracil was also reduced in response to 1X MIC of 12-bis-THA particles (**Figure 5.9**). Adenosine and guanosine were also identified but were not differentially abundant following incubation with 12-bis-THA particles. Similarly, hypoxanthine is a purine derivative and was not differentially abundant in response to 12-bis-THA particles.

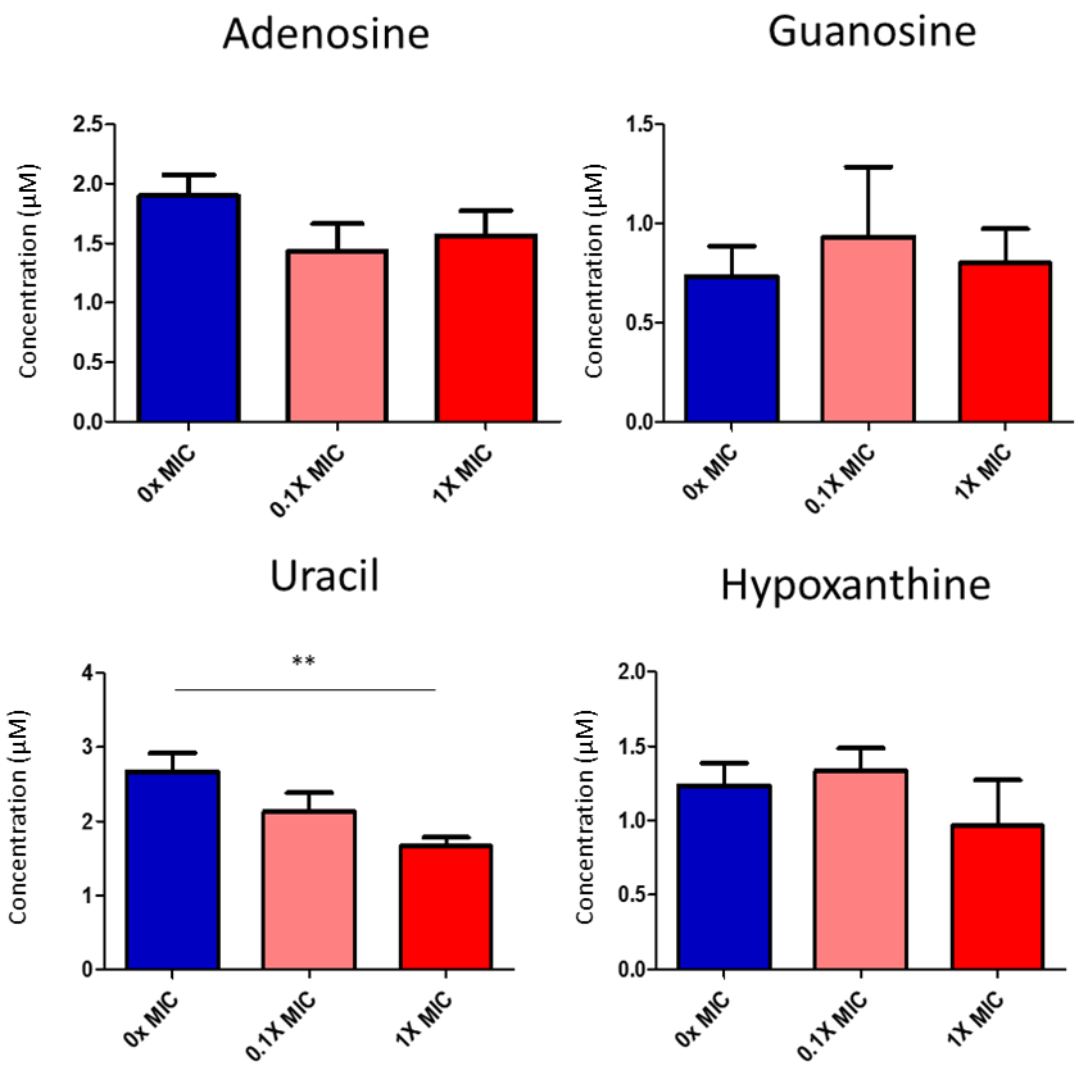

Figure 5.9: Cytoplasmic abundance of nucleotides and nucleotide derivatives in *B. thailandensis* in untreated bacteria or those incubated with 0.1X MIC or 1X MIC of 12-bis-THA particles. Metabolite concentration was calculated using Chenomx NMR Suite 7.0 and comparing peak area to a known concentration of TSP. Statistical significance was determined using a one-way ANOVA followed by a Bonferroni correction. Significance was denoted using the following markers *P < 0.05; **P < 0.01; ***P < 0.001.

Twelve amino acids were identified in the metabolomic data set (**Figure 5.10** and **Figure 5.11**). Lysine was the only metabolite that increased in abundance in response to 12-bis-THA particles and increased from 2.5 $\pm$ 0.2 µM in the untreated control to 9.1 $\pm$ 1.8 µM in the samples treated with 1X MIC of 12-bis-THA particles. In contrast, tyrosine was reduced in response to 1X MIC of 12-bis-THA particles as it was not detected in these samples. Despite this, the reduction in tyrosine was not significant and had a p-value of 0.0634.

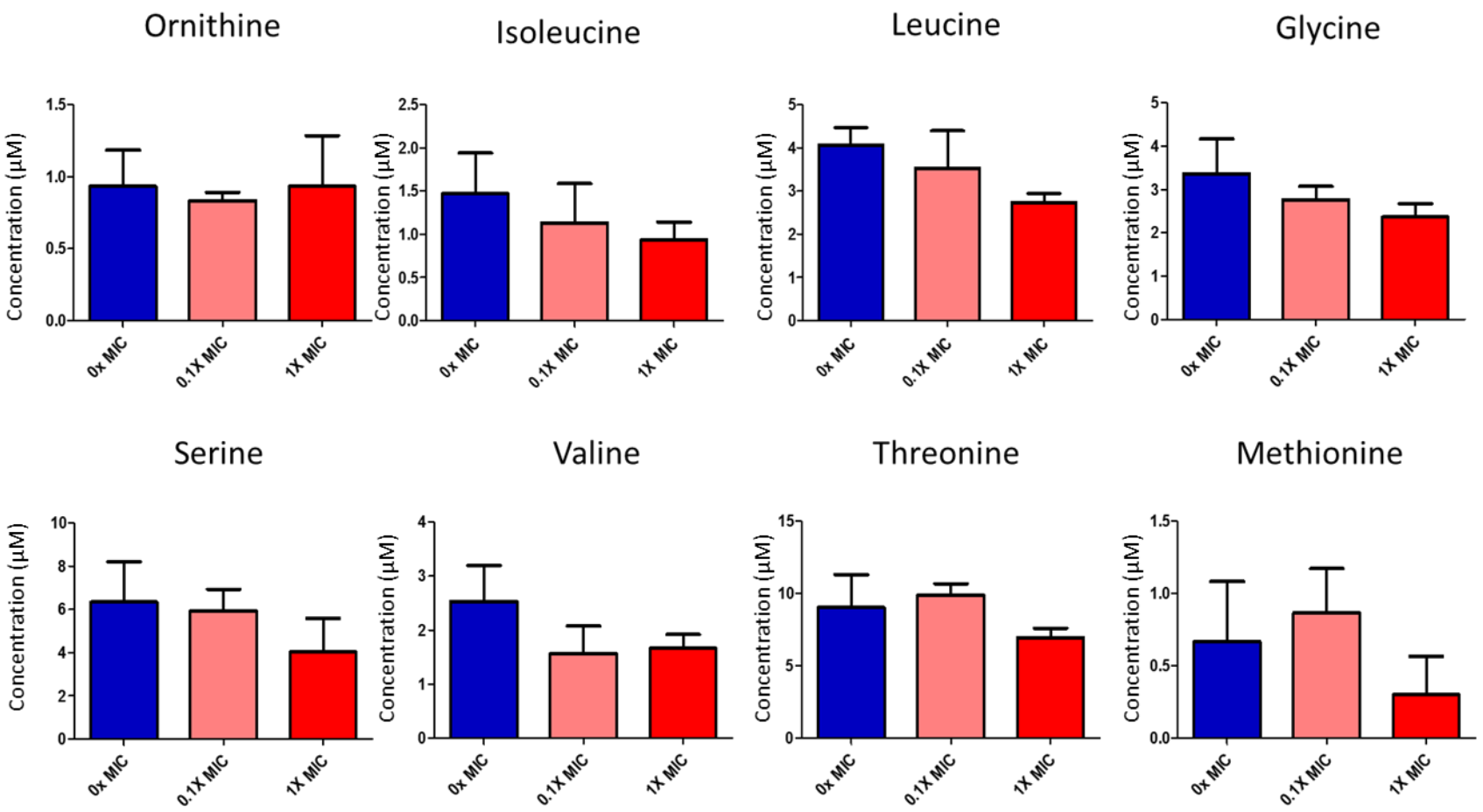

Figure 5.10: Cytoplasmic abundance of amino acids in *B. thailandensis* in untreated bacteria or those incubated with 0.1X MIC or 1X MIC of 12-bis-THA particles. Metabolite concentration was calculated using Chenomx NMR Suite 7.0 and comparing peak area to a known concentration of TSP. Statistical significance was determined using a one-way ANOVA followed by a Bonferroni correction. Significance was denoted using the following markers *P < 0.05; **P < 0.01; ***P < 0.001.

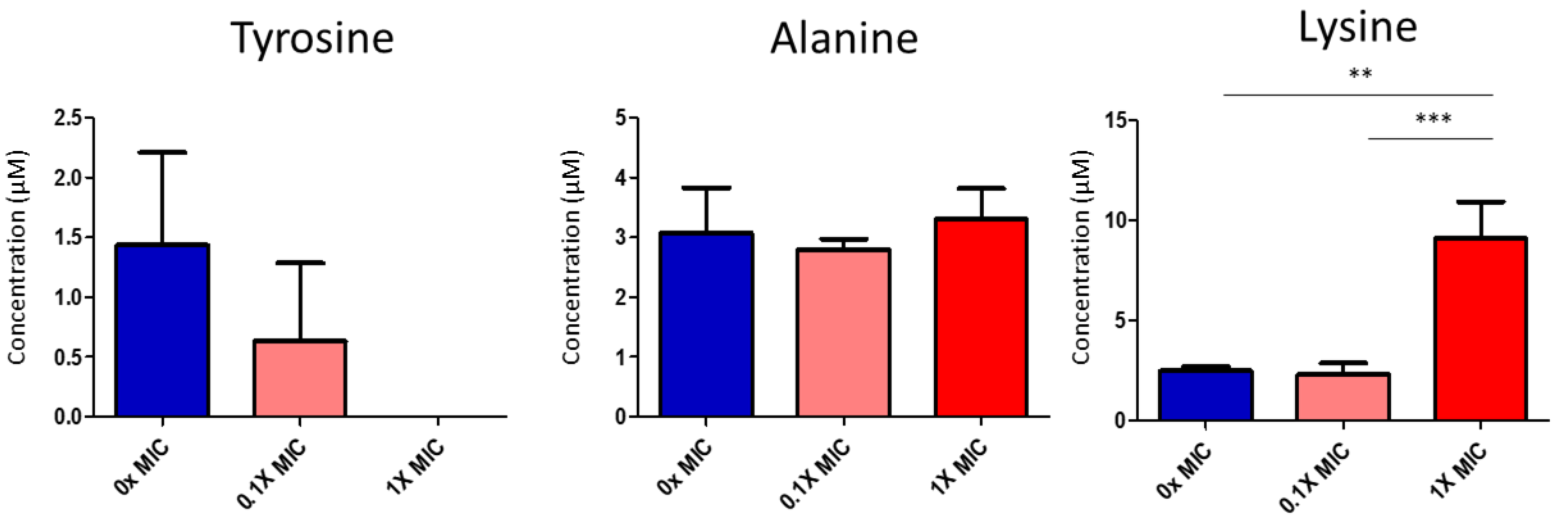

Figure 5.11: Cytoplasmic abundance of amino acids in *B. thailandensis* in untreated bacteria or those incubated with 0.1X MIC or 1X MIC of 12-bis-THA particles. Metabolite concentration was calculated using Chenomx NMR Suite 7.0 and comparing peak area to a known concentration of TSP. Statistical significance was determined using a one-way ANOVA followed by a Bonferroni correction. Significance was denoted using the following markers *P < 0.05; **P < 0.01; ***P < 0.001.

5.3 DISCUSSION

5.3.1 Integrated proteomics and metabolomics can provide insight into bacterial stress responses

Integrated untargeted 'omics is an approach which can provide a holistic overview of bacterial changes in response to stimuli. To provide insight into their mechanism of action of 12-bis-THA particles against *B. thailandensis* strain E555, a proteomic-metabolomic study was performed to provide an overview of the resulting stress responses. Additionally, the proteomic data can later be mined to identify candidates for TFD discovery by selecting transcription factors that govern the stress response to 12-bis-THA particles and are conserved in *B. pseudomallei*.

Gel free methods were chosen over gel based methods as they provide better proteome coverage and resolution (304). However, while mass spectrometry-based label-free quantification is highly sensitive and capable of identifying approximately 3000 proteins per run, variability between runs can make hypothesis testing challenging (data not shown). Therefore, tandem mass tagging (TMT) was used in our study to identify a large number of proteins and to limit inter-run variability which had been observed in previous proteomic investigations.

The raw proteomic data was processed with Proteome Discoverer where peptide reads were mapped to the UNIPROT proteome of *B. thailandensis* strain E264 as the UNIPROT proteome of *B. thailandensis* E555 was not complete at the time of analysis. The limitation of this is that the expression of proteins involved with the production and export of the capsular polysaccharide will not be observed. In this work, 3150 proteins were identified to give a proteome coverage of 56.6%. These are in line with Li *et al* who identified 2,463 proteins and 2,524 proteins in *B. thailandensis* E264 representing proteome coverages of 43% and 45% respectively (305).

The Proteome Discoverer output was then processed using Perseus, a software package for the statistical analysis and visualisation of large proteomics datasets (146). Before statistical analysis could be performed, the proteomics data sets were first investigated for missing values. Missing values were computationally replaced using Perseus by drawing values from the distribution to stimulate the expression of data that are below the limit of detection. These were visualised using histograms where true data is shown in blue and the imputed data in orange. In the context of our data, the histograms show a low amount of missing data values meaning that proteins that were identified were consistent between biological and technical replicates. This suggests that exposure of *B. thailandensis* E555 to 12-bis-THA particles does not change the proteins present but rather changes the abundance of some proteins.

Perseus was used to investigate differences in the protein abundance when comparing the proteomes of bacteria challenged with 12-bis-THA particles compared to the untreated control. This was visualized by producing volcano plots using an FDR of 0.01 and an S0 value of 1 that is consistent with CoxDocs (306), which are the supporting documents for Perseus by Jurgen Cox's group, and was used to emulate a 1-fold $\log_2$ cut off for proteins. The values described in this section is centre on zero and a 1-fold increase in abundance is indicative of a doubling of peptides associated with a specific protein. In contrast a 1-fold decrease in abundance is representative of a 50% reduction in peptides associated with a specific protein.

No proteins were differentially abundant when *B. thailandensis* was incubated with 0.1X MIC of 12-bis-THA particles. This may be due to multiple reasons. Stringent statistical parameters were selected to limit the number of false positives which may mean that proteins that change subtly in abundance may be excluded. Alternatively, 0.1X MIC of 12-bis-THA particles may have been insufficient to stimulate a proteomic response which is consistent with the growth curves which showed that this concentration did not affect bacteria growth. This concentration was selected to represent a sub-inhibitory concentration of 12-bis-THA particles which had been determined by MIC assay. However, this assay predicts the inhibition of bacteria at a starting density of 10^5 CFU/mL of bacterial whereas the bacteria in the proteomic study were at a concentration of approximately ~10^{10} CFU/mL. In contrast, the volcano plots show that 1X MIC of 12-bis-THA particles caused in increase in the abundance of 139 proteins and a decrease in the abundance of 671 proteins in *B. thailandensis* E555 (**Figure 5.5**). The observed fold changes of differentially abundant proteins were comparable to those observed by Li *et al.* As our data set was consistent within the literature with regards to fold change and proteome coverage, it is therefore suitable for downstream analysis to provide insight into the mechanism of action of 12-bis-THA particles.

NMR-based metabolomics has also been used to investigate bacteria stress adaption in response to environmental stimuli or antimicrobial exposure (307). An NMR-based study was performed in parallel to produce a complementary data set to support the proteomic study. 45 metabolites were identified in the cytoplasm of *B. thailandensis* which is comparable with Moreira *et al* who identified 25 metabolites in the cytoplasm of *B. cenocepacia* (147). In the dataset present in this thesis, there were several metabolites such as fumarate ($p = 0.0603$) or pyruvate ($p = 0.11$), where fold-changes were not significantly different but were considered in the attempt to deduce the mechanism of action. These metabolites were identified as concentrations near the limit of detection of NMR (1 µM) and are therefore difficult to distinguish the difference between

metabolite signal and noise. Targeted d based metabolomics are ongoing to identify changes in metabolite concentration as this technique is more sensitive than NMR. Despite this, the NMR based study has provided a complementary data set supporting the hypothesis that 12-bis-THA particles induce changes in central metabolism and osmotic balancing.

5.3.2 12-bis-THA particles induce changes in central metabolism

The proteomic and metabolomic studies both identified changes in central metabolism in response to 12-bis-THA. The proteomic data shows that 12-bis-THA particles caused a decrease in the abundance of 6-phosphofructokinase and phosphoglycerate mutase which are enzymes associated with glycolysis, a conserved pathway that is responsible for the conversion of glucose to pyruvate. Similarly, the metabolomic data showed that both pyruvate and glucose were also reduced under the same conditions suggesting a reduction in glycolytic flux. Glycolysis breaks down a single glucose monomer to produce two ATP, two NADH, two H^+ and two pyruvate molecules, the latter of which is converted into acetyl-CoA which is essential for the TCA cycle. The proteomics data set showed strong induction of the four enzymes comprising the β-oxidation cycle (BTH_I0564 – BTH_I0567). This pathway is responsible for the catabolism of long-chain fatty acids and produces $FADH_2$, NADH and acetyl-CoA per completion of the cycle. This data suggests that 12-bis-THA particles cause a shift from glucose metabolism to fatty acid metabolism. A reduction in glycolysis may occur if glucose reserves were depleted in response to osmotic balancing. Induction of β-oxidation may then accommodate the suppression of glycolysis and support maintained activation of the TCA cycle and the ETC.

The ETC is a series of redox reactions whereby electrons are transferred from cytoplasmic high-energy donors (e.g NADH and $FADH_2$) to electron acceptors (e.g cytochrome c). This is coupled with the transfer of protons from the cytoplasm to periplasm to produce a proton gradient which is then exploited by processes such as ATP synthesis and flagella-based motility. The proteomic data set showed that 12-bis-THA induced changes in the ETC as proteins associated with respiratory complex II (succinate dehydrogenase) respiratory complex III (cytochrome c reductase), respiratory complex IV (cytochrome c oxidase), and respiratory complex V (ATP synthase) deceased in abundance (**Figure 5.12B**).

Succinate dehydrogenase differs from the other respiratory complexes as it contributes to both the TCA cycle and the ETC (308). Succinate is a metabolic intermediate of the TCA cycle and is oxidised by the succinate dehydrogenase subunit SdhA to form fumarate which re-enters the TCA cycle. The free electrons from this reaction reduce SdhA-bound FAD to form $FADH_2$ which is then oxidised, and protons are trafficked along Fe-S clusters to reduce ubiquinone (Q) to ubiquinol (QH_2),

a lipid-soluble molecule that freely diffuses within the inner membrane, and is utilised in respiratory complex III. Unlike complexes I and III, complex II does not release H^+ ions into the periplasm but produces QH_2 which are later processed by complex III (**Figure 5.12A**). Of the five proteins subunits identified in the proteomic data set only one was differentially abundant. Succinate dehydrogenase subunit B (BTH_II0362) deceased in abundance 1.66-fold which is a Fe-S domain-containing protein that facilitates the trafficking of H^+ ions from oxidised $FADH_2$. Inhibitors of succinate dehydrogenase, such as carboxin, are well characterised and have industrial applications in agriculture as a fungicide. Interestingly this suggests that 12-bis-THA may be useful to counter fungal pathogens which is consistent with data produced by DiBlasio which demonstrated the potent activity of 12-bis-THA and its analogues against a panel of clinical fungal isolates (138).

Three protein subunits of cytochrome c reductase (respiratory complex III) were observed in the proteomics data set and all deceased in abundance in response to 12-bis-THA particles. Cytochrome c reductase is responsible for the oxidation of QH_2 to Q (**Figure 5.12A**). Upon interacting with complex III, QH_2 releases two H+ ions into the periplasmic space. Two electrons are also released and concomitantly enter the Q-cycle within complex III. The Q-cycle is separated into two sections. In the first, an electron is released by QH_2 which reduces the Fe^{2+} atom within the Fe-S of the Rieske center (309). The electron is then transferred to the heme group of cytochrome c1 and then finally onto cytochrome c which is bound on the periplasmic face of complex III (309). The reduced cytochrome c detaches from complex III and interacts with respiratory complex IV. The second electron is transferred to the heme group of cytochrome b which is transferred to a second ubiquinone to form a semi-quinone radical ion. The Q-cycle is repeated and the semi-quinone radical is reduced to QH_2. PetA, PetB and PetC all deceased in abundance 2.03-fold, 1.36-fold and 1.21-fold, respectively. This suggests that 12-bis-THA shares a similar mechanism of action to its parental molecule dequalinium which inhibits cytochrome c reductase in mitochondria (197).

Respiratory complex IV, also known as cytochrome c oxidase, is responsible for the transfer of electrons from cytochrome c to O_2 to form H_2O within the cytoplasm (**Figure 5.12A**) (310,311). Two reduced cytochrome c molecules release two electrons that are transferred through the metal-containing components of complex IV resulting in the reduction of CuB and heme a3. A diatomic oxygen molecule binds with the reduced form of Heme a3 and CuB to form a peroxide bridge. Another reduced cytochrome c molecule provides another two electrons that, in combination with two H^+ ions from the cytoplasm, break the peroxide bridge by forming a hydroxyl group on Heme a3 and CuB. A further two protons are taken from the cytoplasm and oxidise the Heme a3 and CuB causing them to revert to their natural state and to release H_2O. During this process, complex IV

expels four protons into the periplasmic space. We identified five proteins subunits of cytochrome c oxidase in the proteomic data set and two deceased in abundance in response to 1X MIC of 12-bis-THA particles. BTH_I2874 (cytochrome c oxidase subunit I) and BTH_I1786 (cytochrome c oxidase subunit III) deceased in abundance 1.26-fold and 2.62-fold respectively. As with cytochrome c reductase, mitochondrial cytochrome c oxidase activity in addition to mitochondria DNA number and cellular growth were all reduced in response to dequalinium chloride (268).

The data also showed a decrease in the abundance of ATP synthase subunits. ATP synthase is an enzyme that is responsible for trafficking protons from the periplasmic space to the cytoplasm and driving the formation of ATP from ADP and inorganic phosphate. It is comprised of two domains: (I) a membrane-bound domain termed F_0 which drives the translocation of protons from the periplasm to the cytoplasm; and (II) a cytoplasmic facing component termed F_1 that is responsible for synthesising ATP from ADP and inorganic phosphate (312). Subunit b acts as an anchor for the F_1 domain and was the only F_0 protein to deceased in abundance (3.39-fold) in response to 12-bis-THA. Conversely, four of the F_1 domain components deceased in abundance under the same conditions. The γ (BTH_II0427) and ε (BTH_II0420) subunits deceased in abundance 2.97-fold and 1.29-fold respectively. The α (BTH_II0426) and β (BTH_II0419) subunits deceased in abundance 1.69-fold and 2.01-fold respectively. This implies that 12-bis-THA inhibits the function of ATP synthase which is consistent with the mechanism of its parental molecule dequalinium which is a known inhibitor of mitochondrial respiratory complex III (197) in addition to eukaryotic and prokaryotic respiratory complex V (313).

Loss of proton motive force (PMF) can be countered by increasing TCA flux. This has been shown through the addition of exogenous glucose (314) or fumarate (200) to the growth medium. PMF may be stimulated through the suppression of the glyoxylate cycle which intersects the TCA cycle and bypasses the oxidation of α-ketoglutarate and succinyl coenzyme A. By doing so, this retains two carbons in the form of acetyl-CoA which would otherwise be converted to CO_2 however this is performed at the loss of two NADH molecules (315). Suppression of this pathway would produce more NADH which could be used to stimulate PMF. The proteomic data showed that AceA and AceB, the enzymatic components of the glyoxalate cycle, deceased in abundance in response to 12-bis-THA. Additionally, α-ketoglutarate dehydrogenase (SucAB) and succinyl coenzyme A synthetase (SucCD) both increased in abundance under the same conditions. The NMR data showed a depletion of succinate and fumarate which is consistent with 12-bis-THA increased TCA flux. Oligomycin and dicyclohexylcarbodiimide are respiratory uncouplers (316) that prevent the movement of protons from the periplasm to the cytoplasm inhibiting the formation of ATP due to

the absence of PMF. Dequalinium has also been shown to dissipate membrane potential in mitochondria therefore we postulate that flux through the TCA cycle is increased to provide high-energy compounds to the ETC to counter the effects of membrane depolarisation (317). Future studies are required to investigate changes in membrane potential in *Burkholderia* species in response to 12-bis-THA particles. For example, PMF levels can be quantified in *B. thailandensis* using the potentiometric probe JC-1 (318).

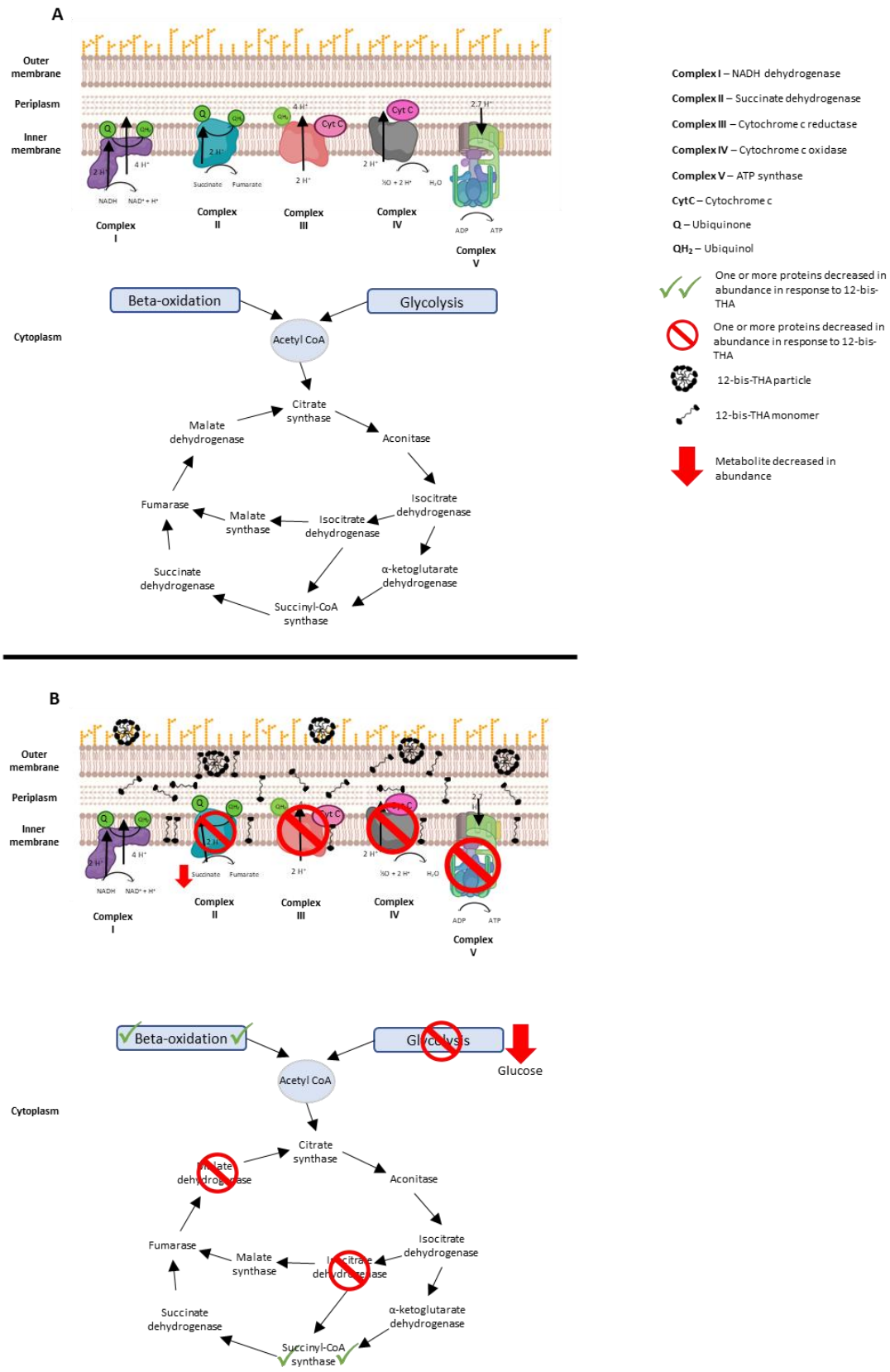

Figure 5.12: The stress response of *B. thailandensis* to 12-bis-THA particles (**A**) A cartoon schematic showing central metabolism under normal physiological conditions. (**B**) A cartoon schematic showing the down regulation of electron transport chain, glyoxylate shunt and glycolysis, and the upregulation of beta-oxidation in response to 12-bis-THA particles.

5.3.3 Induction of oxidative stress pathways

Dysregulation of respiration may induce oxidative stress. The proteomic data set was interrogated to investigate changes in the abundance of oxidative stress proteins. We identified eight proteins known to play roles in regulating oxidative stress including AhpC, KatG, OxyR, and DspA. KatG and DpsA were the only proteins that deceased in abundance in response to 12-bis-THA particles. KatG is a bifunctional catalase-peroxidase enzyme that is responsible for the degradation of hydrogen peroxide (H_2O_2) as either a peroxidase ($H_2O_2 + 2AH \rightarrow 2H_2O + 2A$) or a catalase ($H_2O_2 \rightarrow 2H_2O + O_2$) (319). Alternatively, DpsA is a member of the Dps family, a group of non-specific DNA-binding polypeptides that confer protection to oxidative damage from peroxides (320,321). This indicates that either 12-bis-THA particles do not induce oxidative stress or that it is managed by other means.

In *B. thailandensis,* oxidative stress can be alleviated through the induction of T6SS-2 (also termed T6SS-4) proteins (322,323). Traditionally, the secretion systems in *Burkholderia* species are important contact-dependent virulence factors that are associated with cellular invasion. In contrast, T6SS-2 functions as contact independent export machinery which expels proteinaceous metallophores into the extracellular milieu. These are responsible for collecting manganese and potentially zinc which can be used as antioxidants and enzyme co-factors. T6SS-2 is conserved in multiple *Burkholderia* species including *B. pseudomallei* and *B. mallei* where it is believed to play an important role in polymicrobial communities and *in vivo* (322,323). Fifteen proteins of the T6SS-2 were identified in the proteomic data set and all increased in abundance in response to 1.0X MIC of 12-bis-THA particles. Ciprofloxacin is known to stimulate the formation of ROS and has been shown to induce the expression of T6SS-2 in *B. pseudomallei* (324). This suggests that 12-bis-THA particles stimulated ROS production and also that the T6SS-2 may be important to counter drug-induced oxidative stress.

5.3.4 Possible resistance mechanisms to 12-bis-THA particles

In **Chapter 3**, we showed that 12-bis-THA particles inhibited the growth of *B. thailandensis* with an MIC of 2 – 8 μg/mL. Time-kill studies showed that *B. thailandensis* displayed regrowth at 24 h despite showing an initial reduction in bacterial density. Additionally, plating of *B. thailandensis* cells that been incubated with 12-bis-THA particles identified the presence of small colonies in addition to the normal colony morphology. No change in the growth kinetics or susceptibility to 12-bis-THA particles was observed suggesting that the small colonies were not a resistant sub-population. Despite this, we interrogated the proteomic data set for changes in the abundance of

antimicrobial resistance mechanisms which may be induced by *B. thailandensis* to alleviate the effects of 12-bis-THA particles.

Beta-lactamases are a class of enzymes that inhibit the activity of beta-lactam antimicrobials by hydrolyzing the beta-lactam ring and inactivating the compound. Seven beta-lactamase family proteins were identified in the proteomic data set and two deceased in abundance. Wagley *et al* have suggested that the export of BTH_II0462 to the extracellular milieu is important for the resistance to the beta-lactam antimicrobials amoxicillin, ampicillin, cefoxitin, and cefazolin but not imipenem. No synergy or additivity was observed between 12-bis-THA particles and meropenem or ceftazidime suggesting that BTH_II0462 does not mediate resistance to these compounds or that it is functionally redundant (325). This data suggests that 12-bis-THA particles do not non-specifically stimulate the expression of all chromosomally encoded resistance mechanisms and instead *B. thailandensis* tailors the expression of appropriate systems.

Chromosomally encoded efflux pumps are important antimicrobial resistance determinants in *Burkholderia* species. AmrAB-OprA is an efflux pump present in *B. thailandensis* and *B. pseudomallei*, and is responsible for the export of aminoglycosides and macrolides from the bacterial cytoplasm (280). AmrA and AmrB were both identified in the proteomic data set and increased in abundance in response to 12-bis-THA particles. BpeA and BpeB also increased in abundance under the same conditions. These proteins are components of BpeAB-OprB which is an efflux pump that also expels aminoglycoside and macrolides in addition to acriflavine (281). MacA and MacB are also efflux pump components. Both were identified in the proteomics data set but only MacA was differentially abundant in response to 12-bis-THA particles. As the cytoplasm is a highly reductive environment and the concentration of nucleic acids, it is thought that 12-bis-THA exists in its monomeric form within the cytoplasm. Therefore, it is possible that an efflux pump exists that is able to expel 12-bis-THA monomers. It is not known which, if any, of these pumps may expel 12-bis-THA monomers. Interestingly, BpeAB-OprB likely expels acriflavine with *ΔbpeAB* of *B. pseudomallei* showing increased sensitivity (281). Acriflavine shares structural similarity to the headgroup of 12-bis-THA suggesting that BpeAB-OprB may confer resistance to 12-bis-THA particles. Phenotypic assays are required to investigate any alignment between efflux pump expression and the susceptibility of *Burkholderia* species to 12-bis-THA particles.

The approach of using 12-bis-THA particles to deliver TFDs to the cytoplasm of bacteria and is not reliant on the sustained antimicrobial activity of the particles. Resistance to TFD activity is unlikely to arise through the expression of efflux pumps. Instead, resistance to TFD activity may occur if resistance to 12-bis-THA particles prevents successful transfection possibly due to the

modification of membrane components. Previously, studies have shown that TFD delivery is driven through a combination of ionic and lipophilic interactions (132,137). Therefore, the proteomics data set was interrogated to investigate changes in the abundance of proteins that control the composition of membrane lipids.

As 12-bis-THA particles are known to interact with bacterial LPS the data set was evaluated to investigate changes in related proteins. Firstly, we evaluated changes in the abundance of Lpx and Lpt proteins. The Lpx operon is responsible for synthesis of lipid A (326) whereas the Lpt operon is responsible for the trafficking of lipid A to the bacterial membrane (327). Mutations that inhibit the functions of these genes have been associated with resistance to membrane active molecules such as the polymyxin class of antimicrobial that includes colistin (328,329). Proteins from both operons were identified in the data set however no changes in abundance was observed suggesting that 12-bis-THA particles do not affect lipid A synthesis or trafficking.

In contrast, we identified the presence of two operons, BTH_II1982 - BTH_II1986 and BTH_II1975 - BTH_II1978, that were annotated as 'O-antigen related' proteins and deceased in abundance. The O-antigen is the repeating sugar component of the LPS and is connected to the lipid A by the core saccharide. BTH_II1982, BTH_II1983, and BTH_II1984 are predicted analogues of RfbH, RfbG and RfbF. The Rfb operon is associated with LPS synthesis and membrane composition. Mutations in RfbH in *Salmonella enterica* serovar *Enteritidis* have been linked with a reduction in motility and an increase in auto-aggregation and sensitivity to oxidative stress (330). Alternatively, the BTH_II1975 - BTH_II1978 operon is poorly annotated where BTH_II1978 (RfaC2) is the only protein to have a defined name. In *E. coli* and *S. enterica*, WaaC (formerly RfaC) contributes to the formation of the core oligosaccharide component of the LPS (331).

The proteomic data set showed a shift in two systems which may cause a reduction in the sensitivity to 12-bis-THA particles in *B. thailandensis*. Firstly, efflux pump components were overexpressed in response to 12-bis-THA particles which may export 12-bis-THA from the cytoplasm but further investigations are required to investigate which, if any, efflux pumps recognise 12-bis-THA as a ligand. However, efflux mediated resistance to 12-bis-THA particle is unlikely to affect its role as a delivery molecule for oligonucleotide TFD antimicrobials. Alternatively, we observed a decrease in the abundance of proteins involved with the production of LPS O-antigen and core oligosaccharide. Previously, Montis *et al* have shown that the cationic headgroup of 12-bis-THA interacts with the negatively charged GlcN-A subunit of the LPS core oligosaccharide potentially facilitating internalisation (137). A reduction in the core oligosaccharide may prevent 12-bis-THA particles from transfecting *B. thailandensis* and potentially reduce the efficiency of TFD delivery

resulting in a reduction of TFD activity. Future studies should be performed to investigate the development of 12-bis-THA particle resistance and changes in LPS chemotype in response to repeat subculture in sub-inhibitory concentrations of 12-bis-THA particles.

5.3.5 12-bis-THA particles cause the suppression of important virulence factors

The proteomic data set showed a decrease in the abundance of virulence factors by *B. thailandensis* in response to 1X MIC of 12-bis-THA particles. Thirty-two flagella components were identified and seventeen had deceased in abundance. Flagella are hair-like fibers that protrude from the bacterial outer membrane where they rotate at high speed to drive locomotion (332). This is driven by the motor proteins MotA and MotB which utilize PMF to rotate the flagella resulting in movement (333). In *B. pseudomallei*, flagella are important virulence factors when delivered intranasally in a mouse model (334). The proteomic data showed that the motor proteins MotA and MotB, in addition to flagellin (BTH_I3196) which makes up the lash component, deceased in abundance in response to 12-bis-THA particles.

We also identified fifteen proteins that were associated with the T3SS comprising of nine apparatus proteins and six secretory proteins. The T3SS-3 is an important virulence factor in *B. pseudomallei, B. thailandensis,* and *B. mallei* where it plays a role in cellular invasion and survival (291). Only one protein associated with the secretion apparatus had deceased in abundance whereas four secreted proteins deceased in abundance in response to 1X MIC of 12-bis-THA particles. BipC and BipB both deceased in abundance and potentially form a complex *in vivo* which is responsible for forming a translocation pore in the eukaryotic membrane. Deletion of either of these proteins greatly attenuates the virulence of *B. pseudomallei* in a murine model (59,62). BicP is a chaperone protein and is predicted to bind to BopA (296), both of which deceased in abundance in the proteomic data set. BopA allows *B. pseudomallei* to escape from the phagosome prior to fusion with the lysosome and is important for virulence *in vivo* (59).

It is unknown as to why *B. thailandensis* might suppress important virulence factors in response to drug stress. One potential reason is that dysregulation of respiration might induce oxidative stress and deplete the cytoplasmic concentration of high-energy molecules resulting in the bacteria needing to suppress superfluous pathways such as the T3SS. Additionally, the dissipation of PMF resulting in a reduction in periplasmic protons uptake would likely prevent bacterial motility. Alternatively, **Chapter 4** suggested that 12-bis-THA particles might stimulate biofilm formation in *B. thailandensis* at low concentrations. Suppresion of motility proteins has been associated with biofilm maturation in *P. aeruginosa* which suggests that 12-bis-THA particles may induce biofilm formation in *B. thailandensis* in response to 12-bis-THA due to the curtailment of motility.

In summary, the multi-omics approach used in this chapter has provided insight into the mechanism of action of 12-bis-THA particles against *B. thailandensis*. The data showed that particles affected a diverse range of pathways including central metabolism, oxidative stress, antimicrobial resistance mechanisms, and virulence factors. These will be considered in the next chapter when developing TFDs with a particular focus on regulatory elements controlling metabolism and oxidative stress in *B. pseudomallei.*

CHAPTER 6 - THE DEVELOPMENT OF TFDS TO INHIBIT THE GROWTH OF *B. THAILANDENSIS*

6.1 INTRODUCTION

Burkholderia species are intrinsically resistant to many antimicrobials which makes treating infections caused by these species clinically challenging. *B. pseudomallei*, the etiological agent of melioidosis, is particularly challenging to treat due to its ability to invade host cells and to form biofilms. Due to this, melioidosis requires a biphasic therapeutic approach that utilises oral and intravenous antimicrobials to prevent patient mortality. The first phase is the treatment of the acute phase of the disease and consists of intravenous ceftazidime or meropenem to prevent to development of sepsis (80). This typically lasts up to fourteen days but can be extended to eight weeks for infection with bone or neurological involvement (335). This is followed by the eradication phase which consists of a three to six-month course of oral co-trimoxazole or co-amoxiclav to prevent relapse (81). Despite the timely initiation of the appropriate treatment strategy, mortality still occurs in 10 to 40% of cases suggesting the need for new antimicrobials with improved efficacy (38,79).

Transcription factor decoys (TFDs) are a new class of precision antimicrobials that are selectively engineered to target specific bacteria without affecting the host microbiota. Previous, They are synthetic oligonucleotides that contain the transcription factor binding motif of an essential bacterial transcription factor from the target species. Upon entering the bacterial cytoplasm, the TFDs act as competitive inhibitors that sequester the target transcription factor. By doing so they inhibit the transcription factor from binding to its genomic target, preventing expression of its regulon. As TFD technology acts on novel targets, spares the host microbiota (139), and is refractory to traditional antimicrobial resistance mechanisms, it is a potential alternative to small molecule-based antimicrobials for the treatment of melioidosis.

One challenge for the development of TFD technology is the identification and characterization of new transcription factors. To do so, the McArthur group have previously used two approaches to identify new candidates for TFD development: by performing literature searches to identify essential, characterised transcription factors, or by performing proteomic studies on the target organism under varying conditions. Using the literature-based approach, the McArthur group developed a TFD to target WalR in methicillin-resistant *Staphylococcus aureus* (336). Alternatively, a combined proteomic and literature approach was used to develop a TFD to target FNR in *Enterobacteriaceae* species (139). Using a combined approach, this chapter will:

- Identify transcription factors from the proteomic data set that regulated the 12-bis-THA stress response that may be targeted using TFD technology

- Review the literature to identify characterised transcription factors in *Burkholderia* species that can be developed into an anti-melioidosis TFD
- To investigate the antimicrobial activity of TFDs against *B. thailandensis* to identify candidates for further testing in *B. pseudomallei*

6.2 RESULTS

6.2.1 Transcription factors that increased in abundance in the proteomic data set

Firstly, the proteomic data that was generated in **Chapter 5** set was interrogated to identify transcription factors that control the stress response to 12-bis-THA particles in *B. thailandensis*. These will regulate genetic pathways necessary for bacteria to survive the treatment, giving insights into the mechanism of action of the particles. The transcription factors represent a novel type of therapeutic target that could be inhibited with the TFD approach. As such, there is potential for synergy between the action of TFD delivery, mediated by the 12-bis-THA particles, and the inhibition of the induced stress response by the selected TFD. A list of transcription factors and regulatory elements was generated by manually curating the Proteome Discoverer outputs.

Proteins with the keywords “transcription”, “factor”, “transcription factor”, “Regulatory”, “DNA-binding protein”, “Sensory kinase” and “two-component system” were transferred to a new database which was analysed with Perseus. Volcano plots with the statistical parameters of FDR: 0.01 and S0: 1 were used to identify differentially abundant regulatory elements in response to 12-bis-THA particles. In response to 0.1X MIC of 12-bis-THA particles, two transcription factors increased in abundance, and none decreased (**Figure 6.1A**). In contrast, fourteen increased in abundance and forty decreased in abundance in response to incubation with 1X MIC of 12-bis-THA particles (**Figure 6.1B**)

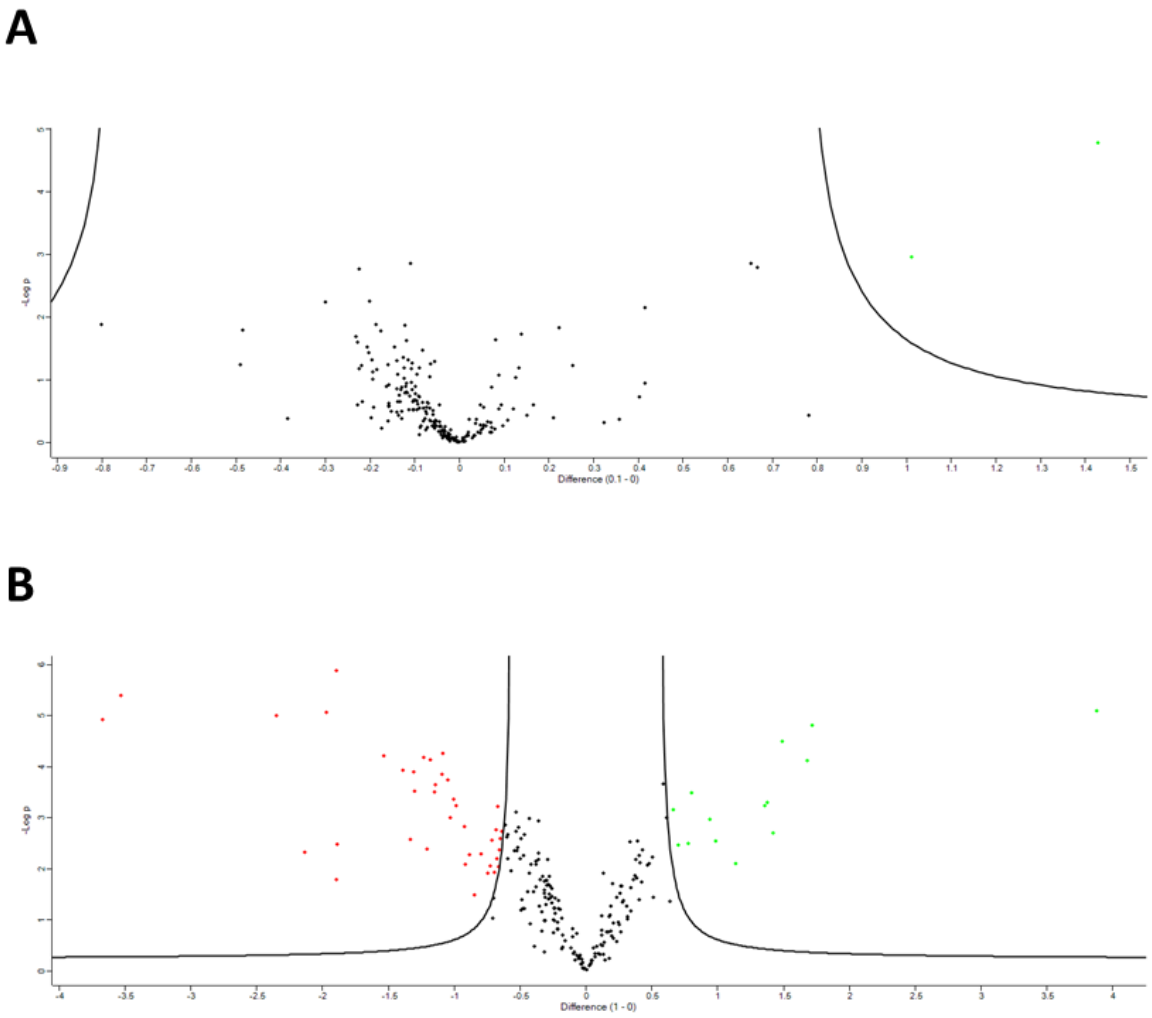

Figure 6.1: Volcano plots showing changes in transcription factor abundance in *B. thailandensis* strain E555 following incubation with 12-bis-THA particles. (**A**) shows the transcription factor proteome of bacteria treated with 0.1X MIC of 12-bis-THA particles compared to the untreated control. (**B**) shows the transcription factor proteome of bacteria treated with 1X MIC of 12-bis-THA particles when compared to the untreated control. Data points in green represents a significant increase in protein abundance whereas data points in red show a significant reduction in protein abundance. Fold change significance was determined using FDR of 0.01 and an S0 value of 1.

The top ten regulatory factors that increased in abundance in response to 1X MIC of 12-bis-THA are shown in **Table 6.1**. As in **Chapter 5**, this data is present as $\log_2$ fold change which is centered on 0. These include the two transcription factors that increased in abundance in response to 0.1X MIC 12-bis-THA particles and also increased in abundance in response to the higher concentration of 12-bis-THA particles. Of the identified regulators, we identified eight transcription factors and two sigma factors. Most of the regulatory factors in **Table 6.1** were poorly annotated therefore blast analysis was performed to better understand the potential biological function of the proteins and to identify candidates for TFD development.

Table 6.19: Top 10 regulatory elements that increased in abundance in response to 12-bis-THA particles. Values in bold indicate statistical significance determined using the volcano parameters FDR: 0.01 and S0: 1.

			Fold change (Log_2)	
Annotation	**Accession number**	**Gene**	**0.1X MIC**	**1X MIC**
RNA polymerase sigma factor RpoD	Q2T2N0	BTH_I0088	-0.49	**3.88**
TetR family transcriptional regulator	Q2T0R4	BTH_I0679	**1.43**	**1.72**
LysR family transcriptional regulator	Q2T3F3	BTH_II2108	0.22	**1.68**
IclR family transcriptional regulator	Q2SYR2	BTH_I1391	-0.08	**1.49**
Transcription regulator LuxR family protein	Q2T5S8	BTH_II1275	0.40	**1.42**
Regulator AmrR	Q2SVT2	BTH_I2446	**1.01**	**1.38**
DNA-binding response regulator	Q2T4G6	BTH_II1739	0.65	**1.36**
RNA polymerase factor sigma-32	Q2T1D5	BTH_I0456	-0.09	**1.14**
Transcriptional regulator	Q2SW09	BTH_I2369	-0.01	**0.98**
LysR family transcriptional regulator	Q2T0W0	BTH_I0632	0.67	**0.94**

6.2.2 Computational prediction of TF function

6.2.2.1 BTH_I0679 – Transcriptional regulator (TetR family)

BTH_I0679 is a TetR family transcriptional regulator that increased in abundance 1.43-fold and 1.72-fold in response to incubation with 0.1X MIC and 1X MIC of 12-bis-THA particles respectively. It is conserved in *B. pseudomallei* sharing substantial amino acid homology with BpeR (coverage – 99%, identity – 98.57%) which is a putative repressor that controls the expression of the BpeAB-OprB resistance-nodulation-division (RND) efflux pump. BTH_I0679 is located upstream of BTH_I0680, BTH_I0681 and BTH_I0682 which are homologues of BpeA, BpeB and OprB respectively. Following exposure to 1X MIC of 12-bis-THA particles, BTH_I0680 and BTH_I0681, which are components of the BpeAB-OprB pump, both increased in abundance in the whole proteomic data set (**Chapter 5**).

6.2.2.2 BTH_I2446 - AmrR

BTH_I2446 (AmrR) increased in abundance in *B. thailandensis* 1.01-fold and 1.38-fold when challenged with 0.1X MIC and 1X MIC concentrations of 12-bis-THA particles respectively. It is conserved in *B. pseudomallei* (coverage – 100%, identity – 95.22%) and is a transcriptional regulator of the AmrAB-OprA RND pump that encodes for aminoglycoside and macrolide resistance (280). To a lesser extent, there was similarity to MexZ (Coverage – 98%, Identity – 59.33%) which is the transcriptional repressor for the MexXY efflux pump in *P. aeruginosa*. AmrR is located upstream from BTH_I2444 and BTH_I2445 which both increased in abundance in response to 1X MIC of 12-bis-THA particles.

6.2.2.3 BTH_II2108 - Transcriptional regulator (LysR family)

BTH_II2108 increased in abundance 1.68-fold in *B. thailandensis* following challenge with 1X MIC of 12-bis-THA particles. It is highly conserved in *B. pseudomallei* sharing significant amino acid homology with BPSS0290 (Coverage – 99%, identity – 97.90%) and encodes BpeT, a transcriptional regulator that controls the expression of the *bpeEF-oprC* operon. *bth_II2109* is located downstream of *bth _II2104, bth _II2105*, *bth _II2106* and *bth_II2107* which encode homologues of the CeoAB-OpcM RND from *B. cenocepacia.* No components of these pumps were identified in the proteomic data set.

6.2.2.4 BTH_I0632 – LysR family transcriptional regulator

BTH_I0632 increased in abundance 0.94-fold in response to 1X MIC of 12-bis-THA particles. It is conserved in *B. pseudomallei* (Coverage 100% and Identity 95.06) where it is annotated as BpeS. This transcription factor acts as a co-activator on the *bpeEF-oprC* operon in conjunction with BpeT (337). The proteins components of the BpeEF-OprC RND pump were not identified in the proteomic data set so it is not possible to infer whether BTH_I0632 was functionally active in response to incubation with 12-bis-THA particles.

6.2.2.5 BTH_I1391 - Transcriptional regulator (IclR family)

BTH_I1391 is an IclR family transcriptional regulator that increased in abundance 1.49-fold in *B. thailandensis* when challenged with 1X MIC of 12-bis-THA particles and is highly conserved in *B. pseudomallei* (coverage – 99%, identity – 94.30%). Homologues of BTH_I1391 were identified in *E. coli, P. aeruginosa* and *Salmonella typhi* (**Table 6.2**).

Table 6.210: Identification of BTH_I1391 homologues in *E. coli*, *P. aeruginosa* and *S. typhi* using BlastP.

Species	Coverage (%)	Identity (%)	E-value	Orthologue
E. coli	58	38.20	2e-14	PcaR
P. aeruginosa	92	42.21	2e-56	IclR family transcriptional regulator
S. typhi	85	25.97	6e-12	Glyoxylate bypass operon transcriptional regulator

PcaR is a transcriptional regulator of the *pca* operon which in *Pseudomonas putida* is responsible for the degradation of aromatic compounds (338). It is a transcriptional activator that acts in association with the pathway intermediate β-ketoadipate to allow for growth on benzoate (339). Also, BTH_I1391 shares homology with IclR, a transcriptional repressor that acts on the glyoxylate

bypass operon (*aceBAK*) which circumvents the two carbon dioxide evolving steps of the Tricarboxylic acid (TCA) cycle (340,341). Proteins associacted with this pathway deceased in abundance in response to 12-bis-THA particles as described in **Chapter 5**.

6.2.2.6 BTH_II1275 – Transcriptional regulator (LuxR family)

The abundance of BTH_II1275 was increased by 1.42-fold following the challenge with 1X MIC of 12-bis-THA particles. It is highly conserved in *B. pseudomallei* (coverage – 100%, identity – 97.39%) but no homologues were identified in *B. mallei, E. coli, S. typhi, P. aeruginosa* or *A. baumannii.* It contains a predicted Per-Arnt-Sim (PAS)-domain which are sensory domains of cytosolic proteins that respond to stimuli such as light, oxygen and redox potential (342). BTH_II1273 and BTH_II1274 encode for 2, 4 dienoyl-CoA reductase and a hypothetical protein, both of which increased in abundance following exposure to 1X MIC of 12-bis-THA particles (**Table 6.3**). The *B. pseudomallei* homologue BPSS1131 is located upstream of *fadH* that encodes 2,4 dienoyl-CoA reductase, an auxiliary enzyme involved in Beta-oxidation (343).

Table 6.3: Expression of differentially abundant proteins in the same operon as BTH_II1275 in response to 12-bis-THA particles. Data were identified in the whole proteome data set with values in bold representing statistical significance in the context of the volcano statistics.

			Fold change (Log_2)	
Accession number	**Protein name**	**Gene**	**0.1X MIC**	**1X MIC**
Q2T5T0	2,4 dienoyl-CoA reductase	BTH_II1273	-0.02	**2.45**
Q2T5S9	Conserved hypothetical transmembrane protein	BTH_II1274	-0.10	**1.85**

6.2.2.7 BTH_II1739 - DNA-binding response regulator

The abundance of BTH_II1739 was increased 1.36-fold in *B. thailandensis* when challenged with 1X MIC of 12-bis-THA particles. This protein shares considerable homology with BprR from *B. pseudomallei* (coverage – 100%, identity – 96.67%). BprRS is a two component system (TCS) in which BprR is the transcription factor activated by histidine kinase protein BprS. BTH_II1740 is also conserved in *B. pseudomallei* where it shares amino acid similarity with BprS (coverage – 100%, identity – 91.86%) however it did not change in abundance in the proteomics data set.

6.2.2.8 BTH_I2369 – Transcriptional regulator

BTH_I2369 is annotated as a transcriptional regulator and increased in abundance 0.98-fold in response to 1X MIC of 12-bis-THA particles. It is not present in *B. pseudomallei* or *B. mallei* but was identified in several BCC species where it was annotated as a AraC family transcriptional regulator. These are transcriptional regulators controlling a diverse range of cellular functions such as carbon metabolism, virulence, and stress (344). The amino acid sequence of BTH_I2369 was compared to the proteome of *E. coli, P. aeruginosa, S. typhi, and A. baumannii* using BlastP to identify possible orthologues which may allow us to infer the function of Bth_I2369 however no characterised orthologues were identified (**Table 6.4**).

Table 6.4: Identification of BTH_I2369 homologues in *E. coli, P. aeruginosa* and *S. typhi* using BlastP.

Species	Coverage (%)	Identity (%)	E-value	Orthologue
E. coli	23	43.68	1e-16	AraC family transcriptional regulator
P. aeruginosa	75	25.94	3e-25	AraC family transcriptional regulator
S. typhi	29	33.94	1e-12	AraC family transcriptional regulator
A. baumannii	23	43.68	7e-18	AraC family transcriptional regulator

6.2.2.9 Sigma factors

Sigma factors are regulatory elements that facilitate the attachment of transcription factors to genomic DNA and control the expression of different sets of genes. The transcription factor database was interrogated to identify differentially abundant sigma factors in response to 12-bis-THA particles (**Table 6.5**). Three sigma factors were differentially abundant in the transcription factor database.

BTH_I0456 which is annotated as RpoH increased in abundance 1.14-fold in response to 1X MIC of 12-bis-THA particles. The *Burkholderia* genome browser identified homologues of BTH_I0456 in *B. pseudomallei*, *B. mallei* and some BCC species where they were annotated as either RpoH or Sigma-32. In *E. coli*, RpoH is an important regulatory factor that controls the expression of heat shock associated proteins (345). Vanaporn *et al* showed that RpoH was induced in *B. pseudomallei* in response to heat shock (346). In *B. pseudomallei*, RpoH slightly increased in abundance under hypoxic conditions suggesting that it might play a role in respiratory adaption (347) or may be induced in response to alternative stress sources.

RpoS (BTH_I2226) was down regulated 1.18-fold in response to 1X MIC of 12-bis-THA particles. As with RpoH, homologues of BTH_I2226 were identified in *B. pseudomallei*, *B. mallei* and some BCC species and all were annotated as RpoS. In *B. pseudomallei*, RpoS is induced in response to oxidative stress and positively regulates the expression of OxyR, DpsA and KatG (348). This is consistent with the observation in **Chapter 5** that showed that DpsA and KatG decreased in abundance in response to 12-bis-THA particles.

BTH_I0088, which is annotated as RNA polymerase sigma factor RpoD, increased in abundance 3.88-fold in response to 12-bis-THA particles. Homologues of BTH_I0088 were identified in *B. pseudomallei* and *B. mallei* where they were annotated as RNA polymerase sigma factor RpoD or RNA polymerase sigma factor. A homologue was also identified in *B. cenocepacia* J2315 that was annotated as SigJ. A study Menard *et al* showed that SigJ is an auxiliary primary sigma factor that is conserved exclusively in *Burkholderia* species making it a potential candidate for TFD development (349). However, to date, no studies have been performed to identify its molecular function or binding motif.

Table 6.5: Sigma factors identified in the transcription factor database. Values in bold represent statistical significance in the context of the volcano statistics

			Fold change (Log_2)	
Accession number	**Protein name**	**Gene**	**0.1X MIC**	**1X MIC**
Q2SU53	RpoA	BTH_I3042	-0.06	0.18
Q2SU19	RpoB	BTH_I3076	-0.06	0.39
Q2SU20	RpoC	BTH_I3075	-0.06	0.37
Q2T7M8	RpoD	BTH_II0621	-0.02	0.36
Q2T1D5	RpoH	BTH_I0456	-0.09	**1.14**
Q2SWF2	RpoS	BTH_I2226	-0.12	**-1.18**
Q2SY71	RpoZ	BTH_I1587	-0.06	0.08
Q2STT9	FliA	BTH_I3166	-0.05	-0.68
Q2T2N0	RNA polymerase sigma factor RpoD	BTH_I0088	-0.49	**3.88**
Q2T1A6	RNA polymerase sigma-54 factor	BTH_I0486	-0.11	-0.35
Q2SZU8	RNA polymerase sigma-70 factor, ECF family	BTH_I0997	-0.06	-0.20
Q2SZQ1	RNA polymerase sigma-70 factor, ECF family	BTH_I1044	0.09	0.39
Q2SXU1	RNA polymerase sigma factor	BTH_I1723	0.02	0.41

6.2.3 Identification of TFD candidates from the literature

One aim of the proteomics study was to identify regulatory elements that controlled the stress response to 12-bis-THA particles in *B. thailandensis*. From this, strains deficient in these genes would have been purchased from a transposon library generated Maniol *et al* and screened for exploitable phenotypes such as sensitivity to 12-bis-THA particles or antimicrobials, or reduction of growth. Unfortunately access to this resource had been discontinued and it was beyond the scope of the project to create fresh knock-outs. Therefore, to identify additional TFD candidates I performed a literature review of essential genes in *Burkholderia* species and computational analysis to deduce their transcriptional regulation.

6.2.3.1 TEX

TEX (toxin expression) protein was first studied in *Bordetella pertussis* where it was shown to be essential for the expression of toxin-associated genes (350). TEX family proteins are ubiquitous in bacteria but exhibit a wide array of molecular functions (351). In *Streptococcus pneumoniae,* it does not affect the expression of major pneumococcus toxin pneumolysin but instead is associated with bacterial fitness (352). In *P. aeruginous*, it is important in establishing chronic lung infections but its function is unknown but it may play an important role in the trafficking of ssRNA to the ribosome (353). In *B. pseudomallei*, a ΔTEX strain was strongly attenuated *in vivo* and displayed a reduction in the ability to invade and replicate within cells (354). Though the mechanism underpinning this phenotype is unknown, it is clear that TEX plays an important role during *in vivo* colonisation

TEX is not a transcription factor but rather a transcriptional accessory protein that preferentially binds single-stranded RNA (351) potentially through the S1 domain (350) contained within the C-terminus of the protein. Spt6 is a eukaryotic elongation factor that interacts with RNAP and mRNA processing factors (355). It has been proposed that TEX may be functionally similar to Spt6 as there is some sequence conservation particularly in important domains including S1 (355). Combining this information with the knowledge that TEX is co-purified with RNAP, RNAse E or PNPase (351) suggests that TEX may play a role in mRNA trafficking and homeostasis. The sequence used in this study was based upon the crystal structure derived from a TEX orthologue in *P. aeruginosa* and was shown to preferentially bind single stranded RNA molecules (351).

6.2.3.2 Bcam1349 - Burkholderia FNR (BFNR)

Fumarate and nitrate reductase (FNR) was identified as a candidate for TFD development in *E. coli* as it increased in abundance in response to sub-inhibitory concentrations of 12-bis-THA particles (data not shown). It is a member of the cyclic adenosine monophosphate (cAMP) receptor protein (CRP) family and a transcription factor that controls the switch from aerobic to anaerobic respiration. The characteristics of the *E. coli* homologue have been thoroughly investigated and has been shown to bind to a $TTGAT_{N4}ATCAA$ consensus sequence (356). In *E. coli*, FNR becomes functionally active through the formation of a homodimer that is held together by the formation of an Fe-S cluster which forms between five conserved cysteine residues under anaerobic conditions (357). FNR family proteins are conserved throughout prokaryotes and not only regulates respiration but also key virulence factors including biofilm formation, motility, and cellular invasion (358).

Bcam1349 is a homologue of FNR in *B. cenocepacia* (359). Sequence searches on 385 partial and 50 full sequenced *B. pseudomallei* genomes in addition to 26 partial and 22 full sequenced *B. thailandensis* genomes show that Bcam1349 homologues are highly conserved in *Burkholderia* species. However upon further investigation, *B. cenocepacia* (Bcam1349), *B. pseudomallei* (BPSL0617) and *B. thailandensis* (BTH_I0534) homologues did not show conservation of Fe-S binding pocket-forming cysteines as shown in **Figure 6.2**. Where characterised, the Fe-S binding domain detects the presence of oxygen or other reactive oxygen species. The loss of this pocket suggests that FNR in *Burkholderia* species is responding to a different stimulus which is consistent with studies by Fazli *et al* which show that Bcam1349 binds to cycli- di-GMP (359).

E. coli strain K12 (FNR): MIPEKRIIRRIQSGGCAIHCQDCSISQLCIPFTLNEHELDQLDNI
B. cenocepacia strain J2315 (Bcam1349): MLHLHSSYSANAILAALPEDSIRTIAPHLELVRIKAGMLDRVGEP
B. pseudomallei strain K96243 (BPSL0617): MRNGILRRGRAAPTNRDTNMLHQNNGFHANALLGSLADDSLRALA
B. thailandensis strain E264 (BTH_II0534): MSGQCLYILRNRTNWHVNRLRVFTPSQEGGASVCKRTTRRAADTI

Figure 6.2: Amino acid sequence alignment of FNR in *E. coli* strain K12 with homologs in *B. cencocepacia* strain J2315, *B. pseudomallei* strain K96243 and *B. thailandensis* strain E264. Residues highlighted in red represent amino acids which are essential for the function of FNR in *E. coli* through the formation of an Fe-S cluster.

A literature review was performed to identify genes regulated by FNR in *E. coli* strain K12 (360,361). A list of these genes was compiled, and homologues were identified in *B. pseudomallei.* Using respective genome browsers, homologous genes were identified with priority given to those that shared comparable synteny based on the *Burkholderia* genome browser and had a known biological function. The 500 bp sequences upstream of each selected gene were searched for potential FNR binding sites using the *E. coli* consensus sequence and the Prodoric search function. Identified sequences were then allocated a position weight matrix score with higher scores pertaining to sequences that were highly similar to the characterised binding motif. For FNR, the maximum score allocated to a newly identified pattern is 8.93 which denotes a sequence that is highly similar to the known binding motif of FNR.

From the upstream regions of the seven genes analysed, Prodoric identified thirteen potential FNR-like binding motifs (**Table 6.6**). Three FNR-like binding motifs were located upstream of *cydA,* a gene that encodes an integral component of cytochrome D ubiquinone oxidase. Two of these motifs displayed position weight matrix scores of 8.93 and 8.92 respectively indicating substantial similarity to the FNR binding motif in *E. coli.*

Table 6.6: The identification of FNR-like binding motifs in *B. pseudomallei*. A list of genes in *B. pseudomallei* was produced by identifying homologues from the FNR regulon in *E. coli*. The 500 base pair nucleotide sequence upstream of each *B. pseudomallei* gene was taken from the *Burkholderia* genome browser and interrogated using Prodoric virtual footprint to identify possible FNR binding domains.

Gene	Start position	End Position	Strand	Position weight matrix score	Sequence
X941_RS19270 (HCP)	245	258	+	6.63	ATGAGATGTATAAA
BURPS1710b_2060 (fimA)	190	203	+	6.49	TTGTTGTATCAAAA
BURPS1710b_2060 (fimA)	113	126	+	6.44	TTGCGAAAAATGAA
BPSL2865 (katG)	173	186	-	8.10	TTGATATATGTAAT
BPSL2865 (katG)	159	172	-	7.70	TTGATAAATTTTAT
BPSL2865 (katG)	471	484	+	7.68	TTGTTTCCCCGCAA
BPSL3304 (tsr)	413	426	-	8.34	TTGCTCGTCATCAG
BPSL3304 (tsr)	413	426	+	7.83	CTGATGACGAGCAA
BPSL1351 (carB)	482	495	-	8.21	TTGGGATTCAGAAA
BPSL2818 (purM)	410	423	+	8.76	TTGCTTTCCCTGAA
BPSL0502 (cydA)	233	246	+	8.93	TTGACTCTCATCAA
BPSL0502 (cydA)	233	246	-	8.92	TTGATGAGAGTCAA
BPSL0502 (cydA)	54	67	-	7.99	TTGCGTTTGCTCAA

A CydA homologue (BTH_I0454) was identified in *B. thailandensis* and three possible binding motifs were identified in its promoter region. All three showed considerable overlap which may result in nucleotides being counted multiple times which might account for position weight matrix scores above 8.93. The sequences highlighted in green showed substantial similarity to the reference FNR

binding sequence from *E. coli*, and with those identified upstream of the *cydA* gene in *B. pseudomallei* (**Table 6.7**). The conservation of these sequences in relation to each other but also the transcription factor binding motif in *E. coli* suggests that these sequences may be useful in the development of TFDs to inhibit Bcam1349.

Table 6.7: The identification of FNR-like binding motifs upstream of CydA in *B. thailandensis* strain E264. The 500 base pair nucleotide sequence upstream of cydA in *B. thailandensis* was taken from the *Burkholderia* genome browser and interrogated using Prodoric virtual footprint to identify possible FNR binding domains.

Gene	Start position	End Position	Strand	Position weight matrix score	Sequence
BTH_I0454	233	246	+	9.37	TTGACTTTCATCAA
BTH_I0454	233	246	-	9.11	TTGATGAAAGTCAA
BTH_I0454	239	252	-	8.07	TTCTTGTTGATGAA

6.2.3.3 GvmR

The global virulence and metabolism regulator (GvmR) is a LysR-type transcriptional regulator in *B. pseudomallei* that controls the response to oxidative stress, cellular invasion, biofilm formation, motility, and secondary metabolism. The proteomic study was performed with *B. thailandensis* with the aim of understanding more about the mechanism of delivery of 12-bis-THA particles and to identify transcription factors that control the stress response, as these would be targets for TFDs to block the bacterium's ability to recover. Interestingly, the data showed an upregulation of proteins associated with the type 6 secretion system cluster 2 (T6SS-2) (15/15 detected) which is under the regulation of GvmR. A homologue of GvmR (BTH_I0124) was also identified in the proteomics dataset but it was not differentially abundant in response to 12-bis-THA particles.

To date, the binding motif of GvmR has not been published therefore we used Prodoric to predict the potential transcription factor binding motif. Some transcriptional regulators including the LysR-type transcriptional regulator have exhibited autoregulatory functions therefore Prodoric was used to analyse the 500 base pair regions upstream of the GvmR promotor in an attempt to identify putative binding sites. For this, the LysR-type transcriptional regulators CynR, CysB, NhaR and OxyR

were selected in Prodoric as no others were available at the time of analysis. Three OxyR-like and one NhaR-like binding motifs were identified in the promotor region of GvmR (**Figure 6.3**).

Promoter Sequence:

ATCTCGAAGC AATTGAGCTT GCGGACGGCG TCCTGGTAGT CGTCGAGGAT GGCAATTTTC ATGGCGTGTT TCGGGATTCG
CGCGAGATGA GCGATGGAAG ACGGTGGCCG CCGCGCACTG TCGCGCGCCG GTCCGGTCCG GTTTGAGGGC CGTAATGATC
CTATGACGGC ACGGCAACAG GTGTATCTCT TTTTAACAGC TTGTTACGCG CGGCCGCAAG CGCCGCCGTC CGGGCGCGGA
TCGCGTTGTT CCGACCCCAC GCGATGCCGA GCCGACAGCG ATTCCGACGT TTCTCGATTG GGCAATTTCG GGAGTGAGAT
TGCTCAATTA TTTCATTTTT AAGAACAATT GGTCTATCTA GCTAGGTAGG CTGAGCAAGT TCGAAGGTTT TTGTCGAGAT
TTCGCGGGAA GTTGAGCAAC TCTGCATCTT TTTCGCTGTC GTAGGAAAAT TACTCATTTG CTTCATATTT TTGAAGCTGT
AACAGCGGTA GGAGCGGAGT

Transcription factor	Start Position	End Position	Strand	Score	Sequence
NhaR | *E.* coli (strain K12)	334	344	-	12.05	TCTTAAAAATG
OxyR | *E. coli* (strain K12)	336	346	-	4.30	GTTCTTAAAAA
OxyR | *E. coli* (strain K12)	428	438	-	4.07	CAGCGAAAAAG
OxyR | *E. coli* (strain K12)	289	299	-	4.05	AATCGAGAAAC

Figure 6.3: Identification of LysR type transcriptional regulator binding motif patterns in the 500 base pair region preceding GvmR in *B. pseudomallei*. The nucleotide sequence was taken from the *Burkholderia* genome browse and interrogated using Prodoric virtual footprint.

Prodoric analysis of the promoter sequences of the 41 genes described in the GvmR regulon was performed (275). All contained at least one potential OxyR binding sites to which GvmR may bind, with the majority containing doublets or triplets. For example, the gene encoding the T6SS-2, that is positively regulated by GvmR, contained three sites. This may suggest that GvmR binds to the promotor region as a multimer. As treatment with 12-bis-THA particles increases the abundance of T6SS-2 (**Chapter 5**), potentially in response to oxidative stress induced by the particles, designing of a TFD to block GvmR binding may have a synergistic effect with the particles: these induce oxidative stress and the TFD inhibits GvmR to diminish bacterial response.

Promoter Sequence:

CTCACGCTGC CGTCGCCGAT ATGGTCGGGC ATCCTGCAGT CGTTCAGGTG TCCGTCGTGA TGCGTCGAGC ATCGGTATTC
ATGCGCCGCA GGGCGCGCAC ACTGGAAAGG AGCAAGACAT GATCGATCCG AAGGAAATCT TTGCGGCATG CAACAACGCG
CACCAGTACG GGCAGGACGC GAGCGGCTCG ATGGCCAAGC CGTTCATGGA TTCGATCCCG GATCTGTCGA CGGCGTCGTC
GAGCAACGCG AGCAACCTGA TCGGCAACGT GCAGCAGGTG GGCTCGAAGA TGCTCGAGCA CATGTCGACG ATCAAGTCGG
CGGTGGACAA GCAGGTGATG ATCCATCAGG ACAACCAGCA GCGTCAGAAG ACGTACGACT TCAACGTCGA CATGCGGGAC
CTGCGGCCGA CCAACGCGGT CGGCTTCCCG GAGGAGATGC CGTCGATCTT CTTCGCGCCG TTCAGGACCG GCAAGTGACG
CGCTTCGGCT GCGTGGGCAG

PWM (species)	Start Position	End Position	Strand	Score	Sequence
OxyR | *E. coli* (strain K12)	139	149	-	3.34	ATGCCGCAAAG
OxyR | *E. coli* (strain K12)	362	372	+	3.29	CGTCAGAAGAC
OxyR | *E. coli* (strain K12)	344	354	+	3.23	CATCAGGACAA

Figure 6.4: Prodoric analysis of the intergenic region preceding BTH_I1883 (TseM).

Considering that 12-bis-THA particles induce the production of T6SS-2 proteins, a TFD that selectively inhibits GvmR might synergise with the delivery agent through suppression of the bacterial stress response. However, TFDs have traditionally developed to inhibit transcription factors that have well-characterized bind motifs such as FNR, NarL, and WalR. As the binding motif of GvmR is currently unknown, TFDs were developed to incorporate multiple predicted binding motifs and the neighbouring sequence (**Figure 6.4**).

6.2.3.4 Zur

The zinc uptake regulator (Zur) is a ubiquitous bacterial transcriptional regulator that controls zinc homeostasis and is a member of the ferric uptake regulatory (FUR) transcription factor family. It predominantly acts as a transcriptional repressor when bound by Zn^{2+} and prevents the expression of downstream genes by blocking the RNAP from binding at the -35 consensus site (362). When the cytoplasmic concentration of Zn^{2+} declines, Zur loses binding activity relieving the repression of its regulon (362).

Zur also has a role in controlling the expression of ribosomal proteins, transcription factors and signal peptides in addition to affecting amino acid metabolism (363). In *Listeria monocytogenes* mutation of Zur results in retardation of growth and reduction of motility *in vitro*, and slight attenuation *in vivo.* However, this attenuation was not observed in mutant strains of *S. enterica* suggesting that the function and importance of Zur can vary depending on the bacterial species

studied (364). It has been proposed that Zur, along with GvmR, OxyR and TctR, regulate the homeostasis of Zn^{2+} and potentially manganese in *B. pseudomallei* through the regulation of the T6SS-2 (365). As 12-bis-THA particles induce the expression of the T6SS-2, Zur is an interesting candidate for TFD development as it may interfere with the ability of *B. thailandensis* and potentially *B. pseudomallei* to induce important stress systems to respond to 12-bis-THA particles.

6.2.4 Phenotypic investigations of TFD activity against *B. thailandensis*

6.2.4.1 The sequences used in this study

Table 6.8 shows the sequences and structures of the TFDs used in this thesis. BFNR1 and BFNR3 were prepared by IDT in the hairpin format where the final three nucleotides were phosphorothioate to prevent endonuclease degradation. TEX1 and TEX2 were also synthesized by IDT but as ssRNA. TEX1 was formed as normal nucleotides whereas TEX2 was formed of O-2 Methyl nucleotides to reduce enzymatic degradation and to improve binding affinity. Alternatively, the Zur and GvmR TFD polymeric particles were made by Professor McArthur using rolling circle amplification.

Table 6.8: The sequence and structure of TFDs tested in this study

TFD	Nucleotide sequence	Structure
BFNR 1	TGG CTT TGA CTT TCA TCA ACA AGA/HEG/TCT TGT TGA TGA AAG TCA AAG* C*C*A	Hairpin structure with three phosphorothioate nucleotides on the 3' end
BFNR 3	TTC TAA ATT CCT AGG GTA CAG TCA/HEG/TGA CTG TAC CCT AGG AAT TTA* G*A*A	Hairpin structure with three phosphorothioate nucleotides on the 3' end
TEX 1	rUrCrUrUrUrUrCrCrUrGrUrGrUrUrUrUrUrCrCrGrCrArArUrC	ssRNA
TEX 2	rUmCmUmUmUmUmCmCmUmGmUmGmUmUmUmUmUmCmCmGmCmAmAmUrC	ssRNA with 2'-O methylation modifications

Zur active	Sequences withheld	TFD polymeric particle
Zur scrambled	Sequences withheld	TFD polymeric particle
GvmR active	Sequences withheld	TFD polymeric particle
GvmR scrambled	Sequences withheld	TFD polymeric particle

6.2.4.2 MIC testing of TEX and BFNR TFDs delivered using 12-bis-THA particles

MIC testing was performed to investigate if TEX or BFNR TFDs exhibited antimicrobial activity against *B. thailandensis* strain E555. **Table 6.9** shows that no difference was observed between the MIC of empty 12-bis-THA particles and those loaded with active or scrambled TFD.

Table 6.9: The MIC of empty 12-bis-THA particles and particles loaded with TEX or BFNR targeting TFDs in *B. thailandensis*. MICs were performed in CAMHB and data are representative of at least 3 independent experiments.

Compound	**Minimum inhibitory concentration (µg/mL)**
BFNR1	2-4
BFNR3	2-4
TEX1	2-4
TEX2	4
12-bis-THA particles	2

6.2.4.3 Delivery of TFDs B. thailandensis strain E555 using 12-bis-THA particles

In **Chapter 3**, we showed that 12-bis-THA particles accumulated in the cytoplasm of both capsulated and unencapsulated strains of *B. thailandensis,* However, no difference in the antimicrobial activity of empty and loaded particles was observed during MIC testing. This may occur if 12-bis-THA is unable to deliver TFD to the bacterial cytoplasm. Confocal microscopy was performed to investigate if 12-bis-THA was able to deliver TFD to the cytoplasm of capsulated *B. thailandensis*.

Figure 6.5A-D shows that no fluorescence was detected in the green (TFD) and blue (12-bis-THA particles) channels with the selected laser settings. This indicates that any fluorescence observed in these channels in the test samples is representative of TFD and 12-bis-THA particles not autofluorescence or bleeding from the red channel (membrane stain FM4-64 FX). **Figure 6.5E-H** shows *B. thailandensis* stained with FM4-64 FX and incubated with 12-bis-THA particles loaded with rhodamine-labelled FUR TFD. As previously observed in **Chapter 3**, the membrane resolution of bacterial cells treated with 12-bis-THA particles was considerably lower than the untreated control. **Chapter 3** showed that 12-bis-THA particles may accumulate within the bacterial membrane potentially causing displacement of FM4-64 FX. However, no membrane binding or accumulation was observed in **Figure 6.5E-H**. Despite this, the fluorescence of the TFDs and 12-bis-THA particles were observed **Figure 6.5E-H** and could be seen to overlap with most but not all the fluorescently labelled *B. thailandensis* cells. Several bacterial cells, such as those highlighted in **Figure 6.5F** using the yellow arrows contained both green and blue fluorescence suggesting accumulation of both 12-bis-THA particles and TFD within the bacterial cytoplasm. Some of the cells demonstrate a high intensity of green signal indicating high levels of TFDs present within this bacterial cell. In contrast, some cells contained only the blue signal suggesting that only 12-bis-THA was present and not TFD (shown by the white arrows in **Figure 6.5G**). This may if the concentration of TFD is low and is not detected with the laser settings used. Alternatively, it may represent the accumulation of 12-bis-THA particles that were not loaded with TFD

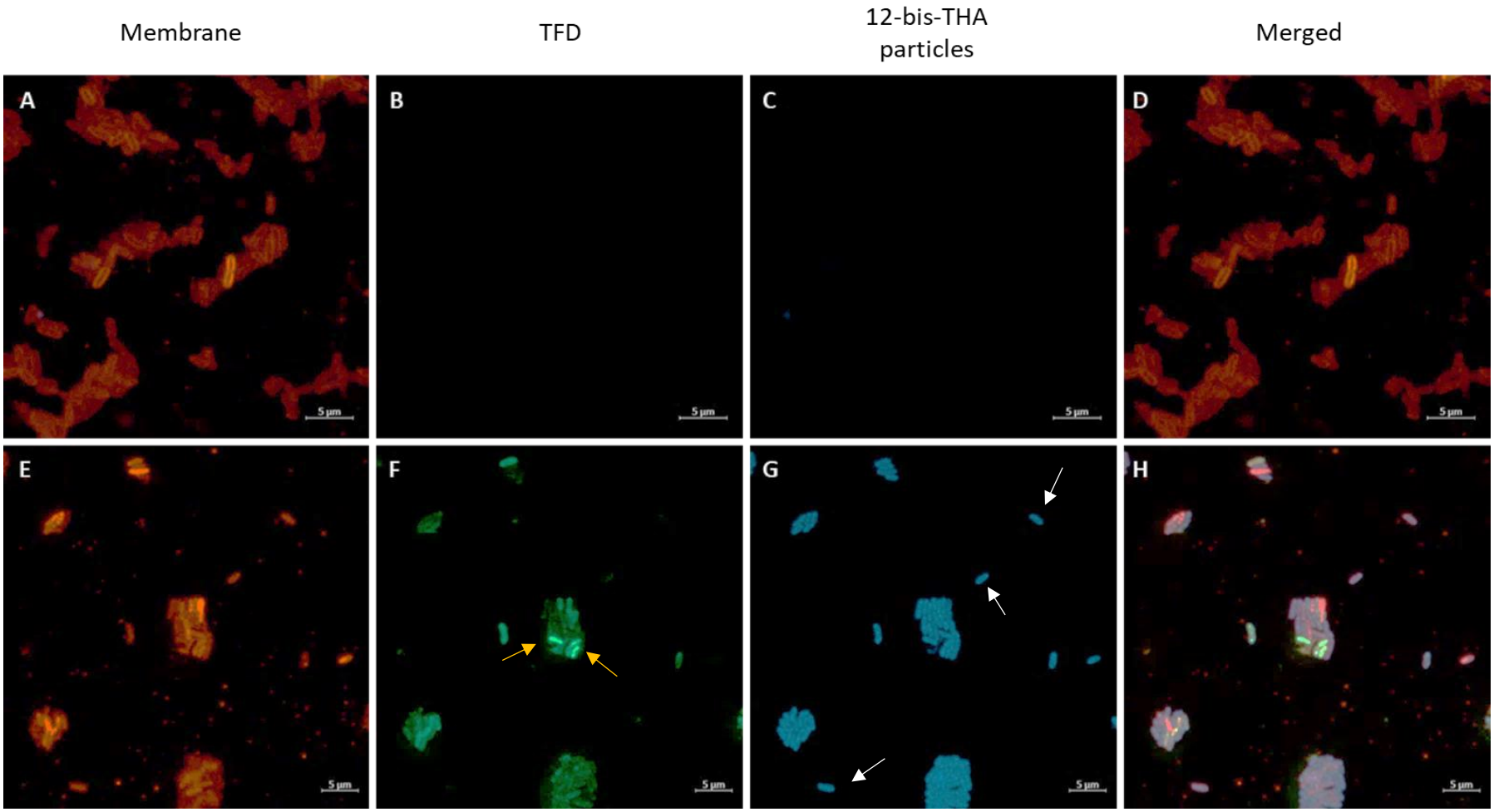

Figure 6.5: Confocal microscopy of TFD delivery to encapsulated *B. thailandensis* strain E555 using 12-bis-THA particles. Bacterial cells grown to mid-log phase were incubated with 50 µg/mL of 12-bis-THA loaded with 5 µg/mL of alexa-488 labelled FUR TFD for 1.5 h. Red, green and blue show the bacteria, TFD and 12-bis-THA particles respectively. Images were captured with a Zeiss LSM 800 microscope and represent 5 fields of view from 3 independent replicates. Scale bars show 5 µm.

6.2.4.4 The activity of BFNR and TEX TFDs against mature B. thailandensis biofilms

Both Bcam1349 and TEX have been associated with biofilm formation in *Burkholderia* species (243,359). Therefore, we investigated if TFDs that targeted BFNR, and TEX demonstrated activity against mature *B. thailandensis* biofilms using the method developed in **Chapter 4**. The data in **Figure 6.6** shows no difference between empty 12-bis-THA particles and those loaded with any of the TFD oligonucleotides. The MBEC curve observed in **Figure 6.6** is remarkably different to that observed in the biofilm chapter (**Figure 4.3** and **4.4**) which is presented as an inverted sigmoidal curve whereas the data in **Figure 6.6** suggests a linear reduction in biofilm biomass when exposed to doubling concentrations of 12-bis-THA particles.

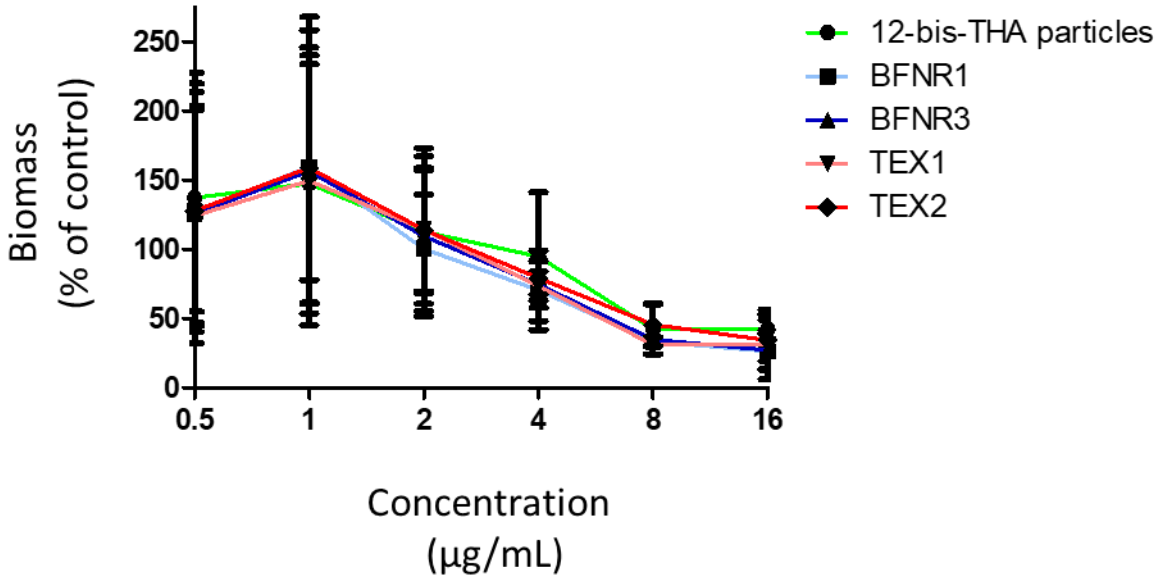

Figure 6.6: Activity of TFD loaded 12-bis-THA particles against preformed *B. thailandensis* strain E555 biofilms. Biofilms were formed using the Calgary biofilm and tested for 24 h in the present of TFD before crystal violet staining and quantification. The values shown are relative to the untreated control. Data are representative of 2 independent replicates and error bars show standard deviation.

The pMIC values for empty and loaded 12-bis-THA particles were also calculated by observing the concentration that inhibited the shedding of the mature biofilms and prevented visible planktonic growth (**Table 6.10**). No difference in the pMIC was observed between any of the treatments. Additionally, the pMIC value for empty 12-bis-THA particles was consistent with that observed in **Chapter 4**.

Table 6.10: The pMIC of empty 12-bis-THA particles and those loaded with TEX or FNR targeting TFDs in *B. thailandensis*. Data are representative of 2 independent experiments.

Compound	Planktonic minimum inhibitory concentration (μg/mL)
BFNR1	2
BFNR3	2-4
TEX1	2
TEX2	2
12-bis-THA particles	2-4

6.2.4.5 The minimum biofilm inhibitory concentration of BFNR and TEX TFDs against planktonic B. thailandensis

The minimum biofilm inhibitory concentration of each compound was investigated to determine whether the TFDs prevented biofilm formation in planktonic *B. thailandensis*. This was performed by placing the Calgary device lid onto a 96-well plate that had been prepared in the same way as the broth microdilution MIC using modified Vogel Bonner medium (MVBM). Planktonic bacteria treated with halving dilutions of empty and loaded 12-bis-THA particles were incubated under agitation before quantification using crystal violet. No significant difference in biofilm formation was observed when comparing cultures incubated with empty and loaded 12-bis-THA particles (**Figure 6.7**)

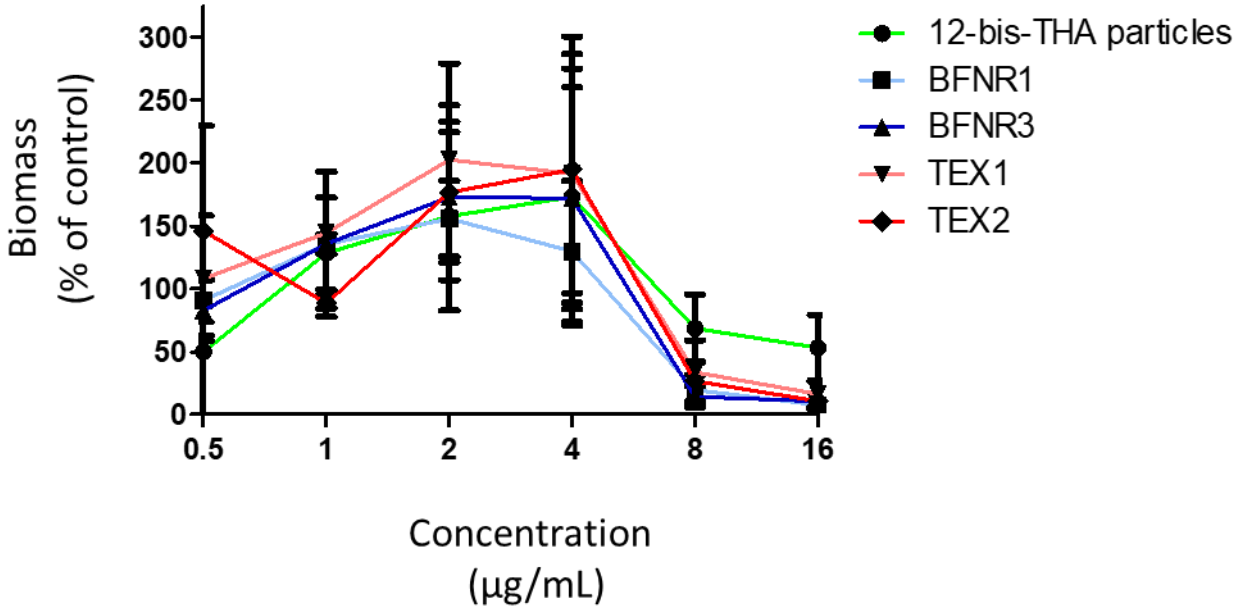

Figure 6.7: Investigation of the minimum biofilm inhibitory concentration (MBIC) for BFNR or TEX targeting TFD in *B. thailandensis*. Empty 12-bis-THA particles or those loaded with TFD were incubated with planktonic bacteria within the Calgary biofilm device and incubated at 37°C for 24 h before using crystal violet staining to quantify the biofilm biomass. The values shown are relative to the untreated control. Data are representative of 2 independent experiment and error bars show the standard deviation.

6.2.4.6 The MIC of GvmR and Zur polymeric TFD particles

Polymeric TFD particles are the next iteration of TFD technology that allows the delivery of exponentially more TFBS sequences without the need for 12-bis-THA particles. Polymeric TFD particles were made by Professor McArthur and contained either the TFBS for Zur or GvmR. Scrambled variants were also produced to act as controls. Additional polymeric particles were made containing a scrambled TFBS to act as negative controls. Broth microdilution MIC assays were performed to investigate if the GvmR and Zur polymeric TFD particles demonstrated antimicrobial activity against *B. thailandensis* E555.

Table 6.11 shows that all of the polymeric TFD particles inhibited bacterial growth. The polymeric TFD particle containing the active GvmR sequence had an MIC of 2.5 µg/mL which was 4-fold lower than the scrambled version which had an MIC of 10 µg/mL. Similarly, the active version of

the Zur TFD particles had MIC values of 0.16 – 0.32 µg/mL that were 16 to 32-fold lower than the scrambles version which had an MIC of 5 µg/mL.

Table 6.1111: The MIC of TFD polymeric particles against *B. thailandensis* strain E555. Assays were performed in CAMHB and data are representative of 2 independent experiments.

Compound	Minimum inhibitory concentration (µg/mL)
GvmR	2.5
GvmR (Scrambled)	10
Zur	**0.16 – 0.31**
Zur (Scrambled)	5

6.2.4.7 Confocal microscopy of polymeric TFD particle delivery to B. thailandensis strain E555

Confocal Microscopy was performed to investigate the transfection efficiency of polymeric TFD particles. Fluorescent microscopy can be used to measure polymeric TFD particle internalization as the delivery moiety, which is TAMRA labelled nucleotides, are intrinsically fluorescent. **Figure 6.8A-C** shows untreated *B. thailandensis* stained with FM4-64. No signal was observed in the green channel (**Figure 6.8B**) indicating that the selected laser parameters had not caused bleeding between the red and green channels or had stimulated bacterial autofluorescence.

Figure 6.8D-F shows *B. thailandensis* strain E555 that were incubated with 5 µg/mL of polymeric TFD particles for 1.5 h and stained with FM4-64 FX. Green fluorescence which represents the polymeric TFD particles were observed to co-localise with bacterial cells stained in red. The TFD signal was observed within the boundaries of the membrane stain suggesting accumulation within the bacterial cytoplasm.

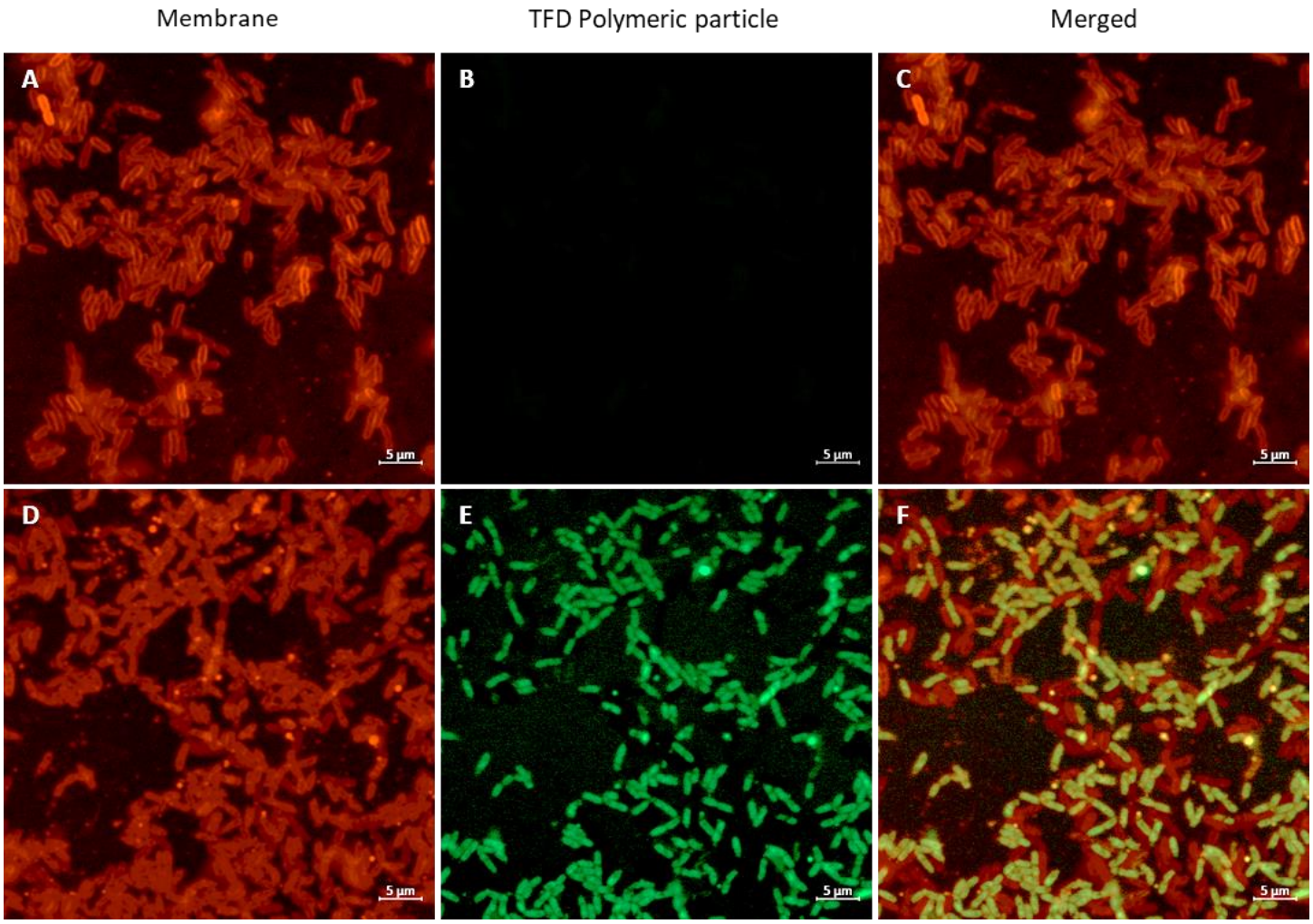

Figure 6.8: TFD polymeric particle delivery to *B. thailandensis* strain E555. Bacterial cells grown to mid-log phase were incubated with 5 µg/mL of TAMRA labelled TFD polymeric particles for 1.5 h. Red and green show the bacteria and TFD respectively. Images were captured with a Zeiss LSM 800 microscope and represent 5 fields of view from 3 independent experiment. Scale bars show 5 µm.

6.3 Discussion

6.3.1 The identification of transcription factors using a proteomic approach

Transcription factor decoys (TFD) are precision oligonucleotide antimicrobials that contain the binding motif of a target transcription factor. This acts as a competitive inhibitor that selectively inhibits the targets resulting in the prevention of downstream gene expression. The main challenge for this technology is identifying new transcription factor candidates particularly in unusual or poorly characterised bacteria. Previously, the McArthur group has performed bottom-up proteomic studies to identify transcription factors that increased in abundance in response to the delivery molecule 12-bis-THA with the perspective that delivery of a TFD that inhibits a transcription factor that controls the stress response. By doing so, the bacteria will be sensitized to 12-bis-THA particles through the prevention of essential gene expression. This has been used to identify transcription factors such as FNR, FUR, and NarPL in *E. coli* and BrlR in *P. aeruginosa.*

In **Chapter 5**, a proteomic study was performed to investigate the stress response in *B. thailandensis* strain E555 to provide insight into its mechanism of action of 12-bis-THA particles in this bacterial species. In this chapter, we mined the proteomic data set to investigate transcription factors that increased in abundance in response to 12-bis-THA particles. This generated a new protein data base containing proteins with annotations such as “Transcription factor”, “regulator” or “DNA-binding” which was then processed using Perseus as previously described in **Chapter 5**. Using this approach, two transcription factors and regulatory elements that increased in abundance in response to 0.1X MIC and fourteen following exposure to 1X MIC of 12-bis-THA particles were identified.

The data shows that four transcription factors which increased in abundance in response to 12-bis-THA particles control the expression of RND efflux pumps in *Burkholderia* species. AmrR and BpeR (BTH_I0679) increased in abundance in response to both 0.1X MIC and 1X MIC concentrations of 12-bis-THA particles and act as transcriptional repressors of AmrAB-OprM and BpeAB-OprB respectively in *B. pseudomallei*. Mutation of these repressors leads to constitutive expression of their respective RND pumps resulting in reduced susceptibility to antimicrobials including clinically important meropenem (366–368). Conversely, the data from the whole proteomic database (**Chapter 5**) showed that downstream genes of both AmrR and BpeR increased in abundance in a response to 12-bis-THA particles regardless of the increased presence of their transcriptional repressors. Homologues of BpeT (BTH_II2108) and BpeS (BTH_I0632) were also identified in the transcription factor database and increased in abundance by *B. thailandensis* in response to 1X MIC of 12-bis-THA particles. In *B. pseudomallei*, BpeT and BpeS co-organize the expression of the BpeEF-OprC pump by binding to LTTR

box upstream of the RND pump (337). The BpeEF-OprC RND efflux system is responsible for the efflux of clinically relevant antimicrobials trimethoprim and sulfamethoxazole (167,369). These proteins were not identified in the proteomic dataset, but it is reasonable to anticipate their upregulation due to an increase in the abundance of their transcription activator in response to 12-bis-THA particles.

It is clear that 12-bis-THA induces changes in the regulation and abundance of RND efflux proteins however the mechanism is not understood. Previously it has been shown that 12-bis-THA particles interact with the membrane of capsulated and unencapsulated strains of *B. thailandensis* which leads to varying degrees of permeabilisation. Both membrane permeability and efflux act together and influence antimicrobial diffusion across the membrane in Gram-negative species including *B. thailandensis* and *B. cepacia* (91). This suggests that 12-bis-THA particles may induce changes in RND efflux activity and regulation for two reasons. Firstly, 12-bis-THA particles may cause a temporary upregulation in efflux activity to expel 12-bis-THA from the cytoplasm or particles passing through the membrane may increase membrane permeability. It was observed in **Chapter 3** that 12-bis-THA particles did not cause the leakage of cytoplasmic enzymes in capsulated *B. thailandensis* strain E555. However, 12-bis-THA particles may still form membrane pores that are too small or transient to allow cytoplasmic proteins to be released but still allow water and metabolites to leak out. The metabolomic data in **Chapter 5** supports this hypothesis as a reduction in osmotically active molecules was observed in response to 12-bis-THA particles. Secondly, the upregulation of transcriptional repressors AmrR and BpeR may act to limit the over activation of efflux pumps which may further increase membrane permeability.

The impact of 12-bis-THA particles on the regulation of RND efflux systems in *B. thailandensis* is not fully understood. Our data suggest that there is a strong link between the two however the proteomic assay performed only provides a snapshot of a single time point. To better understand the role of 12-bis-THA particles plays on RND efflux pumps further times points are required. Alternatively, the activity of efflux pumps could be monitored in response to 12-bis-THA particles using a method described by Paixão *et al* (370). In the context of TFD development, transcriptional activators such as BpeT and BpeS are potential candidates for TFD development as their inhibition would likely give rise to increased sensitivity to antimicrobials such as trimethoprim that would otherwise be expelled (102). However further work is required to identify the transcription binding motifs of these transcription factors.

Four other transcription factors increased in abundance in response to 12-bis-THA particles but required further analysis as those identified were less characterised. For example, BTH_I1391 increased in abundance 1.49-fold in response to 12-bis-THA particles and was annotated as an IclR

family transcriptional regulator. While it is conserved in both *B. pseudomallei* and *B. mallei,* it is not characterised and has no known function in *Burkholderia* species. To provide insight into its possible molecular function, the amino acid sequence for BTH_I1391 was analysed using BlastP to identify homologues in well-characterised species, such as *E. coli* and *P. aeruginosa*, to infer its function. An uncharacterised homologue was identified in *P. aeruginosa* whereas characterised ones were observed in *E. coli* (PcaR) and *S. typhi* (glyoxylate bypass operon regulator).

PcaR is an IclR family transcriptional regulator that is best characterised in *P. putida* where it enables bacteria to grow using benzoate derivatives as a carbon source (339). No evidence of changes to benzoate metabolism was observed in the proteomic or metabolomic data set which suggests that PcaR is functionally different in *B. thailandensis.* Alternatively, the *S. typhi* homologue glyoxylate bypass operon regulator, which is called IclR in *E. coli*, is responsible for suppressing the activity of the glyoxylate bypass (340,371). This is consistent with the observation in **Chapter 5** where the downregulation of the glyoxylate bypass in response to 12-bis-THA particles was observed. Overall, it is difficult to predict the function of BTH_I1391 from the BlastP output as the coverage and E-values were low. However, it is interesting to note that possible homologues identified were associated with central metabolism. With the data that is currently available, BTH_I1391 is not a good candidate for TFD development as its function and binding site are unknown.

BTH_II1275 is a LuxR family transcriptional regulator that increased in abundance 1.42-fold in response to 1X MIC of 12-bis-THA particles. The *Burkholderia* genome browser showed that this protein was conserved in *B. pseudomallei* but not *B. mallei*. Additionally, BlastP identified no homologue in *E. coli, A. baumannni, P. aeruginosa,* or *S. typhi*, however it did identify a PAS-domain within the amino acid sequence. These sensory domains can control the dimerisation and activity of their transcription factors as they respond to a wide range of environmental stimuli including oxygen and redox potential. For example, Aer is a PAS-domain containing protein in *E. coli* that senses changes in proton motive force through FAD binding (372,373). Another remarkable feature of BTH_II1275 and its *B. pseudomallei* homologue (BPSS 1131) was its location upstream of two genes associated with fatty acid metabolism both of which had increased in abundance when the proteomic data set was analysed. As with BTH_I1391, it is challenging to predict the function of BTH_II1275 as it has no characterised homologue. Interestingly, the data suggests that it could have a role in β-oxidation and fatty acid metabolism however further studies are needed to substantiate this. In the context of TFD development, considerably more work is required to investigate the potential of BTH_II1275 as a candidate particularly the characterisation of its molecular function however this lies beyond the scope of this project.

BTH_II1739 increased in abundance 1.36-fold in response to 1X MIC of 12-bis-THA particles and is a homologue of BprR in *B. pseudomallei*. BprR is a part of the BprRS two-component system that regulates virulence in addition to being an important virulence factor *in vivo* (374). Deletion of either or both components resulted in moderate attenuation in intranasally infected mice. Adler *et al* showed that a Δ*bprR* strain of *B. pseudomallei* displayed reduced swimming motility aligning with transcriptomic data showing an increase in the abundance of mRNA transcripts associated with motility (374). This suggests that BprR acts as a transcriptional repressor for these genes which is consistent with the findings in **Chapter 5** which show a reduction in the abundance of flagella proteins combined with an increase in the abundance of BprR. BprR is a potential candidate for TFD development as the deletion of this gene results in a reduction in virulence both *in vivo* and *in vitro* however further studies are required to identify its transcription factor binding motif.

BTH_I2369 is annotated as a transcriptional regulator and increased in abundance 0.98-fold in response to 1X MIC of 12-bis-THA particles. The *Burkholderia* genome browser showed that it is not conserved in *B. pseudomallei* or *B. mallei* but can be found in some BCC species including *B. cepacia, B. dolosa* and *B, vietnamiensis* where it is annotated as an AraC family transcriptional regulator. Additionally, no characterised homologue was detected in *E. coli, P. aeruginosa, A. baummanni* or *S. typhi* as homologues were also annotated as an AraC family transcriptional regulator

6.3.2 Sigma factors as potential TFD candidates.

Of the ten regulatory elements to increase in abundance in response to 12-bis-THA particles, two were sigma factors. Sigma factors are transcription initiation proteins that reversibly bind to RNA polymerase to direct its binding to DNA and initiate transcription. Hence, they affect the specificity of the polymerase via the selection of binding site, and its efficiency by controlling the rate of RNA synthesis. First characterised in E. coli they are historically grouped by their mass, structure and binding site. For example, RpoD is a primary sigma factor and regulates the transcription of 'housekeeping' genes that are required for growth (375,376). It controls the expression of important genes by recognising two binding motifs (–35 5'-TTGACA-3' and –10 5'-TATAAT-3') (377) and is essential for viability in multiple species (378–380). Sigma factors are potentially attractive candidates for TFD development as they are functionally similar to traditional TFDs with the difference that a sigma factor decoy may suppressor a larger array of genes. The caveat of this is that sigma factor binding motifs are conserved across bacterial species resulting in a reduction or loss in precision antimicrobial activity compared to a traditional TFD. Additionally, the very large number of RNA

polymerases within a bacterial cell will require efficient delivery of the TFD so it can act as a competitive inhibitor.

SigJ increased in abundance 3.88-fold in response to 12-bis-THA particles. It is annotated by Menard *et al* as a novel lineage of the primary sigma factor RpoD (349). This is consistent with the finding in this chapter that showes the presence of both SigJ and RpoD. It is difficult to determine whether SigJ is a good candidate for TFD development as its function is unknown. Mutations of primary sigma factors can be lethal (381) but deletion of *sigJ* in has been observed in *Burkholderia* sp. 383 and *B. cenocepacia* PC184 suggesting that it is not essential for bacterial viability (349). The function of SigJ is unknown but it has been proposed to act as an auxiliary primary factor to support the function of RpoD (349). Further studies are required to investigate the molecular function and binding motif of SigJ before a TFD can be developed.

BTH_I0456 which is annotated as RpoH also increased in abundance 1.14-fold in response to 12-bis-THA particles. In *E. coli,* RpoH is a sigma factor that increased in abundance in response to heat stress and controls the expression of chaperone proteins and proteases to counter the accumulation of misfolded proteins (382). This is consistent with our findings which showed that HslUV, which are known members of the RpoH regulon (383), were significantly increased in abundance in response to 1X MIC of 12-bis-THA particles (1.32-fold and 2.13-fold, respectively). In *B. pseudomallei*, the expression of RpoH and its regulon is coregulated by RpoE (384). A mutant of RpoE was constructed in *B. pseudomallei* which exhibited sensitivity to oxidative and osmotic shock (385) in addition to a reduction in intracellular viability and biofilm formation suggesting a function outside of heat-induced stress. This is consistent with the findings in **Chapter 5** which suggests that 12-bis-THA particles induce oxidative stress in *B. thailandensis.* Further, in *E. coli* the consensus binding site for RpoH is distinct from that of the housekeeping RpoD making it possible to design TFDs just to target the RpoH regulon however further studies are required to gain insight into the role and binding specificity of RpoH in *B. pseudomallei*.

6.3.3 Using the literature to identify candidates for TFD development

Though the proteomics assay successfully identified several candidates for TFD development, all required further characterisation which is beyond the scope of this project. As an alternative approach, a literature review was performed to identify alternative TFD candidates that had been characterised in *Burkholderia* species. By doing so, we identified four candidates for a *B. pseudomallei* specific TFD.

Zur is a transcription factor that is ubiquitous in bacteria and is responsible for regulating cytoplasmic zinc homeostasis (386). It is proposed that Zur regulates cytoplasmic zinc levels in *B. pseudomallei* by acting on the T6SS-4 as the promoter region contains a Zur binding box which had considerable similarity to that identified in *E. coli* (365). Deletion of zur in *B. thailandensis* results in an increase in the expression of T6SS-4 genes suggesting that it acts as a transcriptional repressor on this operon (365). However, there is evidence in *Caulobacter crescentus* that also acts as a transcriptional activator but it can also, directly or indirectly, activate genes in the FUR regulon which is responsible for orchestrating iron homeostasis(387). Though the Zur regulon is not fully characterised in *B. thailandensis* or *B. pseudomallei*, it is an attractive candidate for TFD development due to its conservation in *Burkholderia* species, known binding box and understood phenotype.

TEX is another candidate for TFD development as a ΔTEX strain of *B. pseudomallei* showed attenuation of virulence in a mouse model (354). TEX is a unique target for TFD development as it is not a traditional transcription factor but rather a transcriptional accessory protein that preferentially binds single-stranded RNA (351). TEX shares sequence and structural homology with Spt6 which is a eukaryotic elongation factor that supports the processing of mRNA into a polypeptide chain (355). Though Spt6 is considerably larger than TEX, Johnson *et al* propose that both proteins share the same molecular function based on the conservation of an S1 domain that is responsible for binding nucleic acids (355). Additionally, TEX has been co-purified with RNAP, RNAse E or PNPase further implicating it with a role in mRNA processing (351). In this study, a TFD was developed using the nucleotide bind motif identified based upon the crystal structure derived from the crystal structure of the TEX orthologue in *P. aeruginosa* binding to a single-stranded RNA molecule (351).

GvmR is a transcription factor in *B. pseudomallei* that acts globally to control the expression genes involved with of metabolism and virulence (275). In addition, GvmR was found to positively regulate the T6SS-2 secretion system in *B. pseudomallei*, which itself is regulated by sensing levels of zinc (365). A *ΔgvmR* strain of *B. pseudomallei* demonstrated attenuation in a mouse model with *in vitro* studies showing that the mutant strain displayed a reduction in the ability to invade and replicate inside cells (275). Due to its phenotype and conservation in *B. thailandensis* and *B. mallei,* in addition to BCC species, GvmR is an excellent candidate for TFD development (365).

Bcam1349 is an FNR family transcriptional regulator in *B. cenocepacia* that regulates biofilm formation and virulence *in vivo*. In *E. coli,* FNR is a global transcriptional regulator that controls the switch from aerobic to anaerobic respiration. Under anaerobic conditions, FNR forms a homodimer that is held together by a Fe-S cluster which forms disulfide bridges at conserved cysteines (388). These cysteines are not conserved in *B. thailandensis* or *B. pseudomallei* which is consistent with studies by

Fazli *et al* which showed that Bcam1349 controls the production and export of extracellular polysaccharides for biofilm formation and is regulated by cytoplasmic levels of cyclic-di-GMP (389). Previously, the McArthur group has focused on developing a TFD the selectivity inhibits FNR in *Enterobacteriaceae* to counter gut dysbiosis and complicated urinary tract infections therefore FNR-family transcriptional regulators in *Burkholderia* are possible candidates for the development of an anti-melioidosis TFD termed BFNR. For both GvmR and Bcam1349, suitable transcription binding motifs had not been identified at the time of the study.

Therefore, to predict the transcription factor binding motif of both GvmR and Bcam1349, a computational tool called Prodoric was used to identify potential conserved nucleotide sequences upstream of genes within the transcription factors regulon. Prodoric compares new nucleotide sequences to a database of known bacterial transcription factor binding motifs (149,390). New binding motifs are then allocated a score based on their similarity to a reference sequence.

To identify a possible transcription factor binding motif the upstream nucleotide sequences of all genes within the GvmR regulon (275) were interrogated with Prodoric. By doing so, an OxyR-like binding domain similar to that found in *E. coli* was identified. All genes within the regulon contained at least one OxyR-like binding motif however the promotor domains consistently contained two or three motifs including upstream of itself and the T6SS-2. In this study, TFD particles were produced from synthetic, circular DNA containing the binding site found using a proprietary methodology.

In parallel, a list of promoters found in the *E. coli* FNR regulon was compiled using papers published by Constantinidou *et al* (360) and Myers *et al* (361). The *Burkholderia* genome browser and BlastN were used to identify homologues in *B. pseudomallei* depending on sequence conservation and gene synteny. Prodoric was then used to interrogate the upstream regions of conserved *B. pseudomallei* homologues to investigate the presence of FNR-like binding motifs. Using this approach, thirteen potential transcription factor binding motifs were identified for Bcam1349. For TFD development, the sequence upstream of *cydA* was selected as the Prodoric score was the maximum possible (8.93/8.93) indicating a match to the FNR binding motif in *E. coli.*

6.3.4 TFD platforms: 12-bis-THA vs polymeric TFD particles

Next, we investigated the antimicrobial activity of the TFDs against *B. thailandensis* strain E555. No difference was observed between empty 12-bis-THA particles and those loaded with active or scrambled TFD. This was not unexpected as both TEX and Bcam1349 do not regulate genes that are essential for viability but rather those which are associated with biofilm formation (243,359).

However, whether the TFD was delivered in sufficient quantity or were stable enough to assert a biological effect needs to be investigated.

No TFD specific activity may have been observed if 12-bis-THA particles were unable to deliver TFD to the cytoplasm of encapsulated *B. thailandensis*. In **Chapter 3**, 12-bis-THA particles were shown to rapidly accumulate within the cytoplasm of encapsulated and unencapsulated strains of *B. thailandensis*. Using the method described in this chapter, it was determined whether 12-bis-THA particles could deliver TFD to the bacterial cytoplasm of encapsulated *B. thailandensis* strain E555. Using CLSM, 12-bis-THA particles were shown to deliver TFD to the cytoplasm. This suggested that 12-bis-THA would be a suitable delivery agent for delivery of TFDs to *B. pseudomallei* due to the similarity between the polysaccharide capsules (391). This could be formed using several methods. Radiolabeled TFD oligonucleotides could be used to determine their presence in the cytoplasm. Alternatively, bacterial reporter strains could be used to evaluate whether they are functionally active whilst in the cytoplasm. This method would also allow for the further optimization of TFDs by changing nucleotide sequences and using chemically modified nucleotides such as phosphorothioate nucleotides.

TEX and BFNR TFDs were tested for antibiofilm activity against *B. thailandensis* strain E555 using two methods. Firstly, the MBEC method described in **Chapter 4** was used to assess the antimicrobial properties of 12-bis-THA particles loaded with TFD against mature *B. thailandensis* biofilms grown on the Calgary biofilm device. The data showed no difference between empty 12-bis-THA particles and those loaded with active or scrambled TFD suggesting that the TFD are not active against mature *B. thailandensis* biofilms. This may occur as the crystal violet method is not sensitive to changes in bacterial viability. The TFDs may exhibit antimicrobial activity against cells within the biofilm but this is not recorded as crystal violet staining binds to viable and dead cells indiscriminately in addition to the biofilm matrix. It is important to note that the MBEC curves observed in this chapter are considerably different to those in **Chapter 4**. Bacterial biofilms are labile and sensitive to changes in media batch or stock culture. The minimum biofilm inhibition concentration (MBIC) was measured by suspending *B. thailandensis* in halving concentrations of empty and loaded 12-bis-THA particles. A Calgary biofilm device was then added to the lid of the 96-well plate and incubated for 16 h before biofilms were quantified using crystal violet staining. This was performed to investigate if the TEX and BFNR TFDs prevented planktonic cultures from forming biofilms. The MBIC studies showed that no difference was observed in biofilm formation following incubation with empty or loaded 12-bis-THA particles. This may occur if TFD activity is transient. Biofilm growth kinetics in the presence of absence active and scrambled TFD are required to further investigate the activity of TEX and BFNR TFDs.

As these assays have only been performed twice, no strong conclusion can be drawn from this data until further replicates have been performed. However, the current data suggest that TEX and BFNR TFDs are not active against *B. thailandensis* when loaded into 12-bis-THA particles. This raises several questions: (1) does the TFD activity persist long enough to observe activity at 24 h? (2) Do 12-bis-THA particles mask TFD activity as it is endowed with its antimicrobial properties? (3) Does 12-bis-THA particles deliver enough TFD to *B. thailandensis* stain E555 to elicit activity?

Polymeric TFD particles are the next generation of TFD technology which allow for exponentially more TFD delivery without the need for 12-bis-THA particles. Polymeric TFD particles were produced by Professor McArthur that contained either the binding site of GvmR or Zur. Antimicrobial susceptibility testing was then performed to investigate the MIC of the TFD particles. **Table 6.11** showed the MIC values of active and scrambled polymeric TFD particles against *B. thailandensis*. The active GvmR TFD particle had an MIC of 2.5 μg/mL which was 4-fold lower than the MIC of the scrambled version which was 10 μg/mL. Similarly, the TFD particle containing the active Zur sequence had an MIC of 0.16/0.32 μg/mL. This was 16 to 32-fold lower than the MIC of the scrambled version which was 5 μg/mL. It is not clear why the MIC of the Zur TFD particles was much lower than the active GvmR TFD particle. One reason may be that the Zur transcription factor binding motif (365) is better characterised in multiple bacteria whereas there are no *in vivo* studies, such as electrophoretic mobility shift assay or DNAase footprinting, studying the GvmR binding site (392). The GvmR TFD particles may have the potential to produce comparable MIC values but likely requires further optimisation following the characterisation of its binding site. Alternatively, the difference in MICs may indicate that Zur is a better candidate than GvmR in the conditions tested.

CLSM showed that polymeric TFD particles transfected *B. thailandensis* E555 in the absence of 12-bis-THA particles. It is not possible to determine if there is a difference in transfection efficiency when compared to those delivered by 12-bis-THA particles as microscopy on the polymeric TFD particles has only been performed once. Despite this, **Figure 6.8** provides evidence that polymeric TFD particles containing TAMRA-labelled nucleotides are sufficient to deliver large volumes of TFD across the Gram-negative membrane in addition to the polysaccharide capsule of *B. thailandensis,* and potentially *B. pseudomallei*.

To conclude, in this chapter using a proteomic and literature review approach, eighteen transcription factors were identified to be considered for TFD development. As few had been characterised, four were taken forward for TFD testing. The TEX and the BFNR TFDs were tested in the traditional format using 12-bis-THA particles as a delivery platform, and no TFD specific activity was observed. In contrast, polymeric TFD particles were produced by Professor McArthur which contained the binding

sites of GvmR and Zur. Both demonstrated TFD specific activity against *B. thailandensis* strain E555 in the absence of 12-bis-THA particles. Further studies should be performed to further optimise the antimicrobial activity of the GvmR polymeric TFD particle through characterisation of the GvmR bind motif. In addition, further *in vitro* screening is required for Zur using time-kill and biofilm assays.

CHAPTER 7 - GENERAL DISCUSSION, CONCLUSIONS, AND FUTURE WORK

This thesis aimed to determine if 12-bis-THA particles loaded with transcription factor decoys (TFDs) were suitable for the development as *Burkholderia* specific antimicrobials to treat melioidosis. The data detailed in this thesis demonstrates that 12-bis-THA particles are a suitable delivery molecule to transfect the surrogate organism *B. thailandensis* strain E555 when complexed with TFDs. Additionally, these can to some extent penetrate *B. thailandensis* biofilms. A combinatory approach using proteomic and computational analysis in parallel with a literature review identified candidates for TFD development Candidate sequences were tested for activity with initial results demonstrating the need to optimise the formulation of the TFD. A novel polyplex formulation did show considerable activity and future work will investigate this agent further.

7.1.1 Do 12-bis-THA particles alone inhibit the growth of *Burkholderia* species?

The aim of **Chapter 3** was to investigate the antimicrobial activity of 12-bis-THA particles against *Burkholderia* species and to investigate if the bacterial cell wall affected antimicrobial activity and transfection efficiency. 12-bis-THA particles had an MIC of 2-8 µg/mL against both capsulated (E555) and unencapsulated (E264) *B. thailandensis* strains tested. MIC testing against a panel of BCC clinical isolates was performed by Dr Laura Rushton in collaboration with Professor Eshwar Mahenthiralingam at Cardiff University.

12-bis-THA particles had MICs against the BCC panel that were comparable to those determined for *B. thailandensis,* with the exception of *B. cenocepacia* strains which were up to 32 µg/mL. It may be that the different LPS typical of BCC species (218) affected the antimicrobial activity of 12-bis-THA particles as they are known to interact with the lipid A (137) component of the LPS layer. The proteomic data in **Chapter 5** studying the stress response of *B. thailandensis* to 12-bis-THA particles showed a decrease in the abundance of proteins involved with O-antigen production of the LPS layer suggesting that the particles may induce changes in the LPS as part of emerging resistance or as a consequence of 12-bis-THA disrupting the LPS layer. It was not possible to determine from the clinical panel data if LPS chemotypes influence the activity as the isolates were from different species within the BCC. A better approach would be to test the antimicrobial activity and transfection efficiency against a panel of deep-rough LPS mutants that had been derived from the same *B. cepacia* strain as described by Gronow *et al* (222).

CLSM studies showed that the capsule present in *B. thailandensis* strain E555 did not affect the transfection of 12-bis-THA particles into the cell. The 12-bis-THA particles are weakly fluorescent so high concentrations (50 µg/mL) are required to be used to get sufficient signal for the CLSM studies, and this may mask a difference in transfection efficiency. It is notable that even after prolonged

exposure of bacteria to 10-20x MIC of particles no lysis was observed. A better approach to investigate if the capsule influences particle uptake would be to treat capsulated, and unencapsulated cells with MIC concentrations of a radiolabelled version of 12-bis-THA. The cytoplasm could be extracted and analysed using LC-MS to investigate the presence of 12-bis-THA particles in the cytoplasm. Additionally it would also provide insight into the uptake kinetics in the presence of absence of the polysaccharide capsule.

The capsule did influence whether 12-bis-THA particles were bacteriostatic or bactericidal: A difference was observed in the time-kill studies which showed that 12-bis-THA particles were bactericidal against the unencapsulated strain but bacteriostatic against the capsulated strain. This suggests that the polysaccharide capsule found in *B. thailandensis* strain E555 affects the transfection of the particles and perturb their internalization. The time-kill studies showed that strain E264 regrew following 24 h of incubation with the particles whereas strain E555 did not. This may have occurred due to the density of the polysaccharide capsule acting as a physical barrier to the 12-bis-THA particles, or if the anionic phosphates within the capsule sequestered the particles.

This suggests that the polysaccharide capsule may absorb the 12-bis-THA particles resulting in bacteriostatic action that is sustained, unlike the unencapsulated strain E264 which showed an initial reduction in CFU counts prior to regrowing at 24 h (**Chapter 3**). *B. thailandensis* cultures that had been exposed to 12-bis-THA particles produced small and normal sized colonies. The small colonies showed no change in growth kinetics or susceptibility to 12-bis-THA particles suggesting that these were not true SCVs. Instead, the formation of the smaller colonies may have occurred the induction of damage to respiratory changes which is known to induce SCV morphology in *S. aureus* (196). This is consistent with the observation in the proteomic data set which showed that 12-bis-THA particles caused a decrease in the abundance of proteins within the ETC which might result in smaller than usual *B. thailandensis* colonies.

The proteomic study performed and is described in **Chapter 5** provided insight into the mechanism of action of 12-bis-THA particles in *B. thailandensis* strain E555. The data indicated that *B. thailandensis* switched from carbon metabolism to fatty acid metabolism by suppressing glycolysis and upregulating β-oxidation. Metabolomic analysis, using NMR, showed a reduction in the cytoplasmic concentration of osmotically active molecules following incubation with 12-bis-THA particles. The switch from glucose metabolism to fatty-acid metabolism may occur if 12-bis-THA particles permeabilise the membrane causing glucose to be released into the supernatant. The proteomic data also showed that 12-bis-THA particles suppressed the glyoxylate shunt forcing the completion of the TCA cycle which may result in the increased production of NADH. In contrast, 12-

bis-THA particles caused the suppression of respiratory complexes cytochrome c reductase, cytochrome c oxidase and ATP synthase. This is consistent with the literature that shows the parental dequalinium molecule inhibits the activity of cytochrome c reductase (197) and ATP synthase (313).

Suppression of the glyoxylate shunt and increased production of NADH may stimulate the ETC in response to 12-bis-THA. An increase in the abundance of the T6SS-2, which is responsible for scavenging extracellular zinc and manganese in response to oxidative stress, suggests that 12-bis-THA particles induce oxidative stress in *B. thailandensis*. The proteomic data suggests that 12-bis-THA particles induce changes in central metabolism through the inhibition of ETC resulting in oxidative stress. Although the mechanism is not fully clear, the data in **Chapter 5** suggests that 12-bis-THA particles may inhibit bacterial growth through the suppression of ATP synthesis and inhibition of the ETC. Further testing is ongoing to quantify the cytoplasmic concentrations of AMP, ADP and ATP in *B. thailandensis* following incubation with 12-bis-THA particles.

7.1.2 Do 12-bis-THA particles synergise with small molecule antimicrobials?

Di Blasio *et al* previously showed that 12-bis-THA particles combined with colistin and tobramycin produced a synergistic effect against *P. aeruginosa* (138). Therefore, synergy testing was performed to investigate interactions between 12-bis-THA particles and antimicrobials against *B. thailandensis*. The data presented in **Chapter 3** provided evidence that 12-bis-THA particles synergise with trimethoprim and co-trimoxazole and have an additive effect with rifampin and tobramycin.

Further studies were planned to assess the antimicrobial activity of the antimicrobial combinations against a panel of clinical BCC isolates by performing MIC testing in collaboration with Professor Eshwar Mahenthiralingam. Due to time restraints, we were unable to perform checkerboard assays on BCC clinical isolates therefore we performed testing to identify which, if any, ratio of antimicrobial to 12-bis-THA particles retained the synergism. The data showed that combining antimicrobials with 12-bis-THA particles in a 3:1 ratio (weight per weight) resulted in the lowest MICs in *B. thailandensis*. Possible synergy of the 3:1 combinations was investigated by performing time-kill studies where synergy was defined as a >2 $\log_{10}$ reduction in CFU at 24 h compared to the most effective monotherapy (145). The time-kills also showed that the tobramycin, and rifampin combinations were bactericidal, whilst the trimethoprim, and co-trimoxazole combinations were bacteriostatic.

Interestingly, the time-kill studies showed that the tobramycin combination was rapidly bactericidal, but bacteria regrew at 24 h and produced colonies that were both normal and smaller in size. Tobramycin is a cationic molecule that exploits PMF to penetrate *E. coli* and *P. aeruginosa*

(393,394). The proteomic data in **Chapter 5** suggests that 12-bis-THA particles may increase membrane potential which could account for the synergy observed between 12-bis-THA particles and tobramycin. The rapid regrowth was observed after 6 h suggesting that the additive effect is transient.

In **Chapter 3**, MIC testing of the antimicrobial combinations was performed on the panel of clinical BCC isolates. The tobramycin combination showed the greatest activity against the panel and improved activity against 9 of 11 bacteria tested. In contrast, the rifampin, and trimethoprim combinations showed little difference in relation to the relevant monotherapies. The combinations of rifampin, and trimethoprim only showed improved antimicrobial activity against 1 of 11 and 2 of 11 panel members respectively. This suggests that 12-bis-THA particles do not synergise with rifampin, and trimethoprim against BCC species, or that they do not synergise in the used ratios. Further studies would seek to optimise combinations and determine whether or not this could lead to a synergistic effect against BCC species.

7.1.3 Are 12-bis-THA particles able to deliver TFD to Burkholderia biofilms?

In **Chapter 3**, it was established that 12-bis-THA particles and the antimicrobial combinations inhibited the growth of planktonic *B. thailandensis*. As *B. thailandensis* and *B. pseudomallei* form biofilms, **Chapter 4** investigated if 12-bis-THA particles and the antimicrobial combinations demonstrated activity against *B. thailandensis* biofilms. An assay was developed using the Calgary biofilm device to produce biofilms that had a starting inoculum equivalent to an MIC plate (5×10^5 CFU/mL) to allow for a fair comparison between MBEC and MIC values. $MBEC_{50}$ values were calculated using non-linear regression to identify the concentration of a compound that reduced the biomass of biofilm by 50% relative to an untreated control. 12-bis-THA particles had an $MBEC_{50}$ of 2.17 µg/mL which was similar to its MIC of 2 – 8 µg/mL. The antimicrobial combinations also showed good antimicrobial activity but it was not possible to determine if this was synergistic. To do so, a synergy time-kill assay described in **Chapter 3** could be performed using bacterial biofilms instead of planktonic cultures (145).

It was interesting to observe that the MBEC values detailed in this thesis were considerably lower than those identified in the literature. This is likely due to methodological differences as the biofilm testing in this thesis was optimised to generate biofilms with starting densities equivalent to an MIC plate whereas the methods used in the literature use generate biofilms with a higher bacterial density (234). Additionally, studies by Sawasdidoln *et al* and Anutrakunchai *et al* define MBEC as the concentration of a compound that chemically sterilises a peg preventing bacterial regrowth in a nutrient-rich medium whereas the investigations in **Chapter 4** measures changes in biofilm biomass (234,252).

Another aim of **Chapter 4** was to investigate if 12-bis-THA particles could deliver TFD to bacteria within a biofilm. A longitudinal study was performed using a *B. thailandensis* strain E555 that expressed RFP to allow the bacteria to be visualised when contained within biofilms. These were formed on a glass slide in MVBM medium in a time-dependent manner. Biofilms that were grown for 72 h were 13 and 22 µm thick which was sufficient for the penetration studies. Though this study was performed once, the 72 h old biofilm in this study and those in the penetration studies showed the formation of three-dimensional structures indicating that they were mature. To further characterise this model fluorescent dyes could be used to detect the presence of extracellular matrix components such as DNA and polysaccharides (230,232).

The penetration studies showed that both empty 12-bis-THA particles and those loaded with fluorescently labelled TFD rapidly interacted with *B. thailandensis* biofilms. However, empty 12-bis-THA particles were homogenously dispersed throughout the body of the biofilm whereas loaded particles penetrated the biofilm in a time-dependent manner. The data showed that 12-bis-THA particles and TFD were mostly co-localised however some diffusion of the TFD was observed. It was not possible to determine whether the 12-bis-THA particles and the TFD were within the bacteria cytoplasm or in the extracellular matrix of the biofilm. Some penetration of 12-bis-THA in the absence of TFD suggested bacterial internalization but may only represent the bacteria on the surface of the biofilm. Further studies with later time points and counterstains for biofilm matrix are required to better investigate the location of 12-bis-THA particles and their TFD cargo. Additionally, the inclusion of a polymeric TFD particle study would provide information on whether this technology was suitable for TFD delivery to biofilms.

TFD-rhodamine conjugates have shown good transfection efficiency against Gram-negative organisms including *E. coli* and *P. aeruginosa.* It shares functional similarities with 12-bis-THA particles as rhodamine is a lipophilic cation able to cross prokaryotic and mitochondrial membranes using PMF (141). Polymeric TFD particles are modified to contain nucleotides labelled with rhodamine molecules which showed moderate transfection efficiency in *B. thailandensis* (**Chapter 6**). TFD-rhodamine conjugates were used as a surrogate for polymeric TFD particles as the cost associated with producing a sufficient concentration of thesis particles was prohibitive. The data in **Chapter 4** suggests that the TFD-rhodamine conjugates did not significantly interact with *B. thailandensis* biofilms however this study was limited to one independent experiment meaning more replicates are required before drawing conclusions.

7.1.4 Identifying candidates for TFD development

In **Chapter 6**, a proteomic and computational workflow was combined with a review of the literature to identify transcription factors and other regulatory elements that were conserved in *Burkholderia* species for TFD development. The proteomic dataset described in **Chapter 5** was interrogated for regulatory elements using a keyword search that identified 217 proteins. Statistical analysis showed that two increased in abundance in response to 0.1X MIC of 12-bis-THA particles whereas fourteen increased in abundance in response to 1X MIC. Further computational characterization was required to investigate the molecular functions of the identified regulatory factors. To do so, Blast searches were performed to identify homologues in organisms such as *E. coli* and *P. aeruginosa.* **Chapter 6** showed that SigJ (BTH_I0088) was an auxiliary group one sigma factor that was conserved in *Burkholderia* species. It is a potential candidate for TFD development but further investigations are required to determine its molecular function and whether it has a unique TFBS. Ultimately, no candidates were identified in the proteomic data set for immediate TFD development as few had been characterised on a molecular level and no transcription factor binding had been identified.

As a complementary approach, a literature review was performed to identify characterised transcription factors with known phenotypes and binding motifs which could be candidates for TFD development. TEX and Zur were both identified using the literature and were taken forward due to their known binding motif. Additionally, Bcam1349 and GvmR were identified in the literature as both being important *in vivo* by regulating virulence factors however, neither had a characterised transcription factor binding motif (275,359). In **Chapter 6**, Prodoric was used to identify potential transcription factor binding motifs GvmR and Bcam1349 by interrogating the promoter of genes within the transcriptional factors regulon. Potential transcription factor binding sequences that had been identified using this method were selected based on the importance of the downstream gene. The caveat of this approach is that these are computationally predicted sequences and there is no experimental data in *Burkholderia* species validating them meaning that an absence of TFD activity may be representative of a falsely predicted binding motif.

7.1.5 Testing the antimicrobial activity of novel anti-Burkholderia TFDs

In **Chapter 6**, it was demonstrated using CLSM that 12-bis-THA particles loaded with TFD accumulated in the cytoplasm of capsulated *B. thailandensis* strain E555. TFD polymeric particles are a new iteration of TFD technology and CLSM showed that these particles transfected strain E555 in the absence of 12-bis-THA particles. Phenotypic assays were performed to investigate the activity of TFDs against *B. thailandensis.* MIC studies of Bcam1349 and TEX TFDs that were delivered by 12-bis-

THA particles showed no difference in the antimicrobial activity of empty particles or those loaded with scrambled TFD. Similar observations were made in the MBEC and MBIC studies which also showed that Bcam1349 and TEX exhibited no difference in antimicrobial activities when compared to the scrambled and empty controls.

Data in **Chapter 4** showed that 12-bis-THA particles loaded with fluorescently labelled TFD could penetrate the biofilm but it was not possible to determine whether the TFD was in the bacterial cytoplasm or within the extracellular matrix. One possibility is that TFDs are sequestered by the extracellular matrix preventing their transfection. Alternatively, 12-bis-THA particles may transfect both planktonic and sessile bacterial cells with levels of TFD that are not sufficient to produce a phenotypic shift. It is also possible that 12-bis-THA particles may mask the effect of the TFD as the particles demonstrate their own antimicrobial activity (**Chapter 3**).

In contrast, MIC testing in **Chapter 6** polymeric TFD particles containing the transcription factor binding motifs of Zur and GvmR demonstrated sequence-specific activity. The polymeric TFD particles containing the Zur binding domain had an MIC of 0.16 – 0.31 µg/mL which was 16 – 32 fold lower than the scrambled control. Similarly, the MIC of the GvmR polymeric TFD particle had an MIC of 2.5 µg/mL. This was 4-fold lower than the MIC of the scrambled control which was 10 µg/mL. The Zur TFD may have a lower MIC than the GvmR TFD particle as its transcription factor binding motif is better characterised whereas the sequence used to develop the GvmR was based on a computational prediction using Prodoric. Further characterization of the structure and binding motif of GvmR may identify an alternative transcription factor binding motif that produces a lower MIC. Overall, the polymeric TFD particles demonstrated superior antimicrobial activity compared to TFDs delivered by 12-bis-THA particles. This may occur for several reasons:

- 12-bis-THA particles may deliver insufficient TFD to the bacterial cytoplasm compared to the polymeric TFD particles whose mass is predominantly comprised of TFD sequences
- 12-bis-THA particles have their own antimicrobial activity which masks the activity of the TFD
- characterisation of Bcam1349 and TEX mutants are required to identify the appropriate conditions to observe TFD activity.

7.2 FUTURE STUDIES

7.2.1 Development and characterization of polymeric TFD particles

The data presented in this thesis showed that polymeric TFD particles demonstrated better antimicrobial activity compared to TFDs delivered by 12-bis-THA particles. The reason for this is unknown but is discussed in section **7.1.5**. To allow for a fair comparison of TFD activity, polymeric TFD particles containing the transcription factor binding motifs of Bcam1349 and TEX should be prepared, and their MIC determined.

In general, to better understand polymeric TFD particles, further characterization should be performed using DLS to determine their biophysical characteristics including size and z-potential. A longitudinal study should be performed to provide insight into their stability which will inform the frequency of their preparation. Additionally, studies should be performed to assess the stability of polymeric TFD particles in biological fluids as described by Marín-Menéndez *et al* (132).

7.2.2 Characterisation of SigJ, GvmR and Zur as therapeutic targets in *Burkholderia* species

It is important when developing TFDs to identify a robust and conserved candidate. For these reasons, SigJ, GvmR and Zur are strong candidates for TFD development. However, development has been slow as data on these transcription factors characterizing their molecular function and binding motifs in *B. pseudomallei* is limited. A mutant strain of Δ*gvmR* has been constructed in *B. pseudomallei* by Duong *et al* (275) however we were unable to study this as we did not have access to Containment Level 3 facilities. Although this is beyond the scope of this project, recombinant expression, and structural characterisation of SigJ, GvmR and Zur are required. Recombinantly expressed proteins can be used to perform DNAse footprinting (116) and electrophoretic motility shift assays (395) to identify the transcription factor binding motifs of these proteins which will allow for the optimisation of TFD sequences. Additionally, the generation of *ΔsigJ* strain of *B.thailandensis* could provide insight into the molecular function of this sigma factor and help determine whether it is a good candidate for TFD development.

7.2.3 Investigating the antimicrobial activity of TFDs against *B. pseudomallei*

The main aim of this project was to identify TFDs that demonstrated antimicrobial activity against *B. pseudomallei*. Due to the lack of Containment Level 3 facilities and the impact of Covid-19, we were unable to perform studies using this organism and instead performed studies on the surrogate organism *B. thailandensis.* Despite this, TFDs were developed based on candidates conserved in *B. pseudomallei* and preliminary MIC testing showing that the polymeric TFD particles inhibit *B. thailandensis* growth at ng/mL concentrations. MIC testing of Zur and GvmR polymeric TFD

particles should be performed on strains of *B. pseudomallei* to determine if the antimicrobial activity is conserved within this species. The inclusion of *B. mallei* strains would help determine if these polymeric TFD particles demonstrated broad-spectrum activity against both *Burkholderia* species.

CONCLUSIONS

TFD based antimicrobials have the potential to be good alternatives to traditional small molecule therapies as they act on novel targets, can spare the host microbiota, and can circumvent antimicrobial resistances mechanisms. The multi-omic workflow presented in this thesis successfully provided insight into the mechanism of action of 12-bis-THA particles against *B. thailandensis* and identified possible candidates for TFD development that were conserved in multiple *Burkholderia* species including *B. pseudomallei*. However, this approach may be more useful in organisms where transcription factors are better characterised.

The data presented also shows that 12-bis-THA particles exhibit antimicrobial activity against planktonic and sessile *B. thailandensis*, they synergises with small molecule antimicrobials, and can deliver TFDs to the cytoplasm of *B. thailandensis*. However, no TFD activity was observed when delivered with 12-bis-THA particles raising questions regarding its suitability as a delivery agent to *Burkholderia* species. In contrast, polymeric TFD particles transfected *B. thailandensis* in the absence of 12-bis-THA particles and had comparatively lower MICs however further testing is required to assess the antimicrobial of polymeric TFD particles in the target organism *B. pseudomallei*.

REFERENCES

1. Compant S, Nowak J, Coenye T, Clément C, Ait Barka E. Diversity and occurrence of Burkholderia spp. in the natural environment. FEMS Microbiology Reviews. 2008 Jul 1;32(4):607–26.

2. Depoorter E, Bull MJ, Peeters C, Coenye T, Vandamme P, Mahenthiralingam E. Burkholderia: an update on taxonomy and biotechnological potential as antibiotic producers. Applied microbiology and biotechnology. 2016 Jun 1;100(12):5215–29.

3. Tavares M, Kozak M, Balola A, Sá-Correia I. Burkholderia cepacia complex bacteria: A feared contamination risk in water-based pharmaceutical products. Clinical Microbiology Reviews. 2020 Jul 1;33(3).

4. Coutinho CP, dos Santos SC, Madeira A, Mira NP, Moreira AS, Sá-Correia I. Long-Term Colonization of the Cystic Fibrosis Lung by Burkholderia cepacia Complex Bacteria: Epidemiology, Clonal Variation, and Genome-Wide Expression Alterations. Frontiers in Cellular and Infection Microbiology. 2011;1:12.

5. Kalish LA, Waltz DA, Dovey M, Potter-Bynoe G, McAdam AJ, LiPuma JJ, et al. Impact of Burkholderia dolosa on lung function and survival in cystic fibrosis. American journal of respiratory and critical care medicine [Internet]. 2006 Feb 15;173(4):421–5.

6. Greenberg DE, Goldberg JB, Stock F, Murray PR, Holland SM, Lipuma JJ. Recurrent Burkholderia Infection in Patients with Chronic Granulomatous Disease: 11-Year Experience at a Large Referral Center. Clinical infectious diseases : an official publication of the Infectious Diseases Society of America. 2009 Jun 1;48(11):1577.

7. Mann T, Ben-David D, Zlotkin A, Shachar D, Keller N, Toren A, et al. An outbreak of Burkholderia cenocepacia bacteremia in immunocompromised oncology patients. Infection. 2010 Jun;38(3):187–94.

8. Singhal T, Shah S, Naik R. Outbreak of Burkholderia cepacia complex bacteremia in a chemotherapy day care unit due to intrinsic contamination of an antiemetic drug. Indian journal of medical microbiology. 2015 Jan 1;33(1):117–9.

9. el Chakhtoura NG, Saade E, Wilson BM, Perez F, Papp-Wallace KM, Bonomo RA. A 17-Year Nationwide Study of Burkholderia cepacia Complex Bloodstream Infections Among Patients in the United States Veterans Health Administration. Clinical Infectious Diseases: An Official Publication of the Infectious Diseases Society of America. 2017 Oct 1;65(8):1327.

10. de Soyza A, Meachery G, Hester KLM, Nicholson A, Parry G, Tocewicz K, et al. Lung transplantation for patients with cystic fibrosis and Burkholderia cepacia complex infection: a single-center experience. The Journal of heart and lung transplantation : the official publication of the International Society for Heart Transplantation. 2010 Dec ;29(12):1395–404.

11. Kreindler JL. Cystic fibrosis: Exploiting its genetic basis in the hunt for new therapies. Pharmacology & therapeutics. 2010 Feb;125(2):219.

12. Ioannou L, Mcclaren BJ, Massie J, Lewis S, Metcalfe SA, Forrest L, et al. Population-based carrier screening for cystic fibrosis: a systematic review of 23 years of research. Genetics in medicine : official journal of the American College of Medical Genetics. 2014 ;16(3):207–16.

13. Li C, Naren AP. CFTR chloride channel in the apical compartments: spatiotemporal coupling to its interacting partners. Integrative biology : quantitative biosciences from nano to macro. 2010;2(4):161–77.

14. Cantin AM, Hartl D, Konstan MW, Chmiel JF. Inflammation in cystic fibrosis lung disease: Pathogenesis and therapy. Journal of cystic fibrosis : official journal of the European Cystic Fibrosis Society. 2015 Jul 1;14(4):419–30.

15. Regamey N, Jeffery PK, Alton EWFW, Bush A, Davies JC. Airway remodelling and its relationship to inflammation in cystic fibrosis. Thorax. 2011 Jul 1;66(7):624–9.

16. Bhagirath AY, Li Y, Somayajula D, Dadashi M, Badr S, Duan K. Cystic fibrosis lung environment and Pseudomonas aeruginosa infection. BMC Pulmonary Medicine. 2016 Dec 5;16(1).

17. Mahenthiralingam E, Urban TA, Goldberg JB. The multifarious, multireplicon Burkholderia cepacia complex. Nature reviews Microbiology. 2005 Feb;3(2):144–56.

18. Whitby PW, Pope LC, Carter KB, LiPuma JJ, Stull TL. Species-specific PCR as a tool for the identification of Burkholderia gladioli. Journal of clinical microbiology. 2000 ;38(1):282–5.

19. LiPuma JJ. The Changing Microbial Epidemiology in Cystic Fibrosis. Clinical Microbiology Reviews. 2010 Apr;23(2):299.

20. Losada L, Ronningf CM, Deshazer D, Woods D, Fedorova N, Kim HS, et al. Continuing Evolution of Burkholderia mallei Through Genome Reduction and Large-Scale Rearrangements. Genome Biology and Evolution. 2010;2(1):102.

21. Song H, Hwang J, Yi H, Ulrich RL, Yu Y, Nierman WC, et al. The Early Stage of Bacterial Genome-Reductive Evolution in the Host. PLoS Pathogens. 2010 May;6(5):1–10.

22. Khan I, Wieler LH, Melzer F, Elschner MC, Muhammad G, Ali S, et al. Glanders in Animals: A Review on Epidemiology, Clinical Presentation, Diagnosis and Countermeasures. Transboundary and Emerging Diseases. 2013 Jun 1;60(3):204–21.

23. Rjun A, Rinivasan S, Raus ANK, Ecker AMB, Ames J, Ick DD, et al. Glanders in a Military Research Microbiologist. New England Journal of Medicine. 2009 Aug 20;345(4):256–8.

24. Peacock SJ, Schweizer HP, Dance DAB, Smith TL, Gee JE, Wuthiekanun V, et al. Management of accidental laboratory exposure to Burkholderia pseudomallei and B. mallei. Emerging infectious diseases. 2008 Jul;14(7).

25. HOWE C, MILLER WR. Human glanders; report of six cases. Annals of internal medicine. 1947 Jan 1;26(1):93–115.

26. Whitmore A. An Account of a Glanders-like Disease occurring in Rangoon. The Journal of Hygiene. 1913;13(1):1.

27. Wuthiekanun V, Smith MD, White NJ. Survival of Burkholderia pseudomallei in the absence of nutrients. Transactions of the Royal Society of Tropical Medicine and Hygiene. 1995;89(5):491.

28. Hoffmaster AR, Aucoin D, Baccam P, Baggett HC, Baird R, Bhengsri S, et al. Melioidosis diagnostic workshop, 2013. Emerging infectious diseases. 2015;21(2):1–9.

29. Limmathurotsakul D, Golding N, Dance DAB, Messina JP, Pigott DM, Moyes CL, et al. Predicted global distribution of Burkholderia pseudomallei and burden of melioidosis. Nature Microbiology. 2016 Jan 11;1(1):15008.

30. Suputtamongkol Y, Hall AJ, Dance DAB, Chaowagul W, Rajchanuvong A, Smith MD, et al. The epidemiology of melioidosis in Ubon Ratchatani, northeast Thailand. International journal of epidemiology. 1994 Oct;23(5):1082–90.

31. Currie BJ, Fisher DA, Howard DM, Burrow JNC, Lo D, Selva-Nayagam S, et al. Endemic melioidosis in tropical northern Australia: a 10-year prospective study and review of the literature. Clinical infectious diseases : an official publication of the Infectious Diseases Society of America. 2000;31(4):981–6.

32. Weber DR, Douglass LE, Brundage WG, Stallkamp TC. Acute varieties of melioidosis occurring in U. S. soldiers in Vietnam. The American Journal of Medicine. 1969 Feb 1;46(2):234–44.

33. Howe C, Sampath A, Spotnitz M. The pseudomallei group: a review. The Journal of infectious diseases. 1971;124(6):598–606.

34. Moore RA, Tuanyok A, Woods DE. Survival of Burkholderia pseudomallei in Water. BMC Research Notes. 2008 May 7;1(1):1–6.

35. Thaipadungpanit J, Chierakul W, Pattanaporkrattana W, Phoodaeng A, Wongsuvan G, Huntrakun V, et al. Burkholderia pseudomallei in Water Supplies, Southern Thailand. Emerging Infectious Diseases. 2014 Nov 1;20(11):1947.

36. Mayo M, Kaestli M, Harrington G, Cheng AC, Ward L, Karp D, et al. Burkholderia pseudomallei in Unchlorinated Domestic Bore Water, Tropical Northern Australia. Emerging Infectious Diseases. 2011 Jul;17(7):1283.

37. Currie BJ, Mayo M, Anstey NM, Donohoe P, Haase A, Kemp DJ. A cluster of melioidosis cases from an endemic region is clonal and is linked to the water supply using molecular typing of Burkholderia pseudomallei isolates. The American journal of tropical medicine and hygiene. 2001;65(3):177–9.

38. Currie BJ, Ward L, Cheng AC. The epidemiology and clinical spectrum of melioidosis: 540 cases from the 20 year Darwin prospective study. PLoS neglected tropical diseases. 2010 Nov;4(11).

39. Suputtamongkol Y, Hall AJ, Dance DAB, Chaowagul W, Rajchanuvong A, Smith MD, et al. The Epidemiology of Melioidosis in Ubon Ratchatani, Northeast Thailand. International Journal of Epidemiology. 1994 Oct 1;23(5):1082–90.

40. Suntornsut P, Wongsuwan N, Malasit M, Kitphati R, Michie S, Peacock SJ, et al. Barriers and Recommended Interventions to Prevent Melioidosis in Northeast Thailand: A Focus Group Study Using the Behaviour Change Wheel. PLoS neglected tropical diseases. 2016 Jul 29;10(7).

41. Zueter AR, Yean CY, Abumarzouq M, Rahman ZA, Deris ZZ, Harun A. The epidemiology and clinical spectrum of melioidosis in a teaching hospital in a North-Eastern state of Malaysia: A fifteen-year review. BMC Infectious Diseases. 2016 Jul 16;16(1):1–11.

42. Wiersinga WJ, Currie BJ, Peacock SJ. Medical progress: Melioidosis. The New England Journal of Medicine. 2012 Sep 12;367(11):1035–44.

43. Meumann EM, Cheng AC, Ward L, Currie BJ. Clinical Features and Epidemiology of Melioidosis Pneumonia: Results From a 21-Year Study and Review of the Literature. Clinical Infectious Diseases: An Official Publication of the Infectious Diseases Society of America. 2012 Feb 1;54(3):362.

44. Stewart JD, Smith S, Binotto E, McBride WJ, Currie BJ, Hanson J. The epidemiology and clinical features of melioidosis in Far North Queensland: Implications for patient management. PLoS Neglected Tropical Diseases. 2017 Mar 6;11(3).

45. Goel A, Bansal R, Sharma S, Singhal S, Kumar A. Chronic melioidosis presenting with multiple abscesses. Oxford medical case reports. 2016;2016(6):113–6.

46. Currie BJ, Fisher DA, Anstey NM, Jacups SP. Melioidosis: acute and chronic disease, relapse and re-activation. Transactions of the Royal Society of Tropical Medicine and Hygiene. 2000;94(3):301–4.

47. Mariappan V, Thavagnanam S, Vellasamy KM, Teh CJS, Atiya N, Ponnampalavanar S, et al. Relapse of chronic melioidosis in a paediatric cystic fibrosis patient: First case report from Malaysia. BMC Infectious Diseases. 2018 Sep 5;18(1):1–5.

48. Schülin T, Steinmetz I. Chronic Melioidosis in a Patient with Cystic Fibrosis. Journal of Clinical Microbiology. 2001;39(4):1676.

49. Essex-Lopresti AE, Boddey JA, Thomas R, Smith MP, Hartley MG, Atkins T, et al. A Type IV Pilin, PilA, Contributes to Adherence of Burkholderia pseudomallei and Virulence In Vivo. Infection and Immunity. 2005 Feb;73(2):1260.

50. Ahmed K, Enciso HDR, Masaki H, Tao M, Omori A, Tharavichikul P, et al. Attachment of Burkholderia pseudomallei to pharyngeal epithelial cells: a highly pathogenic bacteria with low attachment ability. The American journal of tropical medicine and hygiene. 1999;60(1):90–3.

51. Chuaygud T, Tungpradabkul S, Sirisinha S, Chua KL, Utaisincharoen P. A role of Burkholderia pseudomallei flagella as a virulent factor. Transactions of The Royal Society of Tropical Medicine and Hygiene. 2008 Dec 1;102(Supplement_1):S140–4.

52. Allwood EM, Devenish RJ, Prescott M, Adler B, Boyce JD. Strategies for Intracellular Survival of Burkholderia pseudomallei. Frontiers in Microbiology. 2011;2.

53. Balder R, Lipski S, Lazarus JJ, Grose W, Wooten RM, Hogan RJ, et al. Identification of Burkholderia mallei and Burkholderia pseudomallei adhesins for human respiratory epithelial cells. BMC microbiology. 2010;10.

54. Stevens MP, Friebel A, Taylor LA, Wood MW, Brown PJ, Hardt WD, et al. A Burkholderia pseudomallei type III secreted protein, BopE, facilitates bacterial invasion of epithelial cells and exhibits guanine nucleotide exchange factor activity. Journal of bacteriology. 2003 Aug;185(16):4992–6.

55. Balder R, Lipski S, Lazarus JJ, Grose W, Wooten RM, Hogan RJ, et al. Identification of Burkholderia mallei and Burkholderia pseudomallei adhesins for human respiratory epithelial cells. BMC microbiology. 2010;10.

56. Valvano MA. Intracellular survival of Burkholderia cepacia complex in phagocytic cells. Canadian journal of microbiology. 2015 Feb 11;61(9):607–15.

57. Jones AL, Beveridge TJ, Woods DE. Intracellular survival of Burkholderia pseudomallei. Infection and Immunity.1996;64(3):782.

58. Stevens MP, Wood MW, Taylor LA, Monaghan P, Hawes P, Jones PW, et al. An Inv/Mxi-Spa-like type III protein secretion system in Burkholderia pseudomallei modulates intracellular behaviour of the pathogen. Molecular microbiology. 2002;46(3):649–59.

59. Stevens MP, Haque A, Atkins T, Hill J, Wood MW, Easton A, et al. Attenuated virulence and protective efficacy of a Burkholderia pseudomallei bsa type III secretion mutant in murine models of melioidosis. Microbiology. 2004;150(Pt 8):2669–76.

60. Suparak S, Kespichayawattana W, Haque A, Easton A, Damnin S, Lertmemongkolchai G, et al. Multinucleated giant cell formation and apoptosis in infected host cells is mediated by Burkholderia pseudomallei type III secretion protein BipB. Journal of bacteriology. 2005 Sep;187(18):6556–60.

61. Lennings J, West TE, Schwarz S. The Burkholderia Type VI secretion system 5: Composition, regulation and role in virulence. Frontiers in Microbiology. 2019;10:3339.

62. Suparak S, Kespichayawattana W, Haque A, Easton A, Damnin S, Lertmemongkolchai G, et al. Multinucleated giant cell formation and apoptosis in infected host cells is mediated by Burkholderia pseudomallei type III secretion protein BipB. Journal of bacteriology. 2005 Sep;187(18):6556–60.

63. Burtnick MN, Brett PJ, Harding S v., Ngugi SA, Ribot WJ, Chantratita N, et al. The Cluster 1 Type VI Secretion System Is a Major Virulence Determinant in Burkholderia pseudomallei. Infection and Immunity. 2011 Apr;79(4):1512.

64. French CT, Toesca IJ, Wu TH, Teslaa T, Beaty SM, Wong W, et al. Dissection of the Burkholderia intracellular life cycle using a photothermal nanoblade. Proceedings of the National Academy of Sciences of the United States of America. 2011 Jul 19;108(29):12095–100.

65. Kespichayawattana W, Rattanachetkul S, Wanun T, Utaisincharoen P, Sirisinha S. Burkholderia pseudomallei induces cell fusion and actin-associated membrane protrusion: a possible mechanism for cell-to-cell spreading. Infection and immunity. 2000;68(9):5377–84.

66. Sun GW, Lu J, Pervaiz S, Cao WP, Gan YH. Caspase-1 dependent macrophage death induced by Burkholderia pseudomallei. Cellular microbiology. 2005 Oct;7(10):1447–58.

67. Wiersinga WJ, Virk HS, Torres AG, Currie BJ, Peacock SJ, Dance DAB, et al. Melioidosis. Nature reviews Disease primers. 2018 Feb 1;4:17107.

68. Limmathurotsakul D, Jamsen K, Arayawichanont A, Simpson JA, White LJ, Lee SJ, et al. Defining the true sensitivity of culture for the diagnosis of melioidosis using Bayesian latent class models. PloS one. 2010;5(8).

69. Ashdown LR. An improved screening technique for isolation of Pseudomonas pseudomallei from clinical specimens. Pathology. 1979;11(2):293–7.

70. Dance DAB, Wuthiekanun V, Naigowit P, White NJ, Hospital B. Identification of Pseudomonas pseudomallei in clinical practice: use of simple screening tests and API 20NE. J Clin Pathol. 1989;42:645–8.

71. Suttisunhakul V, Pumpuang A, Ekchariyawat P, Wuthiekanun V, Elrod MG, Turner P, et al. Matrix-assisted laser desorption/ionization time-of-flight mass spectrometry for the identification of Burkholderia pseudomallei from Asia and Australia and differentiation between Burkholderia species. PloS one. 2017 Apr 1;12(4).

72. Gee JE, Sacchi CT, Glass MB, De BK, Weyant RS, Levett PN, et al. Use of 16S rRNA gene sequencing for rapid identification and differentiation of Burkholderia pseudomallei and B. mallei. Journal of clinical microbiology. 2003 Oct 1;41(10):4647–54.

73. Koh SF, Tay ST, Sermswan R, Wongratanacheewin S, Chua KH, Puthucheary SD. Development of a multiplex PCR assay for rapid identification of Burkholderia pseudomallei, Burkholderia thailandensis, Burkholderia mallei and Burkholderia cepacia complex. Journal of microbiological methods. 2012 Sep;90(3):305–8.

74. Kaestli M, Richardson LJ, Colman RE, Tuanyok A, Price EP, Bowers JR, et al. Comparison of TaqMan PCR assays for detection of the melioidosis agent Burkholderia pseudomallei in clinical specimens. Journal of clinical microbiology. 2012 Jun;50(6):2059–62.

75. Alexander AD, Huxsoll DL, Albert R. Warner Jr, Shepler V, Dorsey A. Serological Diagnosis of Human Melioidosis with Indirect Hemagglutination and Complement Fixation Tests. Applied Microbiology. 1970 Nov;20(5):825–33.

76. Chaichana P, Jenjaroen K, Amornchai P, Chumseng S, Langla S, Rongkard P, et al. Antibodies in Melioidosis: The Role of the Indirect Hemagglutination Assay in Evaluating Patients and Exposed Populations. The American journal of tropical medicine and hygiene. 2018;99(6):1378–85.

77. Cheng AC, Wuthiekanun V, Limmathurotsakul D, Chierakul W, Peacock SJ. Intensity of exposure and incidence of melioidosis in Thai children. Transactions of the Royal Society of Tropical Medicine and Hygiene. 2008 Dec;102 Suppl 1(SUPPL. 1).

78. Duval BD, Elrod MG, Gee JE, Chantratita N, Tandhavanant S, Limmathurotsakul D, et al. Evaluation of a latex agglutination assay for the identification of Burkholderia pseudomallei and Burkholderia mallei. The American journal of tropical medicine and hygiene. 2014;90(6):1043–6.

79. Limmathurotsakul D, Wongratanacheewin S, Teerawattanasook N, Wongsuvan G, Chaisuksant S, Chetchotisakd P, et al. Increasing incidence of human melioidosis in northeast Thailand. American Journal of Tropical Medicine and Hygiene. 2010 Jun;82(6):1113–7.

80. Dance D. Treatment and prophylaxis of melioidosis-review. International Journal of Antimicrobial Agents. 2014 Apr; 43(4):310–8.

81. Pitman MC, Luck T, Marshall CS, Anstey NM, Ward L, Currie BJ. Intravenous Therapy Duration and Outcomes in Melioidosis: A New Treatment Paradigm. PLoS Neglected Tropical Diseases. 2015 Mar 26;9(3).

82. Chetchotisakd P, Chierakul W, Chaowagul W, Anunnatsiri S, Phimda K, Mootsikapun P, et al. Trimethoprim-sulfamethoxazole versus trimethoprim-sulfamethoxazole plus doxycycline as oral eradicative treatment for melioidosis (MERTH): a multicentre, double-blind, non-inferiority, randomised controlled trial. Lancet.2014;383(9919):807–14.

83. Wuthiekanun V, Cheng AC, Chierakul W, Amornchai P, Limmathurotsakul D, Chaowagul W, et al. Trimethoprim/sulfamethoxazole resistance in clinical isolates of Burkholderia pseudomallei. The Journal of antimicrobial chemotherapy. 2005 Jun55(6):1029–31.

84. Rao C, Hu Z, Chen J, Tang M, Chen H, Lu X, et al. Molecular epidemiology and antibiotic resistance of Burkholderia pseudomallei isolates from Hainan, China: A STROBE compliant observational study. Medicine. 2019;98(9).

85. Wuthiekanun V, Amornchai P, Saiprom N, Chantratita N, Chierakul W, Koh GCKW, et al. Survey of Antimicrobial Resistance in Clinical Burkholderia pseudomallei Isolates over Two Decades in Northeast Thailand. Antimicrobial Agents and Chemotherapy. 2011 Nov;55(11):5388.

86. Rao C, Hu Z, Chen J, Tang M, Chen H, Lu X, et al. Molecular epidemiology and antibiotic resistance of Burkholderia pseudomallei isolates from Hainan, China: A STROBE compliant observational study. Medicine. 2019;98(9).

87. Godfrey AJ, Wong S, Dance DAB, Chaowagul W, Bryan LE. Pseudomonas pseudomallei resistance to beta-lactam antibiotics due to alterations in the chromosomally encoded beta-lactamase. Antimicrobial Agents and Chemotherapy. 1991;35(8):1635.

88. Sarovich DS, Price EP, von Schulze AT, Cook JM, Mayo M, Watson LM, et al. Characterization of ceftazidime resistance mechanisms in clinical isolates of Burkholderia pseudomallei from Australia. PloS one. 2012 Feb 21;7(2).

89. Chantratita N, Rholl DA, Sim B, Wuthiekanun V, Limmathurotsakul D, Amornchai P, et al. Antimicrobial resistance to ceftazidime involving loss of penicillin-binding protein 3 in Burkholderia pseudomallei. Proceedings of the National Academy of Sciences of the United States of America. 2011 Oct 11;108(41):17165–70.

90. Rhodes KA, Schweizer HP. Antibiotic resistance in Burkholderia species. Drug resistance updates : reviews and commentaries in antimicrobial and anticancer chemotherapy. 2016 Sep 1;28:82–90.

91. Krishnamoorthy G, Leus I v., Weeks JW, Wolloscheck D, Rybenkov V v., Zgurskaya HI. Synergy between Active Efflux and Outer Membrane Diffusion Defines Rules of Antibiotic Permeation into Gram-Negative Bacteria. mBio. 2017 Sep 1;8(5).

92. Podnecky NL, Rhodes KA, Schweizer HP. Efflux pump-mediated drug resistance in Burkholderia. Frontiers in Microbiology. 2015;6:1–25.

93. Trunck LA, Propst KL, Wuthiekanun V, Tuanyok A, Beckstrom-Sternberg SM, Beckstrom-Sternberg JS, et al. Molecular basis of rare aminoglycoside susceptibility and pathogenesis of Burkholderia pseudomallei clinical isolates from Thailand. PLoS neglected tropical diseases. 2009 Sep;3(9).

94. Podin Y, Sarovich DS, Price EP, Kaestli M, Mayo M, Hii K, et al. Burkholderia pseudomallei isolates from Sarawak, Malaysian Borneo, are predominantly susceptible to aminoglycosides and macrolides. Antimicrobial agents and chemotherapy. 2014 Jan;58(1):162–6.

95. Morita Y, Tomida J, Kawamura Y. MexXY multidrug efflux system of Pseudomonas aeruginosa. Frontiers in microbiology. 2012;3.

96. Chan YY, Tan TMC, Ong YM, Chua KL. BpeAB-OprB, a Multidrug Efflux Pump in Burkholderia pseudomallei. Antimicrobial Agents and Chemotherapy. 2004 Apr;48(4):1128.

97. Podnecky NL, Rhodes KA, Schweizer HP. Efflux pump-mediated drug resistance in Burkholderia. Frontiers in Microbiology. 2015;6:1–25.

98. Mima T, Schweizer HP. The BpeAB-OprB efflux pump of Burkholderia pseudomallei 1026b does not play a role in quorum sensing, virulence factor production, or extrusion of aminoglycosides but is a broad-spectrum drug efflux system. Antimicrobial agents and chemotherapy. 2010 Aug 1;54(8):3113–20.

99. Li XZ, Nikaido H, Poole K. Role of mexA-mexB-oprM in antibiotic efflux in Pseudomonas aeruginosa. Antimicrobial Agents and Chemotherapy. 1995;39(9):1948.

100. Kumar A, Chua KL, Schweizer HP. Method for regulated expression of single-copy efflux pump genes in a surrogate Pseudomonas aeruginosa strain: identification of the BpeEF-OprC chloramphenicol and trimethoprim efflux pump of Burkholderia pseudomallei 1026b. Antimicrobial agents and chemotherapy. 2006 Oct;50(10):3460–3.

101. Hayden HS, Lim R, Brittnacher MJ, Sims EH, Ramage ER, Fong C, et al. Evolution of Burkholderia pseudomallei in recurrent melioidosis. PloS one. 2012;7(5).

102. Podnecky NL, Wuthiekanun V, Peacock SJ, Schweizer HP. The BpeEF-OprC Efflux Pump Is Responsible for Widespread Trimethoprim Resistance in Clinical and Environmental Burkholderia pseudomallei Isolates. Antimicrobial Agents and Chemotherapy. 2013 Sep;57(9):4381.

103. Nikaido H. Molecular basis of bacterial outer membrane permeability revisited. Microbiology and molecular biology reviews : MMBR. 2003 Dec;67(4):593–653

104. Bertani B, Ruiz N. Function and Biogenesis of Lipopolysaccharides. EcoSal Plus. 2018 Feb 8;8(1).

105. Hancock REW, Hancock RE. Resistance Mechanisms in Pseudomonas aeruginosa and Other Nonfermentative Gram-Negative Bacteria. Clin Infect Dis.1998 Aug; 27(1):93-6

106. Gatzeva-Topalova PZ, May AP, Sousa MC. Structure and Mechanism of ArnA: Conformational Change Implies Ordered Dehydrogenase Mechanism in Key Enzyme for Polymyxin Resistance. Structure (London, England : 1993). 2005 Jun;13(6):929.

107. NIAID Emerging Infectious Diseases/ Pathogens | NIH: National Institute of Allergy and Infectious Diseases [Internet]. [cited 2021 Dec 31]. Available from: https://www.niaid.nih.gov/research/emerging-infectious-diseases-pathogens

108. Federal Select Agent Program [Internet]. [cited 2021 Dec 31]. Available from: https://www.selectagents.gov/

109. Brett PJ, DeShazer D, Woods DE. Burkholderia thailandensis sp. nov., a Burkholderia pseudomallei-like species. International journal of systematic bacteriology. 1998;48 Pt 1(1):317–20.

110. Yu Y, Kim HS, Hui HC, Chi HL, Siew HS, Lin D, et al. Genomic patterns of pathogen evolution revealed by comparison of Burkholderia pseudomallei, the causative agent of melioidosis, to avirulent Burkholderia thailandensis. BMC microbiology. 2006 May 26;6.

111. Smith MD, Angus BJ, Wuthiekanun V, White NJ. Arabinose assimilation defines a nonvirulent biotype of Burkholderia pseudomallei. Infection and immunity. 1997;65(10):4319–21.

112. Sim BMQ, Chantratita N, Ooi WF, Nandi T, Tewhey R, Wuthiekanun V, et al. Genomic acquisition of a capsular polysaccharide virulence cluster by non-pathogenic Burkholderia isolates. Genome Biology. 2010 Aug 27;11(1):1–17.

113. Scott AE, Laws TR, D'Elia R v., Stokes MGM, Nandi T, Williamson ED, et al. Protection against Experimental Melioidosis following Immunization with Live Burkholderia thailandensis Expressing a manno-Heptose Capsule. Clinical and Vaccine Immunology. 2013 Jul;20(7):1041.

114. Amiss AS, Webb JR, Mayo M, Currie BJ, Craik DJ, Henriques ST, et al. Safer In Vitro Drug Screening Models for Melioidosis Therapy Development. The American journal of tropical medicine and hygiene. 2020 Nov 1;103(5):1846–51.

115. Barker S, Harding S v., Gray D, Richards MI, Atkins HS, Harmer NJ. Drug screening to identify compounds to act as co-therapies for the treatment of Burkholderia species. PLOS ONE. 2021 Mar 1;16(3):e0248119.

116. Galas DJ, Schmitz A. DNAse footprinting: a simple method for the detection of protein-DNA binding specificity. Nucleic acids research. 1978 Sep;5(9):3157–70.

117. Mundade R, Ozer HG, Wei H, Prabhu L, Lu T. Role of ChIP-seq in the discovery of transcription factor binding sites, differential gene regulation mechanism, epigenetic marks and beyond. Cell Cycle. 2014 Sep 15;13(18):2847–52.

118. Ireland WT, Beeler SM, Flores-Bautista E, McCarty NS, Röschinger T, Belliveau NM, et al. Deciphering the regulatory genome of Escherichia coli, one hundred promoters at a time. eLife. 2020 Sep 1;9:1–76.

119. Griffith KL, Wolf J. Systematic mutagenesis of the DNA binding sites for SoxS in the Escherichia coli zwf and fpr promoters: identifying nucleotides required for DNA binding and transcription activation. Molecular microbiology. 2001;40(5):1141–54.

120. Münch R, Hiller K, Barg H, Heldt D, Linz S, Wingender E, et al. PRODORIC: prokaryotic database of gene regulation. Nucleic acids research. 2003 Jan 1;31(1):266–9.

121. Mann MJ, Dzau VJ. Therapeutic applications of transcription factor decoy oligonucleotides. Journal of Clinical Investigation. 2000;106(9):1071.

122. McArthur M, Bibb MJ. Manipulating and understanding antibiotic production in Streptomyces coelicolor A3(2) with decoy oligonucleotides. Proceedings of the National Academy of Sciences. 2008 Jan 22;105(3):1020–5.

123. Nakanishi K. Anatomy of RISC: how do small RNAs and chaperones activate Argonaute proteins? Wiley interdisciplinary reviews RNA. 2016 Sep 1;7(5):637–60.

124. Hagedorn PH, Persson R, Funder ED, Albæk N, Diemer SL, Hansen DJ, et al. Locked nucleic acid: modality, diversity, and drug discovery. Drug Discovery Today. 2018 Jan 1;23(1):101–14.

125. Daly SM, Sturge CR, Marshall-Batty KR, Felder-Scott CF, Jain R, Geller BL, et al. Antisense Inhibitors Retain Activity in Pulmonary Models of Burkholderia Infection. ACS Infectious Diseases. 2018 May 11;4(5):806–14.

126. Goltermann L, Yavari N, Zhang M, Ghosal A, Nielsen PE. PNA length restriction of antibacterial activity of peptide-PNA conjugates in Escherichia coli through effects of the inner membrane. Frontiers in Microbiology. 2019;10(MAY):1032.

127. Ishihama A, Kori A, Koshio E, Yamada K, Maeda H, Shimada T, et al. Intracellular concentrations of 65 species of transcription factors with known regulatory functions in Escherichia coli. Journal of Bacteriology. 2014;196(15):2718–27.

128. Vickers TA, Wyatt JR, Freier SM. Effects of RNA secondary structure on cellular antisense activity. Nucleic Acids Research. 2000 Mar 15;28(6):1340.

129. Grainger DC, Aiba H, Hurd D, Browning DF, Busby SJW. Transcription factor distribution in Escherichia coli: studies with FNR protein. Nucleic acids research. 2007 Jan;35(1):269–78.

130. Wang T, Sun W, Fan L, Hua C, Wu N, Fan S, et al. An atlas of the binding specificities of transcription factors in pseudomonas aeruginosa directs prediction of novel regulators in virulence. eLife. 2021 Mar 1;10.

131. Fraley AW, Pons B, Dalkara D, Nullans G, Behr JP, Zuber G. Cationic oligonucleotide-peptide conjugates with aggregating properties enter efficiently into cells while maintaining hybridization properties and enzymatic recognition. Journal of the American Chemical Society. 2006 Aug 23;128(33):10763–71.

132. Marín-Menéndez A, Montis C, Díaz-Calvo T, Carta D, Hatzixanthis K, Morris CJ, et al. Antimicrobial Nanoplexes meet Model Bacterial Membranes: the key role of Cardiolipin. Scientific Reports 2017 7:1. 2017 Jan 25;7(1):1–13.

133. Hegarty JP, Krzeminski J, Sharma AK, Guzman-Villanueva D, Weissig V, Stewart DB. Bolaamphiphile-based nanocomplex delivery of phosphorothioate gapmer antisense oligonucleotides as a treatment for Clostridium difficile. International journal of nanomedicine. 2016 Aug 1;11:3607–19.

134. Epand RM, Epand RF. Lipid domains in bacterial membranes and the action of antimicrobial agents. Biochimica et Biophysica Acta (BBA) - Biomembranes. 2009 Jan 1;1788(1):289–94.

135. Gidden J, Denson J, Liyanage R, Ivey DM, Lay JO. Lipid Compositions in Escherichia coli and Bacillus subtilis During Growth as Determined by MALDI-TOF and TOF/TOF Mass Spectrometry. International journal of mass spectrometry. 2009 Jun 1;283(1–3):178–84.

136. Sohlenkamp C, Geiger O. Bacterial membrane lipids: diversity in structures and pathways. FEMS Microbiology Reviews. 2016 Jan 1;40(1):133–59.

137. Montis C, Joseph P, Magnani C, Marín-Menéndez A, Barbero F, Estrada AR, et al. Multifunctional nanoassemblies target bacterial lipopolysaccharides for enhanced antimicrobial DNA delivery. Colloids and surfaces B, Biointerfaces. 2020 Nov 1;195.

138. Simona Di Blasio. Cationic Bolalipid Antimicrobials:Mechanism of Action and SAR. [London]; 2019.

139. Nichola Wong. Developing nanoparticulate oligonucleotides as a target-specific antimicrobial for modulation of complex gut microbiota. [Norwich]; 2018.

140. Rieger B, Arroum T, Borowski M-T, Villalta J, Busch KB. Mitochondrial F1FO ATP synthase determines the local proton motive force at cristae rims. EMBO reports. 2021 Dec 6 ;22(12):e52727.

141. Baracca A, Sgarbi G, Solaini G, Lenaz G. Rhodamine 123 as a probe of mitochondrial membrane potential: evaluation of proton flux through F0 during ATP synthesis. Biochimica et Biophysica Acta (BBA) - Bioenergetics. 2003 Sep 30;1606(1–3):137–46.

142. Santos J, Sousa F, Queiroz J, Costa D. Rhodamine based plasmid DNA nanoparticles for mitochondrial gene therapy. Colloids and surfaces B, Biointerfaces. 2014 Sep 1;121:129–40.

143. Yuan X, Xiao F, Zhao H, Huang Y, Shao C, Weizmann Y, et al. High-yield method to fabricate and functionalize DNA nanoparticles from the products of rolling circle amplification. ACS Applied Bio Materials. 2018 Aug 20;1(2):511–9.

144. Lam J, Chan R, Lam K, Costerton JW. Production of mucoid microcolonies by Pseudomonas aeruginosa within infected lungs in cystic fibrosis. Infection and immunity. 1980 ;28(2):546–56.

145. Brennan-Krohn T, Kirby JE. Antimicrobial Synergy Testing by the Inkjet Printer-assisted Automated Checkerboard Array and the Manual Time-kill Method. JoVE (Journal of Visualized Experiments)2019 Apr 18;2019(146):e58636.

146. Tyanova S, Temu T, Sinitcyn P, Carlson A, Hein MY, Geiger T, et al. The Perseus computational platform for comprehensive analysis of (prote)omics data. Vol. 13, Nature Methods. Nature Publishing Group; 2016. p. 731–40.

147. Moreira AS, Lourenço AB, Sá-Correia I. 1H-NMR-based endometabolome profiles of burkholderia cenocepacia clonal variants retrieved from a cystic fibrosis patient during chronic infection. Frontiers in Microbiology. 2016;7(DEC):2024.

148. Winsor GL, Khaira B, van Rossum T, Lo R, Whiteside MD, Brinkman FSL. The Burkholderia Genome Database: facilitating flexible queries and comparative analyses. Bioinformatics (Oxford, England). 2008 Dec;24(23):2803–4.

149. Munch R, Hiller K, Grote A, Scheer M, Klein J, Schobert M, et al. Virtual Footprint and PRODORIC: an integrative framework for regulon prediction in prokaryotes. Bioinformatics. 2005 Nov 15;21(22):4187–9.

150. O'Toole GA. Microtiter Dish Biofilm Formation Assay. JoVE (Journal of Visualized Experiments) 2011;(47).

151. A Brief History of the Center for Drug Evaluation and Research | FDA [Internet]. [cited 2021 Dec 31]. Available from: https://www.fda.gov/about-fda/fda-history-exhibits/brief-history-center-drug-evaluation-and-research

152. Abraham EP, Chain E. An Enzyme from Bacteria able to Destroy Penicillin. Nature 1940 146:3713. 1940;146(3713):837–837.

153. Sir Alexander Fleming - Nobel Lecture: Penicillin - NobelPrize.org [Internet]. [cited 2021 Dec 31]. Available from: https://www.nobelprize.org/prizes/medicine/1945/fleming/lecture/

154. Nguyen TVA, Anthony RM, Bañuls AL, Vu DH, Alffenaar JWC. Bedaquiline Resistance: Its Emergence, Mechanism, and Prevention. Clinical infectious diseases : an official publication of the Infectious Diseases Society of America. 2018 May 2;66(10):1625–30.

155. Schwaber MJ, Carmeli Y. Carbapenem-resistant Enterobacteriaceae: a potential threat. JAMA . 2008 Dec 24;300(24):2911–3.

156. Liu YY, Wang Y, Walsh TR, Yi LX, Zhang R, Spencer J, et al. Emergence of plasmid-mediated colistin resistance mechanism MCR-1 in animals and human beings in China: a microbiological and molecular biological study. The Lancet Infectious diseases. 2016 Feb 1 16(2):161–8.

157. 2019 Antibiotic Resistance Threats Report | CDC [Internet]. [cited 2021 Dec 31]. Available from: https://www.cdc.gov/drugresistance/biggest-threats.html

158. TACKLING DRUG-RESISTANT INFECTIONS GLOBALLY: FINAL REPORT AND RECOMMENDATIONS THE REVIEW ON ANTIMICROBIAL RESISTANCE CHAIRED BY JIM O'NEILL. 2016;

159. Shlaes DM. The Perfect Storm. Antibiotics. 2010;1–7.

160. UK aims to cut antibiotics 15% in 5-year AMR plan | CIDRAP [Internet]. [cited 2021 Dec 31]. Available from: https://www.cidrap.umn.edu/news-perspective/2019/01/uk-aims-cut-antibiotics-15-5-year-amr-plan

161. Mullard A. UK outlines its antibiotic pull incentive plan. Nature reviews Drug discovery. 2020 May 1;19(5):298.

162. Tracking the Global Pipeline of Antibiotics in Development, April 2020 | The Pew Charitable Trusts [Internet]. [cited 2021 Dec 31]. Available from: https://www.pewtrusts.org/en/research-and-analysis/issue-briefs/2020/04/tracking-the-global-pipeline-of-antibiotics-in-development

163. Bushby SR, Hitchings GH. Trimethoprim, a sulphonamide potentiator. British Journal of Pharmacology and Chemotherapy. 1968;33(1):72.

164. Yadav R, Bulitta JB, Schneider EK, Shin BS, Velkov T, Nation RL, et al. Aminoglycoside Concentrations Required for Synergy with Carbapenems against Pseudomonas aeruginosa Determined via Mechanistic Studies and Modeling. Antimicrobial agents and chemotherapy. 2017 Dec 1;61(12).

165. Bush K. Past and Present Perspectives on β-Lactamases. Antimicrobial agents and chemotherapy. 2018 Oct 1;62(10).

166. Bush K, Bradford PA. β-Lactams and β-Lactamase Inhibitors: An Overview. Cold Spring Harbor perspectives in medicine. 2016 Aug 1;6(8).

167. Schweizer HP. Mechanisms of antibiotic resistance in Burkholderia pseudomallei: implications for treatment of melioidosis. Future microbiology. 2012 Dec;7(12):1389–99.

168. Panta PR, Kumar S, Stafford CF, Billiot CE, Douglass M v., Herrera CM, et al. A DedA Family Membrane Protein Is Required for Burkholderia thailandensis Colistin Resistance. Frontiers in Microbiology. 2019 Nov 5;10:2532.

169. Wang X, Zheng X, Huang M, Liu L. A comparative genomic analysis of small-colony variant and wild-type Burkholderia pseudomallei in a patient with bacterial liver abscess. Journal of Global Antimicrobial Resistance. 2020 Jun 1;21:16–21.

170. Rigal A, Doyle SM, Robert S. Live cell imaging of FM4-64, a tool for tracing the endocytic pathways in Arabidopsis root cells. Methods in Molecular Biology. 2015;1242:93–103.

171. Bazaka K, Crawford RJ, Nazarenko EL, Ivanova EP. Bacterial extracellular polysaccharides. Advances in Experimental Medicine and Biology. 2011;715:213–26.

172. Marín-Menéndez A, Montis C, Díaz-Calvo T, Carta D, Hatzixanthis K, Morris CJ, et al. Antimicrobial Nanoplexes meet Model Bacterial Membranes: the key role of Cardiolipin. Scientific Reports. 2017 Dec 25;7(1):41242.

173. CO-AMOXICLAV | Drug | BNF content published by NICE [Internet]. [cited 2021 Dec 31]. Available from: https://bnf.nice.org.uk/drug/co-amoxiclav.html

174. Holden MTG, Seth-Smith HMB, Crossman LC, Sebaihia M, Bentley SD, Cerdeño-Tárraga AM, et al. The genome of Burkholderia cenocepacia J2315, an epidemic pathogen of cystic fibrosis patients. Journal of Bacteriology. 2009 Jan 1;91(1):261–77.

175. Loutet SA, Valvano MA. Extreme Antimicrobial Peptide and Polymyxin B Resistance in the Genus Burkholderia. Frontiers in Microbiology. 2011;2.

176. Peschel A. How do bacteria resist human antimicrobial peptides? Vol. 10, Trends in Microbiology. Elsevier Current Trends; 2002. p. 179–86.

177. Ortega XP, Cardona ST, Brown AR, Loutet SA, Flannagan RS, Campopiano DJ, et al. A putative gene cluster for aminoarabinose biosynthesis is essential for Burkholderia cenocepacia viability. Journal of Bacteriology. 2007 May;189(9):3639–44.

178. Lin TY, Weibel DB. Organization and function of anionic phospholipids in bacteria. Vol. 100, Applied Microbiology and Biotechnology. Springer Verlag; 2016. p. 4255–67.

179. Renner LD, Weibel DB. Cardiolipin microdomains localize to negatively curved regions of Escherichia coli membranes. Proceedings of the National Academy of Sciences of the United States of America. 2011 Apr 12;108(15):6264–9.

180. Kawai F, Shoda M, Harashima R, Sadaie Y, Hara H, Matsumoto K. Cardiolipin Domains in Bacillus subtilis Marburg Membranes. Journal of Bacteriology. 2004 Mar;186(5):1475–83.

181. Pfeiffer K, Gohil V, Stuart RA, Hunte C, Brandt U, Greenberg ML, et al. Cardiolipin Stabilizes Respiratory Chain Supercomplexes. Journal of Biological Chemistry. 2003 Dec 26;278(52):52873–80.

182. Zhang M, Mileykovskaya E, Dowhan W. Gluing the respiratory chain together: Cardiolipin is required for supercomplex formation in the inner mitochondrial membrane. Journal of Biological Chemistry. 2002 Nov 15;277(46):43553–6.

183. Huang KC, Mukhopadhyay R, Wingreen NS. A curvature-mediated mechanism for localization of lipids to bacterial poles. PLoS Computational Biology. 2006 Nov;2(11):1357–64.

184. Reckseidler-Zenteno SL, DeVinney R, Woods DE. The capsular polysaccharide of Burkholderia pseudomallei contributes to survival in serum by reducing complement factor C3b deposition. Infection and immunity. 2005 Feb 1;73(2):1106–15.

185. Egan AM, Gordon DL. Burkholderia pseudomallei activates complement and is ingested but not killed by polymorphonuclear leukocytes. Infection and Immunity. 1996;64(12):4952–9.

186. El-Halfawy OM, Valvano MA. Antimicrobial heteroresistance: An emerging field in need of clarity. Vol. 28, Clinical Microbiology Reviews. American Society for Microbiology; 2015. p. 191–207.

187. Napier BA, Band V, Burd EM, Weiss DS. Colistin heteroresistance in Enterobacter cloacae is associated with cross-resistance to the host antimicrobial lysozyme. Antimicrobial Agents and Chemotherapy. 2014;58(9):5594–7.

188. Wood TK, Knabel SJ, Kwan BW. Bacterial persister cell formation and dormancy. Vol. 79, Applied and Environmental Microbiology. American Society for Microbiology (ASM); 2013. p. 7116–21.

189. Andersson DI, Nicoloff H, Hjort K. Mechanisms and clinical relevance of bacterial heteroresistance. Vol. 17, Nature Reviews Microbiology. Nature Publishing Group; 2019. p. 479–96.

190. Nicoloff H, Hjort K, Levin BR, Andersson DI. The high prevalence of antibiotic heteroresistance in pathogenic bacteria is mainly caused by gene amplification. Nature Microbiology. 2019 Mar 1;4(3):504–14.

191. Low DA, Weyand NJ, Mahan MJ. Roles of DNA Adenine Methylation in Regulating Bacterial Gene Expression and Virulence. Infection and Immunity. 2001;69(12):7197.

192. Haagmans W, van der Woude M. Phase variation of Ag43 in Escherichia coli: Dam-dependent methylation abrogates OxyR binding and OxyR-mediated repression of transcription. Molecular microbiology. 2000;35(4):877–87.

193. Roberts D, Hoopes BC, McClure WR, Kleckner N. IS10 transposition is regulated by DNA adenine methylation. Cell. 1985;43(1):117–30.

194. Stephenson SAM, Brown PD. Epigenetic Influence of Dam Methylation on Gene Expression and Attachment in Uropathogenic Escherichia coli. Frontiers in Public Health. 2016 Jun 27;4:131.

195. Marinus MG. DNA methylation and mutator genes in Escherichia coli K-12. Mutation research. 2010 Oct;705(2):71–6.

196. Vestergaard M, Paulander W, Leng B, Nielsen JB, Westh HT, Ingmer H. Novel pathways for ameliorating the fitness cost of gentamicin resistant small colony variants. Frontiers in Microbiology. 2016 Nov 22;7.

197. Betosludtsev KN, Belosludtseva N v., Tenkov KS, Sharapov VA, Kosareva EA, Dubinin M v. Effect of dequalinium on respiration rates and permeabilization of the inner membrane of rat liver mitochondria. Biologicheskie Membrany. 2017;34(6):101–8.

198. Loh B, Grant C, Hancock REW. Use of the fluorescent probe 1-N-phenylnaphthylamine to study the interactions of aminoglycoside antibiotics with the outer membrane of Pseudomonas aeruginosa. Antimicrobial Agents and Chemotherapy. 1984;26(4):546–51.

199. Davis BD. Mechanism of bactericidal action of aminoglycosides. Vol. 51, Microbiological Reviews. American Society for Microbiology Journals; 1987. p. 341–50.

200. Meylan S, Porter CBM, Yang JH, Belenky P, Gutierrez A, Lobritz MA, et al. Carbon Sources Tune Antibiotic Susceptibility in Pseudomonas aeruginosa via Tricarboxylic Acid Cycle Control. Cell Chemical Biology. 2017 Feb 16;24(2):195–206.

201. Slachmuylders L, Van Acker H, Brackman G, Sass A, Van Nieuwerburgh F, Coenye T. Elucidation of the mechanism behind the potentiating activity of baicalin against Burkholderia cenocepacia biofilms. George AM, editor. PLoS ONE. 2018 Jan 2;13(1):e0190533.

202. Veloira WG, Domenico P, LiPuma JJ, Davis JM, Gurzenda E, Kazzaz JA. In vitro activity and synergy of bismuth thiols and tobramycin against Burkholderia cepacia complex. Journal of Antimicrobial Chemotherapy. 2003 Dec;52(6):915–9.

203. Sox TE, Olson CA. Binding and killing of bacteria by bismuth subsalicylate. Antimicrobial Agents and Chemotherapy. 1989;33(12):2075–82.

204. Jussupow A, Di Luca A, Kaila VRI. How cardiolipin modulates the dynamics of respiratory complex I. Science Advances. 2019 Mar 1;5(3):eaav1850.

205. Wikström M, Hummer G. Stoichiometry of proton translocation by respiratory complex I and its mechanistic implications. Proceedings of the National Academy of Sciences of the United States of America. 2012 Mar 20;109(12):4431–6.

206. Stock D, Gibbons C, Arechaga I, Leslie AGW, Walker JE. The rotary mechanism of ATP synthase. Vol. 10, Current Opinion in Structural Biology. Curr Opin Struct Biol; 2000. p. 672–9.

207. Pedersen PL. Transport ATPases into the year 2008: A brief overview related to types, structures, functions and roles in health and disease. Vol. 39, Journal of Bioenergetics and Biomembranes. J Bioenerg Biomembr; 2007. p. 349–55.

208. Gleckman R, Blagg N, Joubert DW. Trimethoprim: Mechanisms of Action, Antimicrobial Activity, Bacterial Resistance, Pharmacokinetics, Adverse Reactions, and Therapeutic Indications. Pharmacotherapy: The Journal of Human Pharmacology and Drug Therapy. 1981;1(1):14–9.

209. Wegkamp A, Van Oorschot W, De Vos WM, Smid EJ. Characterization of the role of para-aminobenzoic acid biosynthesis in folate production by Lactococcus lactis. Applied and Environmental Microbiology. 2007 Apr;73(8):2673–81.

210. Chevereau G, Bollenbach T. Systematic discovery of drug interaction mechanisms. Molecular Systems Biology. 2015 Apr;11(4):807.

211. Lambden PR, Guest JR. Mutants of Escherichia coli K12 unable to use fumarate as an anaerobic electron acceptor. Journal of General Microbiology. 1976 Dec 1;97(2):145–60.

212. Sevilla E, Bes MT, González A, Peleato ML, Fillat MF. Redox-Based Transcriptional Regulation in Prokaryotes: Revisiting Model Mechanisms. Antioxidants and Redox Signaling. 2019 May 1;30(13):1651–96.

213. Buroni S, Pasca MR, Flannagan RS, Bazzini S, Milano A, Bertani I, et al. Assessment of three Resistance-Nodulation-Cell Division drug efflux transporters of Burkholderia cenocepacia in intrinsic antibiotic resistance. BMC Microbiology. 2009;9:200.

214. Buroni S, Matthijs N, Spadaro F, Van Acker H, Scoffone VC, Pasca MR, et al. Differential roles of rnd efflux pumps in antimicrobial drug resistance of sessile and planktonic burkholderia cenocepacia cells. Antimicrobial Agents and Chemotherapy. 2014 Dec 1;58(12):7424–9.

215. Coenye T, Van Acker H, Peeters E, Sass A, Buroni S, Riccardi G, et al. Molecular mechanisms of chlorhexidine tolerance in Burkholderia cenocepacia biofilms. Antimicrobial Agents and Chemotherapy. 2011 May;55(5):1912–9.

216. Hancock REW. Resistance Mechanisms in Pseudomonas aeruginosa and Other Nonfermentative Gram-Negative Bacteria. Clin Infect Dis. 1998 Aug;27:S93–9.

217. Moore RA, Hancock REW. Involvement of outer membrane of Pseudomonas cepacia in aminoglycoside and polymyxin resistance. Antimicrobial Agents and Chemotherapy. 1986;30(6):923–6.

218. Evans E, Poxton IR, Govan JRW. Lipopolysaccharide chemotypes of Burkholderia cepacia. Journal of Medical Microbiology. 1999 Sep;48(9):825–32.

219. Burtnick MN, Woods DE. Isolation of polymyxin B-susceptible mutants of Burkholderia pseudomallei and molecular characterization of genetic loci involved in polymyxin B resistance. Antimicrobial Agents and Chemotherapy. 1999 Nov;43(11):2648–56.

220. Loutet SA, Flannagan RS, Kooi C, Sokol PA, Valvano MA. A complete lipopolysaccharide inner core oligosaccharide is required for resistance of Burkholderia cenocepacia to antimicrobial peptides and bacterial survival in vivo. Journal of Bacteriology. 2006 Mar;188(6):2073–80.

221. Burtnick MN, Woods DE. Isolation of polymyxin B-susceptible mutants of Burkholderia pseudomallei and molecular characterization of genetic loci involved in polymyxin B resistance. Antimicrobial agents and chemotherapy. 1999 Nov;43(11):2648–56.

222. Gronow S, Noah C, Blumenthal A, Lindner B, Brade H. Construction of a Deep-rough Mutant of Burkholderia cepacia ATCC 25416 and Characterization of Its Chemical and Biological Properties. Glycobiology and Extracellular Matrices. 2003;278(3):1647-1655.

223. Davies D. Understanding biofilm resistance to antibacterial agents. Nature reviews Drug discovery. 2003 Feb;2(2):114–22.

224. Sharma D, Misba L, Khan AU. Antibiotics versus biofilm: an emerging battleground in microbial communities. Antimicrobial Resistance & Infection Control 2019 8:1. 2019 May ;8(1):1–10.

225. Bridier A, Briandet R, Thomas V, Dubois-Brissonnet F. Resistance of bacterial biofilms to disinfectants: a review. Biofouling. 2011 Oct;27(9):1017–32.

226. Bjarnsholt T. The role of bacterial biofilms in chronic infections. APMIS. 2013;121(136):1–58.

227. Limmathurotsakul D, Paeyao A, Wongratanacheewin S, Saiprom N, Takpho N, Thaipadungpanit J, et al. Role of Burkholderia pseudomallei biofilm formation and lipopolysaccharide in relapse of melioidosis. Clinical microbiology and infection : the official publication of the European Society of Clinical Microbiology and Infectious Diseases. 2014 Nov;20(11):O854–6.

228. Chin CY, Hara Y, Ghazali AK, Yap SJ, Kong C, Wong YC, et al. Global transcriptional analysis of Burkholderia pseudomallei high and low biofilm producers reveals insights into biofilm production and virulence. BMC Genomics. 2015 Jun;16(1):1–15.

229. Borlee GI, Plumley BA, Martin KH, Somprasong N, Mangalea MR, Islam MN, et al. Genome-scale analysis of the genes that contribute to Burkholderia pseudomallei biofilm formation identifies a crucial exopolysaccharide biosynthesis gene cluster. PLoS Neglected Tropical Diseases. 2017 Jun;11(6).

230. Pakkulnan R, Anutrakunchai C, Kanthawong S, Taweechaisupapong S, Chareonsudjai P, Chareonsudjai S. Extracellular DNA facilitates bacterial adhesion during Burkholderia pseudomallei biofilm formation. PloS one. 2019 Mar;14(3).

231. Novotny LA, Amer AO, Brockson ME, Goodman SD, Bakaletz LO. Structural Stability of Burkholderia cenocepacia Biofilms Is Reliant on eDNA Structure and Presence of a Bacterial Nucleic Acid Binding Protein. PLOS one. 2013 Jun 14;8(6):e67629.

232. Tseng BS, Majerczyk CD, da Silva DP, Chandler JR, Greenberg EP, Parsek MR. Quorum sensing influences Burkholderia thailandensis biofilm development and matrix production. Journal of Bacteriology. 2016 ;198(19):2643–50.

233. Wilking JN, Zaburdaev V, de Volder M, Losick R, Brenner MP, Weitz DA. Liquid transport facilitated by channels in Bacillus subtilis biofilms. Proceedings of the National Academy of Sciences of the United States of America. 2013 Jan;110(3):848–52.

234. Sawasdidoln C, Taweechaisupapong S, Sermswan RW, Tattawasart U, Tungpradabkul S, Wongratanacheewin S. Growing Burkholderia pseudomallei in Biofilm Stimulating Conditions Significantly Induces Antimicrobial Resistance. PLoS one. 2010 Feb 12;5(2).

235. Ross BN, Micheva-Viteva S, Hong-Geller E, Torres AG. Evaluating the role of Burkholderia pseudomallei K96243 toxins BPSS0390, BPSS0395, and BPSS1584 in persistent infection. Cellular Microbiology. 2019 Dec;21(12):e13096.

236. Nierman WC, Yu Y, Losada L. The In vitro Antibiotic Tolerant Persister Population in Burkholderia pseudomallei is Altered by Environmental Factors. Frontiers in microbiology. 2015;6.

237. Hamad MA, Austin CR, Stewart AL, Higgins M, Vázquez-Torres A, Voskuil MI. Adaptation and Antibiotic Tolerance of Anaerobic Burkholderia pseudomallei. Antimicrobial Agents and Chemotherapy [Internet]. 2011 Jul;55(7):3313.

238. Butt A, Higman VA, Williams C, Crump MP, Hemsley CM, Harmer N, et al. The HicA toxin from Burkholderia pseudomallei has a role in persister cell formation. The Biochemical journal. 2014 Apr 15;459(2):333–44.

239. Pibalpakdee P, Wongratanacheewin S, Taweechaisupapong S, Niumsup PR. Diffusion and activity of antibiotics against Burkholderia pseudomallei biofilms. International journal of antimicrobial agents. 2012 April;39(4):356–9.

240. Messiaen AS, Nelis H, Coenye T. Investigating the role of matrix components in protection of Burkholderia cepacia complex biofilms against tobramycin. Journal of Cystic Fibrosis. 2014 Jan;13(1):56–62.

241. Bylund J, Burgess LA, Cescutti P, Ernst RK, Speert DP. Exopolysaccharides from Burkholderia cenocepacia inhibit neutrophil chemotaxis and scavenge reactive oxygen species. The Journal of biological chemistry. 2006 Feb;281(5):2526–32.

242. Alav I, Sutton JM, Rahman KM. Role of bacterial efflux pumps in biofilm formation. Journal of Antimicrobial Chemotherapy. 2018 Aug;73(8):2003–20.

243. Khan MM, Chattagul S, Tran BQ, Freiberg JA, Nita-Lazar A, Shirtliff ME, et al. Temporal proteomic profiling reveals changes that support Burkholderia biofilms. Pathogens and Disease. 2019 Mar;77(2).

244. Nakao R, Ramstedt M, Wai SN, Uhlin BE. Enhanced biofilm formation by Escherichia coli LPS mutants defective in Hep biosynthesis. PloS one. 2012 Dec 28;7(12).

245. Maldonado RF, Sá-Correia I, Valvano MA. Lipopolysaccharide modification in Gram-negative bacteria during chronic infection. FEMS microbiology reviews. 2016 Jul;40(4):480–93.

246. Campion M, Scully G. Antibiotic Use in the Intensive Care Unit: Optimization and De-Escalation. Journal of Intensive Care Medicine. 2018 Dec 1;33(12):647–55.

247. Gao Y, Wang J, Chai M, Li X, Deng Y, Jin Q, et al. Size and Charge Adaptive Clustered Nanoparticles Targeting the Biofilm Microenvironment for Chronic Lung Infection Management. ACS Nano. 2020 May 26;14(5):5686–99.

248. Li X, Yeh YC, Giri K, Mout R, Landis RF, Prakash YS, et al. Control of nanoparticle penetration into biofilms through surface design. Chemical Communications. 2014 Dec;51(2):282–5.

249. Fulaz S, Devlin H, Vitale S, Quinn L, O'gara JP, Casey E. Tailoring Nanoparticle-Biofilm Interactions to Increase the Efficacy of Antimicrobial Agents Against Staphylococcus aureus . International Journal of Nanomedicine. 2020 Jul;15:4779–91.

250. Anutrakunchai C, Bolscher JGM, Krom BP, Kanthawong S, Chareonsudjai S, Taweechaisupapong S. Impact of nutritional stress on drug susceptibility and biofilm structures of Burkholderia pseudomallei and Burkholderia thailandensis grown in static and microfluidic systems. PloS one. 2018 Mar;13(3):e0194946.

251. Gleckman R, Blagg N, Joubert DW. Trimethoprim: Mechanisms of Action, Antimicrobial Activity, Bacterial Resistance, Pharmacokinetics, Adverse Reactions, and Therapeutic Indications. Pharmacotherapy: The Journal of Human Pharmacology and Drug Therapy. 1981;1(1):14–9.

252. Anutrakunchai C, Bolscher JGM, Krom BP, Kanthawong S, Chareonsudjai S, Taweechaisupapong S. Impact of nutritional stress on drug susceptibility and biofilm structures of Burkholderia pseudomallei and Burkholderia thailandensis grown in static and microfluidic systems. PLOS one. 2018 Mar;13(3):e0194946.

253. Ranieri MR, Whitchurch CB, Burrows LL. Mechanisms of biofilm stimulation by subinhibitory concentrations of antimicrobials. Current opinion in microbiology. 2018 Oct ;45:164–9.

254. Hoffman LR, D'Argenio DA, MacCoss MJ, Zhang Z, Jones RA, Miller SI. Aminoglycoside antibiotics induce bacterial biofilm formation. Nature 2005 436:7054. 2005 Aug 25 ;436(7054):1171–5.

255. Lima-e-Silva AA, Silva-Filho RG, Fernandes HMZ, Saramago CSM, Viana AS, Souza MJ, et al. Sub-Inhibitory Concentrations of Rifampicin Strongly Stimulated Biofilm Production in S. aureus. The Open Microbiology Journal. 2017 Jul;11(1):142.

256. Ranieri MR, Whitchurch CB, Burrows LL. Mechanisms of biofilm stimulation by subinhibitory concentrations of antimicrobials. Current opinion in microbiology. 2018 Oct ;45:164–9.

257. Turnbull L, Toyofuku M, Hynen AL, Kurosawa M, Pessi G, Petty NK, et al. Explosive cell lysis as a mechanism for the biogenesis of bacterial membrane vesicles and biofilms. Nature Communications 2016 7:1. 2016 Apr;7(1):1–13.

258. Oh E, Jeon B. Role of Alkyl Hydroperoxide Reductase (AhpC) in the Biofilm Formation of Campylobacter jejuni. PLoS ONE. 2014 Jan;9(1).

259. Strempel N, Nusser M, Neidig A, Brenner-Weiss G, Overhage J. The oxidative stress agent hypochlorite stimulates c-di-GMP synthesis and biofilm formation in Pseudomonas aeruginosa. Frontiers in Microbiology. 2017 Nov;8:2311.

260. Geier H, Mostowy S, Cangelosi GA, Behr MA, Ford TE. Autoinducer-2 triggers the oxidative stress response in Mycobacterium avium, leading to biofilm formation. Applied and Environmental Microbiology. 2008 Mar.74(6):1798–804.

261. Katharios-Lanwermeyer S, Whitfield GB, Howell PL, O'toole GA. Pseudomonas aeruginosa Uses c-di-GMP Phosphodiesterases RmcA and MorA To Regulate Biofilm Maintenance. mBio. 2021 Jan;12(1):1–19.

262. Pellizzoni E, Ravalico F, Scaini D, Delneri A, Rizzo R, Cescutti P. Biofilms produced by Burkholderia cenocepacia: Influence of media and solid supports on composition of matrix exopolysaccharides. Microbiology. 2016 Feb;162(2):283–94.

263. Narayanaswamy VP, Duncan AP, LiPuma JJ, Wiesmann WP, Baker SM, Townsend SM. In Vitro Activity of a Novel Glycopolymer against Biofilms of Burkholderia cepacia Complex Cystic Fibrosis Clinical Isolates. Antimicrobial agents and chemotherapy. 2019 Jun ;63(6).

264. Kunyanee C, Kamjumphol W, Taweechaisupapong S, Kanthawong S, Wongwajana S, Wongratanacheewin S, et al. Burkholderia pseudomallei Biofilm Promotes Adhesion, Internalization and Stimulates Proinflammatory Cytokines in Human Epithelial A549 Cells. PLoS one. 2016 Aug;11(8):e0160741.

265. Ghanbari A, Dehghany J, Schwebs T, Müsken M, Häussler S, Meyer-Hermann M. Inoculation density and nutrient level determine the formation of mushroom-shaped structures in Pseudomonas aeruginosa biofilms. Scientific Reports 2016 6:1. 2016 Sep 9;6(1):1–12.

266. Tran HM, Tran H, Booth MA, Fox KE, Nguyen TH, Tran N, et al. Nanomaterials for Treating Bacterial Biofilms on Implantable Medical Devices. Nanomaterials. 2020 Nov;10(11):1–19.

267. Forier K, Messiaen AS, Raemdonck K, Nelis H, de Smedt S, Demeester J, et al. Probing the size limit for nanomedicine penetration into Burkholderia multivorans and Pseudomonas aeruginosa biofilms. Journal of controlled release : official journal of the Controlled Release Society. 2014 Dec;195:21–8.

268. Schneider Berlin KR, Ammini C v., Rowe TC. Dequalinium Induces a Selective Depletion of Mitochondrial DNA from HeLa Human Cervical Carcinoma Cells. Experimental Cell Research. 1998 Nov 25;245(1):137–45.

269. Anderson WM, Chambers BB, Wood JM, Benninger L. Inhibitory effects of two structurally related carbocyanine laser dyes on the activity of bovine heart mitochondrial and paracoccus denitrificans nadh-ubiquinone reductase. Evidence for a rotenone-type mechanism. Biochemical Pharmacology. 1991 Mar 1;41(5):677–84.

270. Anderson WM, Wood JM, Anderson AC. Inhibition of mitochondrial and Paracoccus denitrificans NADH-ubiquinone reductase by oxacarbocyanine dyes. A structure-activity study. Biochemical Pharmacology. 1993 Apr 25;45(10):2115–22.

271. Mendling W, Weissenbacher ER, Gerber S, Prasauskas V, Grob P. Use of locally delivered dequalinium chloride in the treatment of vaginal infections: a review. Archives of gynecology and obstetrics. 2016 Mar;293(3):469–84.

272. Podnecky NL, Rhodes KA, Schweizer HP. Efflux pump-mediated drug resistance in burkholderia. Frontiers in Microbiology. 2015;6:1–25.

273. Schurek KN, Marr AK, Taylor PK, Wiegand I, Semenec L, Khaira BK, et al. Novel genetic determinants of low-level aminoglycoside resistance in Pseudomonas aeruginosa. Antimicrobial agents and chemotherapy. 2008 Dec;52(12):4213–9.

274. Price EP, Viberg LT, Kidd TJ, Bell SC, Currie BJ, Sarovich DS. Transcriptomic analysis of longitudinal Burkholderia pseudomallei infecting the cystic fibrosis lung. Microbial genomics [Internet]. 2018 Aug 1 [cited 2021 Dec 31];4(8).

275. Duong LT, Schwarz S, Gross H, Breitbach K, Hochgräfe F, Mostertz J, et al. GvmR - A Novel LysR-Type Transcriptional Regulator Involved in Virulence and Primary and Secondary Metabolism of Burkholderia pseudomallei. Frontiers in microbiology. 2018;9:935.

276. Kovacs-Simon A, Hemsley CM, Scott AE, Prior JL, Titball RW. Burkholderia thailandensis strain E555 is a surrogate for the investigation of Burkholderia pseudomallei replication and survival in macrophages. BMC Microbiology. 2019 May;19(1):1–16.

277. Gierok P, Kohler C, Steinmetz I, Lalk M. Burkholderia pseudomallei Colony Morphotypes Show a Synchronized Metabolic Pattern after Acute Infection. PLOS Neglected Tropical Diseases. 2016 Mar;10(3):e0004483.

278. Luo Q, Dong Y, Chen H, Gao H. Mislocalization of Rieske protein PetA predominantly accounts for the aerobic growth defect of Tat mutants in Shewanella oneidensis. PloS one. 2013 Apr 11;8(4).

279. Dwivedi K, Sen A, Bullerjahn GS. Expression and mutagenesis of the dpsA gene of Synechococcus sp. PCC7942, encoding a DNA-binding protein involved in oxidative stress protection. FEMS Microbiology Letters. 1997 Oct;155(1):85–91.

280. Moore RA, Deshazer D, Reckseidler S, Weissman A, Woods DE. Efflux-Mediated Aminoglycoside and Macrolide Resistance in Burkholderia pseudomallei. Antimicrobial Agents and Chemotherapy. 1999;43(3):465.

281. Chan YY, Tan TMC, Ong YM, Chua KL. BpeAB-OprB, a Multidrug Efflux Pump in Burkholderia pseudomallei. Antimicrobial Agents and Chemotherapy. 2004 Apr;48(4):1128.

282. Kobayashi N, Nishino K, Yamaguchi A. Novel Macrolide-Specific ABC-Type Efflux Transporter in Escherichia coli. Journal of Bacteriology. 2001;183(19):5639.

283. Lu S, Zgurskaya HI. MacA, a Periplasmic Membrane Fusion Protein of the Macrolide Transporter MacAB-TolC, Binds Lipopolysaccharide Core Specifically and with High Affinity. Journal of Bacteriology. 2013;195(21):4865.

284. Vallet-Gely I, Novikov A, Augusto L, Liehl P, Bolbach G, Péchy-Tarr M, et al. Association of Hemolytic Activity of Pseudomonas entomophila, a Versatile Soil Bacterium, with Cyclic Lipopeptide Production. Applied and Environmental Microbiology. 2010 Feb;76(3):910.

285. Cho H, Kang H. The PseEF efflux system is a virulence factor of Pseudomonas syringae pv. syringae. Journal of microbiology. 2012 Feb;50(1):79–90.

286. Klein G, Raina S. Regulated Assembly of LPS, Its Structural Alterations and Cellular Response to LPS Defects. International Journal of Molecular Sciences. 2019 Jan 2;20(2).

287. Moosavian M, Emam N, Pletzer D, Savari M. Rough-type and loss of the LPS due to lpx genes deletions are associated with colistin resistance in multidrug-resistant clinical Escherichia coli isolates not harbouring mcr genes. PLoS one. 2020 May:15(5):e0233518.

288. Boels IC, Beerthuyzen MM, Kosters MHW, van Kaauwen MPW, Kleerebezem M, de Vos WM. Identification and Functional Characterization of the Lactococcus lactis rfb Operon, Required for dTDP-Rhamnose Biosynthesis. Journal of Bacteriology. 2004 Mar;186(5):1239–48.

289. Liu D, Cole RA, Reeves PR. An O-Antigen Processing Function for Wzx (RfbX): a Promising Candidate for O-Unit Flippase. JOURNAL OF BACTERIOLOGY. 1996;178(7):2102–7.

290. Fitzgerald C, Sherwood R, Gheesling LL, Brenner FW, Fields PI. Molecular Analysis of the rfb O Antigen Gene Cluster of Salmonella enterica Serogroup O:6,14 and Development of a Serogroup-Specific PCR Assay. Applied and Environmental Microbiology. 2003 Oct;69(10):6099.

291. vander Broek CW, Stevens JM. Type III Secretion in the Melioidosis Pathogen Burkholderia pseudomallei. Frontiers in cellular and infection microbiology. 2017 Jun 15;7.

292. Chen Y, Schröder I, French CT, Jaroszewicz A, Yee XJ, Teh BE, et al. Characterization and analysis of the Burkholderia pseudomallei BsaN virulence regulon. BMC microbiology. 2014 Aug;14(1).

293. Galán JE, Wolf-Watz H. Protein delivery into eukaryotic cells by type III secretion machines. Nature. 2006;444(7119):567–73.

294. Lorenz C, Büttner D. Functional characterization of the type iii secretion ATPase HrcN from the plant pathogen Xanthomonas campestris pv. vesicatoria. Journal of Bacteriology. 2009 Mar;191(5):1414–28.

295. Burkinshaw BJ, Strynadka NCJ. Assembly and structure of the T3SS. Biochimica et Biophysica Acta (BBA) - Molecular Cell Research. 2014 Aug 1;1843(8):1649–63.

296. Panina EM, Mattoo S, Griffith N, Kozak NA, Yuk MH, Miller JF. A genome-wide screen identifies a Bordetella type III secretion effector and candidate effectors in other species. Molecular microbiology. 2005 Oct;58(1):267–79.

297. Konishi M, Kanbe M, McMurry JL, Aizawa SI. Flagellar formation in C-ring-defective mutants by overproduction of FliI, the ATPase specific for flagellar type III secretion. Journal of Bacteriology. 2009 Oct;191(19):6186–91.

298. Grünenfelder B, Gehrig S, Jena U. Role of the cytoplasmic C terminus of the FliF motor protein in flagellar assembly and rotation. Journal of Bacteriology. 2003 Mar;185(5):1624–33.

299. Schoenhals GJ, Macnab RM. Physiological and biochemical analyses of FlgH, a lipoprotein forming the outer membrane L ring of the flagellar basal body of Salmonella typhimurium. Journal of Bacteriology. 1996;178(14):4200–7.

300. Auvray F, Thomas J, Fraser GM, Hughes C. Flagellin polymerisation control by a cytosolic export chaperone. Journal of Molecular Biology. 2001 Apr 27;308(2):221–9.

301. Samatey FA, Matsunami H, Imada K, Nagashima S, Shaikh TR, Thomas DR, et al. Structure of the bacterial flagellar hook and implication for the molecular universal joint mechanism. Nature 2004 431:7012. 2004 Oct 28;431(7012):1062–8.

302. Blair DF. Flagellar movement driven by proton translocation. FEBS Letters. 2003 Jun 12;545(1):86–95.

303. Paul K, Nieto V, Carlquist WC, Blair DF, Harshey RM. The c-di-GMP Binding Protein YcgR Controls Flagellar Motor Direction and Speed to Affect Chemotaxis by a "Backstop Brake" Mechanism. Molecular Cell. 2010 Apr 9;38(1):128–39.

304. Al-Maleki AR, Mariappan V, Vellasamy KM, Tay ST, Vadivelu J. Altered Proteome of Burkholderia pseudomallei Colony Variants Induced by Exposure to Human Lung Epithelial Cells. PLoS one. 2015 May 21;10(5):e0127398.

305. Li A, Mao D, Yoshimura A, Rosen PC, Martin WL, Gallant É, et al. Multi-omic analyses provide links between low-dose antibiotic treatment and induction of secondary metabolism in Burkholderia thailandensis. mBio. 2020 Jan 1;11(1).

306. perseus:user:use_cases:interactions [Perseus documentation] [Internet]. Available from: http://www.coxdocs.org/doku.php?id=perseus:user:use_cases:interactions

307. Hoerr V, Duggan GE, Zbytnuik L, Poon KKH, Große C, Neugebauer U, et al. Characterization and prediction of the mechanism of action of antibiotics through NMR metabolomics. BMC Microbiology. 2016 May 10;16(1):1–14.

308. Rizwan M, Rasheed H al, Tarjan G. Succinate Dehydrogenase Complex: An Updated Review. Archives of pathology & laboratory medicine [Internet]. 2018 Dec;142(12):1564–70.

309. Cramer WA, Hasan SS, Yamashita E. The Q cycle of cytochrome bc complexes: a structure perspective. Biochimica et biophysica acta [Internet]. 2011 Jul;1807(7):788–802.

310. Wikström M, Krab K, Sharma V. Oxygen Activation and Energy Conservation by Cytochrome c Oxidase. Chemical Reviews. 2018 Mar 14;118(5):2469–90.

311. Yoshikawa S, Shimada A. Reaction Mechanism of Cytochrome c Oxidase. Chemical Reviews. 2015 Feb;115(4):1936–89.

312. Nath S. The molecular mechanism of ATP synthesis by F1F0-ATP synthase: a scrutiny of the major possibilities. Advances in biochemical engineering/biotechnology. 2002;74:65–98.

313. Hong S, Pedersen PL. ATP Synthase and the Actions of Inhibitors Utilized To Study Its Roles in Human Health, Disease, and Other Scientific Areas. Microbiology and Molecular Biology Reviews. 2008 Dec;72(4):590–641.

314. Su Y bin, Peng B, Li H, Cheng Z xue, Zhang T tuo, Zhu J xin, et al. Pyruvate cycle increases aminoglycoside efficacy and provides respiratory energy in bacteria. Proceedings of the National Academy of Sciences of the United States of America. 2018 Feb;115(7):E1578–87.

315. Cronan, Jr. JE, Laporte D. Tricarboxylic Acid Cycle and Glyoxylate Bypass. EcoSal Plus. 2005 May;1(2).

316. Guerrieri F, Lorusso M, Pansini A, Ferrarese V, Papa S. On the mechanism of action of oligomycin and acidic uncouplers on proton translocation and energy transfer in “sonic” submitochondrial particles. Journal of bioenergetics and biomembranes. 1976 Jun;8(3):131–42.

317. Bae Y, Jung MK, Lee S, Song SJ, Mun JY, Green ES, et al. Dequalinium-based functional nanosomes show increased mitochondria targeting and anticancer effect. European Journal of Pharmaceutics and Biopharmaceutics. 2018 Mar 1;124:104–15.

318. Panta PR, Kumar S, Stafford CF, Billiot CE, Douglass M v., Herrera CM, et al. A DedA Family Membrane Protein Is Required for Burkholderia thailandensis Colistin Resistance. Frontiers in Microbiology. 2019 Nov 5;10.

319. Carpena X, Loprasert S, Mongkolsuk S, Switala J, Loewen PC, Fita I. Catalase-peroxidase KatG of Burkholderia pseudomallei at 1.7 Å resolution. Journal of Molecular Biology. 2003 Mar 21;327(2):475–89.

320. Almiron M, Link AJ, Furlong D, Kolter R. A novel DNA-binding protein with regulatory and protective roles in starved Escherichia coli. Genes & development. 1992;6(12B):2646–54.

321. Dwivedi K, Sen A, Bullerjahn GS. Expression and mutagenesis of the dpsA gene of Synechococcus sp. PCC7942, encoding a DNA-binding protein involved in oxidative stress protection. FEMS Microbiology Letters. 1997 Oct;155(1):85–91.

322. Si M, Zhao C, Burkinshaw B, Zhang B, Wei D, Wang Y, et al. Manganese scavenging and oxidative stress response mediated by type VI secretion system in Burkholderia thailandensis. Proceedings of the National Academy of Sciences of the United States of America. 2017 Mar;114(11):E2233–42.

323. Si M, Wang Y, Zhang B, Zhao C, Kang Y, Bai H, et al. The Type VI Secretion System Engages a Redox-Regulated Dual-Functional Heme Transporter for Zinc Acquisition. Cell Reports. 2017 Jul 25;20(4):949–59.

324. Losada L, Shea AA, DeShazer D. A MarR family transcriptional regulator and subinhibitory antibiotics regulate type VI secretion gene clusters in Burkholderia pseudomallei. Microbiology. 2018 Sep;164(9):1196.

325. Wagley S, Hemsley C, Thomas R, Moule MG, Vanaporn M, Andreae C, et al. The Twin Arginine Translocation System Is Essential for Aerobic Growth and Full Virulence of Burkholderia thailandensis. Journal of Bacteriology. 2014 Jan;196(2):407.

326. Polissi A, Sperandeo P. The Lipopolysaccharide Export Pathway in Escherichia coli: Structure, Organization and Regulated Assembly of the Lpt Machinery. Marine Drugs. 2014;12(2):1023.

327. Okuda S, Sherman DJ, Silhavy TJ, Ruiz N, Kahne D. Lipopolysaccharide transport and assembly at the outer membrane: the PEZ model. Nature reviews Microbiology. 2016 Jun 1;14(6):337–45.

328. Moosavian M, Emam N, Pletzer D, Savari M. Rough-type and loss of the LPS due to lpx genes deletions are associated with colistin resistance in multidrug-resistant clinical Escherichia coli isolates not harbouring mcr genes. PLoS one. 2020 May 1;15(5):e0233518.

329. Moffatt JH, Harper M, Adler B, Nation RL, Li J, Boyce JD. Insertion sequence ISAba11 is involved in colistin resistance and loss of lipopolysaccharide in Acinetobacter baumannii. Antimicrobial Agents and Chemotherapy. 2011 Jun;55(6):3022–4.

330. Jiao Y, Xia Z, Zhou X, Guo Y, Guo R, Kang X, et al. Signature-tagged mutagenesis screening revealed the role of lipopolysaccharide biosynthesis gene rfbH in smooth-to-rough transition in Salmonella Enteritidis. Microbiological Research. 2018 Jul 1;212–213:75–9.

331. Heinrichs DE, Monteiro MA, Perry MB, Whitfield C. The Assembly System for the Lipopolysaccharide R2 Core-type ofEscherichia coli Is a Hybrid of Those Found inEscherichia coli K-12 and Salmonella enterica: STRUCTURE AND FUNCTION OF THE R2 WaaK AND WaaL HOMOLOGS. Journal of Biological Chemistry. 1998 Apr 10;273(15):8849–59.

332. Scharf BE, Fahrner KA, Turner L, Berg HC. Control of direction of flagellar rotation in bacterial chemotaxis. Proceedings of the National Academy of Sciences. 1998 Jan ;95(1):201–6.

333. Vartanian AS, Pazs A, Fortgang EA, Abramsons J, Dahlquist FW. Structure of Flagellar Motor Proteins in Complex Allows for Insights into Motor Structure and Switching. Journal of Biological Chemistry. 2012 Oct 19;287(43):35779–83.

334. Chua KL, Chan YY, Gan YH. Flagella are virulence determinants of Burkholderia pseudomallei. Infection and immunity. 2003 Apr;71(4):1622–9.

335. Lipsitz R, Garges S, Aurigemma R, Baccam P, Blaney DD, Cheng AC, et al. Workshop on treatment of and postexposure prophylaxis for Burkholderia pseudomallei and B. mallei Infection, 2010. Emerging infectious diseases. 2012 Dec;18(12):e2.

336. Hibbitts A, Lucía A, Serrano-Sevilla I, de Matteis L, McArthur M, de La Fuente JM, et al. Co-delivery of free vancomycin and transcription factor decoy-nanostructured lipid carriers can enhance inhibition of methicillin resistant Staphylococcus aureus (MRSA). PloS one. 2019 Sep;14(9).

337. Rhodes KA, Somprasong N, Podnecky NL, Mima T, Chirakul S, Schweizer HP. Molecular determinants of Burkholderia pseudomallei BpeEF-OprC efflux pump expression. Microbiology (United Kingdom). 2018 Sep 1;164(9):1156–67.

338. Romero-Steiner S, Parales RE, Harwood CS, Houghton JE. Characterization of the pcaR regulatory gene from Pseudomonas putida, which is required for the complete degradation of p-hydroxybenzoate. Journal of Bacteriology. 1994;176(18):5771–9.

339. Harwood CS, Nichols NN, Kim MK, Ditty JL, Parales RE. Identification of the pcaRKF gene cluster from Pseudomonas putida: Involvement in chemotaxis, biodegradation, and transport of 4-hydroxybenzoate. Journal of Bacteriology. 1994;176(21):6479–88.

340. Gui L, Sunnarborg A, Pan B, Laporte DC. Autoregulation of iclR, the gene encoding the repressor of the glyoxylate bypass operon. Journal of Bacteriology. 1996;178(1):321–4.

341. Jo M, Noh MH, Lim HG, Kang CW, Im DK, Oh MK, et al. Precise tuning of the glyoxylate cycle in Escherichia coli for efficient tyrosine production from acetate. Microbial Cell Factories. 2019 Dec 19;18(1):57.

342. Taylor BL, Zhulin IB. PAS domains: internal sensors of oxygen, redox potential, and light. Microbiology and molecular biology reviews : MMBR. 1999 Jun 63(2):479–506.

343. Liang X, Thorpe C, Schulz H. 2,4-Dienoyl-CoA reductase from Escherichia coli is a novel iron-sulfur flavoprotein that functions in fatty acid beta-oxidation. Archives of biochemistry and biophysics. 2000 Aug;380(2):373–9.

344. Mari´ M, Gallegos M-T, Schleif † Robert, Bairoch A, Hofmann K, Ramos JL. Arac/XylS family of transcriptional regulators. Microbiology and Molecular Biology Reviews. 1997 Dec ;61(4):393.

345. Narberhaus F, Balsiger S. Structure-Function Studies of Escherichia coli RpoH (σ32) by In Vitro Linker Insertion Mutagenesis. Journal of Bacteriology. 2003 May;185(9):2731.

346. Vanaporn M, Vattanaviboon P, Thongboonkerd V, Korbsrisate S. The rpoE operon regulates heat stress response in Burkholderia pseudomallei. FEMS microbiology letters. 2008 Jul;284(2):191–6.

347. Hamad MA, Austin CR, Stewart AL, Higgins M, Vázquez-Torres A, Voskuil MI. Adaptation and antibiotic tolerance of anaerobic Burkholderia pseudomallei. Antimicrobial agents and chemotherapy. 2011 Jul;55(7):3313–23.

348. Jangiam W, Loprasert S, Smith DR, Tungpradabkul S. Burkholderia pseudomallei RpoS regulates OxyR and the katG-dpsA operon under conditions of oxidative stress. Microbiology and Immunology. 2010 Jul;54(7):389–97.

349. Menard A, de los Santos P, Graindorge A, Cournoyer B. Architecture of Burkholderia cepacia complex σ70 gene family: evidence of alternative primary and clade-specific factors, and genomic instability. BMC Genomics. 2007 Sep;8:308.

350. Fuchs TM, Deppisch H, Scarlato V, Gross R. A new gene locus of Bordetella pertussis defines a novel family of prokaryotic transcriptional accessory proteins. Journal of bacteriology. 1996;178(15):4445–52.

351. Johnson SJ, Close D, Robinson H, Vallet-Gely I, Dove SL, Hill CP. Crystal structure and RNA binding of the Tex protein from Pseudomonas aeruginosa. Journal of molecular biology. 2008 Apr;377(5):1460–73.

352. He X, Thornton J, Carmicle-Davis S, McDaniel LS. Tex, a putative transcriptional accessory factor, is involved in pathogen fitness in Streptococcus pneumoniae. Microbial pathogenesis. 2006 Dec;41(6):199–206.

353. Potvin E, Lehoux DE, Kukavica-Ibrulj I, Richard KL, Sanschagrin F, Lau GW, et al. In vivo functional genomics of Pseudomonas aeruginosa for high-throughput screening of new virulence factors and antibacterial targets. Environmental microbiology. 2003 Dec :5(12):1294–308.

354. Moule MG, Spink N, Willcocks S, Lim J, Guerra-Assunção JA, Cia F, et al. Characterization of New Virulence Factors Involved in the Intracellular Growth and Survival of Burkholderia pseudomallei. Infection and Immunity. 2016 Mar;84(3):701.

355. Ponting CP. Novel domains and orthologues of eukaryotic transcription elongation factors. Nucleic acids research. 2002 Sep;30(17):3643–52.

356. Scott C, Partridge JD, Stephenson JR, Green J. DNA target sequence and FNR-dependent gene expression. FEBS letters. 2003 Apr;541(1–3):97–101.

357. Volbeda A, Darnault C, Renoux O, Nicolet Y, Fontecilla-Camps JC. The crystal structure of the global anaerobic transcriptional regulator FNR explains its extremely fine-tuned monomer-dimer equilibrium. Science Advances. 2015 Dec;1(11):e1501086.

358. Barbieri NL, Nicholson B, Hussein A, Cai W, Wannemuehler YM, Dell'Anna G, et al. FNR regulates expression of important virulence factors contributing to pathogenicity of uropathogenic Escherichia coli. Infection and Immunity. 2014 Dec;82(12):5086–98.

359. Fazli M, O'Connell A, Nilsson M, Niehaus K, Dow JM, Givskov M, et al. The CRP/FNR family protein Bcam1349 is a c-di-GMP effector that regulates biofilm formation in the respiratory pathogen Burkholderia cenocepacia. Molecular Microbiology. 2011 Oct;82(2):327–41.

360. Constantinidou C, Hobman JL, Griffiths L, Patel MD, Penn CW, Cole JA, et al. A reassessment of the FNR regulon and transcriptomic analysis of the effects of nitrate, nitrite, NarXL, and NarQP as Escherichia coli K12 adapts from aerobic to anaerobic growth. Journal of Biological Chemistry. 2006 Feb;281(8):4802–15.

361. Myers KS, Yan H, Ong IM, Chung D, Liang K, Tran F, et al. Genome-scale Analysis of Escherichia coli FNR Reveals Complex Features of Transcription Factor Binding. PLOS Genetics. 2013 Jun;9(6):e1003565.

362. Mikhaylina A, Ksibe AZ, Scanlan DJ, Blindauer CA. Bacterial zinc uptake regulator proteins and their regulons. Biochemical Society Transactions. 2018 Jul;46(4):983.

363. Mortensen BL, Rathi S, Chazin WJ, Skaar EP. Acinetobacter baumannii response to host-mediated zinc limitation requires the transcriptional regulator Zur. Journal of bacteriology. 2014;196(14):2616–26.

364. Campoy S, Jara M, Busquets N, Pérez De Rozas AM, Badiola I, Barbé J. Role of the high-affinity zinc uptake znuABC system in Salmonella enterica serovar typhimurium virulence. Infection and immunity. 2002;70(8):4721–5.

365. DeShazer D. A novel contact-independent T6SS that maintains redox homeostasis via Zn2+ and Mn2+ acquisition is conserved in the Burkholderia pseudomallei complex. Microbiological Research. 2019 Sep 1;226:48–54.

366. Sarovich DS, Webb JR, Pitman MC, Viberg LT, Mayo M, Baird RW, et al. Raising the Stakes: Loss of Efflux Pump Regulation Decreases Meropenem Susceptibility in Burkholderia pseudomallei. Clinical infectious diseases : an official publication of the Infectious Diseases Society of America [Internet]. 2018 Jul; 67(2):243–50

367. Schweizer HP. When it comes to drug discovery not all Gram-negative bacterial biodefence pathogens are created equal: Burkholderia pseudomallei is different. Microbial biotechnology [Internet]. 2012 Sep [cited 2021 Dec 31];5(5):581–3.

368. Webb JR, Price EP, Currie BJ, Sarovich DS. Loss of Methyltransferase Function and Increased Efflux Activity Leads to Doxycycline Resistance in Burkholderia pseudomallei. Antimicrobial agents and chemotherapy. 2017 Jun;61(6).

369. Podnecky NL, Rhodes KA, Mima T, Drew HR, Chirakul S, Wuthiekanun V, et al. Mechanisms of resistance to folate pathway inhibitors in Burkholderia pseudomallei: Deviation from the norm. mBio. 2017 Sep 1;8(5).

370. Paixão L, Rodrigues L, Couto I, Martins M, Fernandes P, de Carvalho CCCR, et al. Fluorometric determination of ethidium bromide efflux kinetics in Escherichia coli. Journal of biological engineering. 2009 Oct 16;3.

371. Lorca GL, Ezersky A, Lunin V v., Walker JR, Altamentova S, Evdokimova E, et al. Glyoxylate and Pyruvate Are Antagonistic Effectors of the Escherichia coli IclR Transcriptional Regulator. Journal of Biological Chemistry. 2007 Jun 1;282(22):16476–91.

372. Bibikov SI, Barnes LA, Gitin Y, Parkinson JS. Domain organization and flavin adenine dinucleotide-binding determinants in the aerotaxis signal transducer Aer of Escherichia coli. Proceedings of the National Academy of Sciences of the United States of America. 2000 May 23;97(11):5830–5.

373. Bibikov SI, Biran R, Rudd KE, Parkinson JS. A signal transducer for aerotaxis in Escherichia coli. Journal of Bacteriology. 1997;179(12):4075–9.

374. Lazar Adler NR, Allwood EM, Lucas DD, Harrison P, Watts S, Dimitropoulos A, et al. Perturbation of the two-component signal transduction system, BprRS, results in attenuated virulence and motility defects in Burkholderia pseudomallei. BMC Genomics. 2016;17(1).

375. Wösten MMSM. Eubacterial sigma-factors. FEMS microbiology review. 1998 Sept;22(3):127–50.

376. Jishage M, Iwata A, Ueda S, Ishihama A. Regulation of RNA polymerase sigma subunit synthesis in Escherichia coli: intracellular levels of four species of sigma subunit under various growth conditions. Journal of bacteriology. 1996;178(18):5447–51.

377. Shimada T, Yamazaki Y, Tanaka K, Ishihama A. The Whole Set of Constitutive Promoters Recognized by RNA Polymerase RpoD Holoenzyme of Escherichia coli. PLoS one. 2014 Mar 6 ;9(3):e90447.

378. Hu JC, Gross CA. Mutations in rpoD that increase expression of genes in the mal regulon of Escherichia coli K-12. Journal of molecular biology. 1988 Sep;203(1):15–27.

379. Schulz S, Eckweiler D, Bielecka A, Nicolai T, Franke R, Dötsch A, et al. Elucidation of Sigma Factor-Associated Networks in Pseudomonas aeruginosa Reveals a Modular Architecture with Limited and Function-Specific Crosstalk. PLOS Pathogens. 2015 Mar ;11(3):e1004744.

380. Versalovic J, Koeuth T, Britton R, Geszvain K, Lupski JR. Conservation and evolution of the rpsU-dnaG-rpoD macromolecular synthesis operon in bacteria. Molecular Microbiology. 1993 Apr;8(2):343–55.

381. Hu JC, Gross CA. Mutations in rpoD that increase expression of genes in the mal regulon of Escherichia coli K-12. Journal of molecular biology. 1988 Sep;203(1):15–27.

382. Obrist M, Langklotz S, Milek S, Führer F, Narberhaus F. Region C of the Escherichia coli heat shock sigma factor RpoH (σ32) contains a turnover element for proteolysis by the FtsH protease. FEMS Microbiology Letters. 2009 Jan;290(2):199–208.

383. Kanemori M, Nishihara K, Yanagi H, Yura T. Synergistic roles of HslVU and other ATP-dependent proteases in controlling in vivo turnover of sigma32 and abnormal proteins in Escherichia coli. Journal of bacteriology. 1997;179(23):7219–25.

384. Vanaporn M, Vattanaviboon P, Thongboonkerd V, Korbsrisate S. The rpoE operon regulates heat stress response in Burkholderia pseudomallei. FEMS microbiology letters [Internet]. 2008 Jul;284(2):191–6.

385. Korbsrisate S, Vanaporn M, Kerdsuk P, Kespichayawattana W, Vattanaviboon P, Kiatpapan P, et al. The Burkholderia pseudomallei RpoE (AlgU) operon is involved in environmental stress tolerance and biofilm formation. undefined. 2005 Nov 15;252(2):243–9.

386. Sein-Echaluce VC, González A, Napolitano M, Luque I, Barja F, Peleato ML, et al. Zur (FurB) is a key factor in the control of the oxidative stress response in Anabaena sp. PCC 7120. Environmental microbiology. 2015 Jun;17(6):2006–17.

387. Mazzon RR, Braz VS, da Silva Neto JF, do Valle Marques M. Analysis of the Caulobacter crescentus Zur regulon reveals novel insights in zinc acquisition by TonB-dependent outer membrane proteins. BMC Genomics. 2014 Aug 28;15(1):1–14.

388. Trageser M, Unden G. Role of cysteine residues and of metal ions in the regulatory functioning of FNR, the transcriptional regulator of anaerobic respiration in Escherichia coli. Molecular microbiology. 1989;3(5):593–9.

389. Fazli M, Mccarthy Y, Givskov M, Ryan RP, Tolker-Nielsen T. The exopolysaccharide gene cluster Bcam1330-Bcam1341 is involved in Burkholderia cenocepacia biofilm formation, and its expression is regulated by c-di-GMP and Bcam1349. MicrobiologyOpen. 2013 Feb;2(1):105–22.

390. Münch R, Hiller K, Barg H, Heldt D, Linz S, Wingender E, et al. PRODORIC: Prokaryotic database of gene regulation. Vol. 31, Nucleic Acids Research. Oxford University Press; 2003. p. 266–9.

391. Bayliss M, Donaldson MI, Nepogodiev SA, Pergolizzi G, Scott AE, Harmer NJ, et al. Structural characterisation of the capsular polysaccharide expressed by Burkholderia thailandensis strain E555:: wbiI (pKnock-KmR) and assessment of the significance of the 2-O-acetyl group in immune protection. Carbohydrate Research. 2017 Nov;452:17–24.

392. Gurevich I, Zhang C, Aneskievich BJ. Scanning for transcription factor binding by a variant EMSA. Methods in molecular biology. 2010;585:147–58.

393. Fraimow HS, Greenman JB, Leviton IM, Dougherty TJ, Miller MH. Tobramycin uptake in Escherichia coli is driven by either electrical potential or ATP. Journal of Bacteriology. 1991;173(9):2800–8.

394. Maiden MM, Waters CM. Triclosan depletes the membrane potential in Pseudomonas aeruginosa biofilms inhibiting aminoglycoside induced adaptive resistance. PLOS Pathogens. 2020 Oct;16(10):e1008529.

395. Hellman LM, Fried MG. Electrophoretic mobility shift assay (EMSA) for detecting protein–nucleic acid interactions. Nature Protocols 2007;2(8):1849–61.

396. Maunders E, Welch M. Matrix exopolysaccharides; the sticky side of biofilm formation. FEMS microbiology letters. 2017 Jul 6;364(13).

397. Morales-Ruíz L, Rodríguez-Cisneros M, Kerber-Díaz J, Rojas-Rojas F, Ibarra J, Estrada-de los Santos P. Burkholderia orbicola sp. nov., a novel species within the Burkholderia cepacia complex. Archives of Microbiology. 2022;204(3).

398. Ong K, Aw Y, Lee L, Yule C, Cheow Y, Lee S. Burkholderia paludis sp. nov., an Antibiotic-Siderophore Producing Novel Burkholderia cepacia Complex Species, Isolated from Malaysian Tropical Peat Swamp Soil. Frontiers in Microbiology. 2016;7.

399. Esmaeel Q, Issa A, Sanchez L, Clément C, Jacquard C, Barka E. Draft Genome Sequence of Burkholderia reimsis BE51, a Plant-Associated Bacterium Isolated from Agricultural Rhizosphere. Microbiology Resource Announcements. 2018;7(13).

400. Moradali M, Ghods S, Rehm B. Pseudomonas aeruginosa Lifestyle: A Paradigm for Adaptation, Survival, and Persistence. Frontiers in Cellular and Infection Microbiology. 2017;7.

401. Lima J, Alves L, Paz J, Rabelo M, Maciel M, Morais M. Analysis of biofilm production by clinical isolates of Pseudomonas aeruginosa from patients with ventilator-associated pneumonia. Revista Brasileira de Terapia Intensiva. 2017;29(3).

402. Lima J, Alves L, Jacomé P, Bezerra Neto J, Maciel M, Morais M. Biofilm production by clinical isolates of Pseudomonas aeruginosa and structural changes in LasR protein of isolates non biofilm-producing. The Brazilian Journal of Infectious Diseases. 2018;22(2):129-136.

403. Cysticfibrosis.ca. 2022 [cited 2 September 2022]. Available from: https://www.cysticfibrosis.ca/uploads/RegistryReport2018/2018RegistryAnnualDataReport.pdf

404. Hatziagorou E, Orenti A, Drevinek P, Kashirskaya N, Mei-Zahav M, De Boeck K et al. Changing epidemiology of the respiratory bacteriology of patients with cystic fibrosis–data from the European cystic fibrosis society patient registry. Journal of Cystic Fibrosis. 2020;19(3):376-383.

405. Graff G, Burns J. Factors Affecting the Incidence of Stenotrophomonas maltophilia Isolation in Cystic Fibrosis. Chest. 2002;121(6):1754-1760.

406. Marchac V, Equi A, Le Bihan-Benjamin C, Hodson M, Bush A. Case-control study of Stenotrophomonas maltophilia acquisition in cystic fibrosis patients. European Respiratory Journal. 2004;23(1):98-102.

407. Talmaciu I, Varlotta L, Mortensen J, Schidlow D. Risk factors for emergence ofStenotrophomonas maltophilia in cystic fibrosis. Pediatric Pulmonology. 2000;30(1):10-15.

408. Denton M, Todd N, Kerr K, Hawkey P, Littlewood J. Molecular Epidemiology of Stenotrophomonas maltophilia Isolated from Clinical Specimens from Patients with Cystic Fibrosis and Associated Environmental Samples. Journal of Clinical Microbiology. 1998;36(7):1953-1958.

409. Skolnik K, Kirkpatrick G, Quon B. Nontuberculous Mycobacteria in Cystic Fibrosis. Current Treatment Options in Infectious Diseases. 2016;8(4):259-274.

410. 14. Viviani L, Harrison M, Zolin A, Haworth C, Floto R. Epidemiology of nontuberculous mycobacteria (NTM) amongst individuals with cystic fibrosis (CF). Journal of Cystic Fibrosis. 2016;15(5):619-623.

411. 15. Martiniano S, Nick J, Daley C. Nontuberculous Mycobacterial Infections in Cystic Fibrosis. Thoracic Surgery Clinics. 2019;29(1):95-108.

412. van Dorn A. Multidrug-resistant Mycobacterium abscessus threatens patients with cystic fibrosis. The Lancet Respiratory Medicine. 2017;5(1):15.

413. Floto R, Olivier K, Saiman L, Daley C, Herrmann J, Nick J et al. US Cystic Fibrosis Foundation and European Cystic Fibrosis Society consensus recommendations for the management of non-tuberculous mycobacteria in individuals with cystic fibrosis. Thorax. 2015;71(Suppl 1):i1-i22.

414. Lambiase A, Catania M, del Pezzo M, Rossano F, Terlizzi V, Sepe A et al. Achromobacter xylosoxidans respiratory tract infection in cystic fibrosis patients. European Journal of Clinical Microbiology & Infectious Diseases. 2011;30(8):973-980.

415. Ridderberg W, Bendstrup K, Olesen H, Jensen-Fangel S, Nørskov-Lauritsen N. Marked increase in incidence of Achromobacter xylosoxidans infections caused by sporadic acquisition from the environment. Journal of Cystic Fibrosis. 2011;10(6):466-469.

416. Amoureux L, Bador J, Siebor E, Taillefumier N, Fanton A, Neuwirth C. Epidemiology and resistance of Achromobacter xylosoxidans from cystic fibrosis patients in Dijon, Burgundy: First French data. Journal of Cystic Fibrosis. 2013;12(2):170-176.

417. Rønne Hansen C, Pressler T, Høiby N, Gormsen M. Chronic infection with Achromobacter xylosoxidans in cystic fibrosis patients; a retrospective case control study. Journal of Cystic Fibrosis. 2006;5(4):245-251.

418. Edwards B, Greysson-Wong J, Somayaji R, Waddell B, Whelan F, Storey D et al. Prevalence and Outcomes of Achromobacter Species Infections in Adults with Cystic Fibrosis: a North American Cohort Study. Journal of Clinical Microbiology. 2017;55(7):2074-2085.

419. Stevens J, Ulrich R, Taylor L, Wood M, DeShazer D, Stevens M et al. Actin-Binding Proteins from Burkholderia mallei and Burkholderia thailandensis Can Functionally Compensate for the Actin-Based Motility Defect of a Burkholderia pseudomallei bimA Mutant. Journal of Bacteriology. 2005;187(22):7857-7862.

420. Srinon V, Chaiwattanarungruengpaisan S, Korbsrisate S, Stevens J. Burkholderia pseudomallei BimC Is Required for Actin-Based Motility, Intracellular Survival, and Virulence. Frontiers in Cellular and Infection Microbiology. 2019;9.

421. Allwood E, Devenish R, Prescott M, Adler B, Boyce J. Strategies for Intracellular Survival of Burkholderia pseudomallei. Frontiers in Microbiology. 2011;2.

422. Holden M, Titball R, Peacock S, Cerdeño-Tárraga A, Atkins T, Crossman L et al. Genomic plasticity of the causative agent of melioidosis, Burkholderia pseudomallei. Proceedings of the National Academy of Sciences. 2004;101(39):14240-14245.

423. Agnoli K, Frauenknecht C, Freitag R, Schwager S, Jenul C, Vergunst A et al. The Third Replicon of Members of the Burkholderia cepacia Complex, Plasmid pC3, Plays a Role in Stress Tolerance. Applied and Environmental Microbiology. 2014;80(4):1340-1348.

424. Agnoli K, Schwager S, Uehlinger S, Vergunst A, Viteri D, Nguyen D et al. Exposing the third chromosome of Burkholderia cepacia complex strains as a virulence plasmid. Molecular Microbiology. 2011;83(2):362-378.

425. Sim S, Yu Y, Lin C, Karuturi R, Wuthiekanun V, Tuanyok A et al. The Core and Accessory Genomes of Burkholderia pseudomallei: Implications for Human Melioidosis. PLoS Pathogens. 2008;4(10):e1000178.

426. Spring-Pearson S, Stone J, Doyle A, Allender C, Okinaka R, Mayo M et al. Pangenome Analysis of Burkholderia pseudomallei: Genome Evolution Preserves Gene Order despite High Recombination Rates. PLOS ONE. 2015;10(10):e0140274.

427. Yu Y, Kim H, Chua H, Lin C, Sim S, Lin D et al. Genomic patterns of pathogen evolution revealed by comparison of Burkholderia pseudomallei, the causative agent of melioidosis, to avirulent Burkholderia thailandensis. BMC Microbiology. 2006;6(1).

428. Tuanyok A, Leadem B, Auerbach R, Beckstrom-Sternberg S, Beckstrom-Sternberg J, Mayo M et al. Genomic islands from five strains of Burkholderia pseudomallei. BMC Genomics. 2008;9(1).

429. Reckseidler-Zenteno S, DeVinney R, Woods D. The Capsular Polysaccharide of Burkholderia pseudomallei Contributes to Survival in Serum by Reducing Complement Factor C3b Deposition. Infection and Immunity. 2005;73(2):1106-1115.

430. Hall C, Baker A, Sahl J, Mayo M, Scholz H, Kaestli M et al. Expanding the Burkholderia pseudomallei Complex with the Addition of Two Novel Species: Burkholderia mayonis sp. nov. and Burkholderia savannae sp. nov. Applied and Environmental Microbiology. 2022;88(1).

431. Brett P, DeShazer D, Woods D. Characterization of Burkholderia pseudomallei and Burkholderia pseudomallei-like strains. Epidemiology and Infection. 1997;118(2):137-148.

432. DeShazer D. Virulence of clinical and environmental isolates ofBurkholderia oklahomensisandBurkholderia thailandensisin hamsters and mice. FEMS Microbiology Letters. 2007;277(1):64-69.

433. Chang K, Luo J, Xu H, Li M, Zhang F, Li J et al. Human Infection with Burkholderia thailandensis, China, 2013. Emerging Infectious Diseases. 2017;23(8):1416-1418.

434. Gee J, Elrod M, Gulvik C, Haselow D, Waters C, Liu L et al. Burkholderia thailandensis Isolated from Infected Wound, Arkansas, USA. Emerging Infectious Diseases. 2018;24(11):2091-2094.

435. Dharakul T, Tassaneetrithep B, Trakulsomboon S, Songsivilai S. Phylogenetic Analysis of Ara + and Ara − Burkholderia pseudomallei Isolates and Development of a Multiplex PCR Procedure for Rapid Discrimination between the Two Biotypes. Journal of Clinical Microbiology. 1999;37(6):1906-1912.

436. Lertpatanasuwan N, Sermsri K, Petkaseam A, Trakulsomboon S, Thamlikitkul V, Suputtamongkol Y. Arabinose-PositiveBurkholderia pseudomalleiInfection in Humans: Case Report. Clinical Infectious Diseases. 1999;28(4):927-928.

437. Franco M, D'haeseleer P, Branda S, Liou M, Haider Y, Segelke B et al. Proteomic Profiling of Burkholderia thailandensis During Host Infection Using Bio-Orthogonal Noncanonical Amino Acid Tagging (BONCAT). Frontiers in Cellular and Infection Microbiology. 2018;8.

438. Kovacs-Simon A, Hemsley C, Scott A, Prior J, Titball R. Burkholderia thailandensis strain E555 is a surrogate for the investigation of Burkholderia pseudomallei replication and survival in macrophages. BMC Microbiology. 2019;19(1).

439. Haraga A, West T, Brittnacher M, Skerrett S, Miller S. Burkholderia thailandensis as a Model System for the Study of the Virulence-Associated Type III Secretion System of Burkholderia pseudomallei. Infection and Immunity. 2008;76(11):5402-5411.

440. Scott A, Laws T, D'Elia R, Stokes M, Nandi T, Williamson E et al. Protection against Experimental Melioidosis following Immunization with Live Burkholderia thailandensis Expressing amanno-Heptose Capsule. Clinical and Vaccine Immunology. 2013;20(7):1041-1047.

441. Nieves W, Petersen H, Judy B, Blumentritt C, Russell-Lodrigue K, Roy C et al. A Burkholderia pseudomallei Outer Membrane Vesicle Vaccine Provides Protection against Lethal Sepsis. Clinical and Vaccine Immunology. 2014;21(5):747-754.

442. Chantratita N, Wuthiekanun V, Thanwisai A, Limmathurotsakul D, Cheng A, Chierakul W et al. Accuracy of Enzyme-Linked Immunosorbent Assay Using Crude and Purified Antigens for Serodiagnosis of Melioidosis. Clinical and Vaccine Immunology. 2007;14(1):110-113.

443. Rhodes K, Schweizer H. Antibiotic resistance in Burkholderia species. Drug Resistance Updates. 2016;28:82-90.

444. Schwab U, Abdullah L, Perlmutt O, Albert D, Davis C, Arnold R et al. Localization of Burkholderia cepacia Complex Bacteria in Cystic Fibrosis Lungs and Interactions with Pseudomonas aeruginosa in Hypoxic Mucus. Infection and Immunity. 2014;82(11):4729-4745.

445. Kennedy S, Beaudoin T, Yau Y, Caraher E, Zlosnik J, Speert D et al. Activity of Tobramycin against Cystic Fibrosis Isolates of Burkholderia cepacia Complex Grown as Biofilms. Antimicrobial Agents and Chemotherapy. 2016;60(1):348-355.

446. Tseng B, Majerczyk C, Passos da Silva D, Chandler J, Greenberg E, Parsek M. Quorum Sensing Influences Burkholderia thailandensis Biofilm Development and Matrix Production. Journal of Bacteriology. 2016;198(19):2643-2650.

447. Garcia E. Burkholderia thailandensis : Genetic Manipulation. Current Protocols in Microbiology. 2017;45(1).

448. Lefebre M, Valvano M. Construction and Evaluation of Plasmid Vectors Optimized for Constitutive and Regulated Gene Expression in Burkholderia cepacia Complex Isolates. Applied and Environmental Microbiology. 2002;68(12):5956-5964.

449. Hassan A, Maldonado R, dos Santos S, Di Lorenzo F, Silipo A, Coutinho C et al. Structure of O-Antigen and Hybrid Biosynthetic Locus in Burkholderia cenocepacia Clonal Variants Recovered from a Cystic Fibrosis Patient. Frontiers in Microbiology. 2017;8.

450. De Soyza A, Ellis C, Khan C, Corris P, de Hormaeche R. Burkholderia cenocepacia Lipopolysaccharide, Lipid A, and Proinflammatory Activity. American Journal of Respiratory and Critical Care Medicine. 2004;170(1):70-77.

451. Ortega X, Hunt T, Loutet S, Vinion-Dubiel A, Datta A, Choudhury B et al. Reconstitution of O-Specific Lipopolysaccharide Expression in Burkholderia cenocepacia Strain J2315, Which Is Associated with Transmissible Infections in Patients with Cystic Fibrosis. Journal of Bacteriology. 2005;187(4):1324-1333.

452. Gronow S, Noah C, Blumenthal A, Lindner B, Brade H. Construction of a Deep-rough Mutant of Burkholderia cepacia ATCC 25416 and Characterization of Its Chemical and Biological Properties. Journal of Biological Chemistry. 2003;278(3):1647-1655.

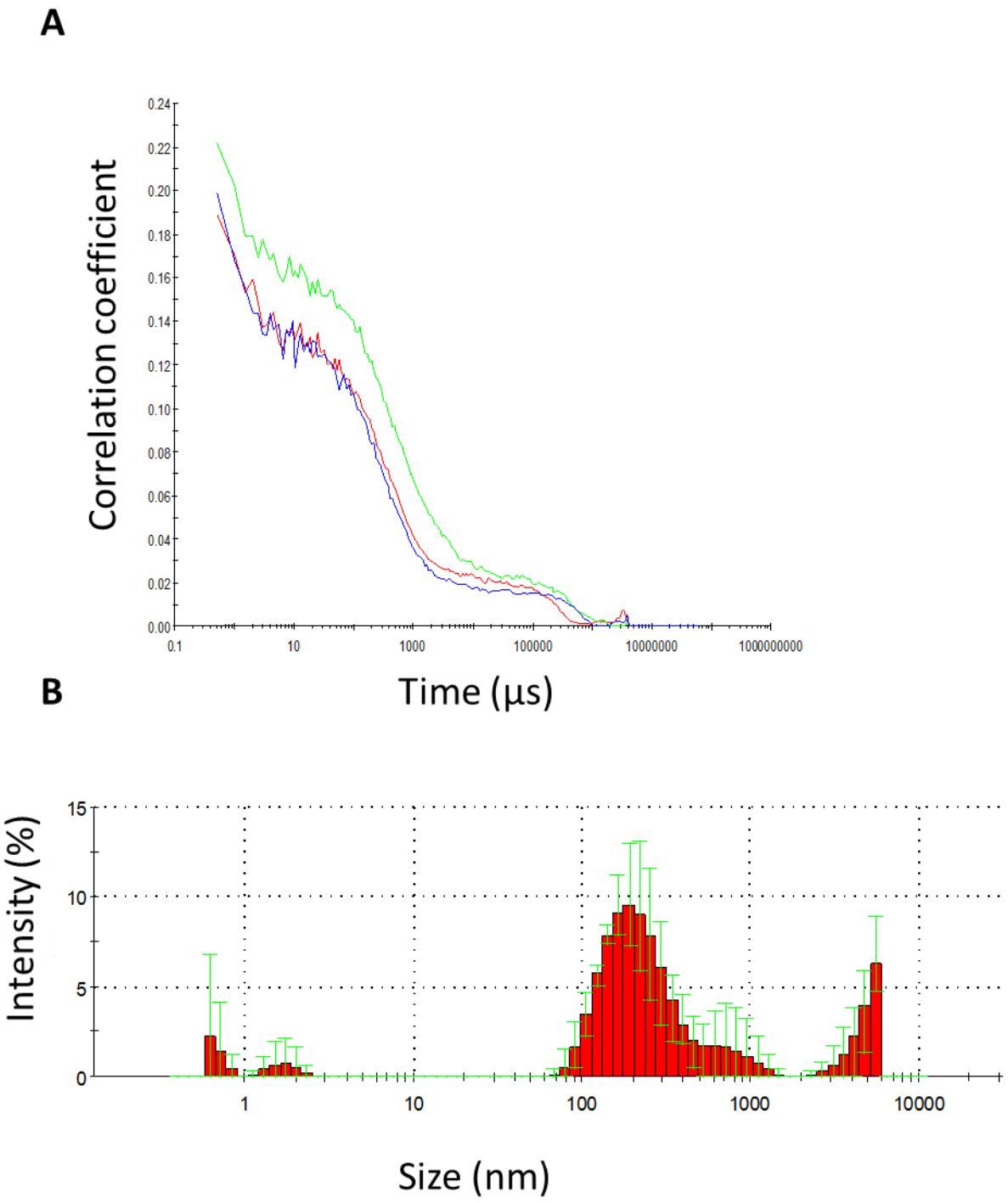

Figure 10.1: Physical characterisation of rifampin suspending in water at 300 µg/mL using dynamic light scatter. (**A**) is a correlogram showing the correlation coefficient of rifampin suggesting it forms unstable, polydispersed particles. (**B**) shows the predicted size of the populations present.

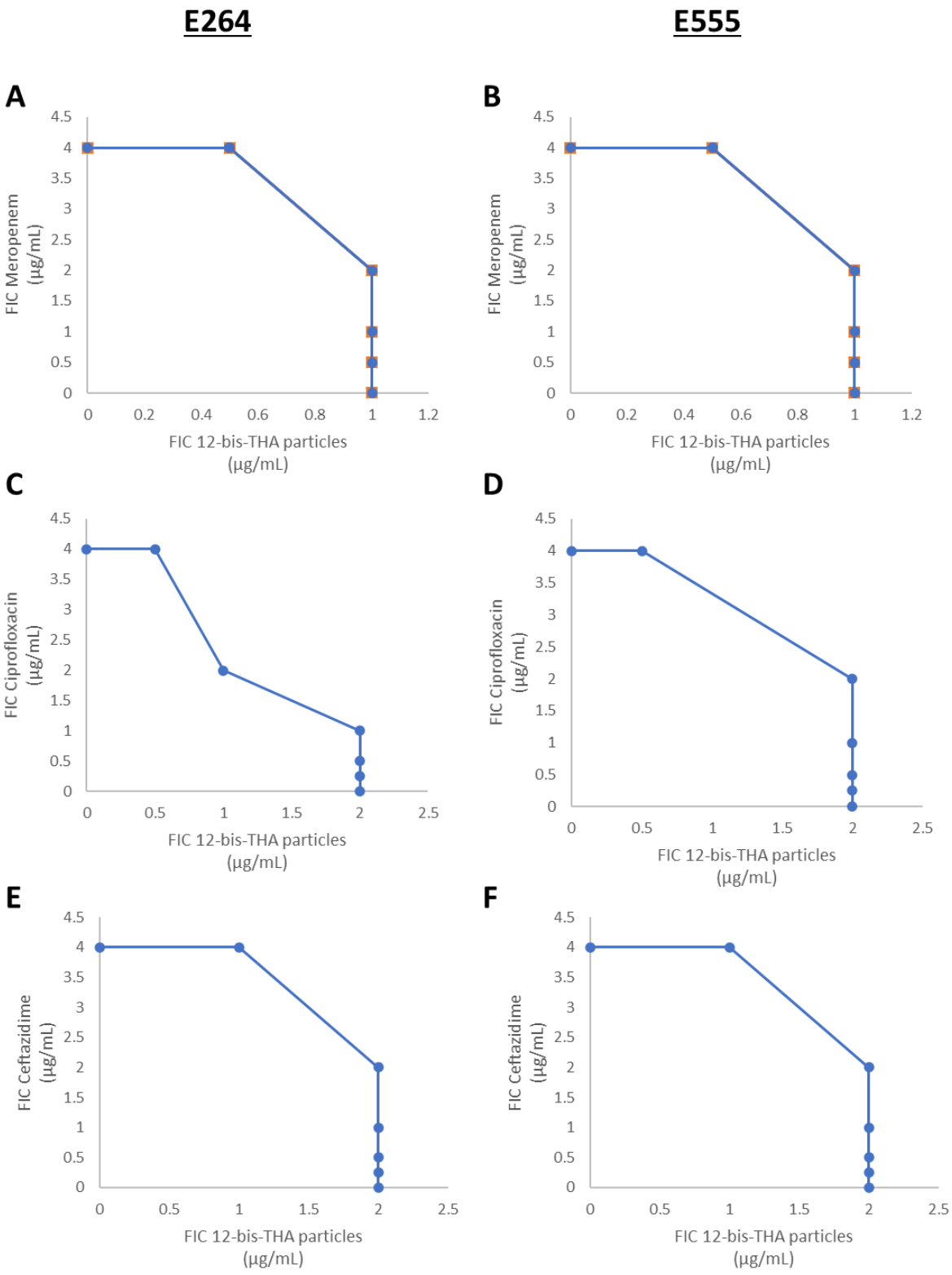

Figure 10.2: Isoboles representative of compounds that did not interact with 12-bis-THA particles in the checkerboard assay. A and **B** show interactions between 12-bis-THA particles and meropenem, **C** and **D** show interactions between 12-bis-THA particles and ciprofloxacin, and **E** and **F** show interactions between 12-bis-THA particles and ceftazidime. Data representative of 1/3 independent replicates.

Table 10.1: LPS chemotypes of BCC isolates used in Table 3.5.

Species	Strain ID	Alternative ID	LPS chemotype	Source
B. multivorans	17616	LMG 17588	Smooth	449
B. multivorans	BCC764	LMG 13010	Rough	450
B. multivorans	BCC710	A1-4	---	---
B. multivorans	BCC008	LMG 16660 C1576	Smooth	450
B. multivorans	BCC032	HA1	---	---
B. cenocepacia	J2315	LMG 16656	Rough	451
B. cenocepacia	K56-2		Smooth	451
B. cenocepacia	AU1054	---	---	---
B. cenocepacia	BCC0018	LMG16659 C1394	Partial rough	450
B. cenocepacia	BCC0020	LMG18830 CEP0511	Partial rough	451
B. cepacia	BCC001	---	Smooth	452
B. Gladioli	MA4	---	---	---

Table 10.2: A comparrison of BCC and *B. gladioli* LPS chemotype with the MIC of 12-bis-THA.

Strain ID	LPS chemotype	12-bis-THA particles MIC (µg/mL)
17616	Smooth	8
BCC008	Smooth	8
K56-2	Smooth	32
BCC001	Smooth	4-8
BCC764	Rough	4-8
J2315	Rough	16
BCC0020	Partial rough	8
BCC0018	Partial rough	8-16
BCC710	Unknown	4
BCC032	Unknown	2
AU1054	Unknown	16
MA4	Unknown	1